CONF-960297--

RECEIVED
OCT 28 1996
OSTI

The Proceedings of the 1st International Workshop on Laboratory Astrophysics Experiments with Large Lasers

B. A. Remington
W. H. Goldstein

August 9, 1996

Lawrence
Livermore
National
Laboratory

MASTER

DISCLAIMER

This document was prepared as an account of work sponsored by an agency of the United States Government. Neither the United States Government nor the University of California nor any of their employees, makes any warranty, express or implied, or assumes any legal liability or responsibility for the accuracy, completeness, or usefulness of any information, apparatus, product, or process disclosed, or represents that its use would not infringe privately owned rights. Reference herein to any specific commercial product, process, or service by trade name, trademark, manufacturer, or otherwise, does not necessarily constitute or imply its endorsement, recommendation, or favoring by the United States Government or the University of California. The views and opinions of authors expressed herein do not necessarily state or reflect those of the United States Government or the University of California, and shall not be used for advertising or product endorsement purposes.

This report has been reproduced
directly from the best available copy.

Available to DOE and DOE contractors from the
Office of Scientific and Technical Information
P.O. Box 62, Oak Ridge, TN 37831
Prices available from (615) 576-8401, FTS 626-8401

Available to the public from the
National Technical Information Service
U.S. Department of Commerce
5285 Port Royal Rd.,
Springfield, VA 22161

Work performed under the auspices of the U.S. Department of Energy by Lawrence Livermore National Laboratory under Contract W-7405-Eng-48.

Contents

I. Hydrodynamics I

II. Hydrodynamics II

III. Radiation Transport

The Proceedings of the

1st International Workshop on Laboratory Astrophysics Experiments with Large Lasers

February 26-27, 1996
Pleasanton, California

Edited by

Bruce A. Remington and William H. Goldstein
Lawrence Livermore National Laboratory
Livermore, CA 94550 USA

Printed by
Document Services Dept.
Lawrence Livermore National Laboratory
Livermore, CA 94550 USA
July 25, 1996

Scientific Committee

John Castor
Defense-Nuclear Technologies Dept.
LLNL

R. Paul Drake
Physics Dept.
University of Michigan

S. Gail Glendinning
Laser Program
Relations
LLNL

William Goldstein
Physics Dept.
LLNL

Bruce A. Hammel
Laser Program
LLNL

Jave Kane
Physics Dept.
University of Arizona

Rich London
Physics Dept.
LLNL

Claire Max
Director of University
LLNL

Bruce A. Remington
Laser Program
LLNL

Alexander Rubenchik
Physics Dept.
University of California-Davis

Organizing Committee

William Goldstein
Physics Directorate
LLNL

Laurie Pinkerton
Laser Program
LLNL

Karen Queheillalt
Laser Program
LLNL

Bruce A. Remington
Laser Program
LLNL

Misty Riendeau
Laser Program
LLNL

Preface

With the advent of modern large telescope facilities (such as the Kitt Peak and Cerro Tololo 4-meter telescopes in Arizona and in Chile, and the Keck 10-m telescope in Hawaii) and orbiting observatories (such as the Hubble Space Telescope and ROSAT) the quality and detail of astrophysical data being taken today is without parallel. Many objects currently under intensive observation exhibit temporal variations with time scales of order weeks, such as Type Ia supernova light curves, and months, such as the evolution of the ejecta from supernova SN1987A on its impact course with its circumstellar nebula. This opens the possibility to test predictions of the macroscopic evolution of such objects in real time with computer models which typically include an immense amount of microscopic physics. Unfortunately, one does not have the luxury in astrophysics of setting up clean, well controlled experiments in the universe to test the ingredients, in particular the microphysics, contained in the astrophysical models. Often times, debates about the details of various models continue for years, and in some cases decades. Creating a surrogate environment to serve as an astrophysics testbed would obviously be very desirable.

On the terrestrial front, the world has stood witness to the development of a number of highly sophisticated and flexible, high power laser facilities (energies and powers of up to 50 kJ and 50 TW), driven largely by the world-wide effort in inertial confinement fusion (ICF). The charter of diagnosing implosions with detailed, quantitative measurements has driven the ICF laser facilities to be exceedingly versatile and well equipped with diagnostics. Interestingly, there is considerable overlap in the physics of ICF and astrophysics. Both typically involve compressible radiative hydrodynamics, radiation transport, complex opacities, and equations of state of dense matter. Surprisingly, however, there has been little communication between these two communities to date.

With the recent declassification of ICF in the USA, and the approval to commence with construction of the next generation "superlasers", the 2 MJ National Ignition Facility in the US, and its equivalent, the LMJ laser in France, the situation is ripe for change. Access to these large laser facilities, present and future, is becoming available to the outside academic community. Given the physics similarities that exist between ICF and astrophysics, one strongly suspects that there should exist regions of overlap where supporting research on the large lasers could be beneficial to the astrophysics community.

As a catalyst for discussions to this end, Lawrence Livermore National Laboratory sponsored the 1st International *Workshop on Laboratory Astrophysics Experiments with Large Lasers* in Pleasanton, California, USA, over a two day period at the end of February, 1996. Approximately 100 scientists attended from around the world, representing eight countries: the USA, Canada, UK, France, Germany, Russia, Japan, and Israel. A total of 30 technical papers were presented. The two day workshop was divided into four sessions, focusing on nonlinear hydrodynamics, radiative hydrodynamics, radiation transport, and atomic physics-opacities. Copies of the presentations are contained in these proceedings.

The conclusion of the meeting was a consensus that there indeed do appear to be areas where careful laser experiments could serve as an astrophysical testing ground, a setting where emerging theories can have a "dry run". The challenge is to match the right astrophysics questions with the right laser experiment. We hope that the outcome of this workshop will be the start of a continuing dialog between the astrophysics and laser experiments communities, which will hopefully lead to more discriminating astrophysics experiments on the large laser facilities around the world.

It is our great pleasure to acknowledge the significant expert assistance we have enjoyed in putting this workshop together. We are particularly indebted to Misty Riendeau, Laurie Pinkerton, and Karen Queheillalt for their assistance in planning, organizing, and running the conference. We also acknowledge the assistance of Sandy Lynn and Cheryl Swinkels from our Document Services Department. We are deeply indebted to Bruce Fryxell for sharing his exquisite color images from his supernova simulations with us, examples of which appear on the announcement poster, the name tags, and on the cover of these proceedings.

*Work performed under the auspices of the U.S. Department of Energy by the Lawrence Livermore National Laboratory under contract number W-7405-ENG-48.

Bruce A. Remington
William H. Goldstein

WORKSHOP SUMMARY

Monday morning: Hydrodynamics I, Bruce Remington presiding

Mike Campbell (LLNL) welcomed the participants to the workshop, and stressed the need to include academia and basic physics experiments into the use of large lasers built for inertial confinement fusion (ICF) research. Mike pointed out that only with outside users of lasers such as Nova and the future National Ignition Facility, can the full potential of these ICF lasers be realized.

Joe Kilkenny (LLNL) gave an overview of large lasers around the world that might potentially be useful for astrophysics experiments. He then focused on laser capabilities at LLNL, covering the parameter regimes accessible with Nova, the 100 TW laser, the petawatt laser, the USP laser, and standard diagnostic capabilities at Nova.

Dave Arnett (University or Arizona) discussed the role of hydrodynamic instabilities, in particular, buoyancy driven convection and Rayleigh-Taylor instability, in the dynamics, evolution, and observables from Supernova 1987A. He stressed the importance of testing current theories and models of supernova in any way experimentally possible. One promising, and hitherto untried testing ground is using large lasers to mock up subsets of the physics of supernova. The current supernova experiment on the Nova laser is a model for designing experimental benchmarks of the supernova codes.

Gail Glendinning (LLNL) discussed an experiment that is being designed, together with Jave Kane (University of Arizona), a graduate student of Dave Arnett's, to test the modeling of deep nonlinear instability evolution using the astrophysics code PROMETHEUS. This appears to be the first experimental test of the nonlinear hydrodynamics predictions of this widely used supernova code. The experiment has progressed past its initial "shake-down" phase, and meaningful comparisons of experimental results with PROMETHEUS simulations has just started.

Dick McCray (University of Colorado, Boulder) discussed the imminent collision predicted to occur in 5 years of the expanding ejecta from SN1987A with its surrounding circumstellar ring nebula. He summarized models and current understanding of the ring, and predictions of x-ray, UV, and optical emissions expected when the collision ensues. He stressed the multiple shock interactions predicted, and pointed out the need to test modeling of these strong radiative shocks in advance of the event.

Paul Drake (LLNL and University of Michigan) discussed the final design of an experiment being developed for Nova, in collaboration with Richard McCray from the University of Colorado at Boulder and Edision Liang from Rice University, to look at the colliding plasma effects relevant to the SN1987A ring collision presented by McCray. This experiment will use the Nova laser to generate the strong shock that produces the laboratory equivalent of the expanding supernova ejecta. This expanding ejecta will then impact a surrounding "ring nebula" of plasma created by foam. The goal of the experiment is to examine the nonlinear shock hydrodynamics expected in the collision, and characterize the radiation emitted in the multiple shock interactions.

James Stone (University of Maryland) described his new model for the formation of hydrodynamic "bullets". The interesting hypothesis of this presentation was that deep nonlinear hydrodynamic instabilities are the cause of a broad array of astrophysical phenomena hitherto unexplained. He stressed the need to access the regime where radiative cooling behind the shock front affects the hydrodynamics. He emphasized that if laser experiments could be designed that investigate any part of this broad area of radiative hydrodynamics, then one might be able to impact the development of astrophysics theories and codes that are still in their infancy. This is exciting, because this is precisely the regime that the Drake-McCray-Liang experiment is being designed to address.

Monday afternoon. Hydrodynamics II, Paul Drake presiding.

The theme of the Monday afternoon session, chaired by Paul Drake, was the study of hydrodynamic phenomena in astrophysics and in the laboratory. Three of the speakers (**Grun** of NRL, **Dimonte** of LLNL, and **Schappert** of LANL) discussed experimental results from laser-based studies of the instability of Taylor-Sedov blast waves. In such experiments, a target immersed in gas is struck by a concentrated laser pulse. This produces a blast wave, similar to those described by Sedov and by Taylor in the 1950's, which takes hundreds of nanoseconds to propagate across the experimental chamber. Such Sedov-Taylor blast waves are believed to occur in a wide range of astrophysical systems including supernova explosions. The experiments found that the blast waves were sometimes stable and sometimes strongly unstable, depending upon a number of factors including the properties of the gas and the presence of a magnetic field.

The instability of Sedov-Taylor blast waves is related to the hydrodynamic instabilities which have produced mixing in supernova 1993J, discussed by **Iwamoto** of the University of Tokyo, who reported that the profiles present in the progenitor star can have a substantial impact on the instabilities which occur when the star explodes. Similarly, the explosion of a type Ia supernova is believed to produce a thin combustion layer which has some similarities to a blast wave and is most definitely subject to strong hydrodynamic instabilities, as discussed by **Khokhlov** of University of Texas at Austin. Both Sedov-Taylor blast waves in astrophysical systems, and the shocks driven by flowing plasmas, can become radiative, in the sense that they radiate power more quickly than they receive power. This can lead to density collapse and strong hydrodynamic instability, as discussed by **Blondin** of North Carolina State University and by **Klein** of LLNL. Although laboratory studies have not yet dealt with radiative shocks, some strongly-nonlinear hydrodynamic systems have been studied. Experiments on the interaction of shock waves, on jets, and on colliding plasmas were reported by **Perry** and **Miller** of LLNL. Additional, possible experiments to look for pair production and to simulate other aspects of supernovae were discussed by Liang of Rice. The general properties of late-time, nonlinear hydrodynamic mixing in non-radiative systems are beginning to yield to theoretical analysis, as **Shvarts**, of Negev Nuclear Research Center in Israel, showed. He also pointed out that the behavior is qualitatively different when a shock passes through a previously-shocked medium, as is common in astrophysical environments, and that this problem deserves study.

Tuesday morning: Atomic physics / opacities, Bill Goldstein presiding

The session on opacity, spectroscopy and radiation transport opened with a historical overview of astrophysical opacity research from **Arthur Cox**, of Los Alamos National Laboratory. Cox introduced the Hertzsprung-Russel diagram, and described the large range of variable stellar systems whose evolution and characteristics depend sensitively on radiative opacity. He identified banner years in the ~55 year history of opacity calculations, including the appearance of Los Alamos opacities in 1964-70, and culminating with the publication of new results from LLNL's OPAL group in 1991-93. These improved tables evinced enhancement factors of three in opacity owing to previously neglected bound-bound transitions in iron. As Cox pointed out, the new calculations affected our understanding of a long list of variable systems, including double-mode cepheids, delta Scuti variables, and solar oscillation frequencies.

Cox went on to describe his recent work on the effects of convection on the behavior of variables, and concluded that modern opacities may not, in fact, fully explain observations of stellar pulsations.

The themes introduced by Cox were elaborated later in the session by **Carlos Iglesias**, who addressed remaining uncertainties in stellar opacities, and by **Paul Springer** who discussed experiments relevant to stellar atmospheres. Iglesias pointed out that uncertainties in the solar interior opacities deduced from code comparisons are as large as 35%, especially near the bottom of the solar convection zone. The source of the discrepancies was traced to uncertainties in the ionization balance. Present theories that describe the behavior of bound states in dense matter do not agree, and there have been few experiments to test them. Iglesias described recent laser-driven absorption measurements that have proven valuable in validating some aspects of these theories, and proposed that these experiments be extended to provide detailed input for ionization balance models.

Paul Springer also pointed to discrepancies between models of stellar opacity, particularly those arising from line-shapes, and the merging of lines into quasi-continua. These uncertainties are most pronounced at densities of 10^{-3} g/cc and lower, and experiments to access this regime are highly constrained in time-duration, spatial size and spectral resolution. Springer concluded by describing a nested-hohlraum design that produces the right conditions in simulations.

Steve Rose, of the Rutherford Appleton Laboratory, and the Department of Physics and Space, University of Birmingham, followed Cox with a wide-ranging review of current and proposed laser experiments in the UK with relevance to radiation flow in astrophysics. Rose showed that the opacity measurements he was describing - including high-density, short pulse laser experiments - mapped out typical temperatures and densities in the sun. He also described line transfer experiments in the presence of large velocity gradients, an important effect Type Ia Supernovae, among other astrophysical systems. Rose also proposed novel experiments to address the role of Compton scattering in the energy balance of accretion-powered objects. He presented simulations showing that the effects of Compton scattering on the radiation emitted from compressed balls of DT gas was profound and measurable.

Rose concluded that the plasma conditions achievable with high-power lasers are comparable to those found in certain astrophysical plasmas. He added that complex laser experiments are underway in which the conditions are controlled to investigate specific, relevant physical processes.

Phil Pinto of the University of Arizona picked up one of Rose's threads in a talk on Radiation Transport in Flows with Large Velocity Gradients. He described the light curve of Type Ia supernovae as a competition between radiaoactive energy deposition, adiabatic decompression, and radiative transport to the surface. The transport is dominated by line absorption in large velocity gradients. Escape is effected through exotic processes like Doppler downshifting of thermal radiation and "photon-splitting." Outside of the supernovae light curve itself, there exists little data to guide the theorists in modeling the opacity of such unique systems. Pinto suggested that laboratory experiments could test elements of the models by measuring transport in laser-produced blow-off plasmas, and by testing iron group atomic physics and branching ratios.

Tim Kallman of NASA and **Duane Liedahl** of LLNL discussed the modeling and laboratory simulation of X-ray photoionized nebulae. The opportunity to perform detailed studies of the X-ray emission from these accretion-powered sources is among the most exciting prospects in astrophysics for the next decade. But the analyses of spectra from accretion-powered X-ray sources, which will comprise a substantial portion of the high-energy astrophysics database, are likely to severely tax the capabilities of the currently available analytical resources. The reason is clear: understanding of atomic physics processes and the matter/radiation interactions in X-ray photoionized plasmas is sketchy.

The essential aspect of an X-ray photoionized plasma is the high degree of overionization relative to a steady-state collision-driven plasma at the same temperature. The ionization state is characterized by the quantity, $\xi = 4\pi F/n$, the ratio of the ionizing radiation flux to the electron density. Whenever ξ exceeds ~10 (cgs), electron impact ionization is less important than photoionization in establishing the charge state distribution. Similarly, the role of electron impact excitation is reduced in comparison to recombination cascades as a population mechanism. At present, the physical processes of "X-ray nebulae" are modeled by complex computer codes which, nevertheless, rely on untested, simplifying assumptions and approximations.

Liedahl pointed out that conditions achievable in targets using the Nova laser, and conditions projected for the planned National Ignition Facility (NIF), have excellent overlap with the parameters expected to characterize accretion-powered plasmas. In proposed experiments, uniform, photoionized plasmas are created by illuminating a low density gas target with broad-band ionizing radiation from a laser-irradiated high-Z converter target. Preliminary experiments and predictions for gas cell targets have already been made and a box-like target has been designed in which argon gas is contained by thin-foil windows. This target allows argon pressures from 25 Torr (corresponding to ion densities near 10^{18} cm^{-3}) down to pressures several orders of magnitude lower. A gold converter spectrum has also been measured on the Nova Two-Beam Facility using .53 mm light in a line-focus geometry at an irradiance of 10^{14} W cm^{-2}. This spectrum has been used to estimate the values of x achievable at laser facilities that are precisely those expected to obtain in the X-ray emitting regions of accretion disks. Design calculations for an argon experiment using the 25-Torr gas cell and the measured gold spectrum have predicted ionization into the middle of the L-shell. Then, using absorption and emission spectroscopy, respectively, to measure ionization distribution and temperature, a direct comparison with the predictions of astrophysical simulation codes could be carried out at known – and controllable – density (gas pressure) and ionization parameter (luminosity).

Tuesday afternoon: Radiation transport, John Castor presiding

In the Tuesday afternoon session **Nigel Woolsey** (LLNL) began with a discussion of "Spectroscopy of Compressed High Energy Density Matter." He reported the results of a series of Nova experiments on implosions of capsules filled with D_2, CD_4, N_2 or Ne, doped with Ar, whose K-line spectrum is measured. The object of the experiment was to make a sensitive test of line-shape theory as applied to the K lines, and in particular to assess the importance of ion dynamics to the line shape, which should be a much greater effect with light perturbing ions (D) than heavy ones (Ne). The same line shapes also provide diagnostics of temperature and electron density. The theoretical comparison was made to the FLY code of Lee, *et al.* The experimental results confirmed that the FWHM of the He-like Ar Kβ line is a good density diagnostic, while the Li-like satellites of the same line provide a T_e diagnostic. The surprising experimental result was that the central dip in He-like Ar Kβ, indicative of a *lack* of ion dynamics, was absent in every case for which the spectrum could be measured, perhaps owing to gradient effects.

Dick More (LLNL) described "Physics on Short Pulse, High Intensity Lasers," referring to the capabilities of LLNL's Ultra-Short-Pulse laser facility. The USP can deliver a pulse of 0.1 Joule with a pulse length of order 100 fs, and the promise is to perform experiments on matter at >1 keV temperatures at solid density, since the heating and ionization time scales can be made short compared with the time scale for hydrodynamic motion. A variety of LASNEX simulations was shown to indicate how the sample approaches LTE and steady-state ionization equilibrium as a function of time and laser intensity. The interferometric techniques for probing the velocity and density distributions in the exploding sample were illustrated. Finally, some results were shown for the spectrum of a sample of germanium.

"Femtosecond-Laser Driven Heat Waves in Solid" was the topic of the presentation by **Andrew Ng** (University of British Columbia). The stimulus was the experiment by Vu, Szöke and Landen with a buried layer of carbon in a glass target exposed to a 5×10^{14} W/cm^2 intensity for 100 fs. The preliminary analysis of the experiment used LASNEX and the classical (Spitzer) conductivity model. In his study, Ng applied a hydrodynamic simulation coupled with a wave equation solver (for the EM field), and used a more sophisticated plasma conductivity theory. These simulations elucidate three different phases of thermal wave propagation: skin-depth deposition, thermal conduction and shock compression. The suggestion is made that the high velocity observed in the Vu, et al., experiment might have been due to laser penetration. It is concluded that accurate measurements of front velocity are a good discriminant for models of electrical and thermal conductivity.

Astrophysics was represented in the session with the presentation "Asteroseismology of White Dwarf Stars" by **Paul Bradley** (LANL). Bradley reviewed the classification of variable (pulsating) white dwarfs into DOV, DBV and DAV, based on surface temperature, ranging from 10^5 K for DOV to 10^4 K for DAV. These stars are oscillating in a mixture of many so-called g-modes, which, like water waves, are based on buoyancy. The evolution of the cooling white dwarfs is modeled, and at each point of its evolution the spectrum of g-mode oscillating frequencies is computed. Fitting the computed spectrum to the observations of individual stars allows their masses and surface temperatures to be inferred, and also the amount of residual hydrogen-rich material left at the outside of the white dwarf. The total masses that are found agree well with other estimates of white dwarf masses, and with masses for white-dwarf progenitor stars. The residual hydrogen masses turn up some surprises, and suggest that DA and DB white dwarfs have different origins.

Anatolly Orishich (Novosibirsk) discussed "Interaction Processes Between Exploding Plasmas and Media in Space," based on experiments with the KI-1 CO_2 laser at the Institute of Laser Physics of Novosibirsk State University, which can deliver 1 kJ to targets up to 100 μg in mass, possibly with a magnetic field of 1 kG. The experiments are intended to simulate the deceleration of nova and supernova ejecta by interstellar material, the movement of plasmoids in the earth's magnetosphere, interplanetary shock waves generated by solar flares, and the influence of the galactic magnetic field on the expansion of planetary nebulae. The governing processes, which are studied using KI-1, are the collisionless interaction of super-Alfvenic plasma flows; collisionless energy coupling to the background gas; interaction of the plasma flow with a magnetic field and the role of turbulence; the formation of compact plasma shells; and ionization waves.

A Quick Look at the Capabilities of Nova and its Accessibility to Outside Users

Joseph D. Kilkenny
Lawrence Livermore National Laboratory

A Quick Look at the Capabilities of Nova and its Accessibility to Outside Users*

Joseph D. Kilkenny
Program Leader,
ICF Target Physics

Lawrence Livermore
National Laboratory

Presented to:
Workshop on Laboratory
Astrophysics Experiments
with Large Lasers
Pleasanton Hilton
February 26, 1995

2

The Nova target chamber with diagnostics in place

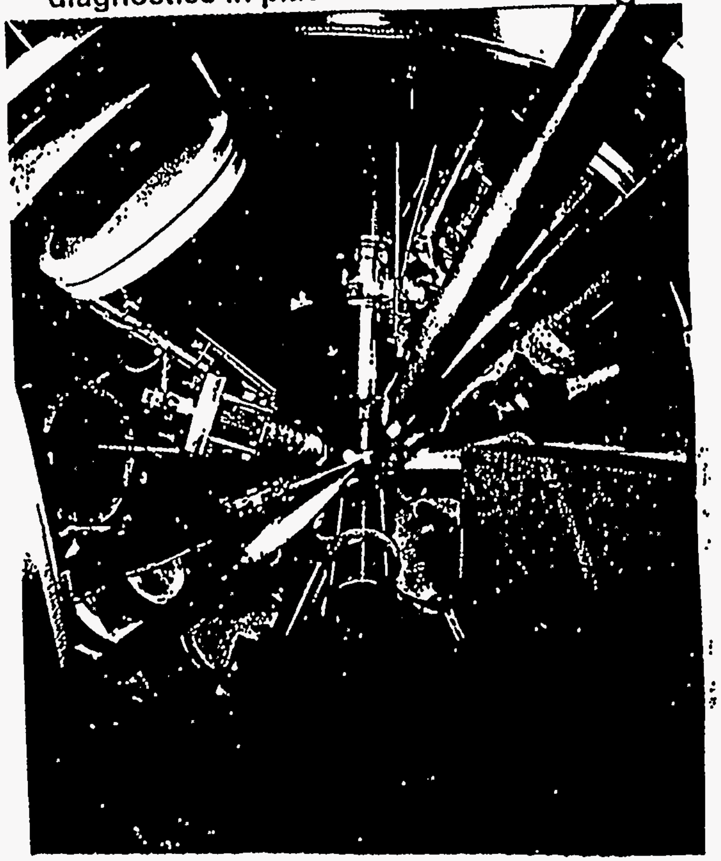

---

*This work was performed under the auspices of the U.S. Department of Energy by Lawrence Livermore National Laboratory under contract No. W-7405-Eng-48.

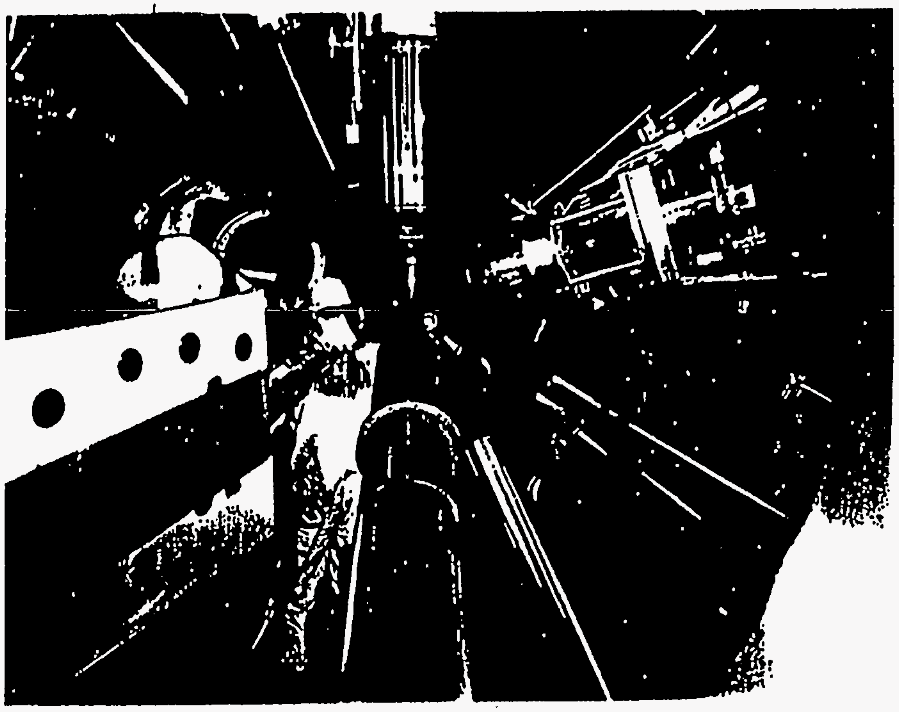

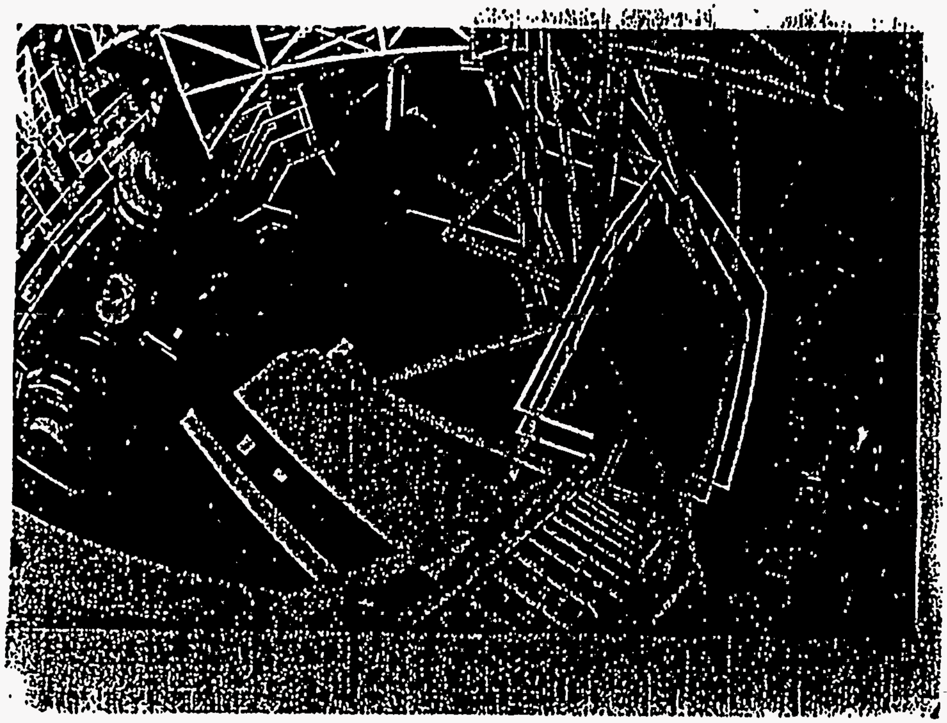

An LDRD-funded Petawatt modification to Nova will be used in FY'97 for Fast Ignitor Physics (FIP) experiments

Deliverables:

FY'93 to FY'95	technology development & hardware installation (LDRD)
FY'96	system integration (LDRD)
FY'97	FIP I, II, & III experiments

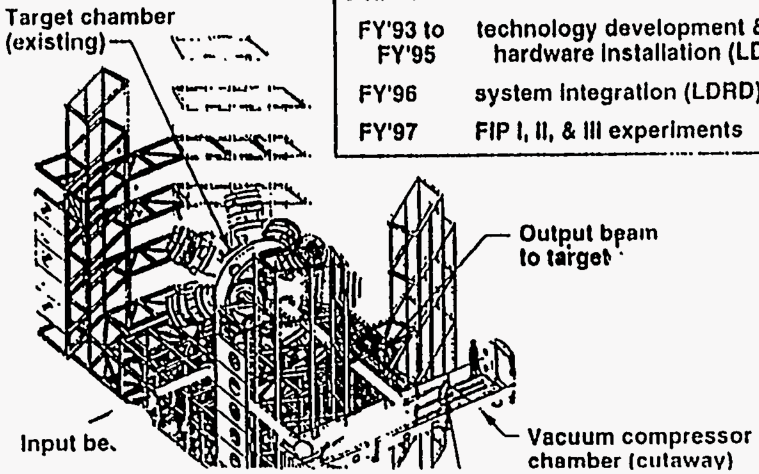

Nova is an unparalleled ICF and high energy density facility and has become a paradigm of interlab collaboration

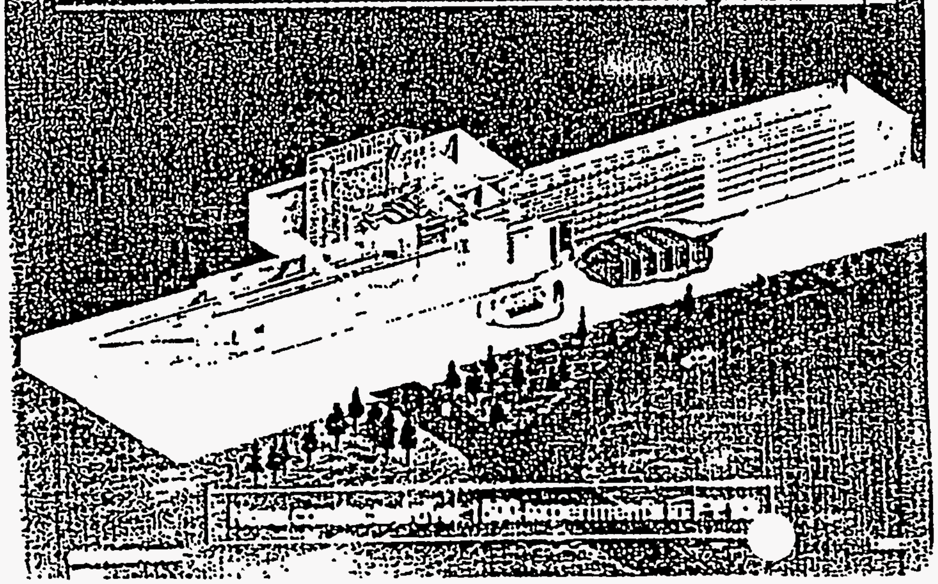

The Target Physics Program Advisory Board Committee (TPPAC) consists of:

Dr. Barrett Ripin, Chairman	American Physical Society
Dr. Don DuBois	Los Alamos National Laboratory
Prof. Roger Falcone	University of California at Berkeley
Dr. Damon Giovanielli	Sumner Associates
Prof. Hans Griem	University of Maryland
Dr. Jacob Grun	Naval Research Laboratory
Prof. Chan Joshi	University of California at Los Angeles
Dr. Michael Key	Daresbury-Rutherford-Appleton Laboratory
Dr. Richard Petrasso	Massachusetts Institute of Technology
Dr. Phillip Rumsby	Exitech Limited
Prof. Wolf Seka	University of Rochester

For FY96, a peer-reviewed pilot scheme for University Use of Nova for high energy density physics is in place and working

- A call for proposals was made in Spring '95 with the criterion of quality high energy density physics, with small funding by ORIF via LLNL for miscellaneous expenses. Shot expenses are paid for by LLNL-ICF.
- Eighteen proposals were received in astrophysics, atomic physics, high density physics, x-ray instrumentation, high magnetic fields, plasma physics and ICF
- An external 13-member committee of scientists (Chaired by Dr. B. Ripin), judged the proposals and recommended proceeding with nine proposals, anticipating using ~100 shots in FY96
- By December '95, ~35 shots had been used with promising results in five of the approved investigation

For FY97, the pilot scheme could be expanded with increased resources identified for supporting research at Universities

The Large Neutron Scintillator Array (LaNSA) is located under the Nova target chamber.

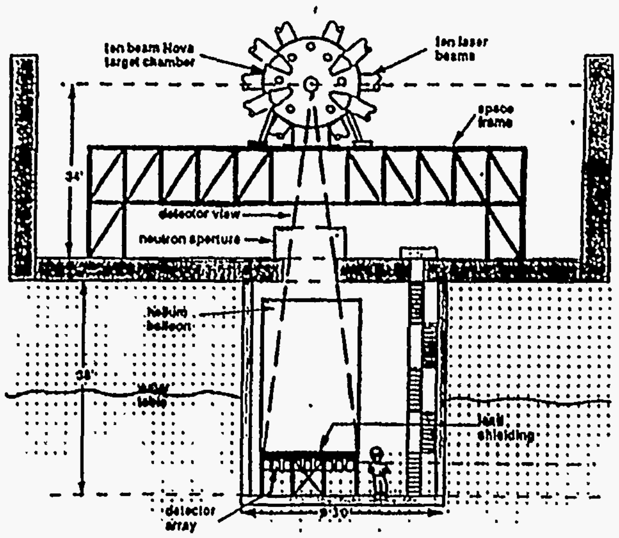

Higher Speed Gating has Clearly Demonstrated Reduced Motional Blurring

Direct drive implosion of a glass microballoon at 1/2 initial radius on the Omega laser

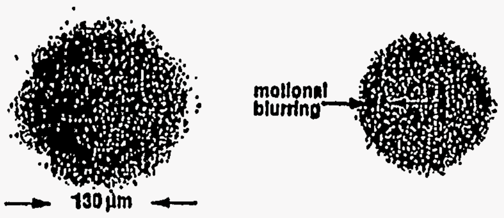

35 psec gating

100 psec gating

The laser and diagnostic capability of Nova has steadily increased

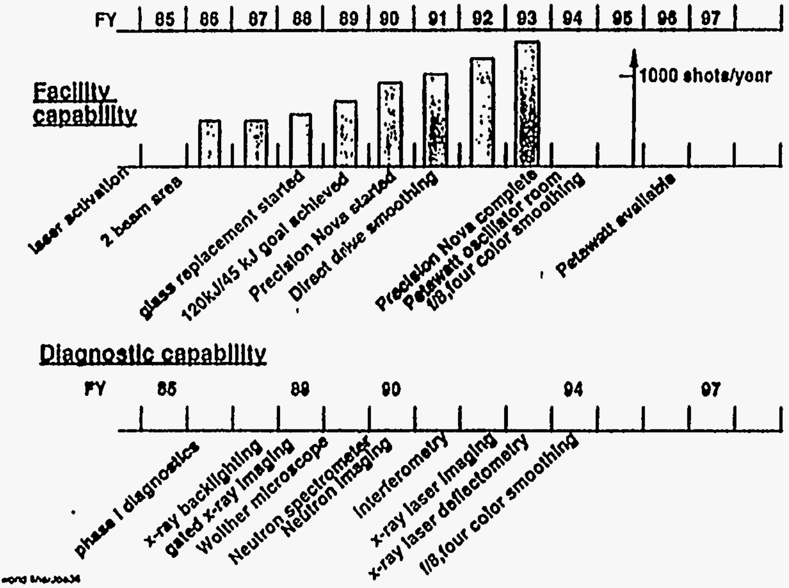

Nova has approximately 60 established diagnostics: most of them are run by the facility

X-ray imagers		no
Wolther x-ray microscope	22X	1
Gated x-ray pin hole camera	GXI,WAX,GACI	4
Gated soft x-ray framing camera	SXRFC	1
Streaked soft x-ray imager	HSDSS	1
Ring aperture microscope	RAM	1
Streaked slit/array imager	SSC/SLIP	2
Kirkpatrick Baez microscopes	8X	2
Axial pin hole cameras	APH	2
Large area backlighting		
Point projection spectroscopy	PPS	2
Soft x-ray microscope		1
XRL beam divergence camera	Cube	1
XRL spatial coherence diagnostic		1

X-ray spectrometers		
Streaked crystal spectrometers	HSCS,[illegible]	2
High resolution streaked spectrometer	HICXS	1
Static crystal spectrometers	Henway,POS	6
High resolution crystal spectrometer	HOPS	1
Gated crystal spectrometer	TOPS	1
Gated imaging XUV spectrometer	DXUVS	
Laue spectrometer	HETS	1
Low resolution x-ray diode array	Dante	2
Low res. high energy fluorescers	FFLEX	2
Spatial coherence diagnostic		1
Grazing incidence spectrometer	COFFIN	1
High resolution spectrometer	HIRES	1
Time resolved soft x-ray spectrometer	SFFD	1
Gated grazing [illegible] spectrometer	McPIGS	1

Neutron diagnostics		no
Yield	Cu,In scn	3
Bang time	NETMCP,Ge	3
Burnwidth	NTD & GaAs	2
High res. high sens. spectrometer	LaNSA	1
Medium res. neutron spectrometer	NTOF	3
Ultra high res spectrometer	INTOF	1
High res high sens spectroscopy	LANL T.	1
Neutron imager	NPAM	
gamma spectrometer		

Optical spectrometers and imagers		
Streaked/gated imager	SOP	2
Streaked optical spectrometers	SOS,BSS	4
Multiple streaked spectroscopy	MATRES	1
Spatially discr. streaked optical spect	SOOSS	1
Calorimeter array	EBM	1
Full beam back scatter	SOSS	1

AN EVEN MORE COMPREHENSIVE SET WILL EVOLVE FOR THE NIF

We have overcome the limitations of spatial and temporal scales for weapon physics on Nova by advanced diagnostic development

- temporal resolution of 30 psec with x-ray framing cameras
- spatial resolution of 3 µm FWHM with xrl microscopy
- soft x-ray backlighting with xrl's for interferometry and deflectometry of hohlraum plasmas
- high-energy x-ray backlighting: photon energies up to 6-9 keV, delay times up to 50 nsec
- high-resolution x-ray spectroscopy

Much development motivated by weapon physics needs

Eighteen proposals for University Use of Nova were received (continued)

Field	Title	Principal Investigator
Plasma Physics	Hot Electron Transport	Kado, CREOL
	Transient 4-Wave Mixing and Thomson Scattering	Joshi, UCLA
	Spectroscopic Investigation of Colliding Plasmas	Clothiaux, Auburn U.
	Fireball Experiments	Peterson, U. of Wisconsin
X-Ray Laser	Nova Experiments in Thomson Scattering	DeGroot, UC Davis
X-Ray Diagnostics	Photopumping for X-Ray Gain at 10-50 Å	Elton, U. of Maryland
ICF	Monochromatic X-Ray Crystal Imaging	Gabel, CREOL
	Direct Drive Implosions with Foam Buffer	Willi, Imperial College
	Energetic Protons for pR and Symmetry in ICF	Petrasso, MIT

Accessibility of U.S. ICF lasers to non-ICF users

Nova
- — FY96 pilot program for University Use in place
- — Shots, targets, miscellaneous support supplied
- — 18 proposals/9 agreed
- — Proposals judged on scientific merit by independent review committee
- — For FY97 new call for proposals expected in Spring '96
- — Shots, targets, miscellaneous support and small contracts expected

Omega
- — National Laser Facility in Place
- — Shots, targets through Rochester, grants through DOE
- — 9 proposals/6 agreed in FY96
- — Call for proposals for FY97 in summer
  - · Contact J. Knauer

Nike (NRL)
Trident (LANL)
- — Less formal arrangements

Contacts — Steve Obenschain (NRL)
— Bob Watt (SNL)

Interferometry using a 155 Å soft x-ray laser was recently demonstrated

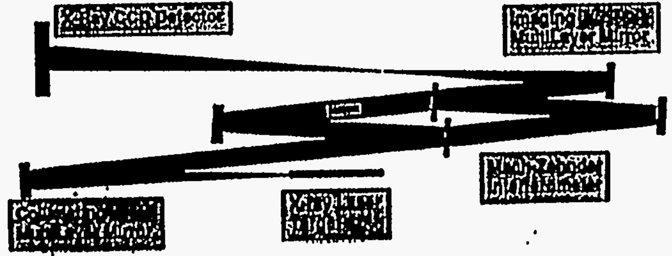

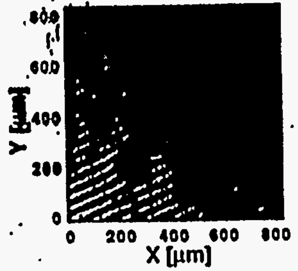

Interferogram obtained without secondary plasma shows excellent fringe visibility. This diagnostic will soon be used to measure electron densities in large scalelength plasmas.

Draft four year plan for use of Nova

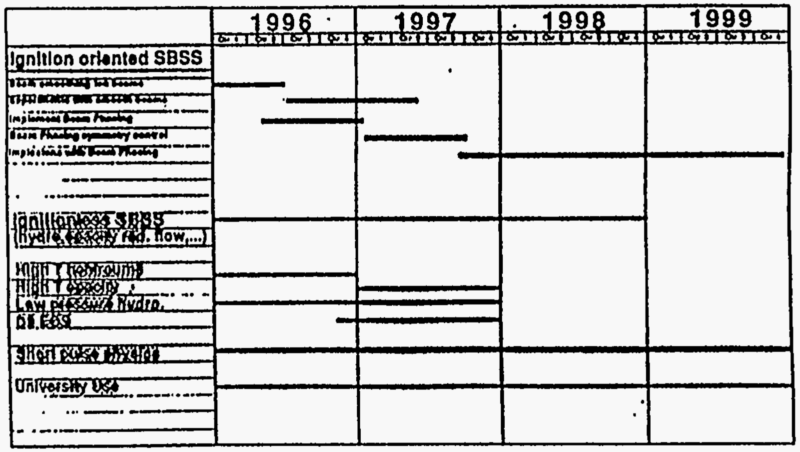

The annual and quinquennial planning processes are in process

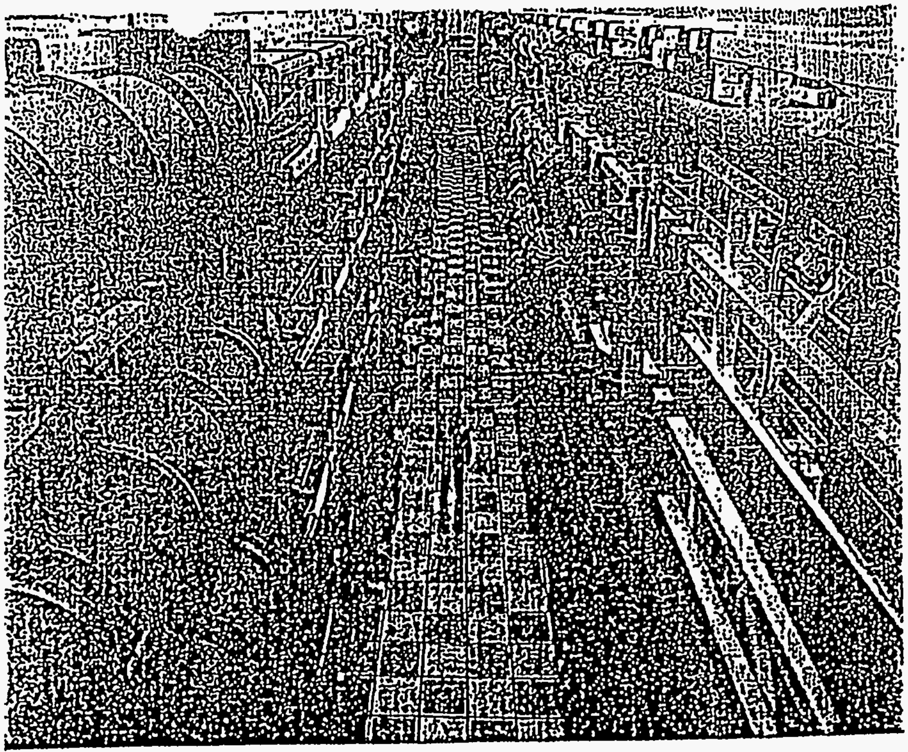

OMEGA has irradiated targets with >37 kJ UV in 60 beams

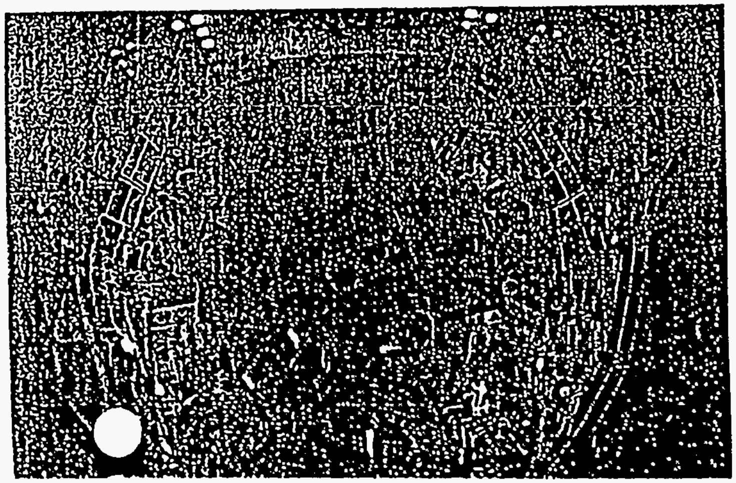

We have achieved >50 joules in a 400-fsec pulse producing a new world record for peak power (125 TW)

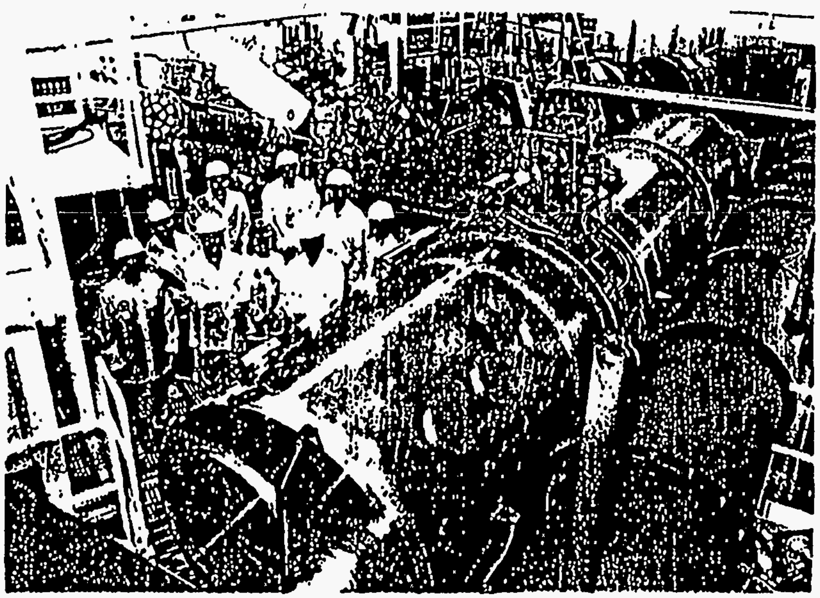

Laser facilities in ICF have large and diverse capabilities for high energy density physics experiments

Nova (LLNL - 1984) – 40 kJ/30 TW, 0.35, 0.53 µm; primarily indirect drive ICF, also planar direct drive ICF; HEDP physics on opacity, rad-hydro, EOS, x-ray laser.
  - 100 TW (1995); 100 TW, 1 ps, 1.05 µm; Independent beam synched with 1 Nova beam; fast ignitor ICF; High density plasmas
  - PetaWatt (1996); 1 PW, 1 ps, 1.05 µm; 1 Nova beam synched with the other nine beams; fast ignitor ICF; High density plasmas

Omega upgrade (U Rochester -1995) – 30 kJ/30 TW, 0.35 µm; primarily direct drive implosion facility; potentially can do indirect drive exps. with ~20 TW.

Trident (LANL - 1992) - 2 beams, 100 J/beam 1.06, 0.53 µm + a backlighter beam; diagnostic development, plasma physics, planar hydro and direct drive .

Nike (NRL - 1995) - 2 kJ/0.4 TW, 0.26 µm + a backlighter beam [illegible] nar direct drive and planar hydro exps.

Hydrodynamic Instabilities in Type II Supernovae

Dave Arnett
University of Arizona

ASTROPHYSICS

(Arnett)

Collaborations:

O and Si burning:
Grant Bazan

87A Rings:
Crystal Martin

Detonation/Deflagration
Willy Benz
Eli Livne

Light Curves
Philip Pinto

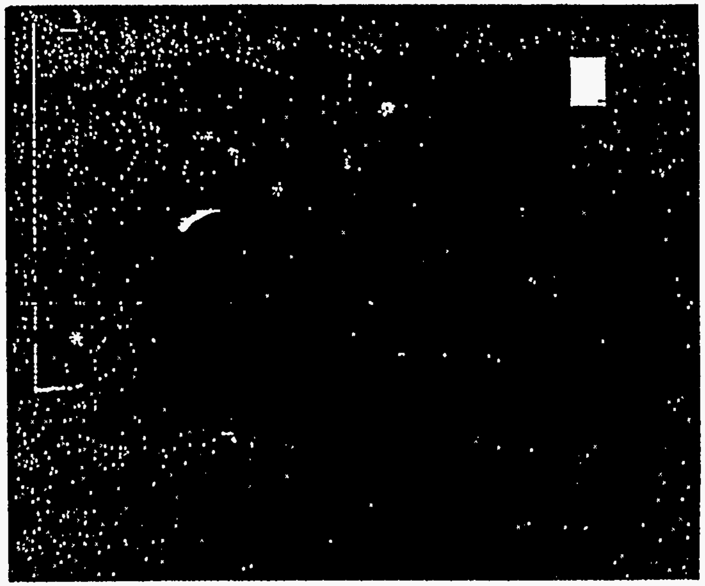

Martin & Arnett 1995 Ap.J.

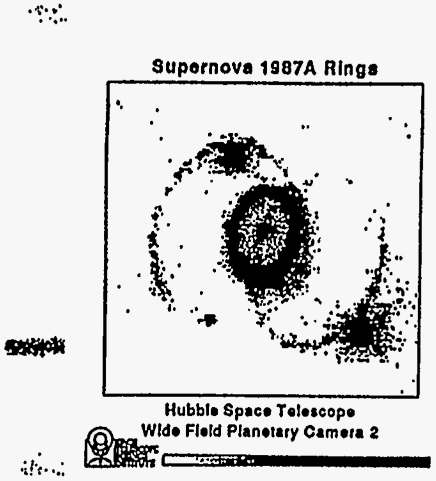

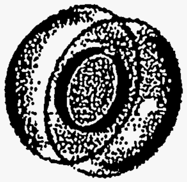

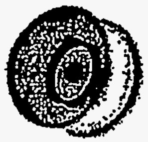

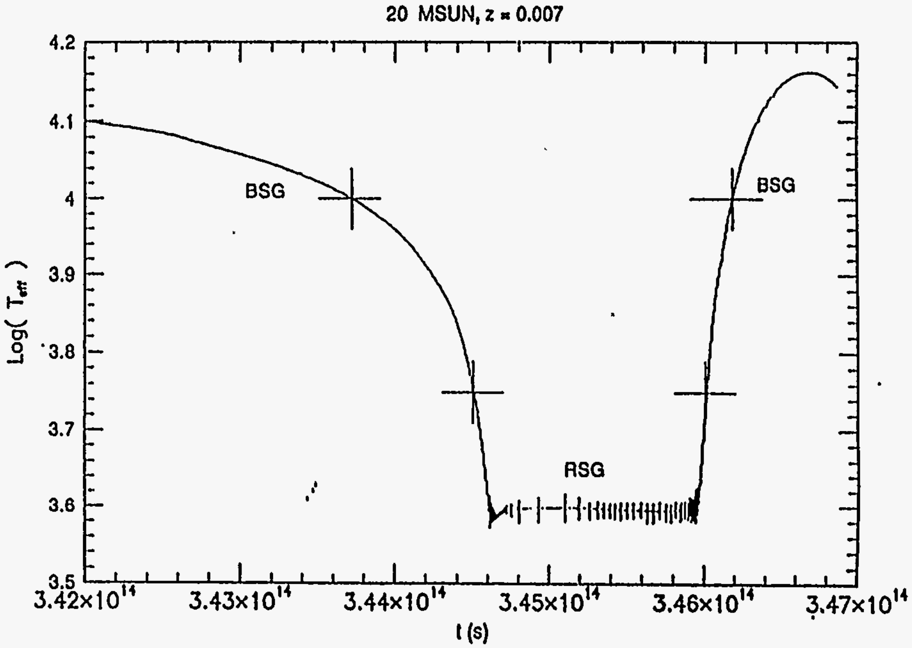

FIGURE 13

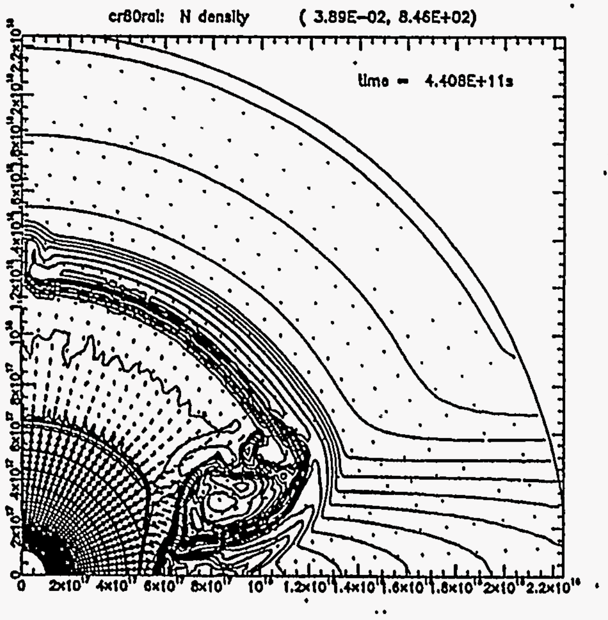
cr80rol: N density (3.89E-02, 8.46E+02)
time = 4.408E+11s
0
2x10¹⁷
4x10¹⁷
6x10¹⁷
8x10¹⁷
10¹⁸
1.2x10¹⁸
1.4x10¹⁸
1.6x10¹⁸
1.8x10¹⁸
2x10¹⁸
2.2x10¹⁸

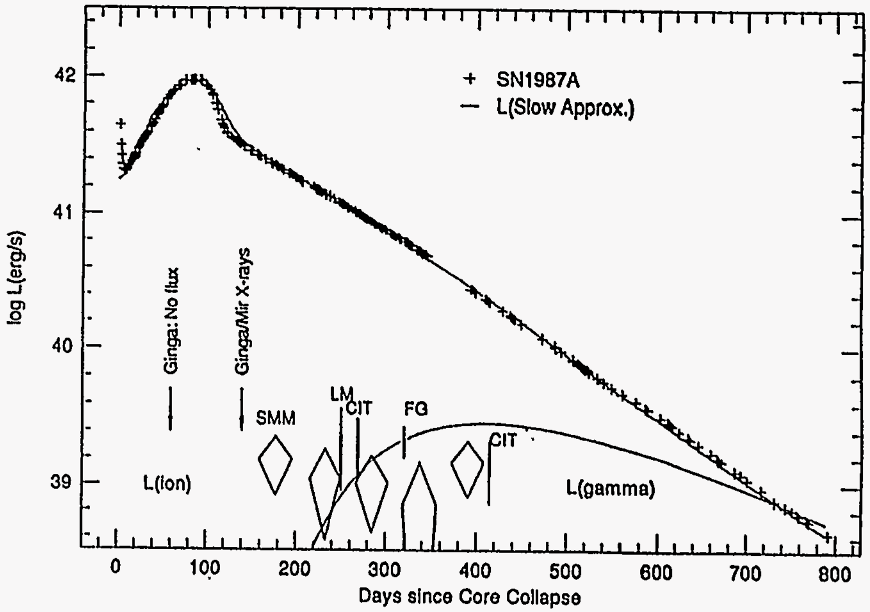
+ SN1987A
— L(Slow Approx.)
log L(erg/s)
42
41
40
39
Ginga: No flux
Ginga/Mir X-rays
SMM
LM
CIT
FG
CIT
L(ion)
L(gamma)
0
100
200
300
400
500
600
700
800
Days since Core Collapse

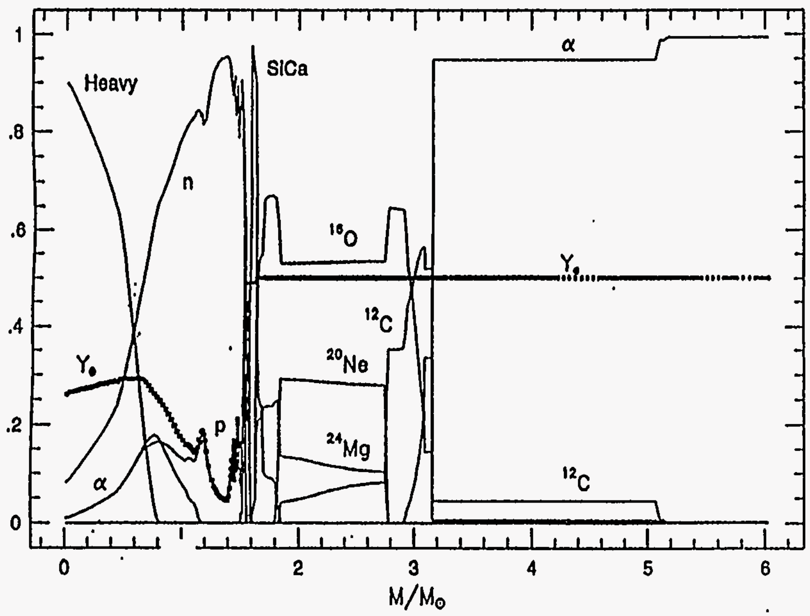
1
.8
.6
.4
.2
0
Heavy
n
SICa
α
¹⁶O
Yₑ
¹²C
²⁰Ne
²⁴Mg
p
α
¹²C
0
2
3
4
5
6
M/M☉

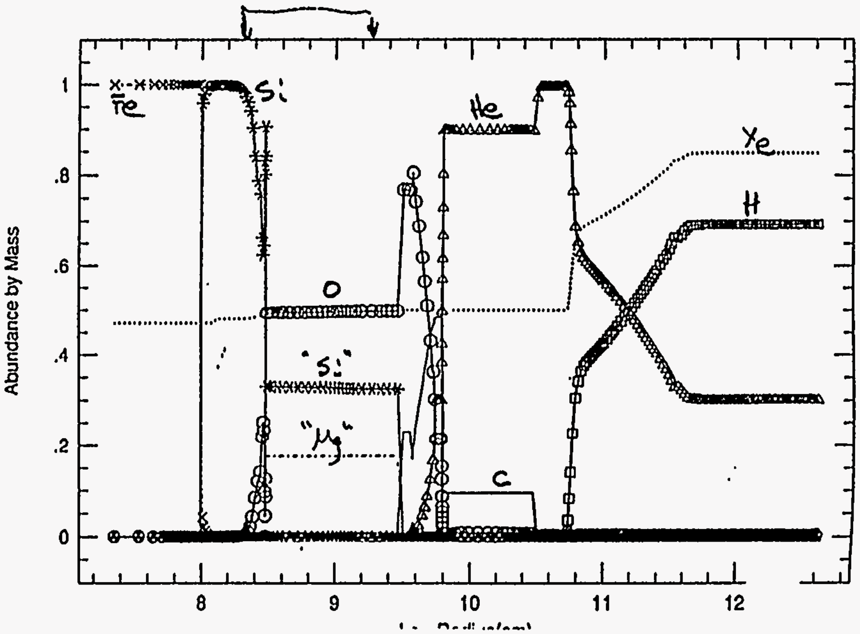
Abundance by Mass
1
.8
.6
.4
.2
0
Fe
Si
He
Xe
H
O
"Si"
"Mg"
C
8
9
10
11
12

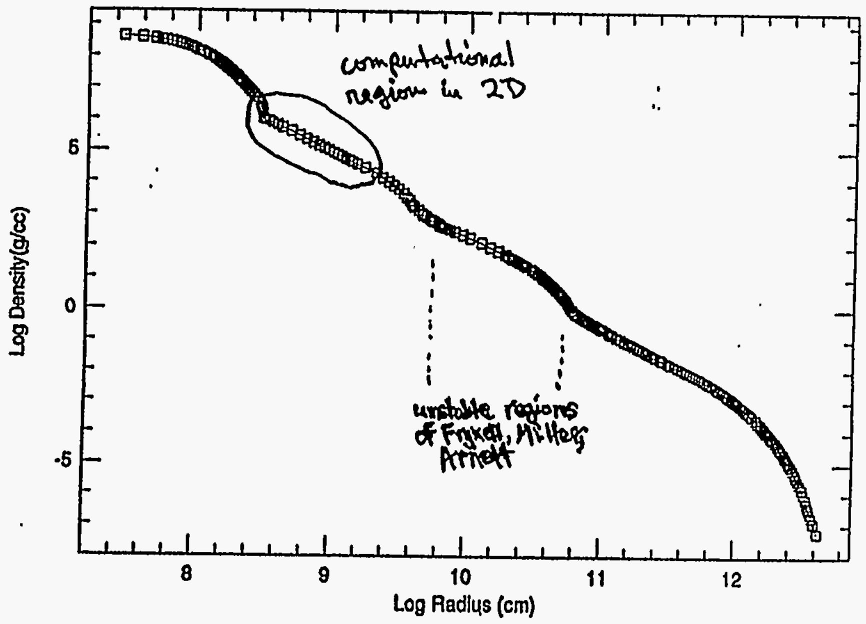

Direct hydrodynamic Simulation:

O shell - "hydrostatic"

Si shell - "hydrostatic"

O shell = explosive

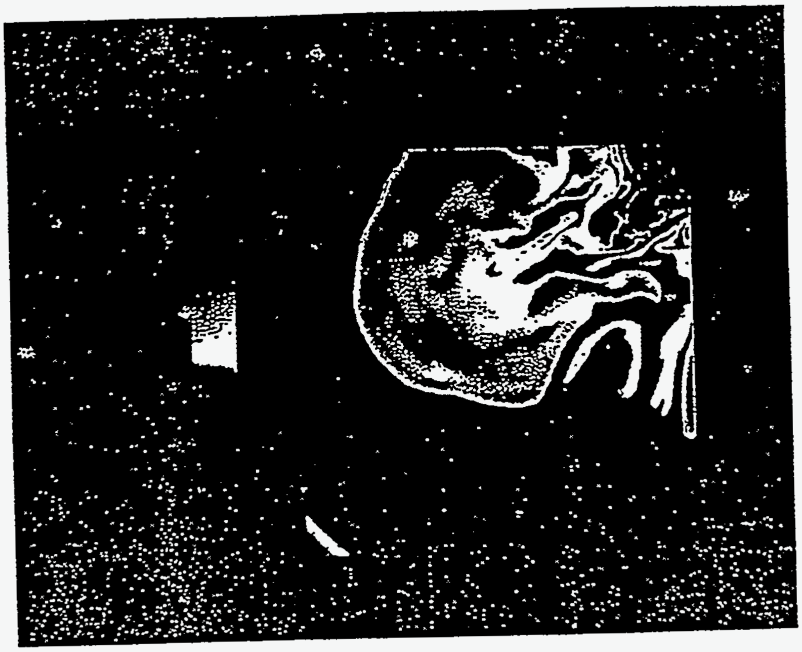

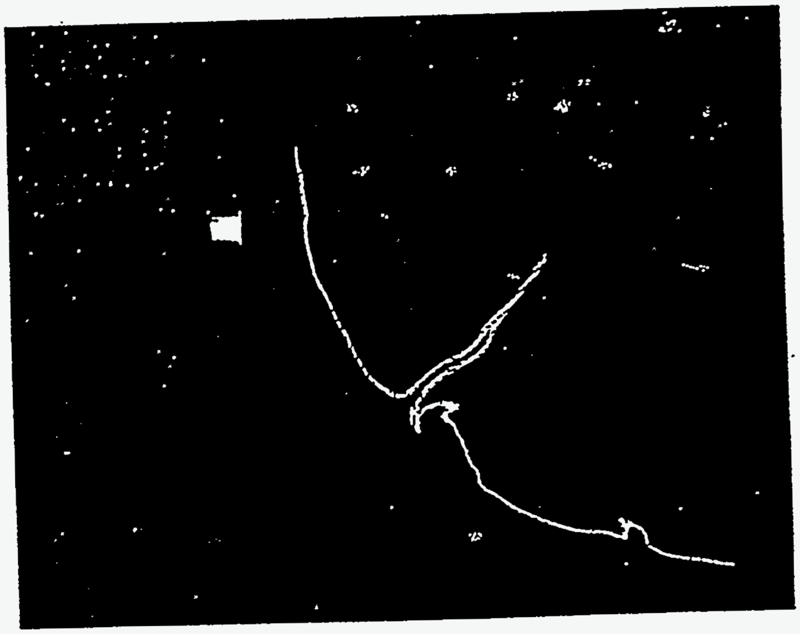

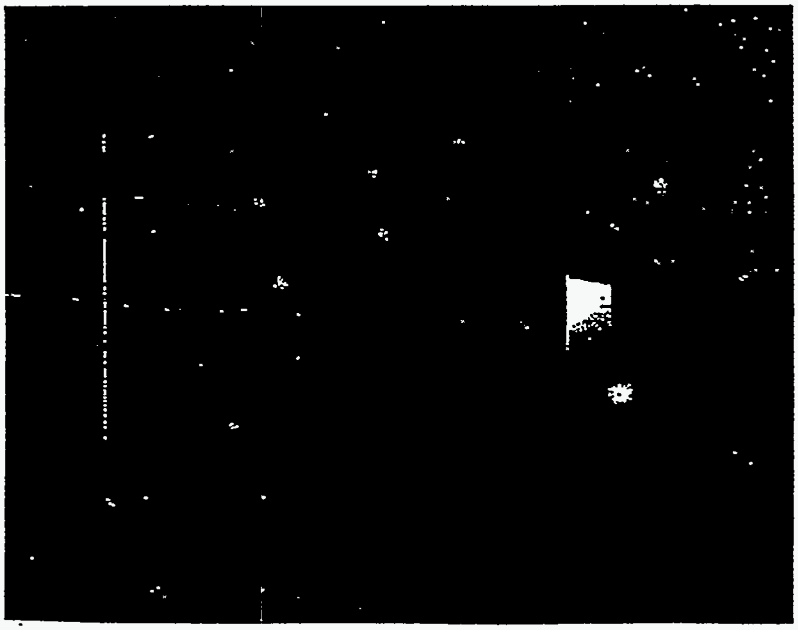

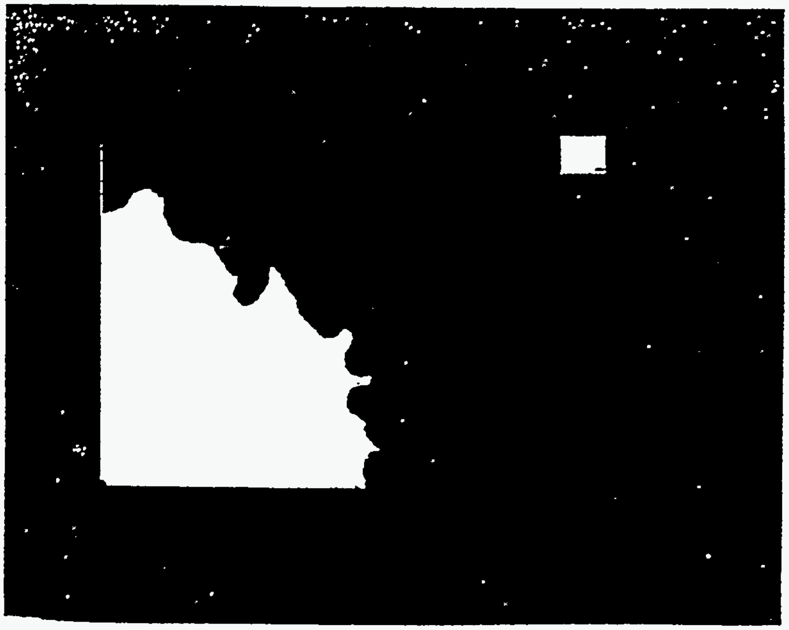

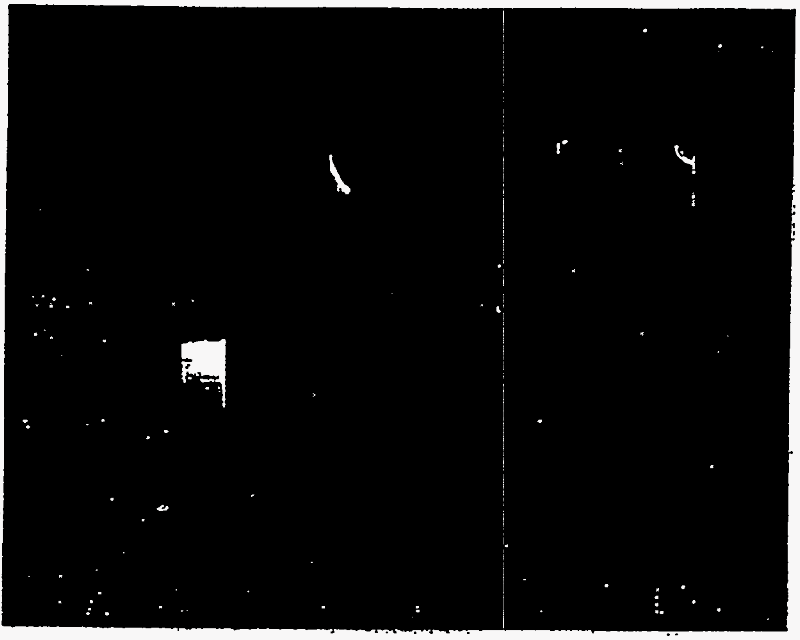

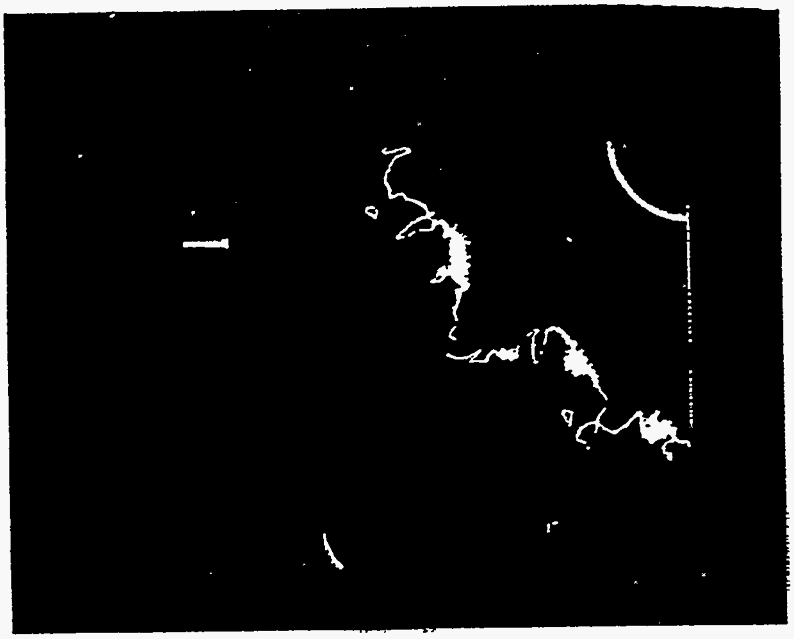

Hydrodynamic Instability Experiments for Supernovae

S. Gail Glendinning
Lawrence Livermore National Laboratory

Hydrodynamic Instability Experiments for Supernovae

Müller et al., density at He-H interface, t=12557 s

Nova experimental data at Cu-CH interface
-log$_e$(exposure) t=34.6 ns

S.G.Glendinning[1], D.Arnett[2], M.Berning[3], J.Castor[1], J.Kane[2], B.A.Remington[1], A.Rubenchik[4]
[1]LLNL; [2]Univ of Ariz, Tuscon; [3]Heinrich-Heine-Universität Düsseldorf; [4]Univ of Calif, Davis

Workshop on Laboratory Astrophysics Experiments with Large Lasers
Pleasanton, CA
26 February, 1996

On Nova, we can examine hydrodynamic growth from well-characterized initial conditions at relevant conditions

Supernova measurements (SN1987A) and simulations indicated important role for turbulence and mix at every interface

Conditions for Nova experiments are similar to SN conditions

- Shock pressures ~100 MBar (10^{14} dyn/cm^2, 10^{13} Pascal)
- Growth scaling (time$\cdot\sqrt{}$acceleration/spatial scale)~10
  - 30 ns laser experiment = about 10 hrs of hydro (SN) growth
- Reynolds number ~ 3×10^6 (about 10^7 for SN)
- Temperatures: 10-30 eV (100-500 eV for SN)

Goals:

- first year:
  - identify and characterize suitable drive and target
  - examine growth (two-dimensional)
  - connect with two-dimensional astrophysical modeling
- second year:
  - two-dimensional experiments
  - feed-through (multiple layers)
  - single and multiple initial modes
  - model with astrophysical codes
- third year: examine effects of three-dimensionality

This talk describes current experimental status

- We have examined various shaped drives and target configurations
- We have best results from single-shock experiments
- Experiments with two-dimensional (single-mode) initial perturbation are in progress
- We have some quantitative comparisons with codes
  - HYADES for one-dimensional predictions
  - CALE and PROMETHEUS predict hydrodynamic evolution of material interface

For thin targets, we can backlight through the target and use the variation in x-ray transmission as a measurement of surface modulation

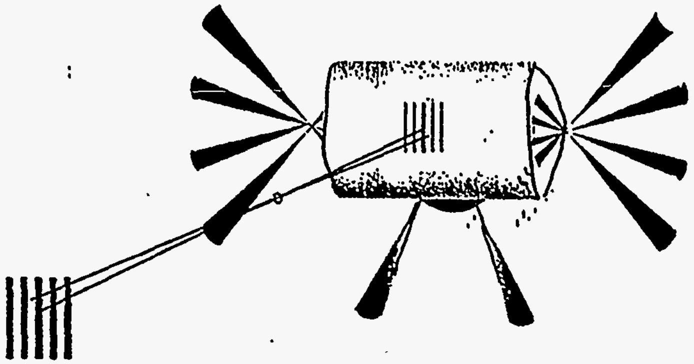

Our experiment uses x-ray drive to drive a planar interface and x-ray radiography to determine the interface position and modulation

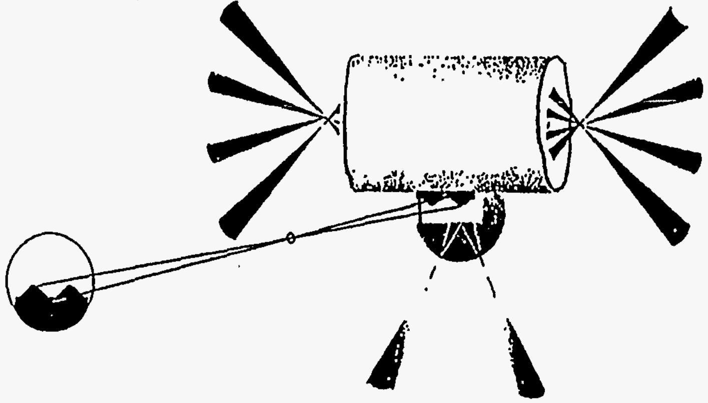

- The primary diagnostic tool is a time-resolving pinhole camera with multiple frames
- Instrument spatial and temporal response functions are well known

We measure the x-ray drive with time- and spectrally- resolved absolutely calibrated x-ray diodes (DANTE)

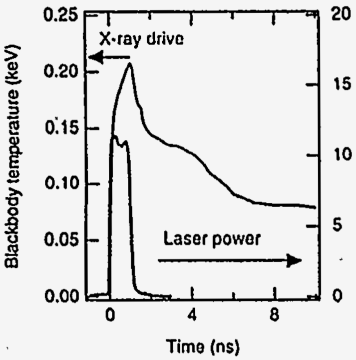

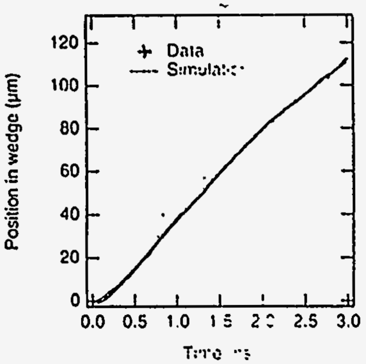

- We check the x-ray drive measurement with shock velocity measurements
- One-dimensional codes (typically HYADES) use x-ray drive measurements to predict conditions within planar targets
- We map 1D results as conditions for two-dimensional codes (CALE, Prometheus) just prior to arrival of shock at interface

Supernova relevant measurements to date include face-on and edge-on views

15 μm Cu decelerated by CH_2, t=7.5 ns

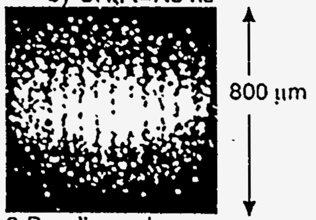

2-D radiograph

15 μm Cu decelerated by CH_2, t=1-5 ns

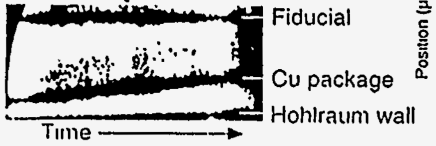

1-D radiograph

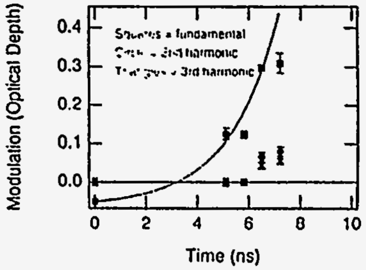

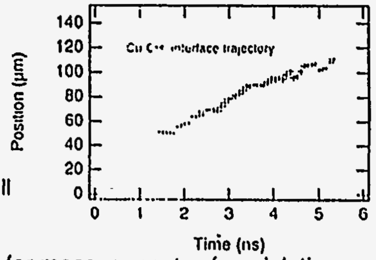

- Two-dimensional imaging is required for measurements of modulations
- Cu package was too thin for this drive; multiple shocks reached the interface (not enough growth)

Increasing the Cu thickness improves the velocity profiles at the interface

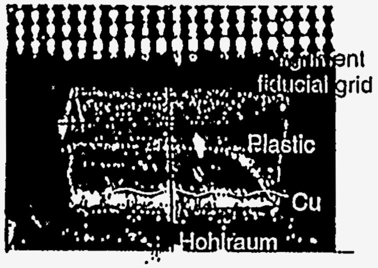

Interface velocity in laser experiments

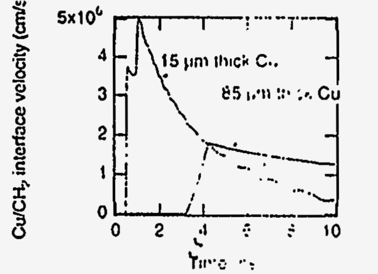

Interface velocity in SN

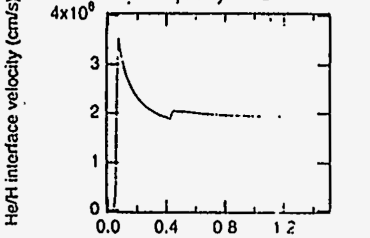

- Cu was 80 μm average thickness (plastic 500 μm thick)
- Ripples in Cu were λ=200 μm. η_0=20 μm
- 1 ns square drive produces shocks which coalesce before reaching the back surface of the Cu
- Hydrodynamic growth continues for 10's of ns after drive turns off

We have a sequence of images vs time (from 3 shots) which extend to 35 ns and show clear evidence of nonlinear behavior

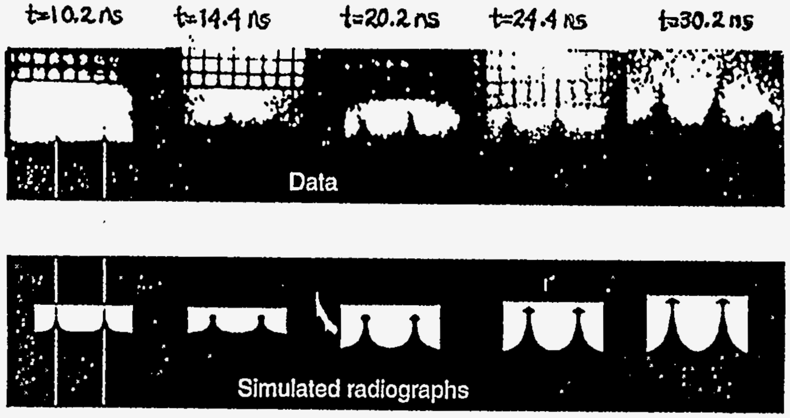

Initial thinnest Cu

- Phase of modulation has inverted, as anticipated

CALE predicts similar structure to that observed

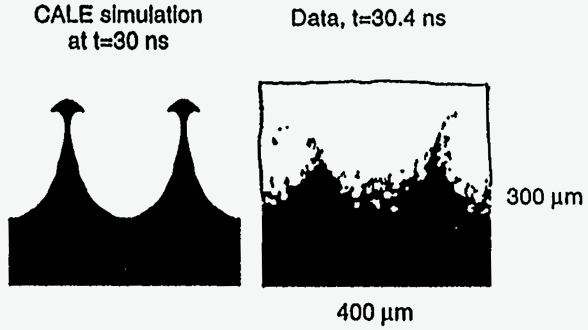

- The code predicts significant spike-formation and roll-up
- Observed structure is more complicated

CALE and PROMETHEUS both predict bubble and spike positions very well

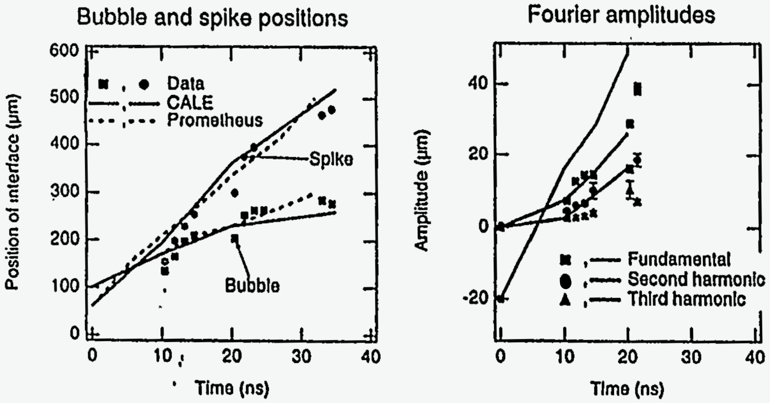

- Early in the evolution, Fourier harmonics are easily determined and show some difference between codes and data

Collisional of SN1987A with Circumstellar Nebular Ring

Richard McCray
JILA, University of Colorado

Richard McCray

DING LUO
JON SLAVIN
} OPTICAL, UV, HST

KAZIK BORKOWSKI
JOHN BLONDIN
} X-RAYS.

CHEVALIER + DWARDAKES 1995

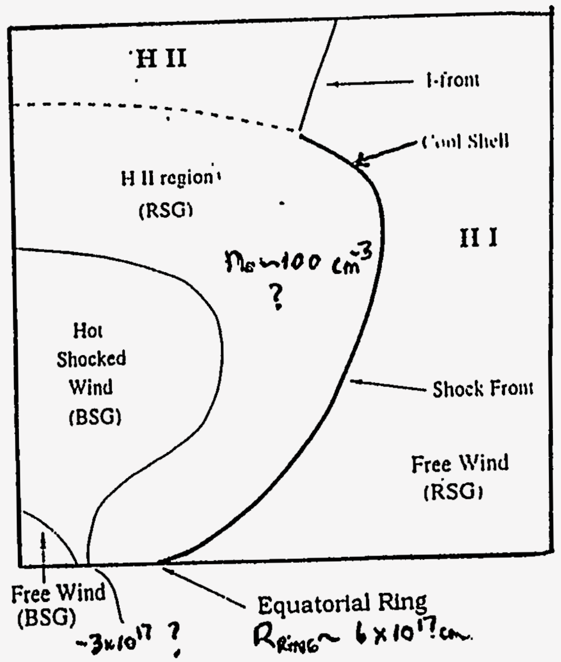

MODEL REQUIRES
- WEAK BSG WIND. ($\sim\frac{1}{50}$ previous estimate)

EXPLAINS
- RADIO TURN-ON
- X-RAY TURN-ON

KEY TEST
X-RAYS.

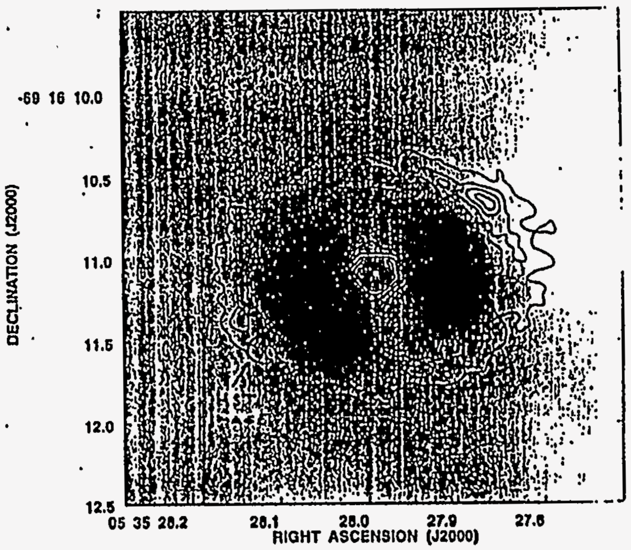

STAVE EX - SMITH ET. AL.

AUSTRALIA TELESCOPE 8.8 GHZ

$t = 5.8$ yr

"IT AIN'T EASY TO PREDICT THINGS
—ESPECIALLY IF THEY'RE
IN THE FUTURE"

— YOGI BERRA

EXPANSION OF SUPERNOVA ENVELOPE
INTO UNIFORM CIRCUMSTELLAR MEDIUM
(CHEVALIER 1982)

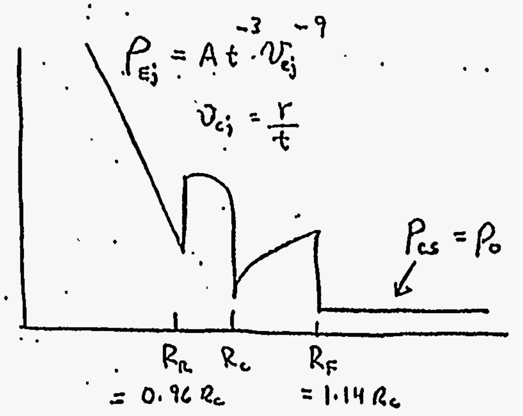

$R_F(t) = K t^{\alpha}$ SELF-SIMILAR SOLUTION.

SET $\rho_{Ej}(v_{ej} - \dot{R}_R)^2 = 0.55 \rho_0 \dot{R}_F^2$

$$\Rightarrow R_F(t) = 0.54 \left(\frac{A}{\rho_0}\right)^{1/9} t^{2/3}$$

$$\Rightarrow \boxed{t_1 = 13 \text{ yr} \left(\frac{n_0}{10 \text{ cm}^{-3}}\right)^{1/6}}$$

A : WELL-MEASURED FROM MODEL-ATMOSPHERE FIT TO EARLY SN PHOTOSPHERIC SPECTRUM

ρ_{Ej} : MUST GUESS, $\left[\begin{array}{l}\text{SHOCKED SN}\\\text{PROGENITOR WIND ?}\end{array}\right.$

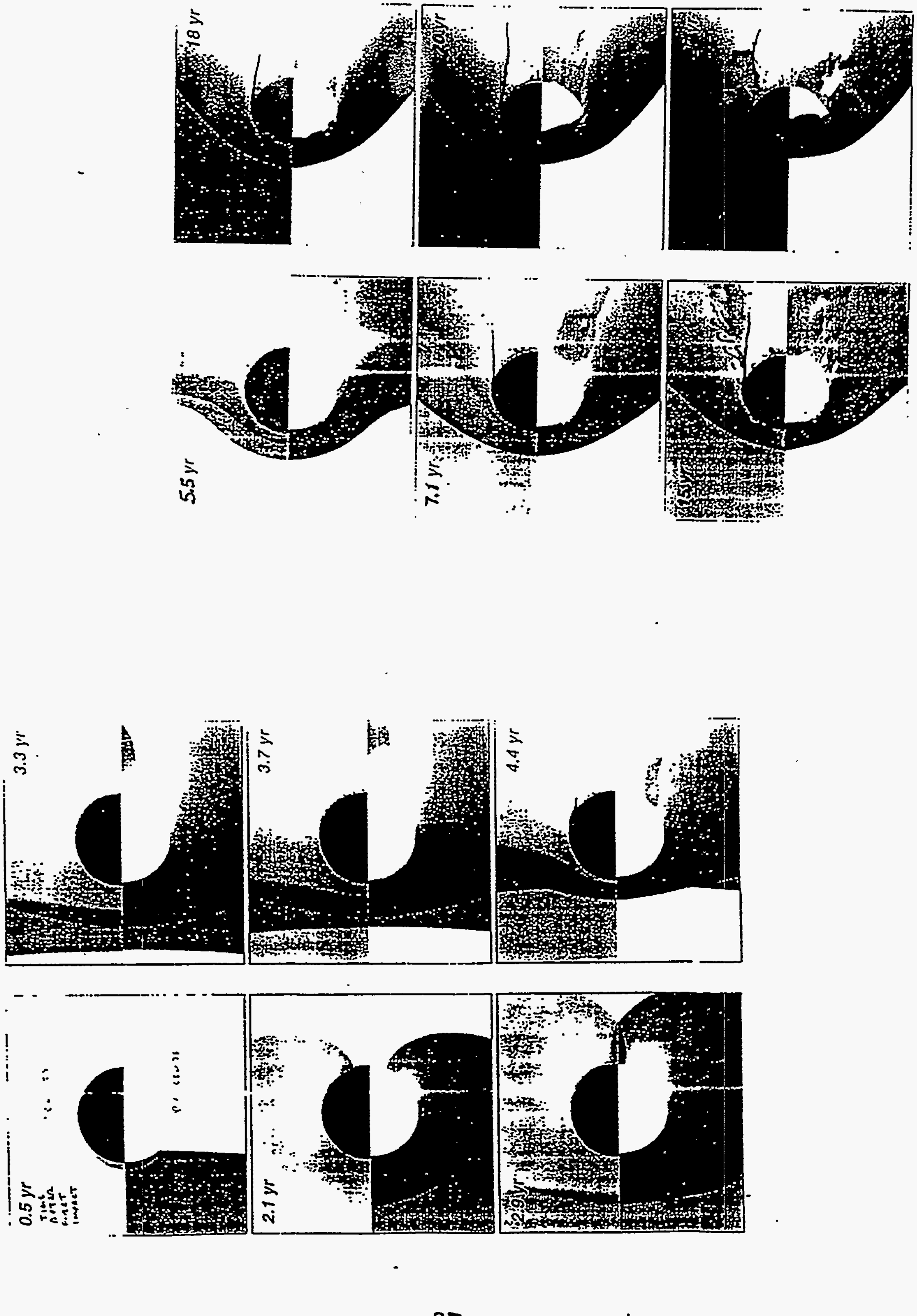
0.5 yr
TIME AFTER FIRST IMPACT
2.1 yr
2.9 yr
3.3 yr
3.7 yr
4.4 yr
5.5 yr
7.1 yr
18 yr
20 yr

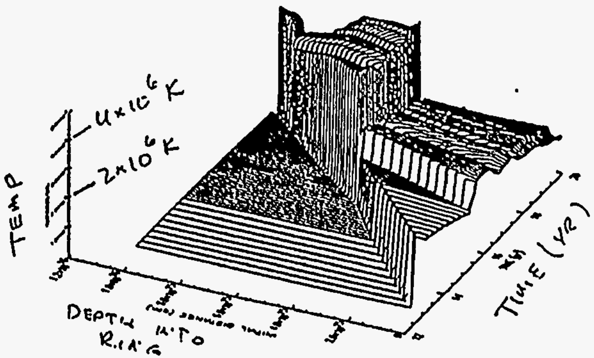

Fig. 6.— Temperature evolution as a function of the initial fluid location.

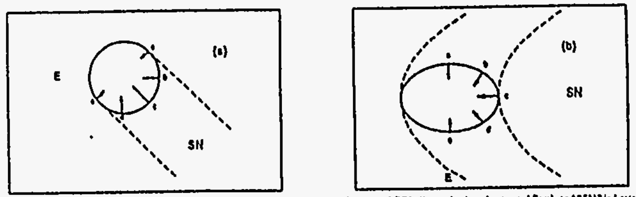

FIG. 6.—Schematic views of cross sections of the ring. (a) Side view of the north side of the ring. "E" indicates the direction toward Earth, and "SN" indicates the direction toward the supernova. The blueshifted peak of the solid emission line profile in Fig. 5a comes from the arc $\overline{abc}$, and the plateau of the same profile, from the arc $\overline{cde}$. The dashed lines indicate the projection of the ring. (b) Top view of the east side of the ring. Again, "E" indicates the direction toward Earth, "SN" indicates the direction toward the supernova, and the dashed curves indicates the projection of the ring. The blue- and redshifted peaks of the dashed emission line profile in Fig. 5a come from the arcs $\overline{ab}$ and $\overline{fe}$, respectively, and the central plateau of the same profile, from the arc $\overline{bcd}$.

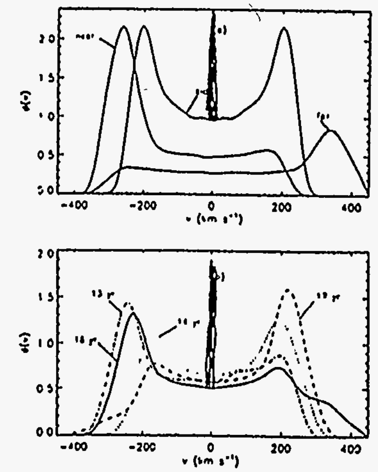

FIG. 7.—Profiles of the [O III] λλ4959, 5007 emission line from the ring for model B. (a) Profiles from equal mass segments of the ring at t = 16 yr: *solid curve*, near side; *dashed curve*, side of ring (along the E-W major axis); *dot-dashed curve*, far side. Normalization is arbitrary. (b) Integrated profiles from the entire ring at various times.

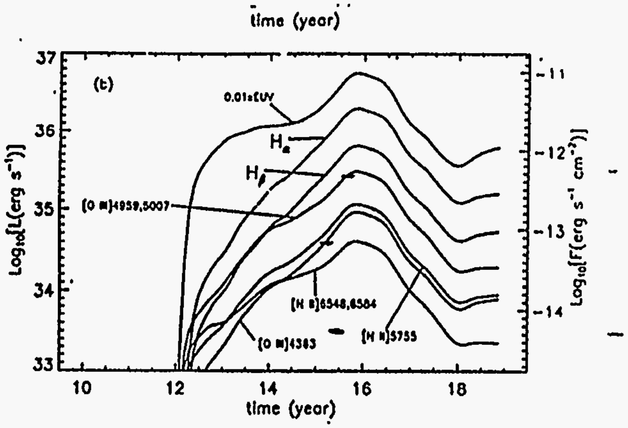
time (year)
(c)
0.01×EUV
H_α
H_β
[O III]4959,5007
[N II]6548,6584
[O III]4363
[N II]5755
37
36
35
34
33
$\mathrm{Log_{10}[L(erg\ s^{-1})]}$
-11
-12
-13
-14
$\mathrm{Log_{10}[F(erg\ s^{-1}\ cm^{-2})]}$
10
12
14
16
18
time (year)

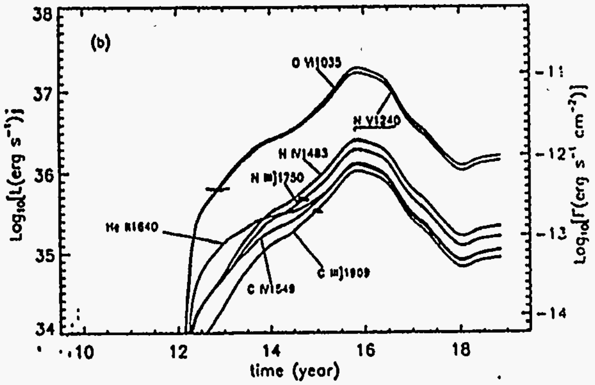
(b)
O VI1035
N V1240
N IV1483
N III]1750
He II1640
C IV1549
C III]1909
38
37
36
35
34
$\mathrm{Log_{10}[L(erg\ s^{-1})]}$
-11
-12
-13
-14
$\mathrm{Log_{10}[F(erg\ s^{-1}\ cm^{-2})]}$
10
12
14
16
18
time (year)

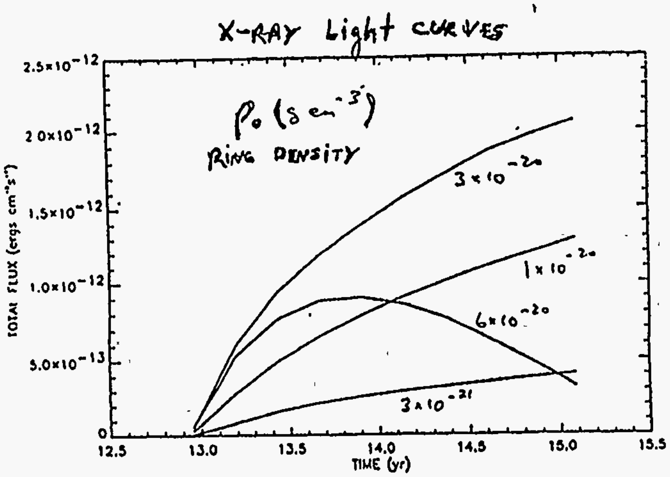
X-RAY Light CURVES
ρ_0 (g cm^{-3})
RING DENSITY
3×10^{-20}
1×10^{-20}
6×10^{-20}
3×10^{-21}
2.5×10^{-12}
2.0×10^{-12}
1.5×10^{-12}
1.0×10^{-12}
5.0×10^{-13}
0
TOTAL FLUX (ergs cm^{-2}s^{-1})
12.5
13.0
13.5
14.0
14.5
15.0
15.5
TIME (yr)

X-RAY SPECTRA AD 2002

(IMPACT + 2ye)

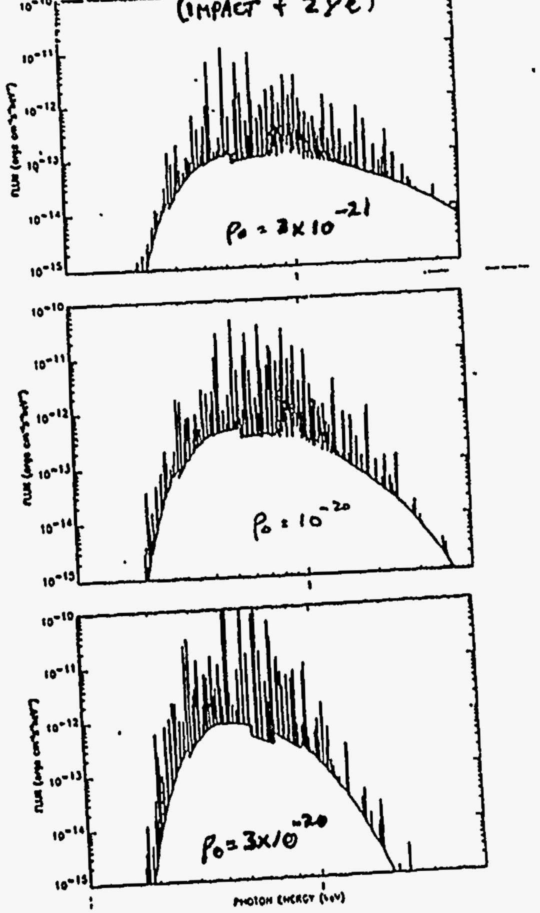

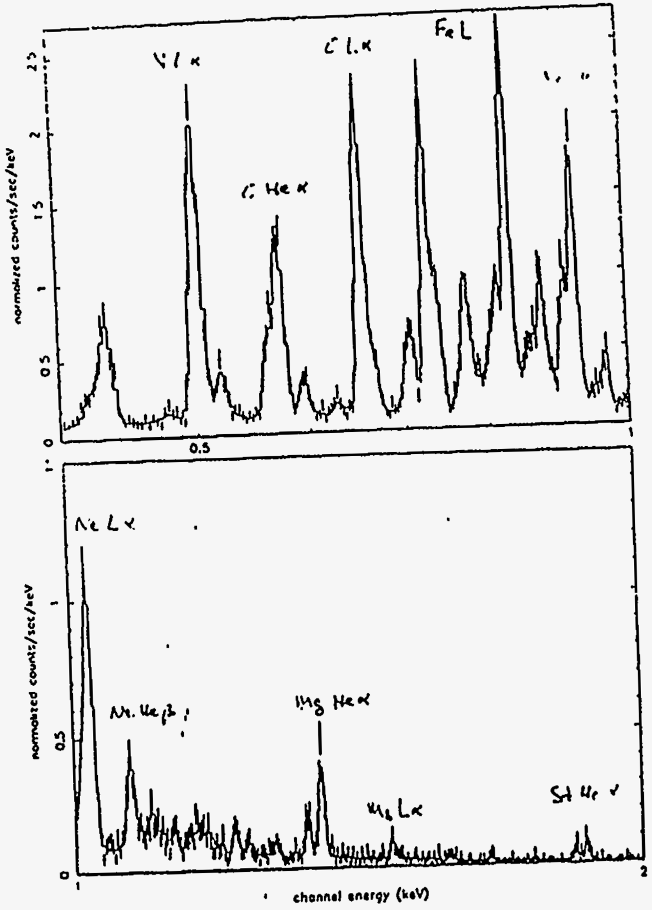

An Experiment Relevant to the Supernovae Ejecta-Ring Collision

R. Paul Drake
Lawrence Livermore National Laboratory
and
University of Michigan

An Experiment Relevant to the Supernova Ejecta-Ring Collision

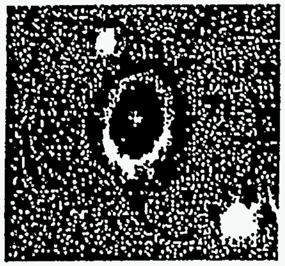

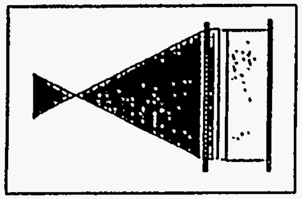

R. Paul Drake
Lawrence Livermore National Laboratory,
and University of Michigan

Workshop on Laboratory
Astrophysics Experiments
With Large Lasers
February, 1996

Work partially performed under the auspices of the U S Department of Energy by the Lawrence Livermore National Laboratory

---

Here's what I'll show you

> SN 1987A provides the context and real-time data

> How we can simulate the SN environment using Nova

> Issues and options for such an experiment

Collaborators:
Lawrence Livermore National Laboratory
Bruce Remington, Kent Estabrook, Gail Glendenning,
John Castor, Rich London, Claire Max
University of Colorado, Boulder
Richard McCray
University of California, Davis
Alexander Rubenchik
Rice University, Houston
Edison Liang

The Ejecta from SN 1987A are now plowing through the circumstellar matter

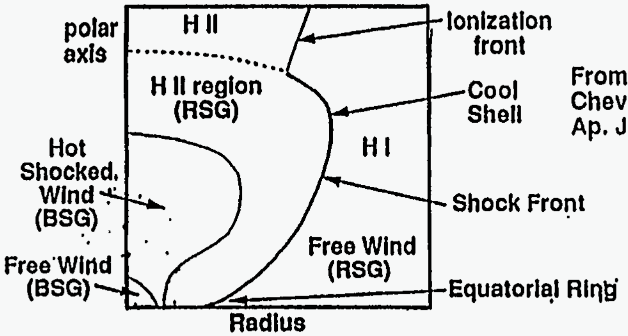

From:
Chevalier & Dwarkadas
Ap. J. 452 L45 (1995)

- The structure developed during this period will determine the emission we observe when the ejecta strike the ring
- In any event, the emission from the ring will be matic and informative

---

A rough schematic of current-day profiles will motivate the layout of a simulation experiment

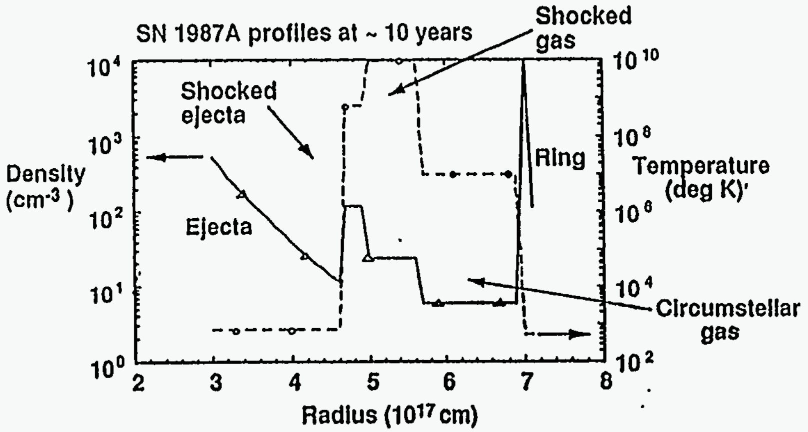

The H II zone, if present, will cause higher densities and lower temperatures in the shocked matter. Both forward and reverse shocks will 'n strong.

Here is one way to simulate the circumstellar environment

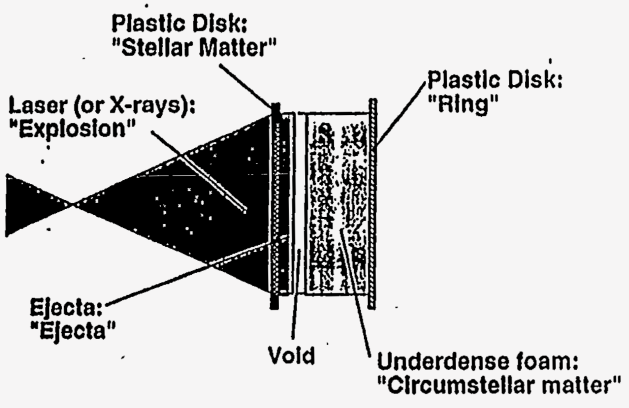

Let's examine this one piece at a time .....

We can make ejecta much like the star does

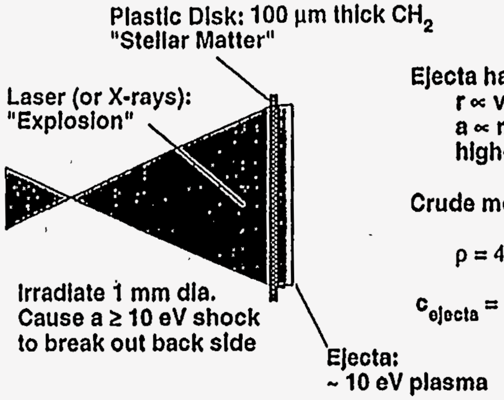

Ejecta have SN-like features :

$r \propto vt$

$a \propto r/t^2$

high-velocity, cool matter

Crude model–isothermal rarefaction:

$$\rho = 4\rho_{solid} \exp - (x/c_{ejecta} t)$$

c_{ejecta} = initial sound speed

For H, c_s = 30 km/s at 10 eV and is $\propto T^{1/2}$

The ejecta can drive a strong shock in low-density foam

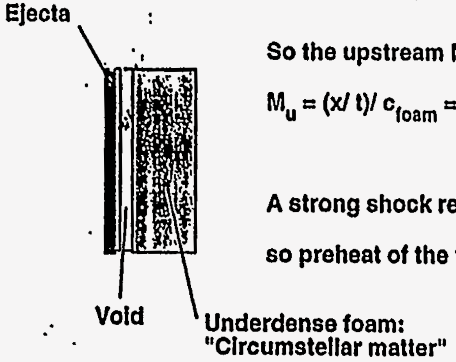

Interaction occurs where $\rho_{ejecta} \sim \rho_{foam}$

Thus $x/t = c_{ejecta} \ln (4\, \rho_{solid} / \rho_{foam})$

So the upstream Mach number is

$$M_u = (x/t)/c_{foam} = (c_{ejecta} / c_{foam}) \ln (4\, \rho_{solid} / \rho_{foam})$$

$\sim \ln 400 = 6$

A strong shock requires $(c_{ejecta} / c_{foam}) > 2$,

so preheat of the foam must be controlled

Foam preheat limits the ejecta velocity

The foam is irradiated by the shocked disk until the ejecta strikes it after ~ 1 ns.

Assume that the foam absorbs σT_{BB}^4 for 1 ns

We can infer a preheat depth by making $T_{foam} = T_{BB}$ in the heated region

For C foam at 20 mg/cc one finds

$$d_{preheat} = 3\ \mu m\ (T_{BB} / 10\ eV)^3$$

Thus, shock temperatures up to several times 10 eV are plausible.

Preheat is more of a problem as density drops and atomic mass increases.

The shocked foam and ejecta can strike the "ring" hard enough to emit

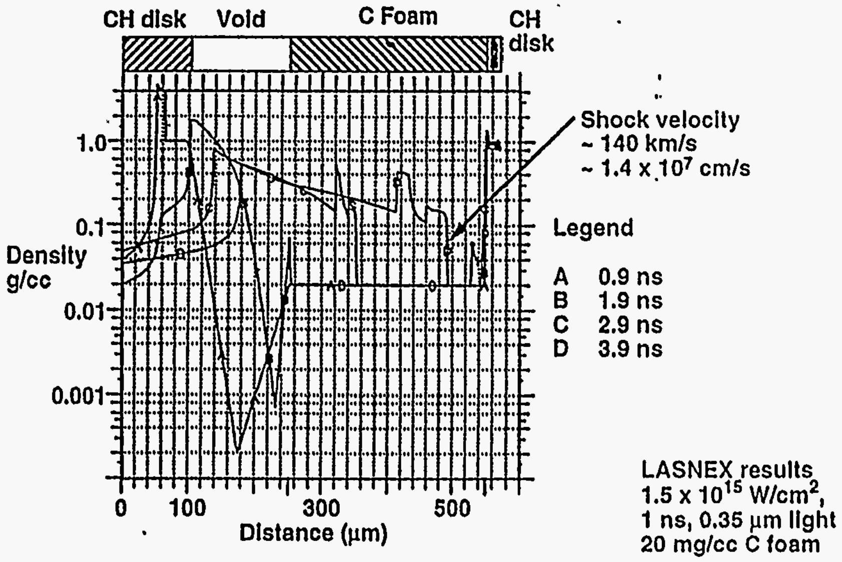

LASNEX results
1.5×10^{15} W/cm^2,
1 ns, 0.35 μm light
20 mg/cc C foam

The shock produces a large pressure impulse

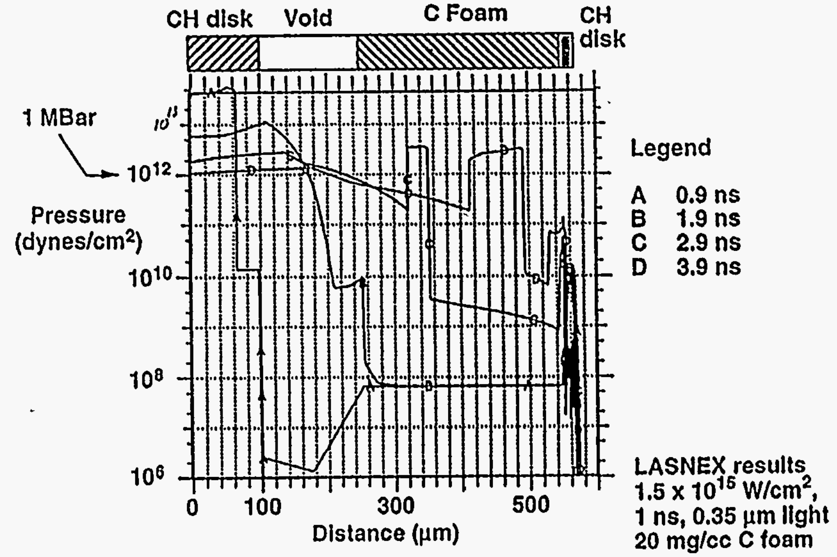

LASNEX results
1.5×10^{15} W/cm^2,
1 ns, 0.35 μm light
20 mg/cc C foam

The ion temperature shows strong heating

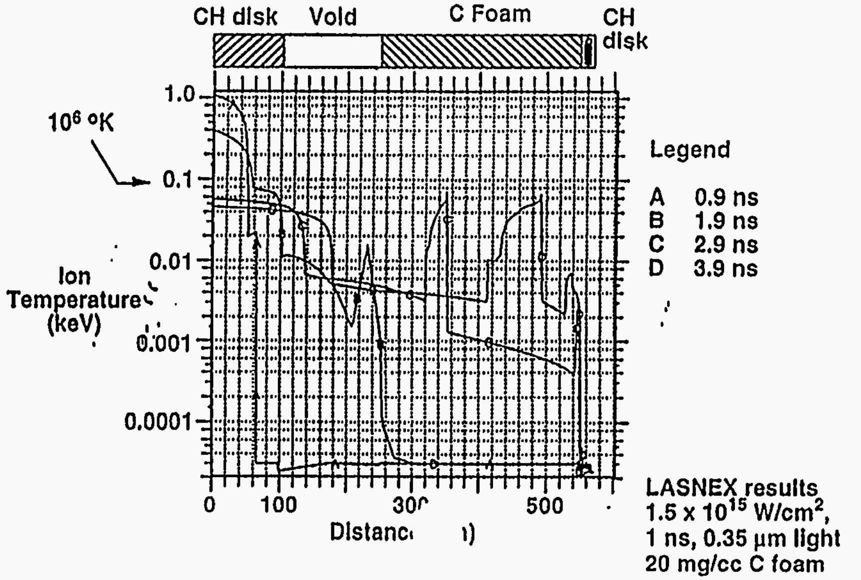

LASNEX results
1.5×10^{15} W/cm^2,
1 ns, 0.35 μm light
20 mg/cc C foam

We can diagnose the shock using established techniques

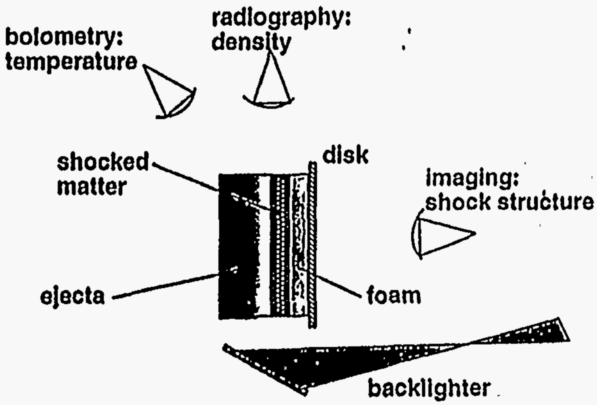

Typical dimension: 1 mm for entire target; 100 µm for shock
Typical resolution: 10 µm
Timescales: 1 ns for shock propagation; 100 ps for diagnostics

---

We are improving this design and working on scaling

- > Modeling x-ray driven designs to get stronger, more uniform shocks
- > Exploring doped foams to obtain radiatively-cooled shocks – plan to greatly vary the hydrodynamic instability growth rates
- > Varying the geometry to seek scale-free behavior
- > Using gas rather than foam to access collisionless shocks
- > We will propose Nova shots this spring and hope to obtain the first data during the next year

Formation of "Bullets" by Hydrodynamical Instabilities in Stellar Outflows

James M. Stone
University of Maryland

Formation of "Bullets" by Hydrodynamical Instabilities in Stellar Outflows

Jim Stone
Lee Mundy
Jianjun Xu
University of Maryland

- Observations of "bullets" in Orion
- An interpretation
- Hydrodynamical Modeling
- "Bullets" in other contexts
- Conclusions

Motivation: IR observations of the star-forming region OMC-1 by Allen & Burton (1993)

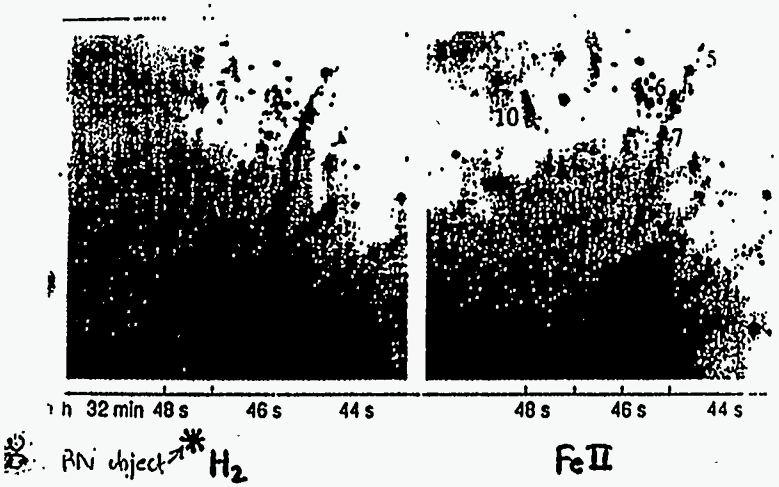

Use of the word "bullet" is provocative

Allen & Burton (1993) refer to "Explosive ejection of matter..."

Implies knots are accelerated to supersonic speeds at source.

But studies of interaction of dense clump with supersonic wind show this is difficult

⇒ clump is fragmented

e.g. Stone & Norman (1992)
Klein, McKee & Colella (1994)
Xu & Stone (1995)

An alternative explanation: "bullets" form <u>in situ</u> in a supersonic wind

Stone & Norman (1993a, 1993b, 1994) demonstrated that dense knots can form in highly collimated outflows (i.e. protostellar jets).

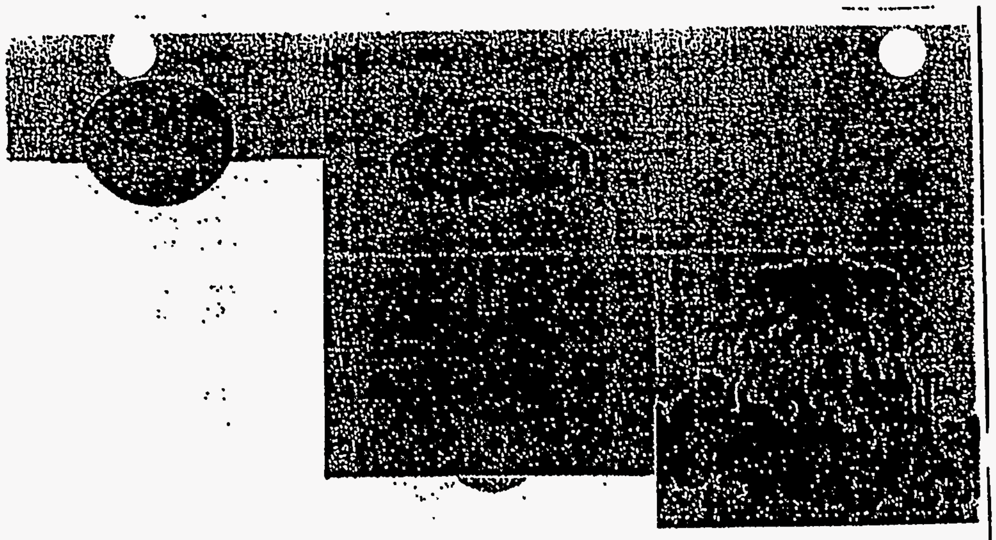

log (density)

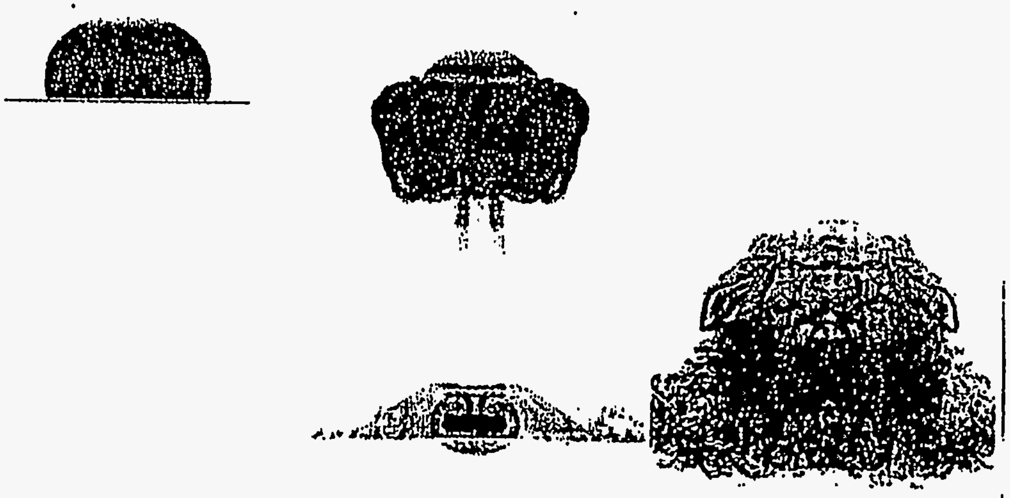

$|\nabla \times v|$ = vorticity

3D Simulation of $\eta=10$, $M=20$ jet:

fragmentation of shell $\Rightarrow$ "interstellar bullets"
"shocked cloudlets" (in $\eta=1$ jet)

[only last 20 yr of jet shown]

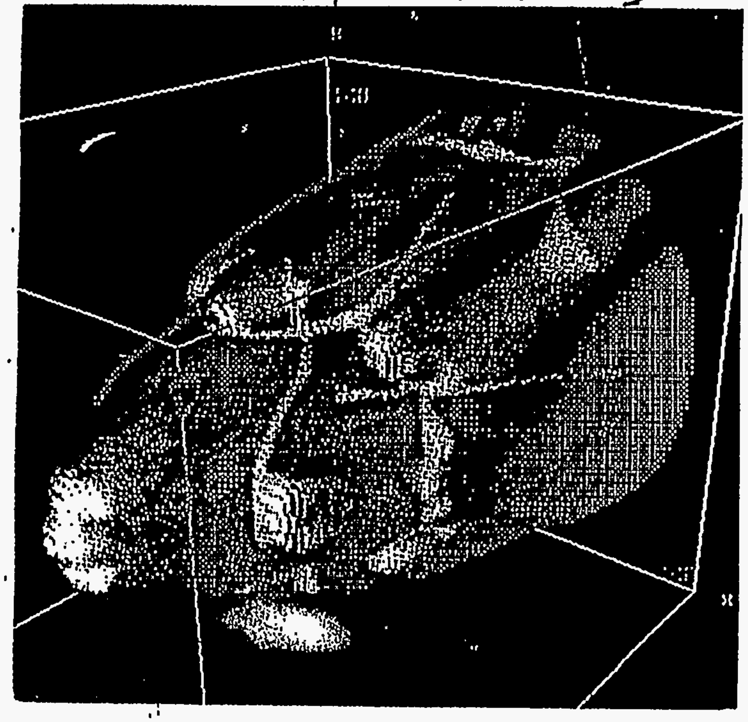

- A key ingredient is that gas must be strongly cooling to form dense structures
- Wind in OMC-1 is also strongly cooling.
  $\tau_{dyn} \sim 10^3$ yrs
  $t_{cool} \sim 1$ yr
- How do "bullets" form in wind?

Spherical wind will sweep up thin, dense shell of shocked ambient + wind gas

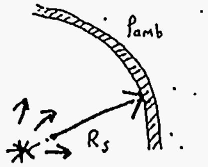

If luminosity of wind
$L_w \propto t^m$

density of ambient gas
$\rho_{amb} \propto r^{-n}$

Then Weaver et al (1977) showed shell will accelerate $\left(\frac{d^2R_s}{dt^2} > 0\right)$ if $n+m > 2$ Acc'n of shell R-T unstable.

Two possibilities: (1) external density gradient is steep $(n>2)$
(2) wind is time-variable

MacLow et al (1989) studied case (1) $\Rightarrow$ "superbubble blowout" from galactic disk

MacLow, McCray, & Norman (1989)

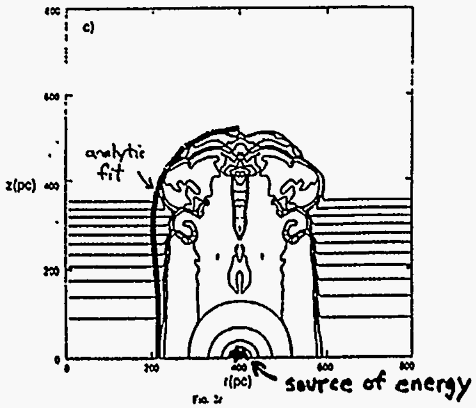

FIG. 2c

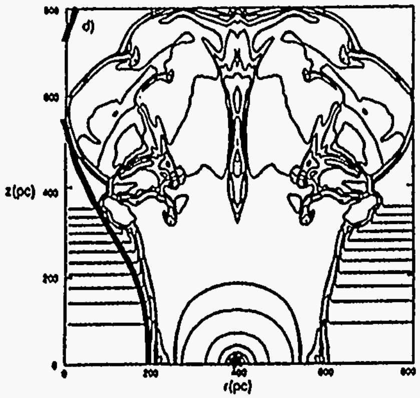

FIG. 2d
147

We have explored case (2).

Hydrodynamical Modeling:

Use PPM code on spherical polar mesh

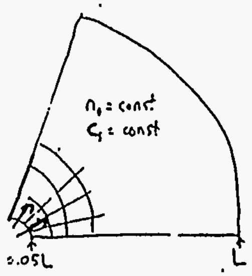

- Introduce wind through Inner B.C
- Ambient gas isothermal, homogeneous
- Small amplitude perturbations near source
- Initial wind velocity corresponds to $M = 10$. At late times, increase to $M = 100$

For OMC-1: $L \sim 0.1$ pc, $C_s = 20$ km/s $\Big\}$ $L/C_s = 5{,}000$ yrs

$V_{wind} = 200$ km/s

$n_0 = 10^3\ cm^{-3}$

$\therefore \dot{M}_{wind} = 10^{-6}\ M_\odot \cdot yr$

What fragments shell?
1) R-T instability
2) Vishniac thin-shell instability

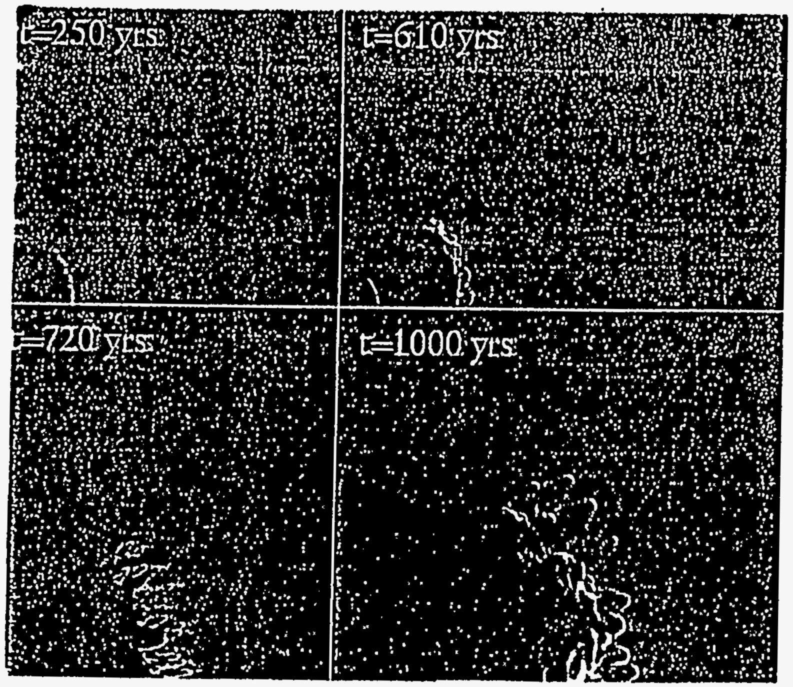

Maclaw & Norman (1993)
Nonlinear evolution of thin-shell instability

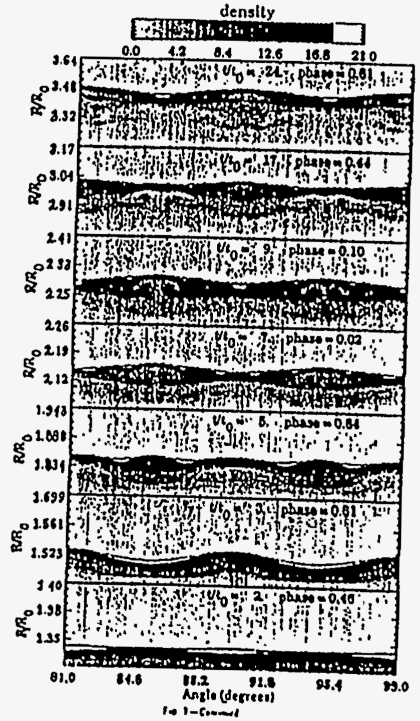

Fig. 1—Continued

213

We expect "bullets" to form in stellar outflows in many other contexts, eg.

1) Evolution of LBV (Garcia-Segura et al 1991)
2) PN (O'Dell & Wang 1996)
3) SNR eg. Crab

HST has observed dense "fingers" in ejecta swept-up by synchrotron nebula

Hester, Stone, et. al. (1996) suggest fingers formed by <u>magnetic</u> R-T instability at surface of expanding synchrotron nebula.

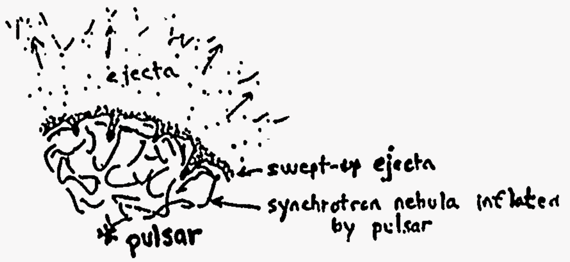

∴ Dense knots formed in this way will catch up to blast wave in ~3,000 yrs.

Perhaps an explanation for the x-ray "bullet" observed in Vela SNR (Strom et al 1995)

G. García-Segura et al.: The dynamical evolution of circumstellar gas

A&A 305, 229 (19

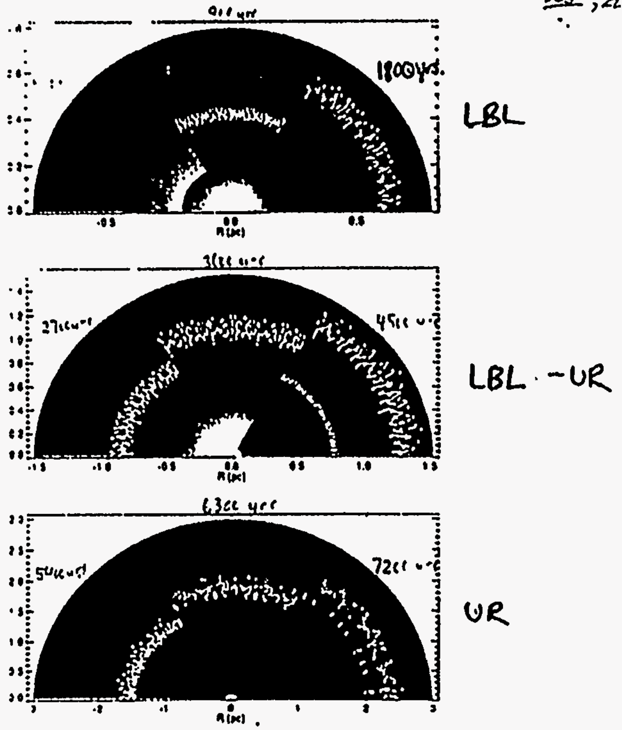

Fig. 10. Logarithm of the circumstellar gas density (in g cm^{-3}) during the LBV and early WR phase, computed on a 3 pc grid with twice the numerical resolution of the run shown in Fig. 9. Note that each 60° slice is now composed of three identical 20° slices. The time difference between consecutive frames is 900 yr. The gray scale minima and maxima given correspond to the density extrema in each frame. Numerical resolution limits the density maxima, so they should be taken as lower limits. a) During the LBV stage (t = 3.337 10^6 yr). The gray scale goes from max=-20.2 (white) to min=-23.2 (black). Only the inner 0.75 pc are shown. b) The late LBV and transition to the WR stage (t = 3.3397 10^6 yr). The gray scale goes from max=-20.8 (white) to min=-24.3 (black). Only the inner 1.5 pc are shown. c) The early WR stage (t = 3.3424 10^6 yr). The gray scale goes from max=-20.8 (white) to min=-24.3 (black).

WFPC-2 image of crab

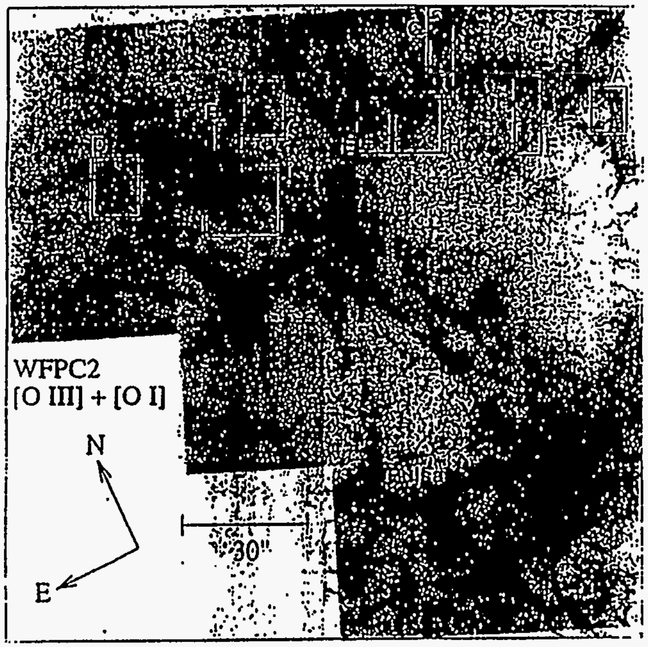

Figure 1.

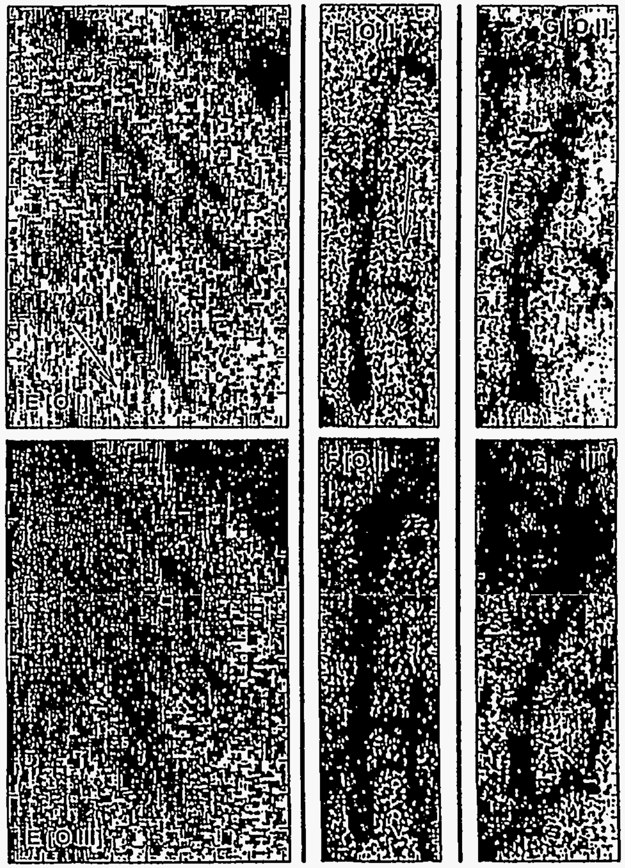

Figure 6.

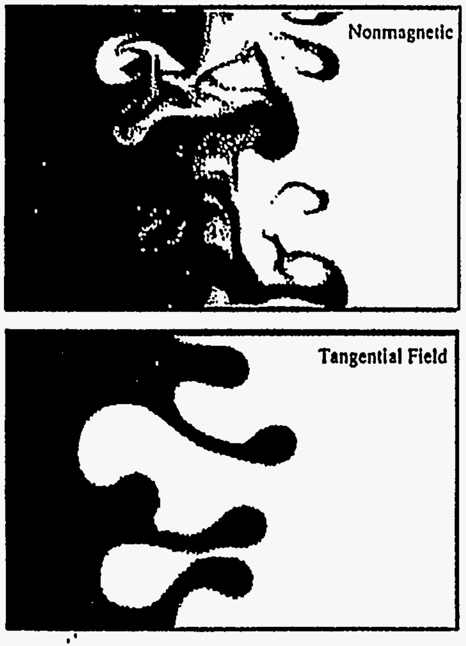

Figure 3.

From Jun, Norman, & Stone (1995)
Nonlinear stage of hydrodynamic vs. magnetic R-T Instability

We conclude:

(1) "bullets" are formed in situ in outflow

(2) Strong cooling is essential for forming dense structures

(3) Many modes of Instability can fragment shell

(4) Provides an interpretation for "bullets" in many contexts

Detailed modeling of line-emission from knots would be fruitful.

The Hydrodynamics of Shock-Cloud Interactions in the Interstellar Medium

Richard I. Klein
Lawrence Livermore National Laboratory

The Hydrodynamics of Shock-Cloud Interactions in The Interstellar Medium.

Richard I. Klein

Collaboration: Chris McKee

Interaction of shock waves with diffuse atomic clouds ($T \sim 10^2 K$) and denser molecular clouds ($T \sim 10-20 K$) in interstellar medium is a problem of fundamental importance in interstellar gas dynamics. It provides us with a space-based laboratory with which to study an array of hydrodynamic instabilities to complement experiments we can do on the Nova Laser.

⇒ Crucial to understanding the evolution of ISM → { shocks develop from supernovae; stellar winds; cloud collisions; spiral density waves. }

Shock waves from SN

- heat the coronal phase of the ISM
- determine the velocity dispersion of clouds ⇒ governs the scale height of the ISM.
- May be effective in destruction of clouds ⇒ Mixing of clouds with ISM.
- Compression of clouds ⇒ gravitational collapse → star formation.

INTERACTION of SNR Blast-Wave - Cloud
can alter the appearance of ISM

⟺ Cloud inhomogeneities can
have a profound effect on
structure and appearance of SNR

[illegible] IC443 (BURTON, '86)

[illegible] filamentation structure

[illegible] (BRAUN '88 → [illegible]
[illegible]
[illegible]

Proposal with James Graham (5×10^{3} sec.
to map entire Cygnus Loop in X-rays
with German X-ray Satellite Rosat
and model entire Cygnus Loop with 3-D, [illegible]

Cygnus Loop X-ray Mosaic (Rosat)
31 FIELDS

J. GRAHAM et al.
+ LEVINSON 1996

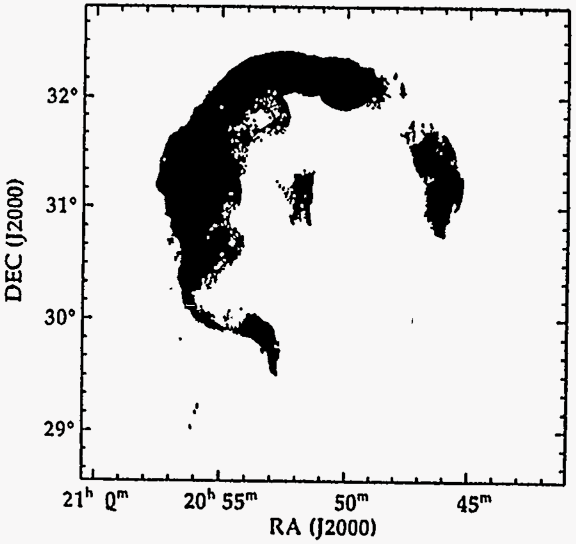

X-RAY (ROSAT) IMAGE OF WESTERN EDGE

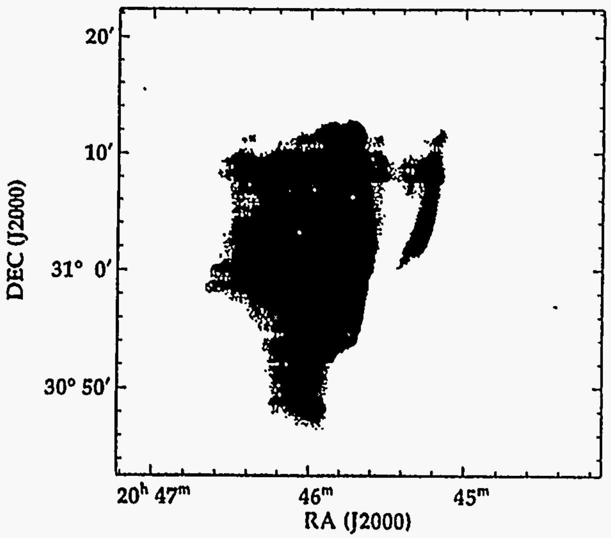

Optical Image of Western Edge (LEVINSON '96)

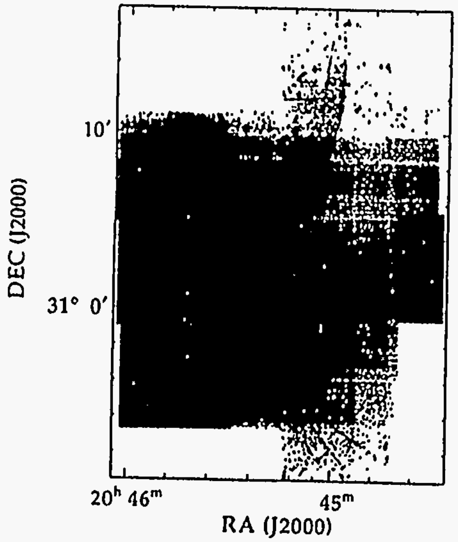

Hα

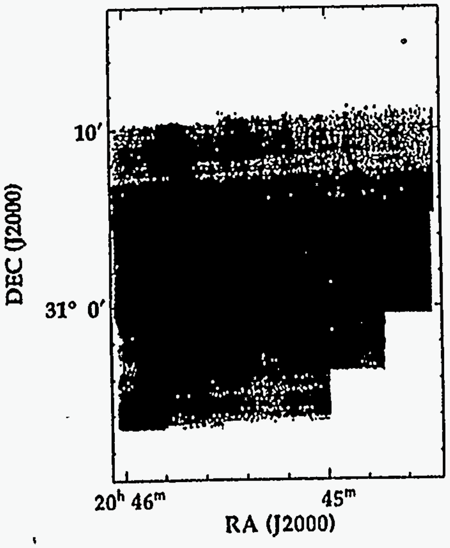

O III

Composite (Hα + OIII + XRAY)

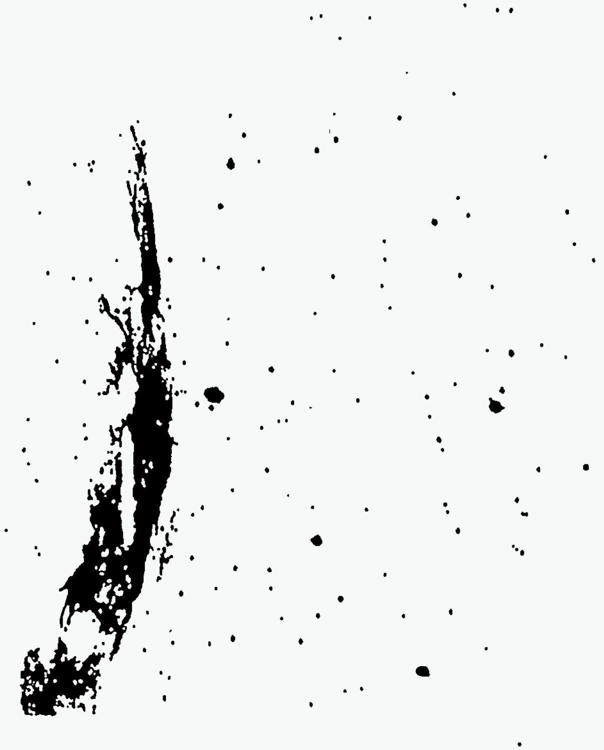

YELLOW = XRAY
TURQOISE = Hα
DARK GREEN = Hα + OIII + XRAY

2.

Initial Conditions specify $M_{shock} = |V_s|/c$

$\chi = \rho_{co}/\rho_{io}$

a_0 = initial cloud radius

$G = 0$

SHOCK PROPAGATION

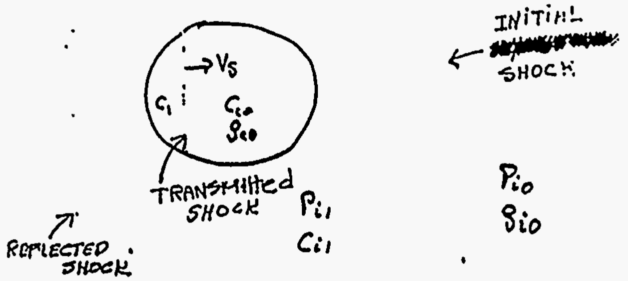

SNR EXPANDS THROUGH ICM ⇒ DRIVES shocks into engulphed clouds.

Assume shocks strong $P_1/P_0 \gg 1$

⇒ Highly supersonic

Pressure behind Blast wave $\sim \rho_{io} V_b^2$

Pressure behind Cloud shock $\sim \rho_{co} V_s^2$

Pressures comparable

$$v_s \approx \left(\rho_{io}/\rho_{co}\right)^{1/2} v_b$$ (Blast Wave NON-RADIATIVE)

If $\dot{v}_s, \dot{v}_b < 0$ then accurate onl.

3.

BLAST WAVE RADIATIVE

$$V_s \simeq \left(\rho_{ii}/\rho_{co}\right)^{1/2} v_b$$

ρ_{ii} = density of shocked ICM $\gtrsim 100\ \rho_{io}$

⇒ V_s (radiative) $\gg$ V_s (NON-RADIATIVE)

TIMES SCALES

Assume SPHERICAL cloud with radius a

For SEDOV-TAYLOR BLAST WAVE

$R_b \propto t^{\alpha}$ $\alpha = 2/5$

Assume $\chi \gg 1$ where $\chi \equiv \rho_c/\rho_{ICM}$

cloud crushing time

(cloud crushed from both sides) $t_{cc} \equiv \dfrac{a}{v_s} = \dfrac{\chi^{1/2} a}{v_b}$

Intercloud crossing time

$t_{ic} \equiv \underline{2a}$

SNR AGE

$t \equiv \frac{\alpha R_b}{v_b} = \frac{2}{5}\frac{R_b}{v_b}$ $\left(v_b = \frac{dR_b}{dt} = \alpha t\right)$

IF $\chi \gg 1 \Rightarrow t_{cc} > t_{ic}$

Clouds are CHARACTERIZED IN 3 SIZES

SMALL CLOUDS $t > t_{cc} \Rightarrow a \ll \frac{0.8R}{\chi^{1/2}}$

SNR DOES NOT evolve SIGNIFICANTLY DURING cloud crushing - CLOUD is promptly CRUSHED. $V_s \sim$ Con
PRESSURE ON CLOUD is STEADY.

MEDIUM CLOUDS $t_{cc} > t > t_{ic}$

$\Rightarrow \frac{0.8R}{\chi^{1/2}} < a < \overset{05}{0.8}R$

Blast wave does evolve during the time to crush the cloud. V_s decelarates

LARGE CLOUDS. $t < t_{ic} \Rightarrow a > \overset{05}{0.8}R$

Blast wave weakens significantly over time to cross cloud

Force on cloud IMPULSIVE

Methodological Approach

Local Adaptive Mesh Refinement

Berger and Oliger 1984

Berger and Colella 1989 2D

Bell et.al. 1991 3D, Stone & Norman 93; Xu & Stone 96
Klein, McKee, Colella, 2D (90, 91, 93, 94), 3D 93

Goals: Avoid unnecessary computation

exploiting high resolution discretization

⇒ Huge advantage in cost of calculation

Approach: Locally refine "patches" of the grid in space and time

Local refinement is necessary to resolve complex ~~shock~~ interactions as well as instabilities and complex evolving structures.

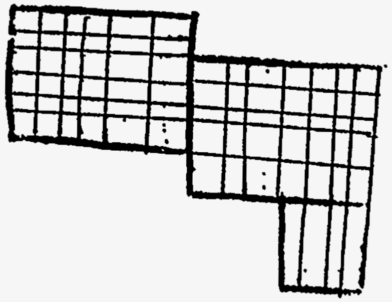

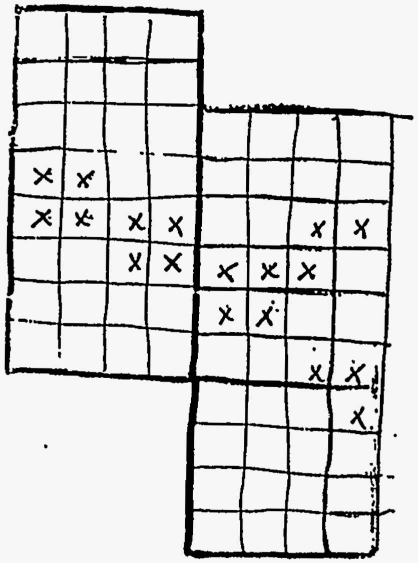

ADAPTIVE MESH REFINEMENT

IDENTIFY CELLS WHERE ADDITIONAL RESOLUTION is
REQUIRED → Refine patches of the grid in space and time

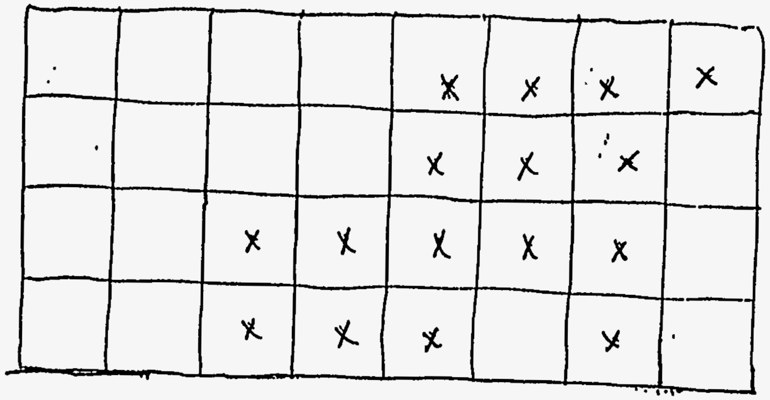

122 Klein, McKee, Colella

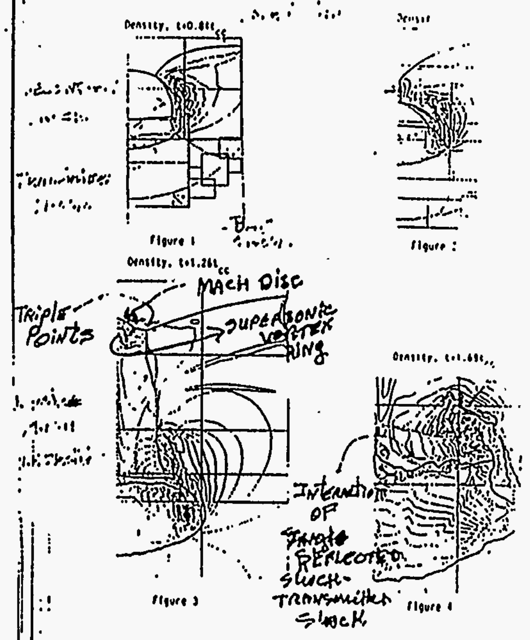

Isodensity contours of cloud and intercloud matter at different times

121 Klein, McKee, Colella

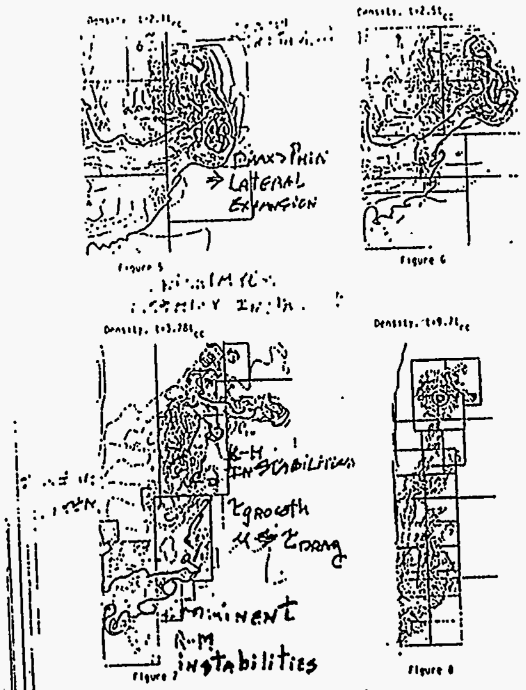

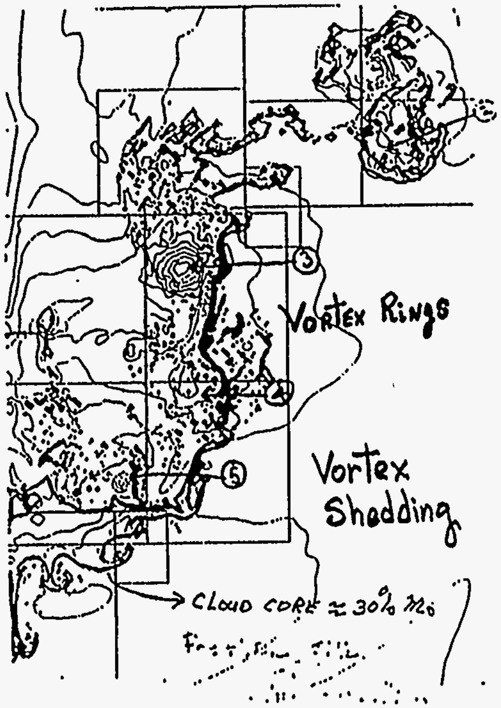

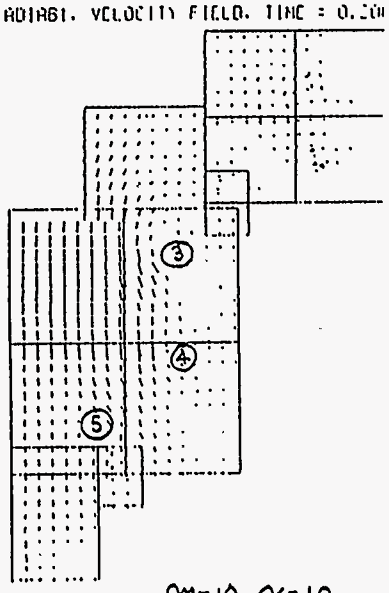

$\mathcal{M}=10,\ \chi=10$
$t=4.2\,t_{cc}$

Vorticity Production

Associated With Cloud-Shock Interactions

$$\Gamma = \int \omega \cdot dA$$

$$\frac{d\Gamma}{dt} = \int (\nabla \times \dot{v}) \cdot dA \ \propto \nabla P \times \nabla (1/\rho)$$

Circulation can be broken into 4 parts

(i) Vorticity produced as shock sweeps over cloud surface

Since there is a large difference in the acceleration of the fluid outside the cloud compared to inside
$\Rightarrow \nabla \times \dot{v} \neq 0 \Rightarrow \frac{d\Gamma}{dt} \neq 0$ so vorticity is generated

$$\Gamma_{shock} \simeq -2.25\, V_b\, a_0 \left(1-\chi^{-1/2}\right)$$ (Klein et al. 1994)

(ii) Vorticity generated in Post-Shock flow by baroclinic term

$$\Gamma_{post} \doteq \frac{9}{64}\left(\frac{\chi^{1/2} t_{drag}}{t_{cc}}\right) v_b a_0$$

(iii) Vorticity generated in intercloud medium behind cloud - Vorticity here is <u>NOT</u> associated with cloud boundary

$\Gamma_{ring} \simeq + \frac{3}{4} v_b a_0$

Vorticity is generated at Triple point.

(iv) Vorticity produced in the cloud near shock triple points associated with MACH reflected shocks

but $V_{cloud} \sim \frac{V_{ICM}}{\chi^{1/2}}$

Γ in cloud is small for $\chi \gg 1$

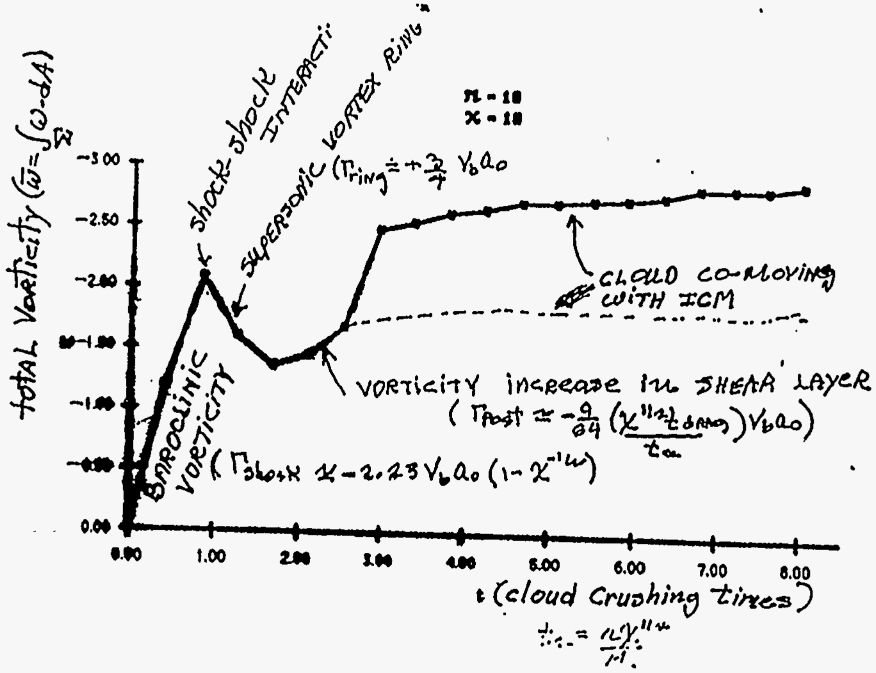

MACH SCALING

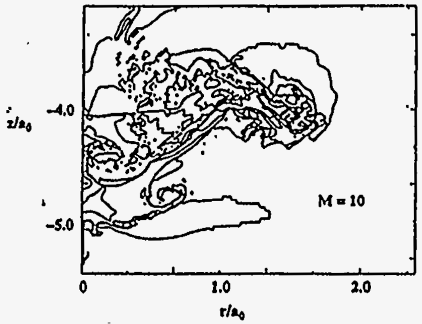

$t = 2.95\, t_{cc}$

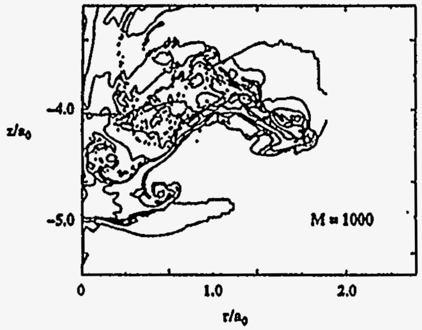

$t = 2.95\, t_{cc}$

Hydrodynamic Equations Invariant

$t \to tM$

$v \to v/M$

$p \to p/M^2$

- Cloud destruction time $\tau_d \sim 3\text{-}4\, t_{cc}$ over a Large dynamic range in χ
  $3 \le \chi < 400$

Destruction proceeds far more rapidly than time for a cloud to clear out its own mass.

- Cloud Accelerated to $v \sim \frac{3}{4} V_b$ in $\tau_{drag} \sim$ few x t_{cc}.

Destruction of shocked cloud due to fragmentation on LARGE AND small SCALES $\longrightarrow$ K-H; R-T; R-M instabilities

2 MEASURES OF CLOUD DESTRUCTION:

I. τ_{dest} = time $m_{core} = m_0/e$
Large SCALE FRAGMENTATION

VERY Robust $\boxed{\tau_{dest} \simeq 3.5\, t_{cc} \quad 3 \le \chi \le 100}$

$\Rightarrow \quad \Delta Z_b(\tau_{dest}) \doteq V_b \tau_{dest} = 3.5 \chi^{1/2} a_0$

$\Rightarrow$ for cloud $\chi = 10$; substantially destroyed when shock-wave advances 10 cloud radii

130 (14) Klein, McKee, Colella 1990

Core Mass vs. time

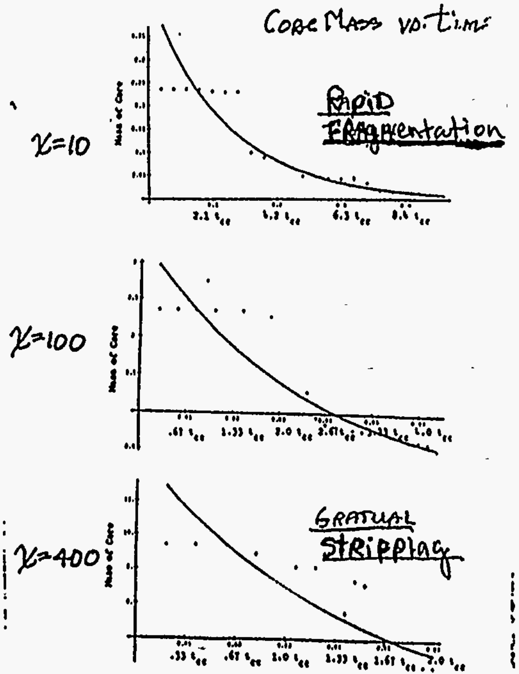

Figure 12 Core mass vs time for χ=10, 100, 400

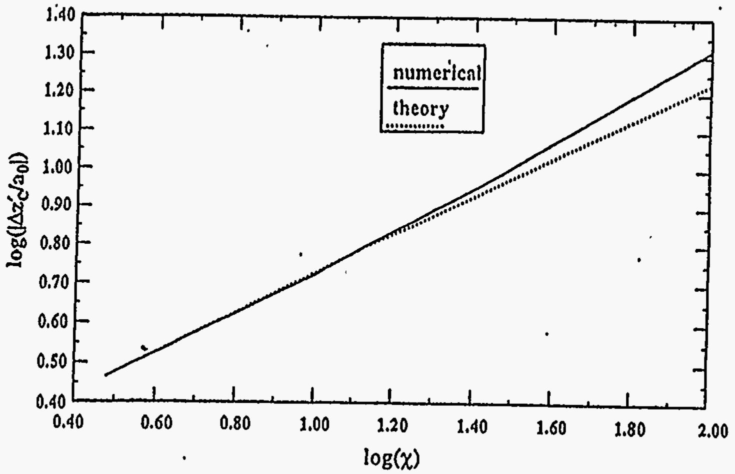

$$\left|\frac{\Delta z}{a_0}\right| \propto \chi^{1/2}$$

Distance cloud travels in ICM over time to fragment to small scales.

$\Rightarrow$ $\chi > 100$, DIFFERENT PROCESS OF FRAGMENTATION

II. Mixing

$\tau_{mix} \rightarrow$ time for a cloud to $\frac{1}{2}$ mass mixed with ICM

$\Rightarrow$ 2-fluid HYDRODYNAMICS

$\rightarrow$ Mixing Most Rapid FOR $\chi \gg 1$

Consider Drag time:

IF area of cloud $A \ni \frac{\partial A}{\partial t} = 0$

$$\tau_{drag} = \frac{\chi a_0}{C_D V_b} = \frac{\chi^{1/2} t_{cc}}{C_D}$$

But, cloud has large lateral expansion

$\Rightarrow$ Drag increased

$\tau_{drag} \ll \chi^{1/2} t_{cc}$

$\Rightarrow$ $\tau_{drag} \simeq$ few $\times\, t_{cc}$ $\quad 3 \lesssim \chi \lesssim 400$

Klein et al. '93

$$\frac{V_c}{V_{c0}} = \frac{1}{1 + \left(\frac{9}{8}\frac{C_D}{\chi^{1/2}}\right)\frac{t}{t_{cc}}\left[1 + \frac{1}{3}\left(\frac{C_c}{V_s}\frac{t}{t_{cc}}\right)^2\right]}$$

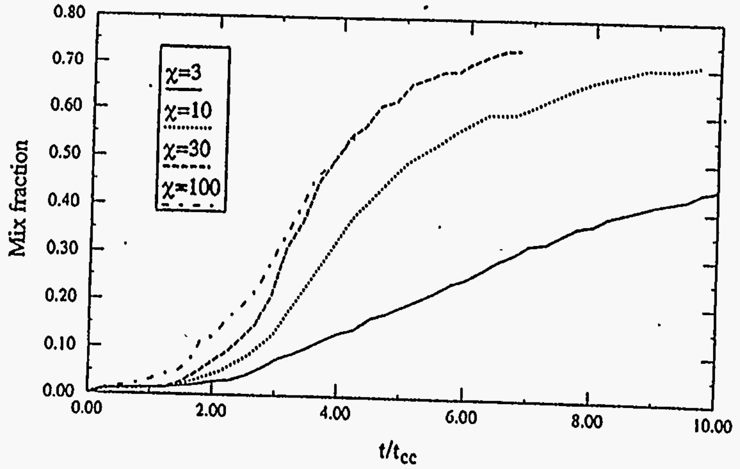

HIERARCHICAL FRAGMENTATION

- Scaling extremely well obeyed

  $3 \le \chi \le 100$

LSF → (Large-scale FRAGMENTATION OF CLOUD CORE

. scaling starts to break down

  $\chi > 100$

⇒ Change in ~~fragmentation~~ fragmentation process

LSF ⟶ small scale stripping OF SURFACE

$\chi \le 100$ $\chi > 100$

Hierarchical Fragmentation is most rapid possible mixing, since it continually exposes interior of cloud to mixing

small scale stripping from surface of cloud is less efficient

FESEN ~~[illegible]~~ AJ 1992

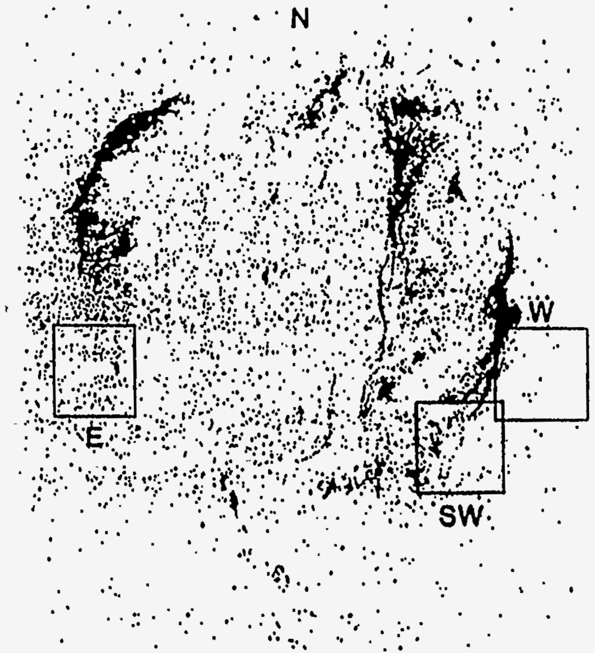

CYGNUS LOOP SNR 30′

Figure 1

Fesen 1992
Hα image
of
EASTERN
cloud
$r_{cl} \sim 0.5$pc.
$n_{cl} \sim 1$
$R_{shell} \sim 3.2\times10^{19}$
$v_b \sim 4\times10^{7}\frac{cm}{s}$
$t \sim 4.1\times10^{3}$ yr.

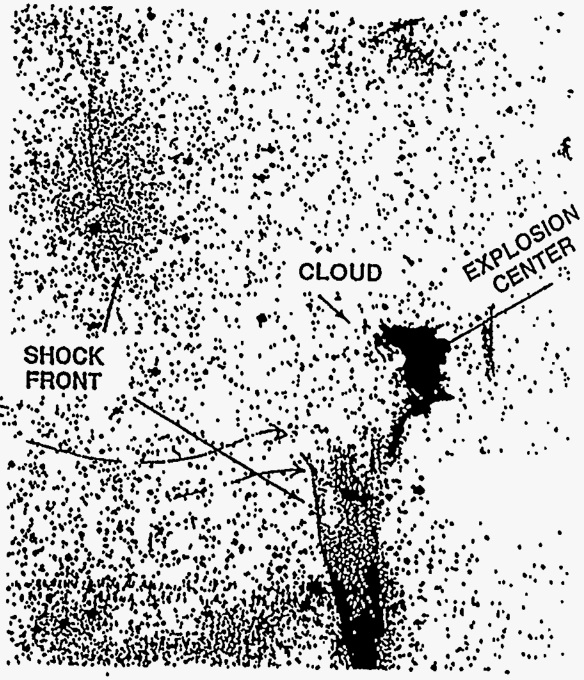

$\gamma_c=1.1$ ("Radiative")
$\chi=10$
$M=10$

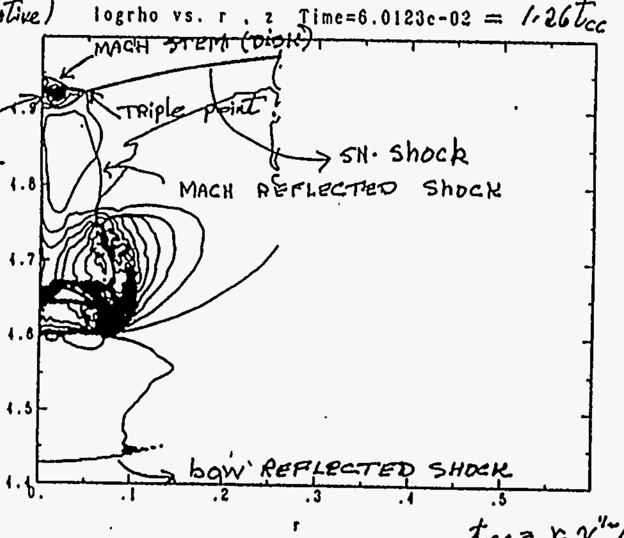

Fig. 10

$t_{cc} = r_c \chi^{1/2}/v_b$

```
                       min                        max
logrho  [ 75,253]=-7.481808e-02 [ 64,169]= 2.718847e+00
r       [  1,  1]= 0.000000e+00 [208,  1]= 2.587500e-01
z       [  1,  1]= 1.400000e+00 [  3, 64]= 1.998750e+00
```

$n_c \approx 1.0$
$n_i \approx 0.1$ $r_c = 0.7$pc; $\chi=10$;
from Chandra's X-ray emission $\Rightarrow v_b = 400\ \frac{km}{s}$.
$t_{cc} = 2.8\times10^{3}$ yr.

Cloud-Shock Interaction Experiments on NOVA

R. KLEIN, T. PERRY

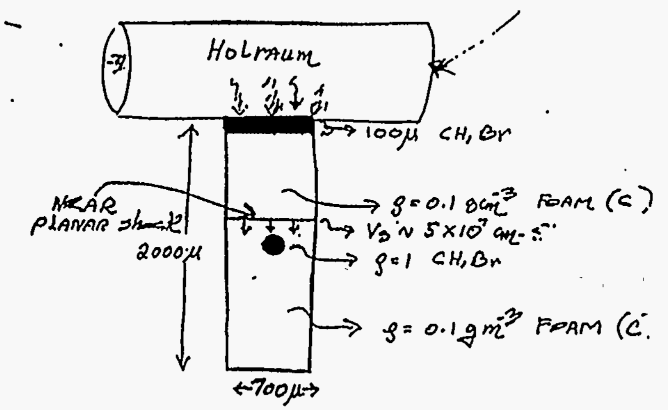

shock propagation for $t \approx 40\times10^{-9}$s ~ 6 t_c

⟹ We can investigate R-M, R-T, R-H instabilities far into the Non-Linear Regime

Experimental Investigation will cover

$\chi \rightarrow 10-100$

$m \rightarrow 1-11$ (TEST MACH ~~[illegible]~~ SCALING AND

Colliding Plasma Experiments

Ted Perry
Lawrence Livermore National Laboratory

Colliding Plasma Experiments

Ted Perry
Defense and Nuclear Technologies
Lawrence Livermore National Laboratory
February 26, 1996

Outline

- Determining temperature by measuring ion balance
- Measuring density through radiography
- Heating samples volumetrically using gold M-band radiation

Point Projection Spectrometry

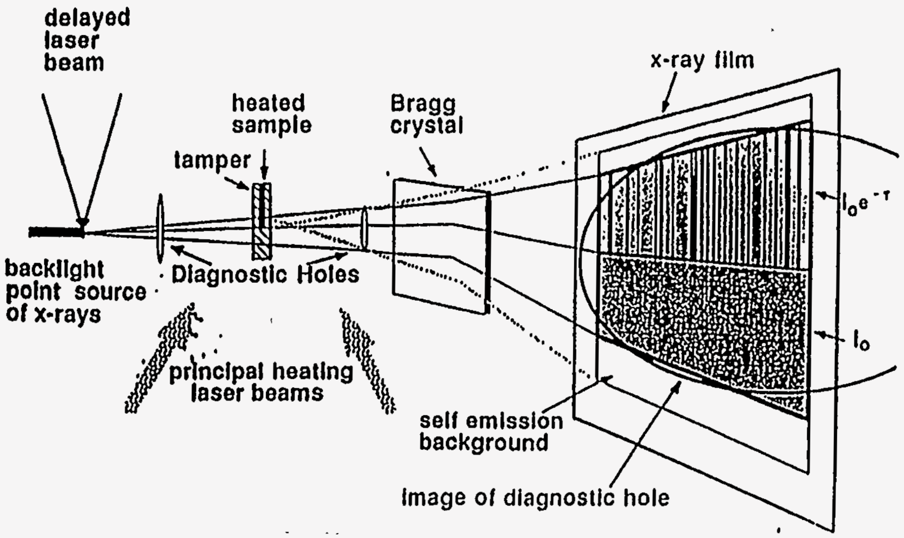

New techniques were developed for opacity experiments

Point projection spectrometry

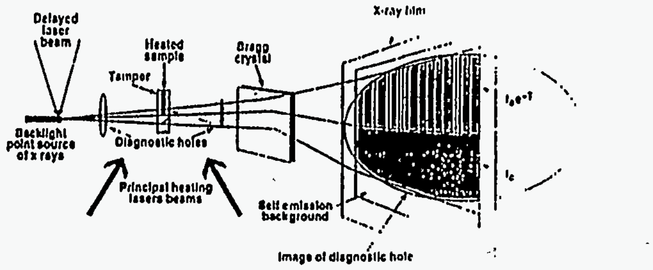

Scale-3 lipped hohlraum

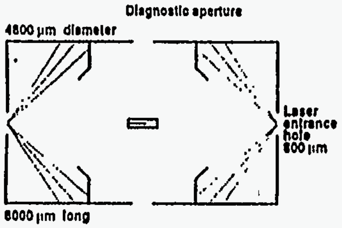

Nearly planckian drive

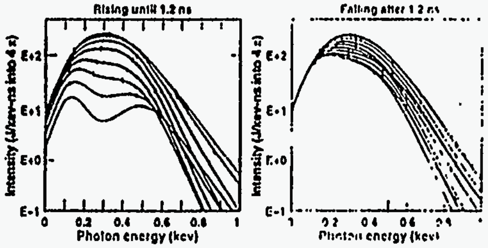

77-77-0196-perry
20-00-0196-0021

First measurements were on aluminum

- Aluminum was used to test accuracy of method and also to investigate using low-Z tracers as a temperature diagnostic
- Two thicknesses (500 Å & 1500Å) were used for consistency check. Cube of thin sample transmission should equal thick sample transmission.

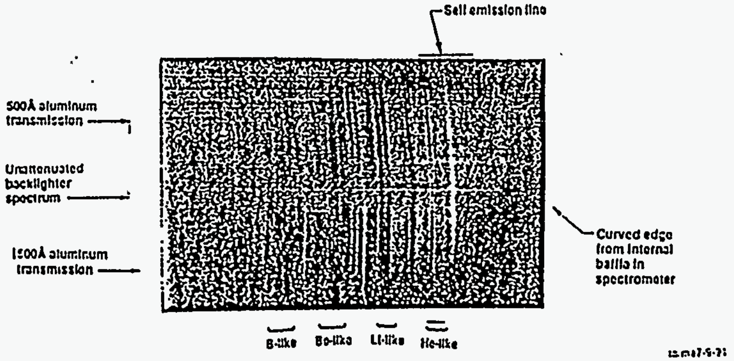

ts-ms17-5-71

The two thicknesses give similar results

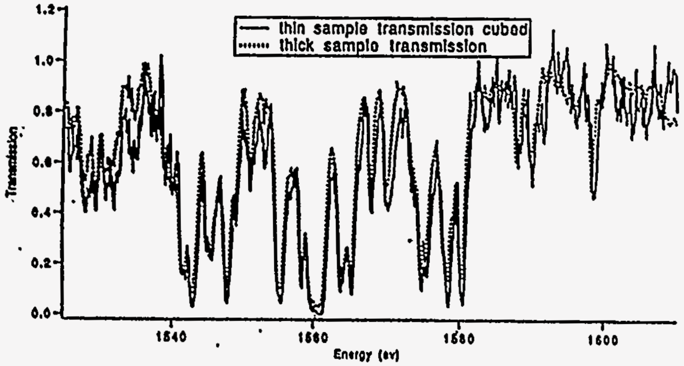

The two different thicknesses of aluminum provide a consistency check on the data reduction. Since the thick sample is three times the thickness of the thin sample, the cube of the transmission of the thin sample should equal the transmission of the thick sample.

1r82090

Experiment agrees well with calculation

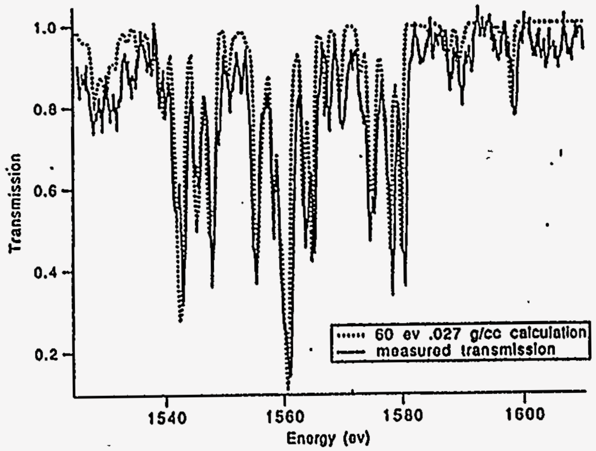

5 ev change in temperature is equivalent to a factor of 2 change in density

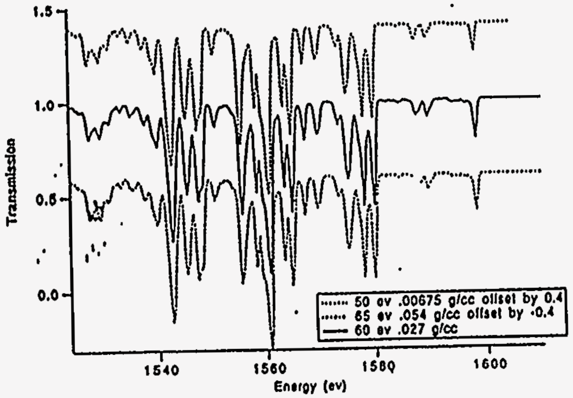

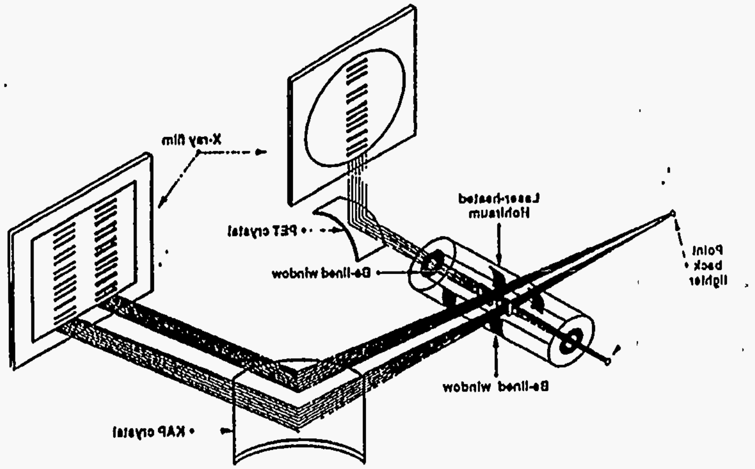

Goal was to have simple, well-characterized system

- We wanted to avoid any problems with laser - matter interactions
- We wanted to have well-characterized x-ray deposition.
- We wanted to avoid strength of material problems
- We wanted to have space and time resolved density and temperature measurements.
- We wanted to be able to make rigorous comparison to code calculations.

ARRANGEMENT OF RADIATIVELY DRIVEN ALUMINUM FOIL EXPERIMENT

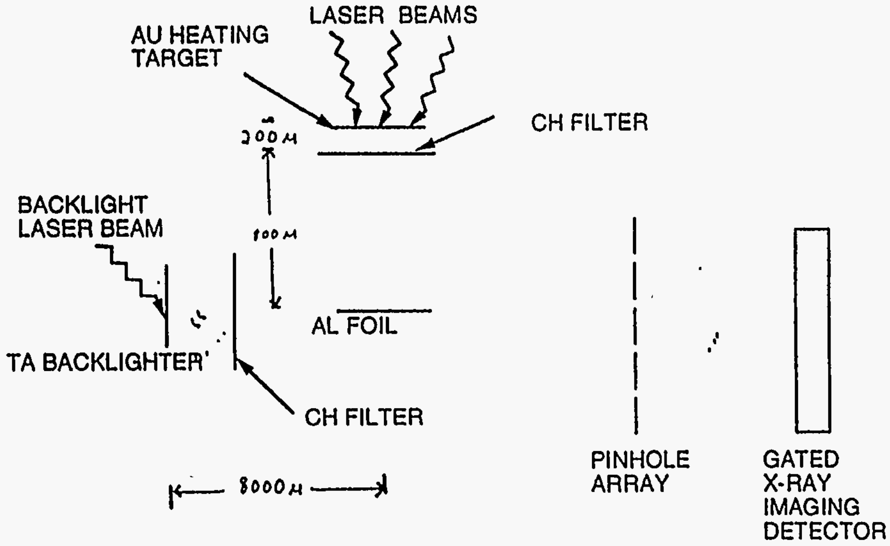

GXI (gated x-ray imager)

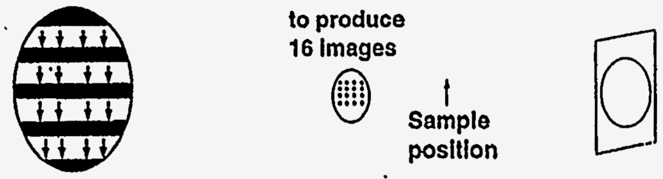

Pinhole array has 16 holes to produce 16 images

Sample position

Microchannel plate x-ray detector has four strips which are gated at four different times.

Laser beam hits piece of tantalum producing x-rays to backlight sample

All 16 GXI channels necessary for proper data analysis

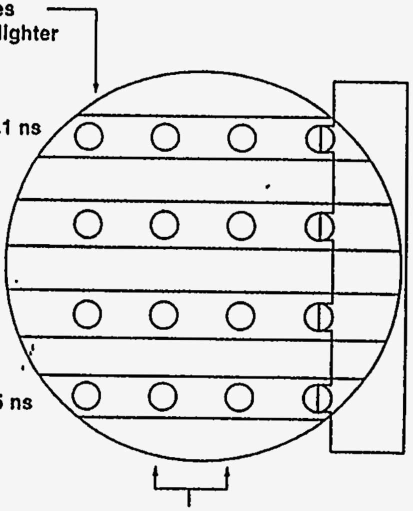

This column of images used to remove backlighter spatial variation.

Strip gated at –0.1 ns

Strip gated at 1.35 ns

Strip gated at 2.80 ns

Strip gated at 4.25 ns

3 μ Al foil is used to check backlighter spectrum.

These columns used to image aluminum sample. (we use column with best alignment.)

Expansion of an x-ray heated Al foil

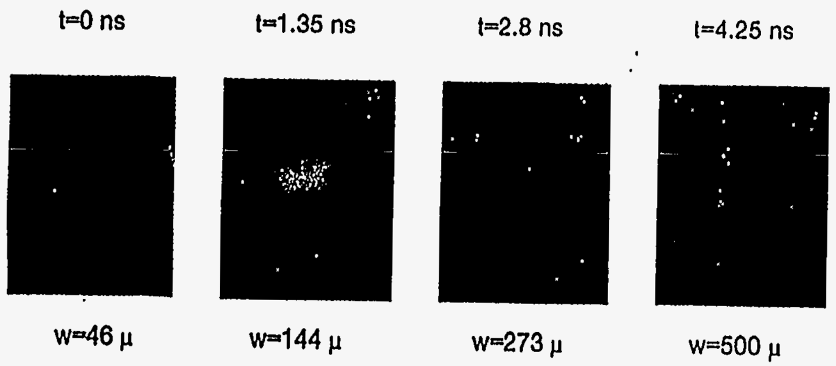

(The foil was 1000 μ long and 2 μ wide viewed at an angle of 2.5°.)

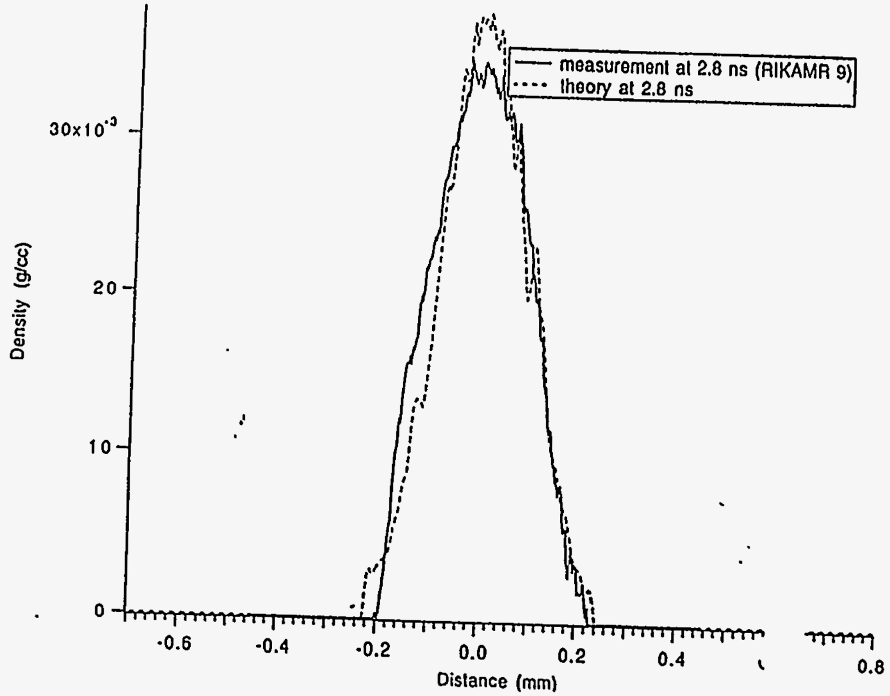

FRAMING CAMERA DATA FROM PARALLEL FOIL EXPERIMENT

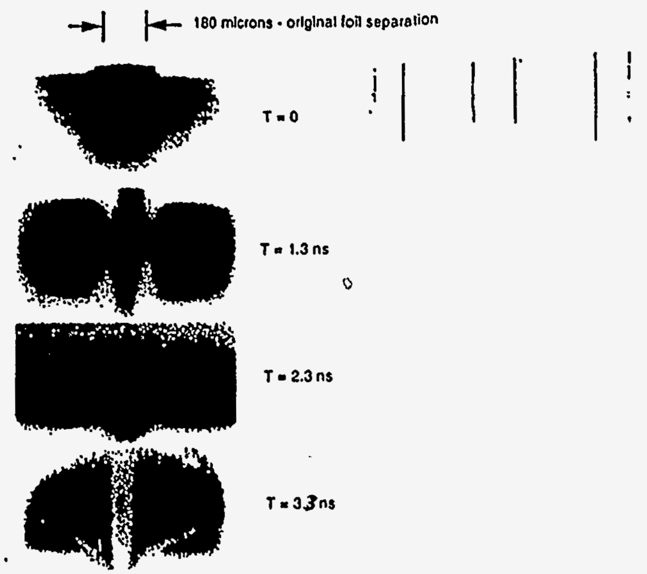

TRANSMISSION OF PARALLEL FOILS AT 1.3 NS

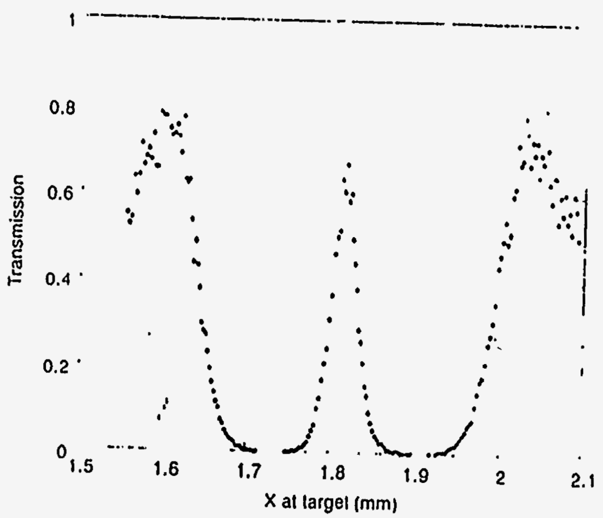

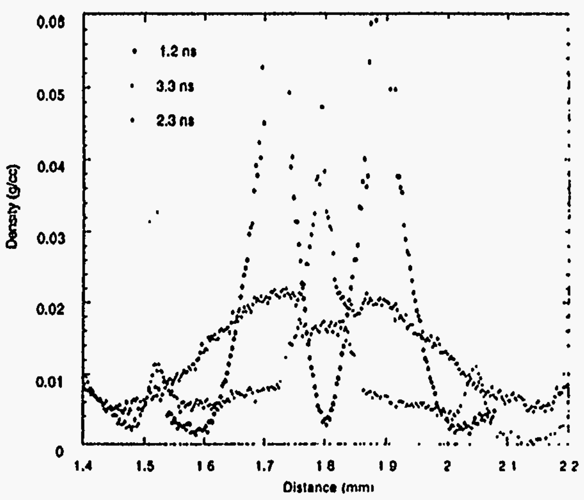
DENSITY DISTRIBUTIONS FOR DOUBLE FOIL EXPERIMENT

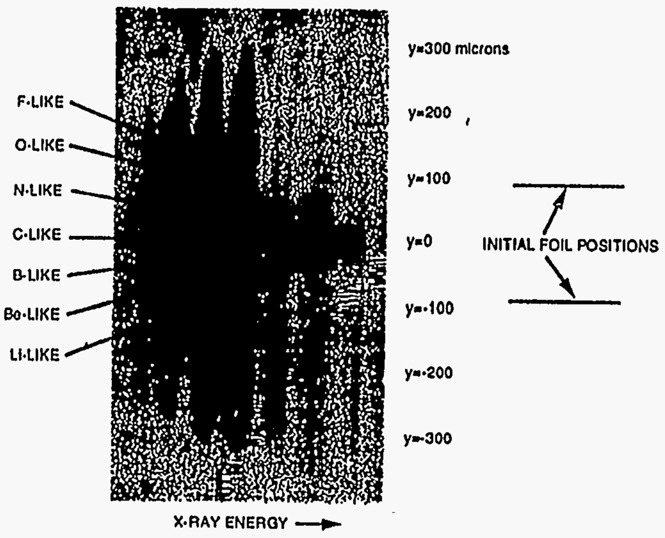
X-RAY IMAGE OF DOUBLE FOIL EXPERIMENT AT 2 NS
SHOWING 1-2 ALUMINUM LINE ABSORPTION

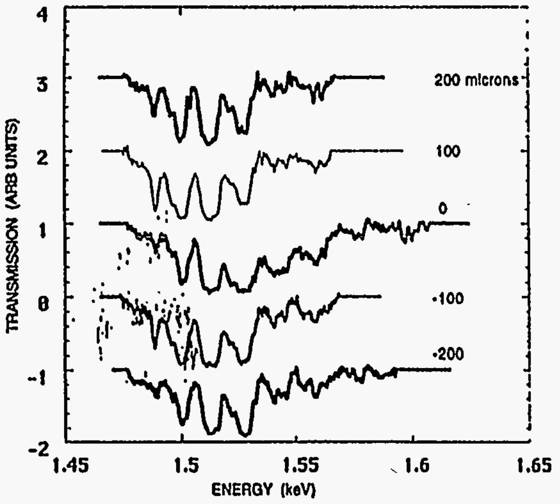
TRANSMISSION AT 2 NS FOR TEMPERATURE DETERMINATIONS

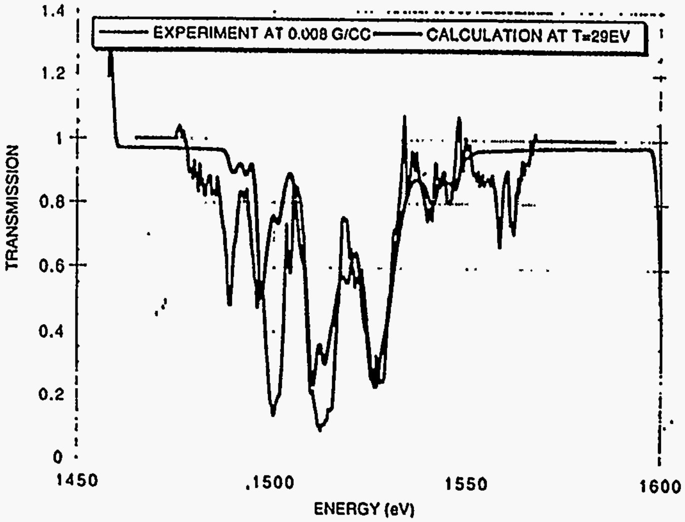
COMPARISON OF MEASURED AND CALCULATED TRANSMISSION
PARALLEL FOIL EXPERIMENT

Temperatures for colliding foils

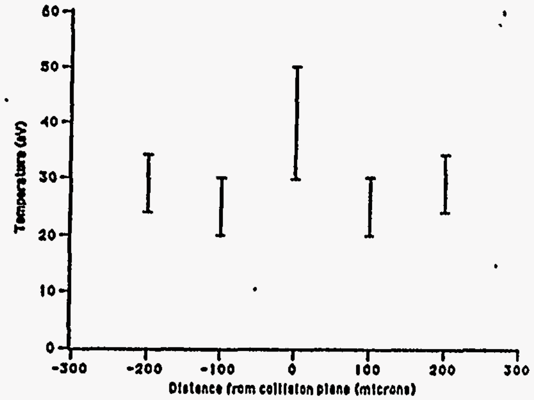

FRAMING CAMERA DATA FROM ANGLED FOIL EXPERIMENT

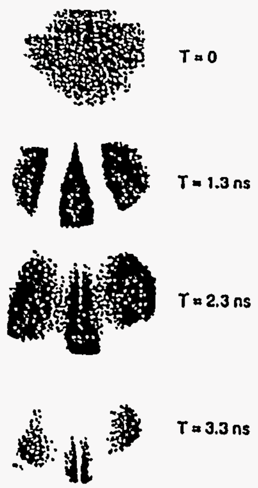

tp2593

Summary

- Temperature can be measured to ±4%.
- Density can be measured to ±25%.
- Gold M-band radiation can be used to heat matter to 10's of eV.
- These techniques have been used to study two colliding plasmas.

Instabilities and Mixing in SN1993J

Kohichi Iwamoto
University of Tokyo

Instabilities and Mixing in SN1993J

K. Iwamoto, T. R. Young, T. Shigeyama, K. Nomoto
and
I. Hachisu
(University of Tokyo)

and
H. Saio

(Tohoku University)

1. Introduction

'peculiar' SN1993J in M81 Mar. 1993

H lines → Type II

2nd peak
Spectral feature change (H → He) } → I-b like

⇓

'Type II-b' model (Podlowski et al 1993
Nomoto et al. 1993
Woosley et al. 1994

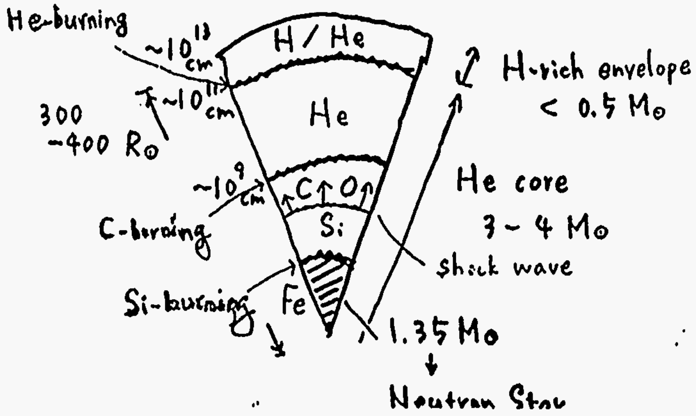

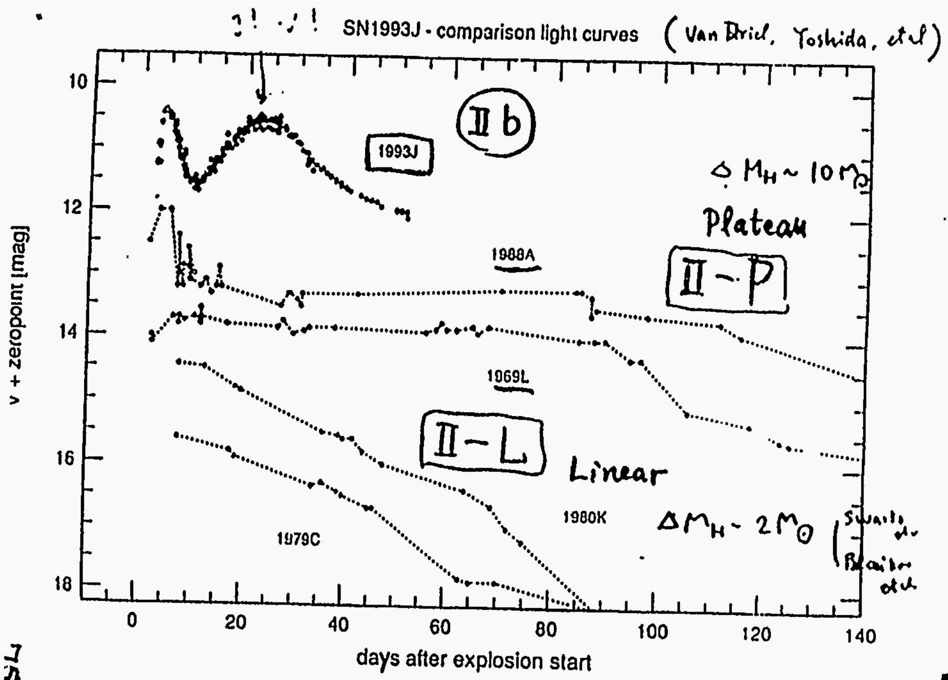
?! ?!
SN1993J - comparison light curves
(Van Driel, Yoshida, et al)
v + zeropoint [mag]
10
12
14
16
18
0
20
40
60
80
100
120
140
days after explosion start
II b
1993J
1988A
1969L
1980K
1979C
Δ M_H ~ 10 M_☉
Plateau
II - P
II - L
Linear
ΔM_H ~ 2 M_☉
Swartz et al
Branch et al

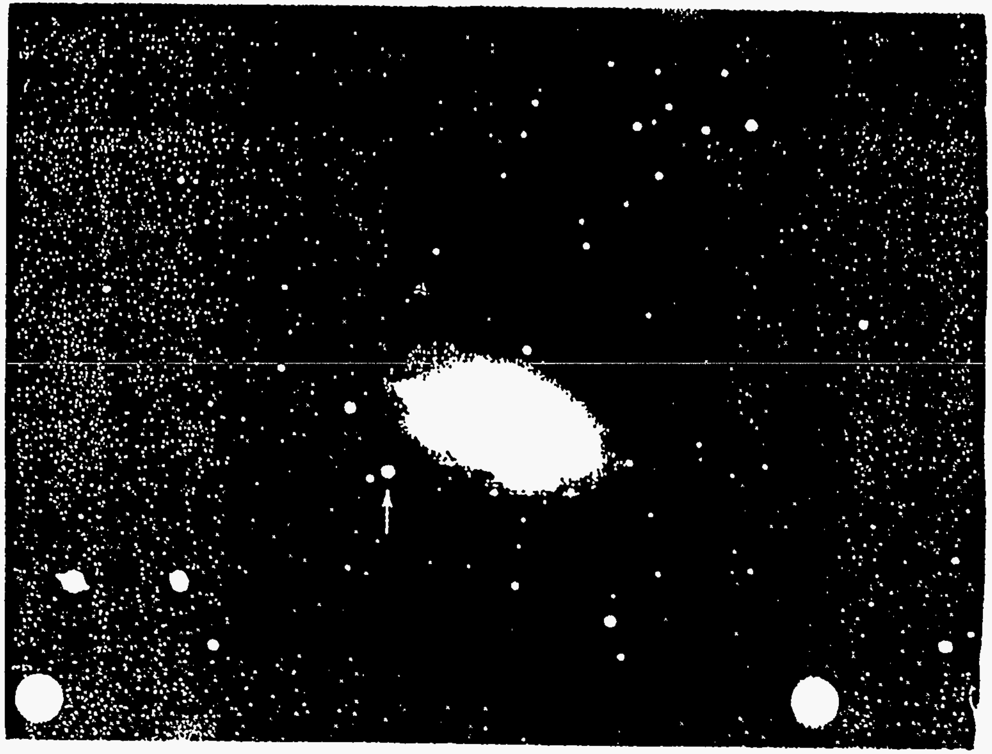

Light Curve Modeling

(Shigeyama et al. 1994)

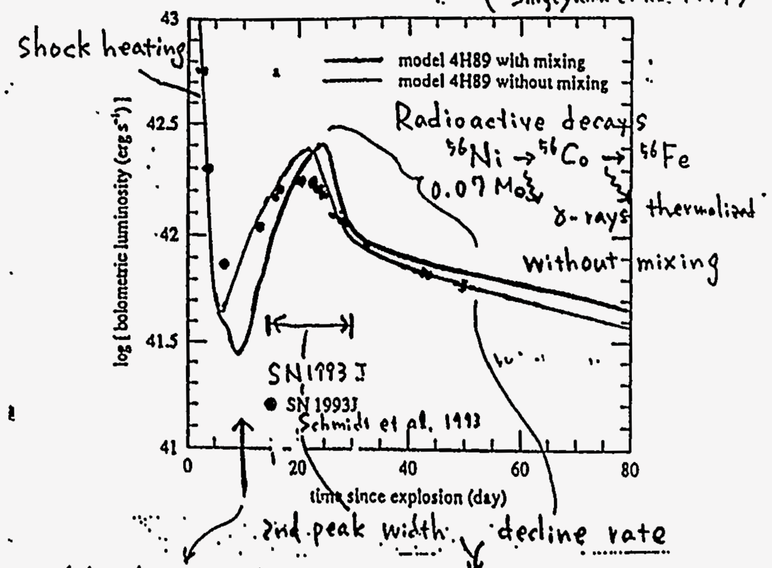

M(H-rich envelope) $< 0.5 M_\odot$

M(He core) = 3 – 4 $M_\odot$

ex.SN1987A

R-T instability

↓

mixing

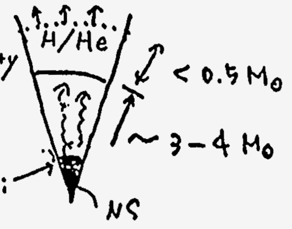

2. Rayleigh-Taylor Instability

ρ_+

ρ_- $\downarrow g$

$$\omega_{RT}^2 = \frac{\rho_+ - \rho_-}{\rho_+ + \rho_-} k g$$

k : wavelength

g : gravity

if $\rho_+ > \rho_-$, R-T unstable

In shocked ejecta of supernovae

acceleration $a = -g - \frac{1}{\rho}\frac{dP}{dr} \simeq \underbrace{-\frac{1}{\rho}}_{}\frac{dP}{dr}$

effective gravity

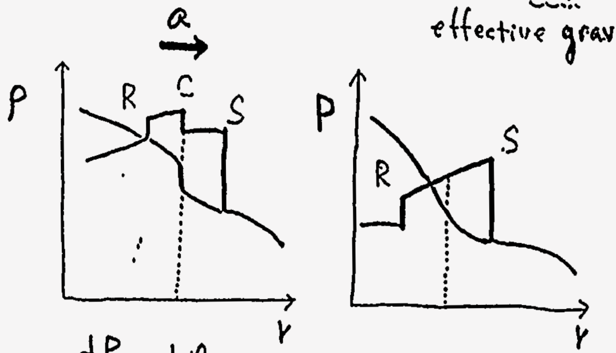

$$\frac{dP}{dr} \cdot \frac{d\rho}{dr} < 0 \rightarrow \text{R-T unstable}$$

Changes in the density and pressure profiles (4H13)

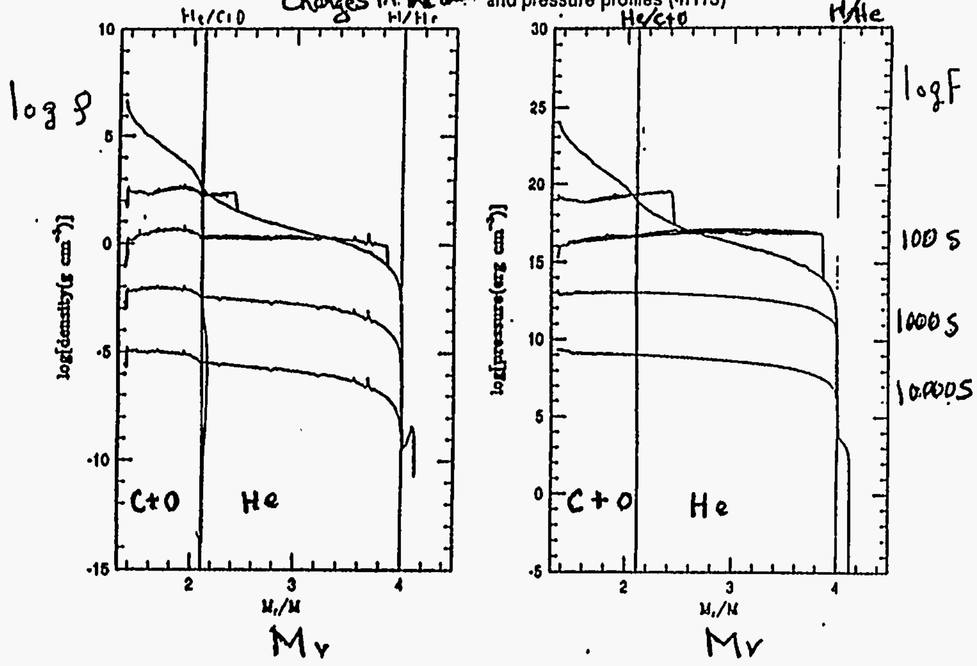

Multi dimensional Simulations of the R-T instability in Supernova Ejecta

previous works
Arnett et al. (1989),
Hachisu et al. (1991),
Müller et al. (1991), ...

Initial Models

	$M_{He}/M_\odot$	$M_H/M_\odot$	$R/R_\odot$	E (10^{51}erg)
3H11	3.3	0.11	450	1.0
4H13	4	0.13	580	1.0

He core from Nomoto & Hashimoto (1988)
hydrostatic envelope model (H. Saio)

Method of Calculation

- 1-D Lagrangian PPM code (~ 10 sec)
- 2-D axisymmetric hydrodynamic code with 3rd order Roe scheme (I. Hachisu)
- EOS .... ideal fluid with $\gamma = 4/3$
- 512^2 grids
- random perturbation (5 %)
- remapping procedure (> 10 times)

3H11 at 120 sec

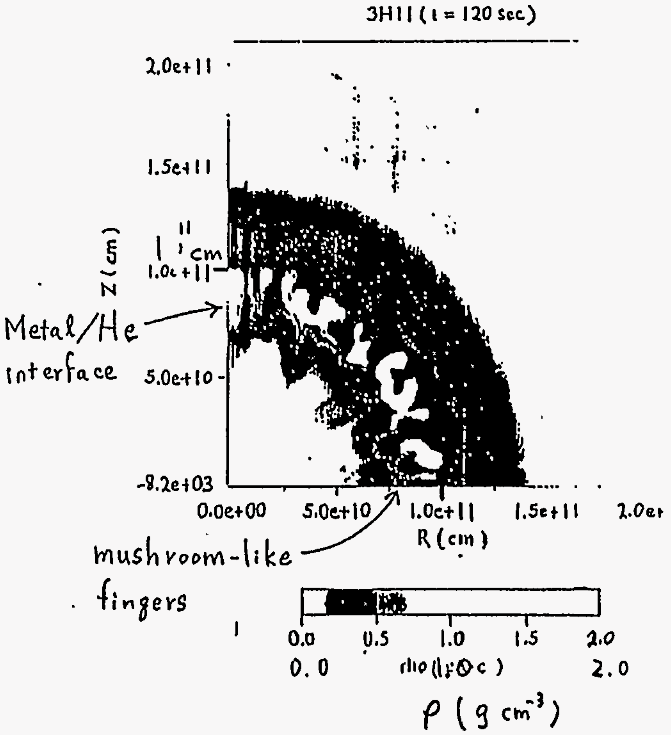

3H11 at 5 × 10⁴ sec

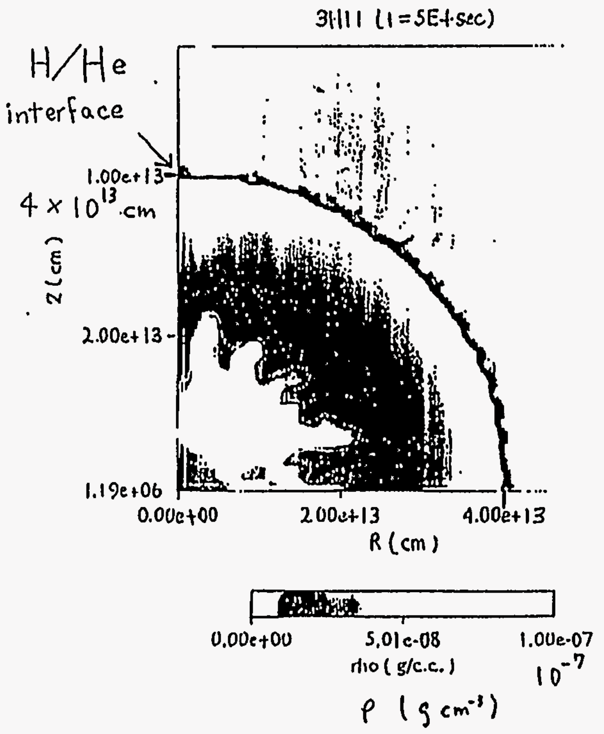

3H11

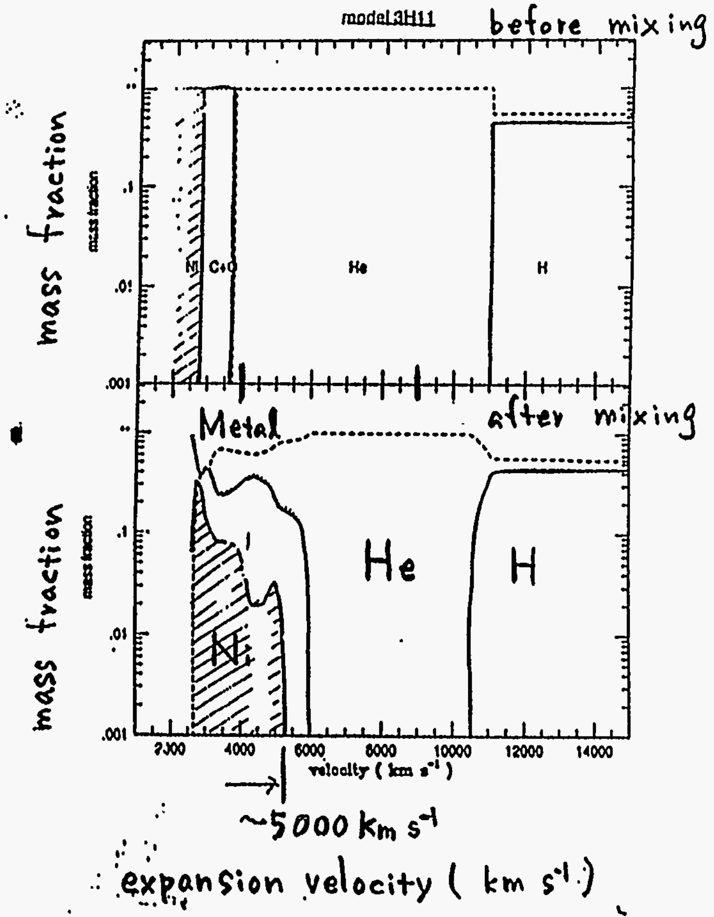

4H13 at 120 sec

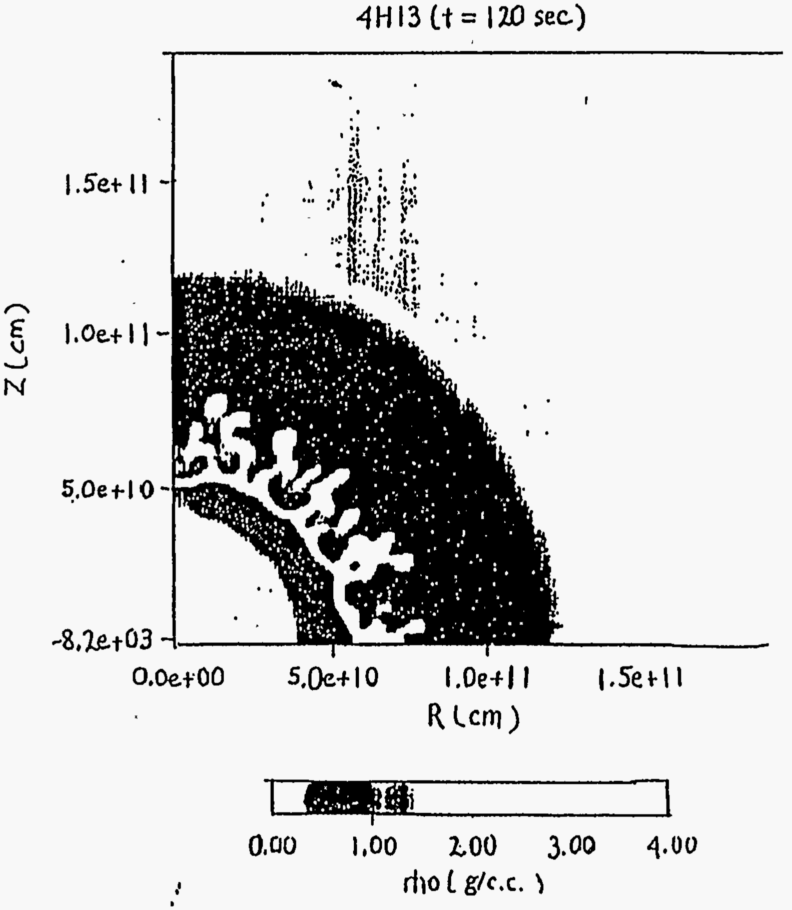

4H13 at . 4×10^4 sec

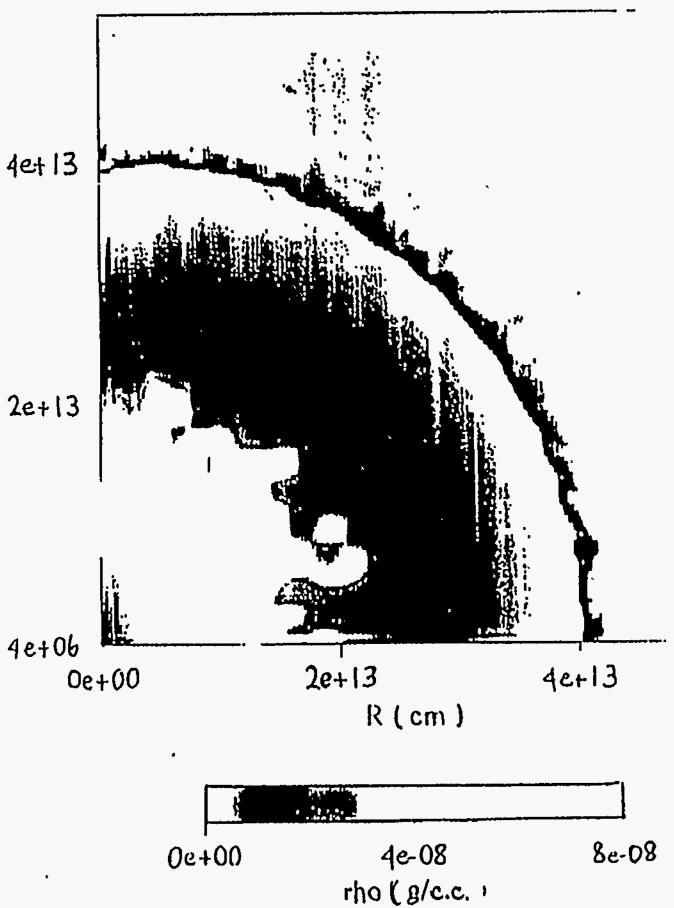

4H13

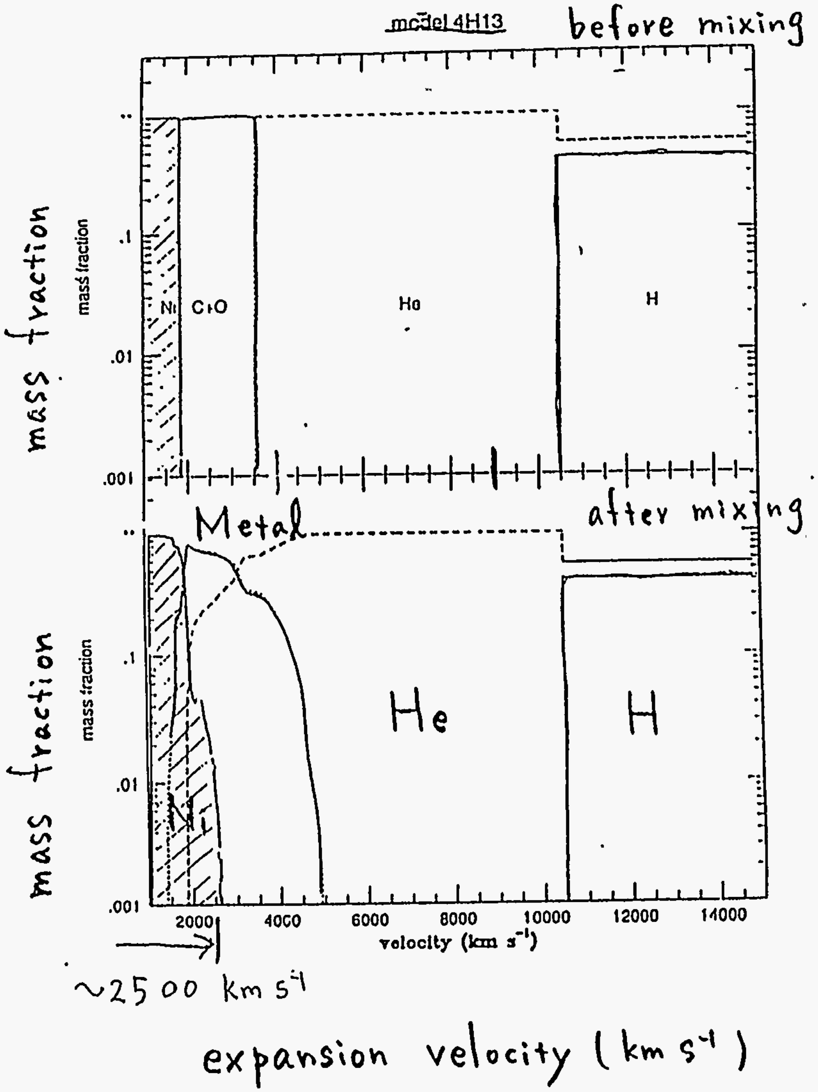

3. Discussions

(1) dependence on progenitor models

Metal/He ⋯ 3H11 has smaller core mass → steeper $d\rho/dr$

→ more R-T unstable → more mixing than 4H13

H/He ⋯ small envelope mass

→ weak deceleration of shock → little mixing

↔ SN1987A larger core mass $\sim 6 M_\odot$

→ little mixing at Metal/He

larger envelope mass $\gtrsim 10 M_\odot$

→ much mixing at H/He

(2) influence on light curve shape

mixing → { earlier 2nd peak, faster decline in tail }

best fit LC

by 3H11 with ^{56}Ni mixing up to 0.6 $M_\odot$

→ consistent with 2-D results

(3) constraints from spectroscopic obs.

O ⋯ $(1-4) \times 10^3$ km/s

H ⋯ $(8.5-10) \times 10^3$ "

Ni max $> 3 \times 10^3$ " → c.f. preferable (3H11) ⋯ 5×10^3 km/s

4H13 ⋯ 2.5×10^2 km/s

Bolometric Light Curves (T. R. Young)

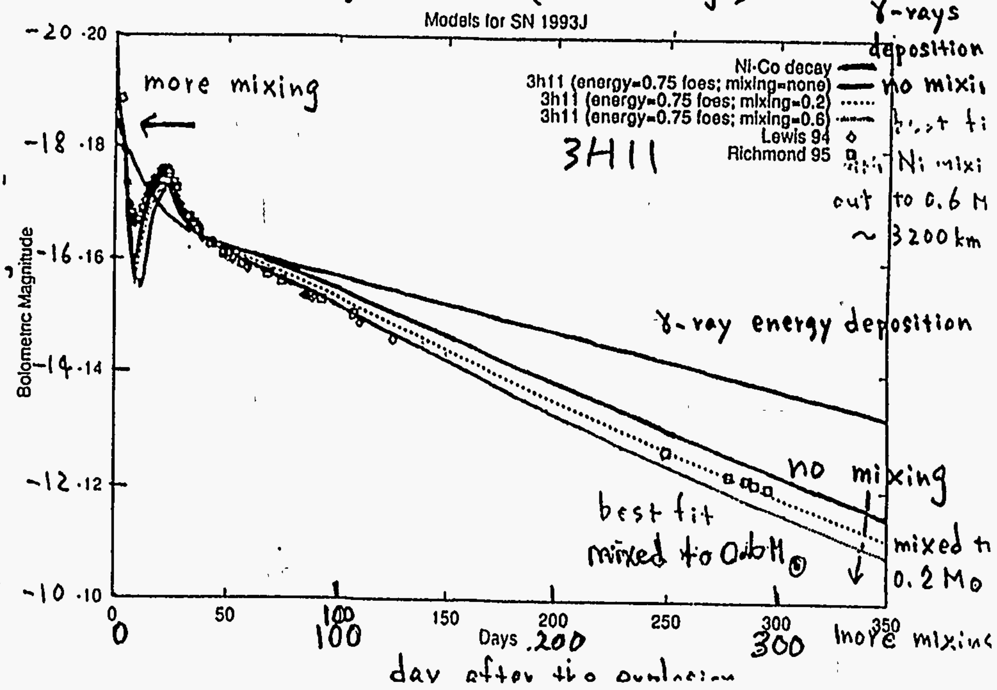

Late time spectrum of SN1993J (J.C.Houck & C.Fransson . 1996)

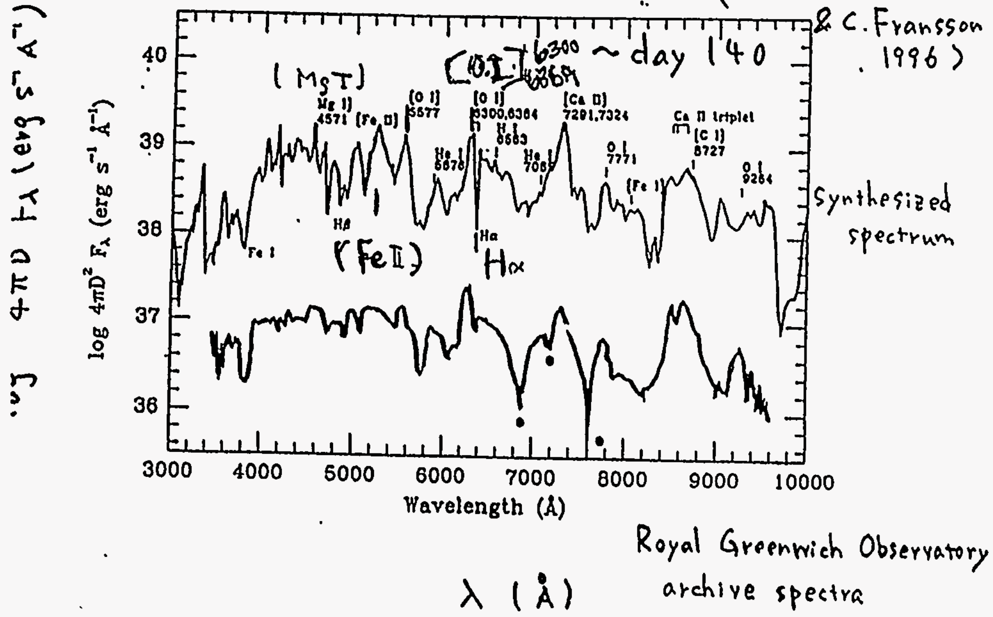

Conclusions :

1. The extent of mixing depends sensitively on the progenitor's structure.

   more mixing with smaller core mass

2. In SN1993J, in contrast to 87A, there appears a large scale mixing at Metal/He interface due to the smaller core mass, but no prominent mixing at H/He interface due to the tiny H-rich envelope.

3 : The study of Rayleigh-Taylor instability is important to identify the progenitor of supernovae.

Shock and Jet Experiments on Nova

Paul Miller
Lawrence Livermore National Laboratory

Shock and Jet Experiments on Nova

Paul Miller, Tom Peyser, Pete Stry,
Kim Budil, Debbie Wojtowicz, Don Griswold,
Bruce Hammel, Ted Perry, Larry Logory, and Gene Burke

Presented to the Workshop on Laboratory Astrophysics,
26 February 1996

Lawrence Livermore National Laboratory
University of California

Work performed under the auspices of the U.S. Department of Energy by the
Lawrence Livermore National Laboratory under Contract W-7405-Eng-48

We are exploring a variety of flows

We are investigating shock-induced hydrodynamics with experiments on the Nova laser and with numerical simulations, including:

- The generation of flat shocks to drive our flows
- Flow peculiar to our non-rigid shock tube
- Hypersonic jet flows generated by a hemispherical protrusion at a density interface*
- The shock-induced mixing region between two materials of different densities with known, nonlinear initial interface perturbations*

The Nova laser delivers 25 KJ (3ω) in 1 ns

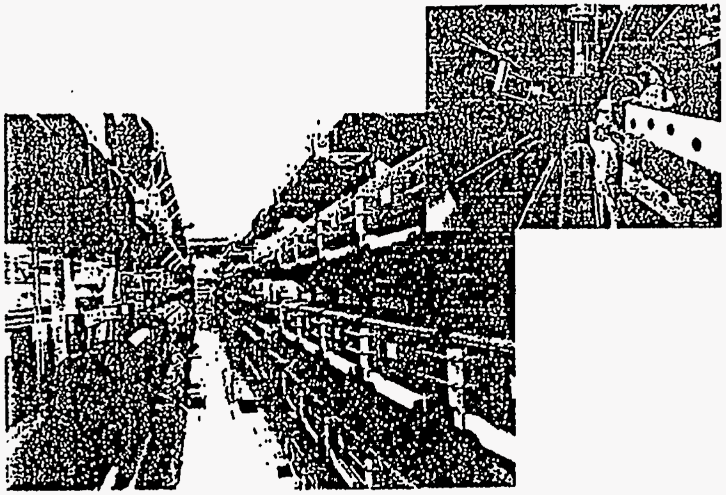

Schematic of the experiment

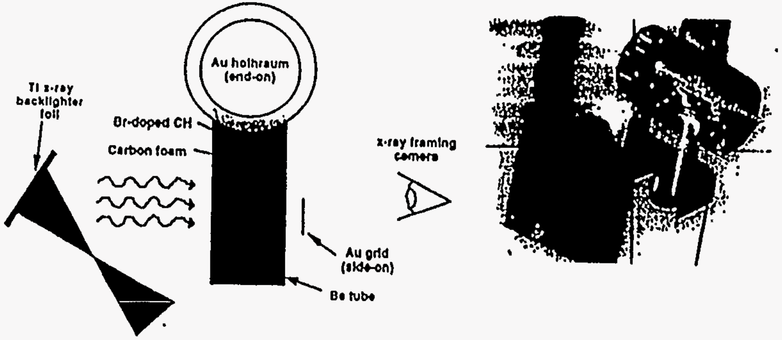

1. Eight of Nova's beams heat the hohlraum to ≈ 230 eV (over 2×10^6 K)
2. Ablation drives a shock into the cylinder
3. The flow is backlit with a titanium backlighter and imaged using a gated 2-D x-ray framing camera

Our shock tube is the size of the "I" on a dime

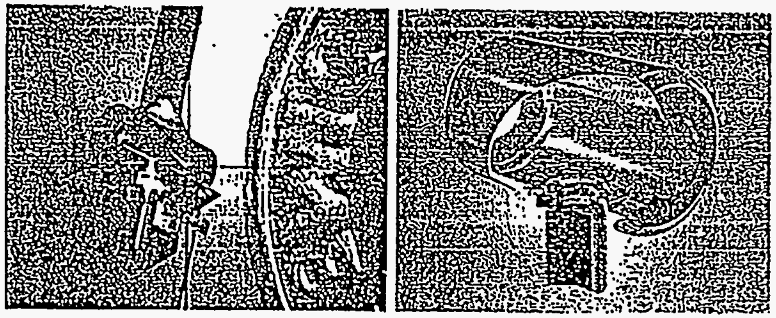

The jet is seeded by a hemispherical feature at a plastic / foam interface (foam part shown)

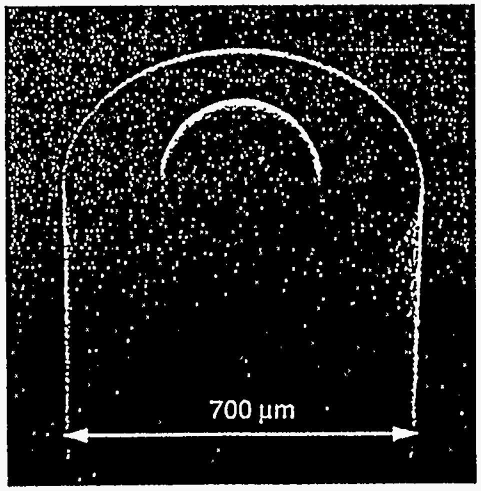

Scanning electron microscope image: low-density, carbon foam piece (oblique view)

- micromachined with diamond tools
- hemisphere radius: 150 µm
- cylinder radius: 350 µm
- foam density: 0.1 gm/cc
- pore size < 1 µm
- surface finish ≈ 3 µm

Temporal progression of the high-speed jet (calc)

Material plots: pink – high density plastic, blue – low density carbon foam

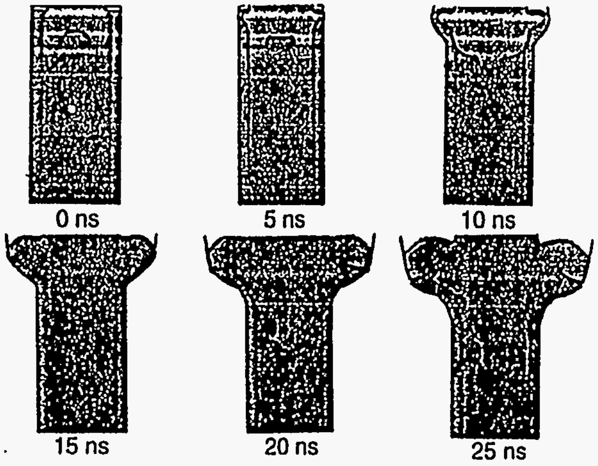

Temporal progression of the high-speed jet (data)

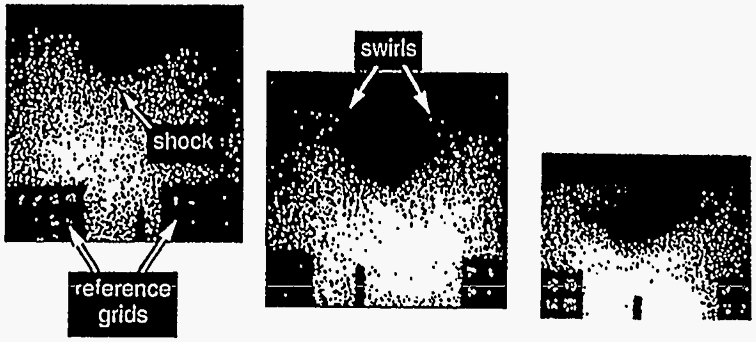

t = 10.4 ns

shock visible, first roll-up

t = 14.8 ns

swirls develop, incipient second roll-up

t = 19.7 ns

jet continues to develop

Comparison of data and simulation images

Simulated radiographs from CALE calculation

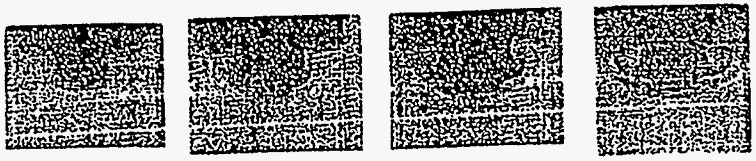

10.5 ns 15.5 ns 19.5 ns 25.5 ns

Data radiographs

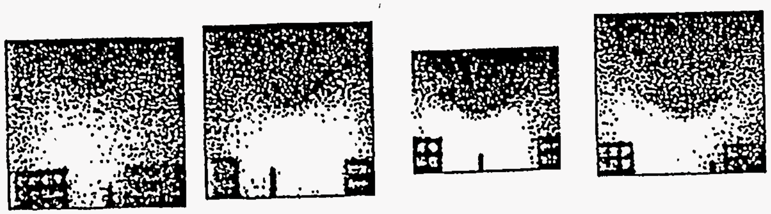

10.6 ns 14.8 ns 19.7 ns 21.9 ns

180

Jet features vs. time from data and simulations

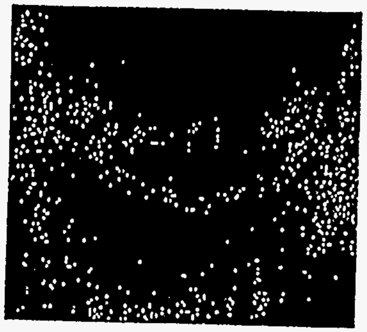

Jet image at 21.9 ns

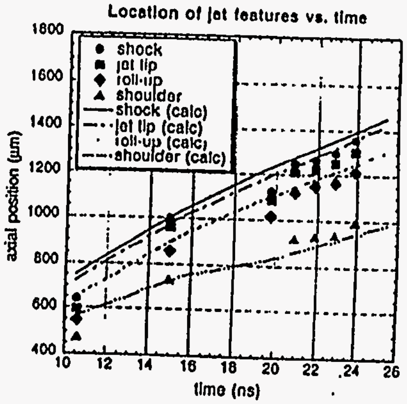

Comparison of lineouts from CALE and data

- both traces at 21.9 ns
- lineouts 100 µm wide
- backlighter nonuniformity removed from the data lineout
- max transmissions normalized to 1.0

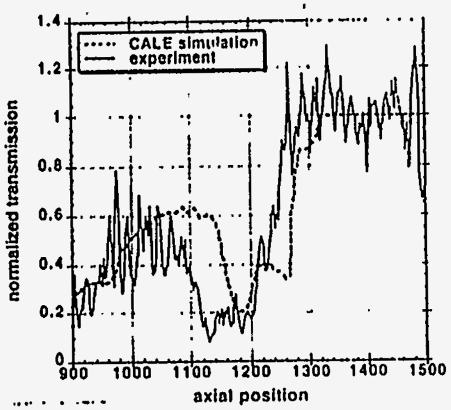
x-ray transmission along centerline

Agreement between experimental and simulated radiographs supports further use of simulations

- 2D CALE calculations of density, axial velocity and vorticity (15.5 ns)


Density Axial velocity Vorticity

Simulations permit examination of unmeasured quantities

Density and axial velocity from CALE simulations at 10.5 ns

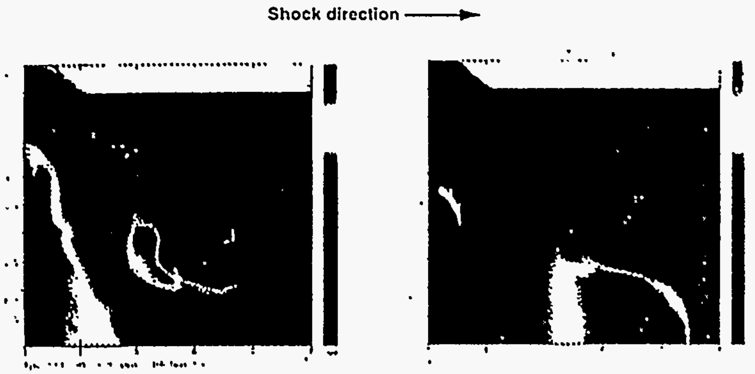

Density (g/cc)

Axial velocity (μm/ns)

The experiment is also being calculated with AMR

Jeff Greenough is using his Adaptive Mesh Refinement code on the jet

- ideal gas, two fluid, equal gammas
- second order Godunov, two levels of 4x refinement (1 μm finest)

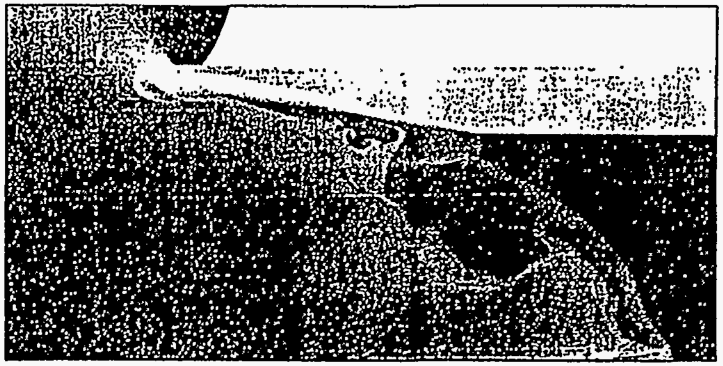

log density contours

Schematic of the experiment

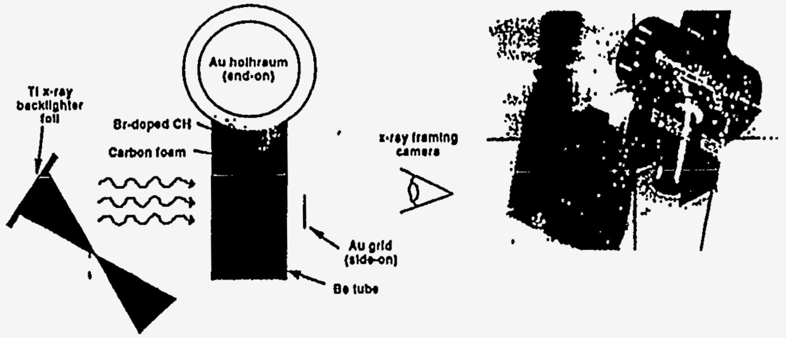

1. Eight of Nova's ten beams heat the hohlraum to about 230 eV
2. Ablation drives a shock into the cylinder
3. The flow is backlit with a titanium backlighter and imaged using a gated 2-D x-ray framing camera

We employ a variety of interface perturbations in our Richtmyer-Meshkov experiments

three types of perturbations used on planar interfaces

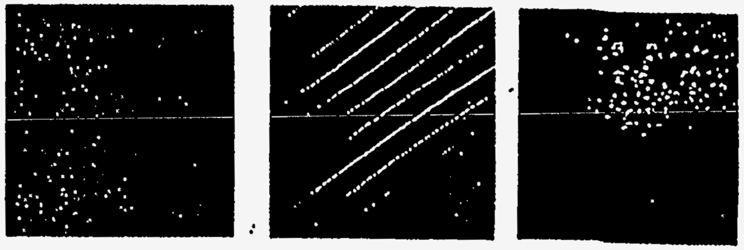

smooth sawtooth "astroturf"

scanning electron microscope images
(80 x 80 μm fields of view)

Temporal progression of sawtooth interface (calc)

- **Density plots from 2D CALE direct numerical simulation**
- **Shock propagation direction** →

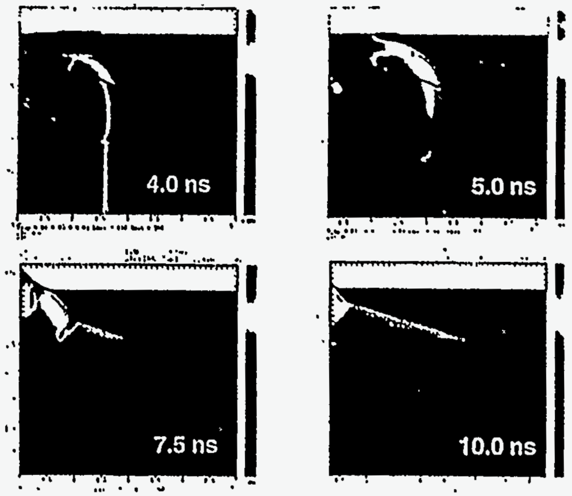

Shock-induced mixing experiments

We are making quantitative measurements of the mixing region widths

This example had a 20 μm sawtooth perturbation

image 5.25 ns after shock arrival

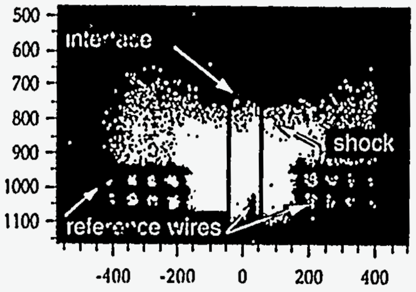

(scales in microns)

100 μm wide lineout

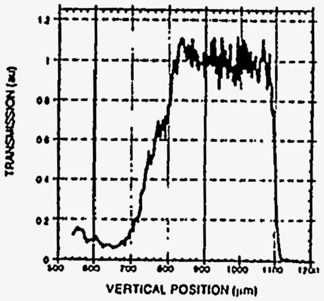

Comparison of mix data and 2-D CALE calculation for 10 μm amplitude sawtooth perturbation

- Mix width for data and calculations based on 5 – 95% transmission criteria
- Effect of decompression obtained from LASNEX and CALE tracer layer calculations
- Experimental values in good agreement with macroscopic mix width results from CALE

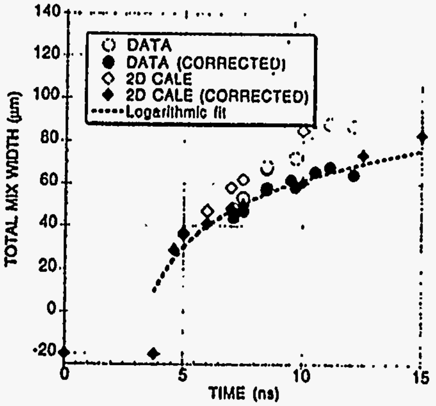

When the effects of target decompression are removed, the width of the mix region is consistent with a theoretical logarithmic behavior

ISSW - 19

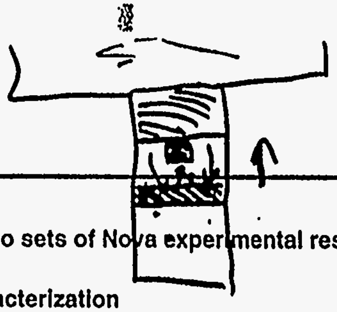

Summary

We have described two sets of Nova experimental results:

- high-speed jet characterization
- Richtmyer-Meshkov instability growth leading to mixing

The experiments:

- demonstrate a general class of experiment which is possible on the laser
- yield data on physical mechanisms such as Richtmyer-Meshkov mixing
- provide well-diagnosed laboratory data in high-speed, compressible plasma flows for potential use in astrophysical code validation

Type Ia Supernovae

John Blondin
North Carolina State University

John Blondin

INSTABILITY OF HYDRODYNAMIC SHOCKS

Radiative Shocks

- What is a **radiative shock**?
- Instabilities on scales $\sim L_{cool}$
- Instabilities on scales $\gg L_{cool}$ (isothermal shocks)

Shock/Shell Collisions in SNRs

Cassiopeia A
Kepler
SN 1987A

Postshock Thermal Energy

$$nkT \sim \rho V^2 \quad \text{ergs/cm}^3$$

Postshock energy loss rate

$$\sim n^2 \Lambda(T) \quad \text{ergs/s/cm}^3$$

$$\Downarrow$$

Cooling timescale

$$t_{cool} \sim \frac{k T_{sh}}{n \Lambda(T_{sh})}$$

How far downstream will gas start to cool

$$L_{cool} = \frac{V_0}{4} t_{cool} = \frac{\bar{m} V_0^3}{85 n_0 \Lambda(T_{sh})}$$

Radiative Shock Profile

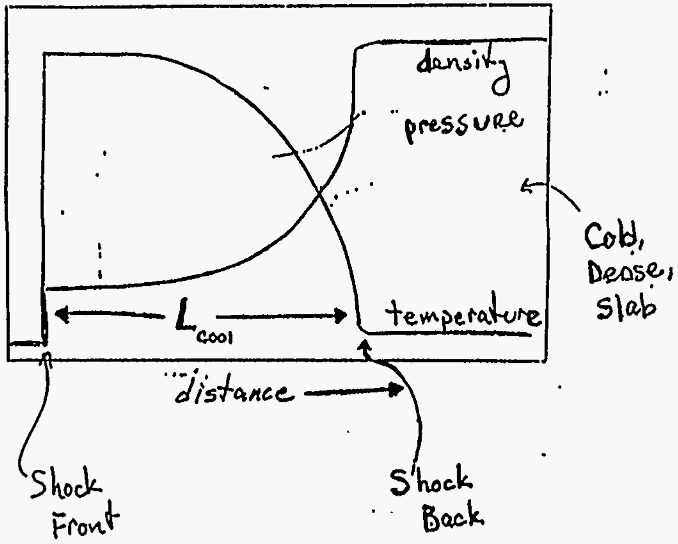

Supersonic Flow Onto a Wall

e.g. accretion onto a white dwarf

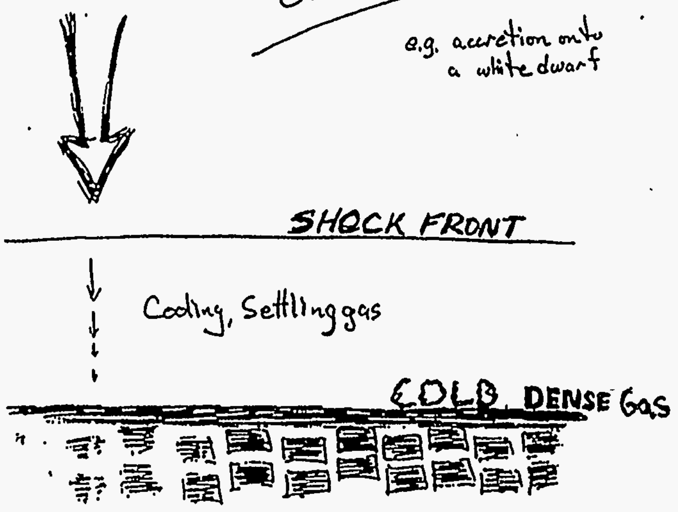

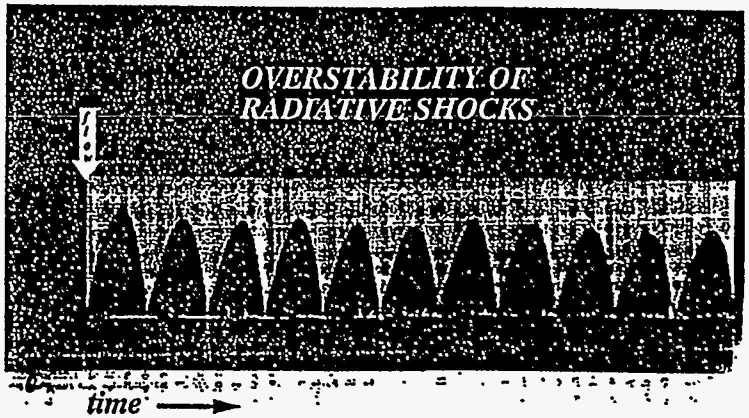

OVERSTABILITY OF RADIATIVE SHOCKS

Overstability of Radiative Shocks

for $\Lambda = \Lambda_0 T^\alpha$ $\quad t_{cool} \approx \frac{kT_{sh}}{n\Lambda_0 T_{sh}^\alpha} \propto V_{sh}^{2(1-\alpha)}$

Consider a radiative shock compressed from equilibrium

The postshock gas does not cool by L', so cooling region is too hot - overpressured.

Extra pressure pushes shock ~~front~~ out.

Now shock velocity is higher ~~than~~ normal

If $\underline{\alpha < 1}$, higher v → longer t_{cool}
postshock continues to push
$\boxed{\text{overstable}}$

If $\alpha > 1$, higher v → shorter t_{cool}
postshock cools, stops pushing

Shocks with α > .75 are stable.

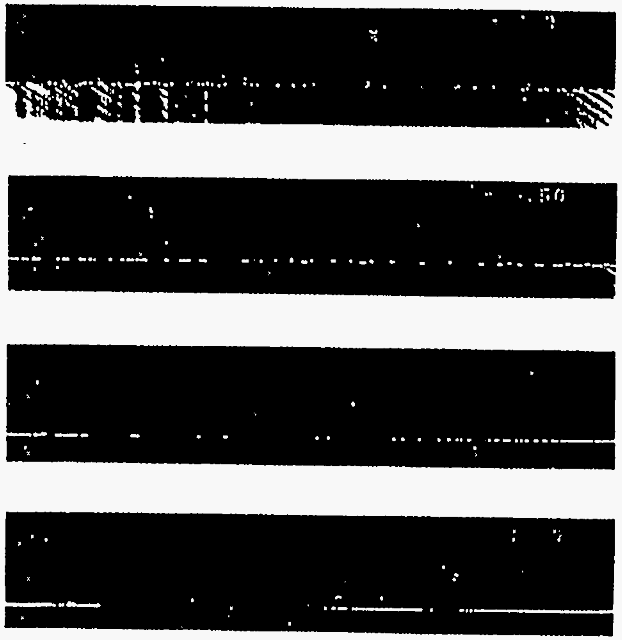

Stability increases with Mach

Instability of Radiative Shock in 2D

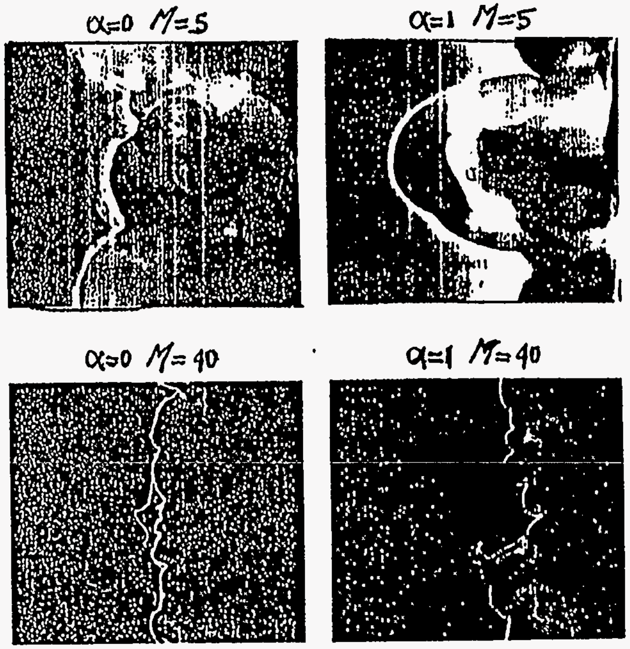

THE SHOCK-BOUNDED SLAB

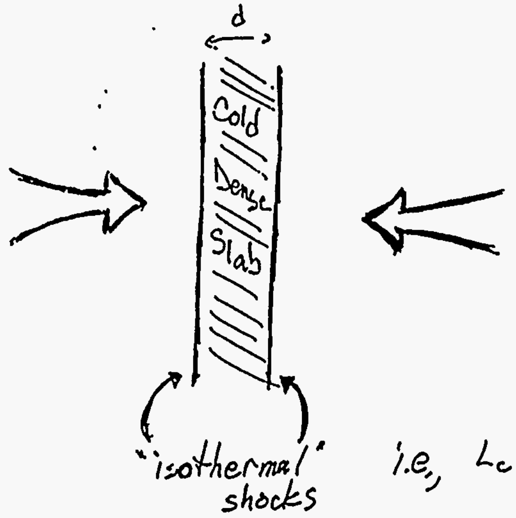

i.e., $L_c \ll d$

[illegible] formation Molecular Clouds.
Stellar Wind.
ff[illegible] - winds, etc.
Formation / Cosmological

Vishniac (1994):

Nonlinear
Thin
Shell
Instability

Cold, Shock-bounded is
- Stable to linear perturbations
- Unstable to nonlinear perturbations

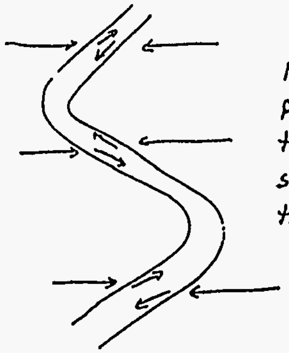

Net transport of positive momentum to parts of the slab displaced in the positive direction.

also Nonlinear Deceleration Instability

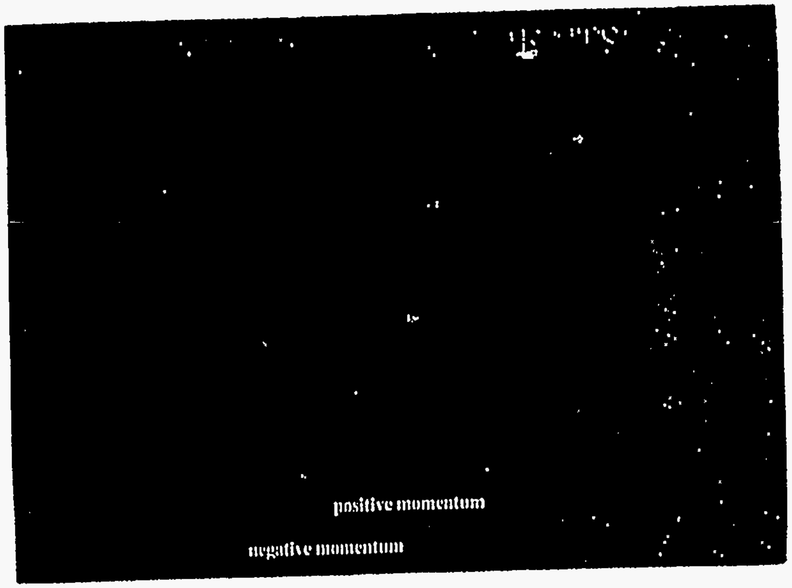
positive momentum
negative momentum

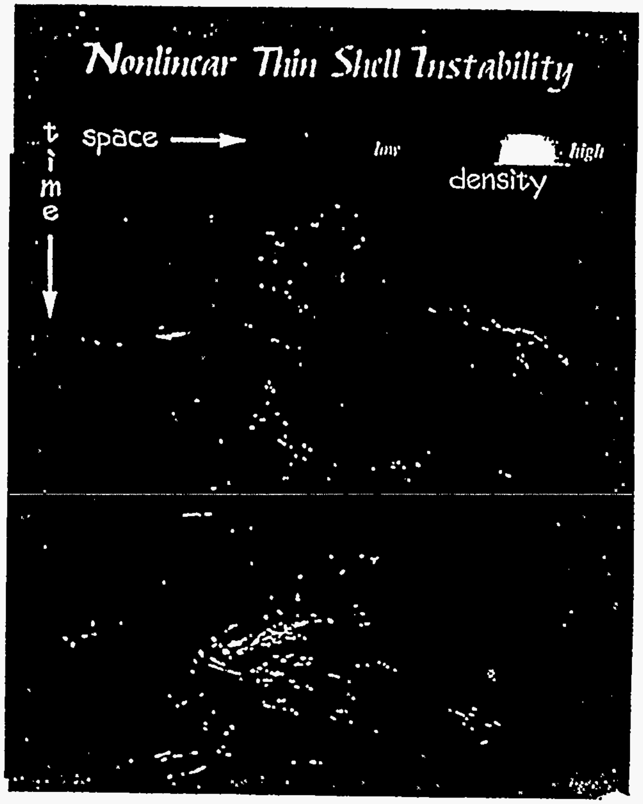
Nonlinear Thin Shell Instability
space
time
low
high
density

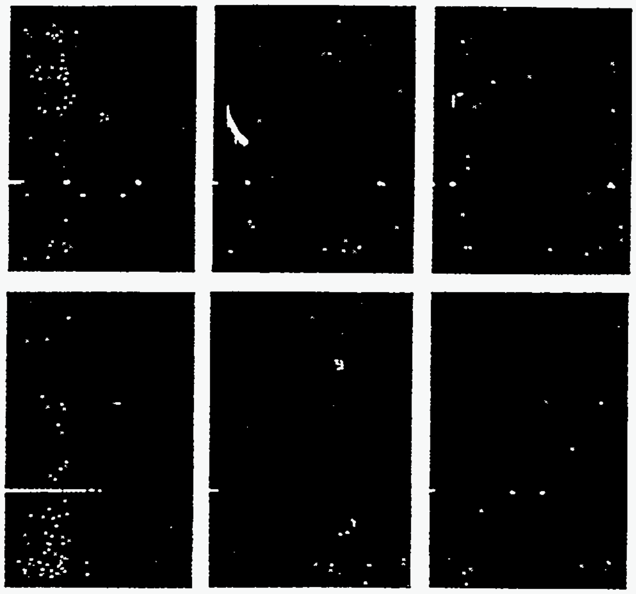

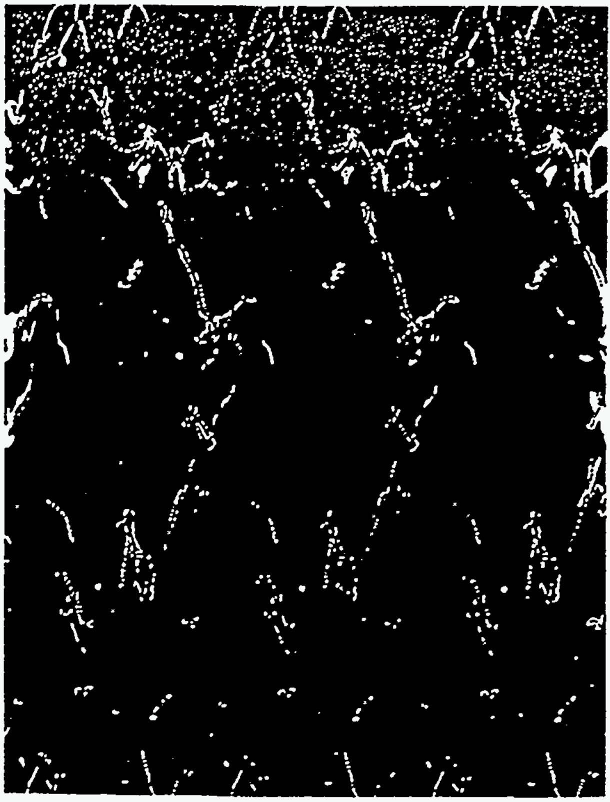

CASSIOPEIA A SUPERNOVA REMNANT: A 2D HYDRODYNAMIC MODEL

Borkowski, Szymkowiak, Blondin Sarazin

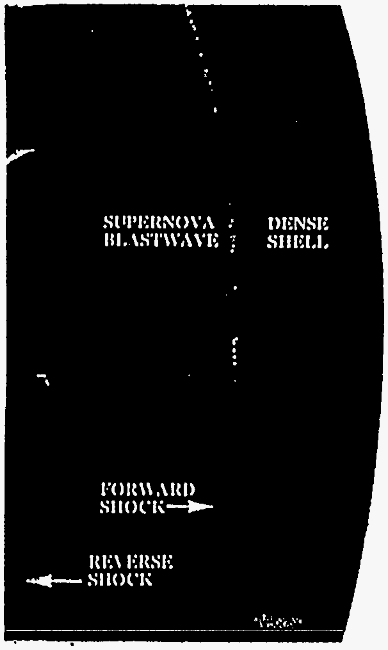

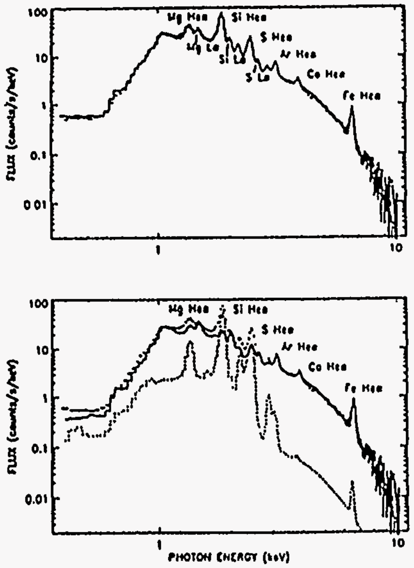

Fig. 2.— The spatially-integrated spectrum of Cas A obtained with the ASCA Solid-state Imaging Spectrometers. The calculated X-ray spectrum is shown by the *solid curve* in the top panel, while the bottom panel shows the contributions from the CSM (*solid curve*) and from the SN ejecta (*dotted curve*) separately. The Ar Heα line at 3 12 keV was not included in these calculations – this line was simply fitted by a Gaussian.

Instability of Hydrodynamic Shocks

Alexei Khokhlov
University of Texas/Austin

Alexi Khokhlov

Type Ia Supernovae

- explosion of a $1.4 \cdot M_\odot$ carbon-oxygen degenerate star.

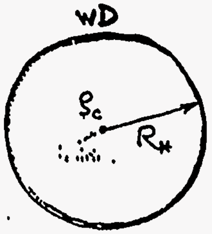

- Mass $\simeq 3.8 \times 10^{33}$ g
  Radius $\simeq 2 \times 10^{8}$ cm
  $\rho_c \simeq 2 \times 10^{9}$ g cm^{-3}
  $a_s \simeq 10^{9}$ cm s^{-1}

- Explosion time $\simeq$ 1 sec.
  Kinetic Energy $\simeq 10^{51}$ ergs.
  Expansion velocity $\simeq 10^{9}$ cm s^{-1}.

- Nickel mass $\simeq 0.5 M_\odot \simeq 10^{33}$ g
  $^{56}Ni \xrightarrow[6.1\,d]{e^-} {}^{56}Co \xrightarrow[78.7\,d]{e^-,\ \beta^+} {}^{56}Fe$
  Luminocity at maximum $\simeq 10^{43}$ ergs per sec.
  $t \simeq 1$ year

FLAME

$^{12}C + {}^{12}C$ heat conduction

δ_ℓ - FLAME THICKNESS : $10^{-2} - 10$ CM
S_ℓ - FLAME SPEED: $10^{7} - 10^{4}$ CM/S

FLAME IS A THIN SURFACE

- $\delta_\ell \ll R_{WD}$
- $U'(\delta_\ell) < S_\ell \iff \lambda_G > \delta_\ell$

$$\lambda_G \simeq \lambda : U'(\lambda) \simeq S_\ell$$

BENCHMARK PROBLEM

FLAME IN A UNIFORM GRAVITY IN A BOX

g, L, S_e, $\frac{\rho_0}{\rho_1}$ $\qquad S_{turb} =:$

- $\frac{\rho_0}{\rho_1} > 1$
- $F_r = \frac{S_e^2}{gL}$
- BOUNDARY CONDITIONS

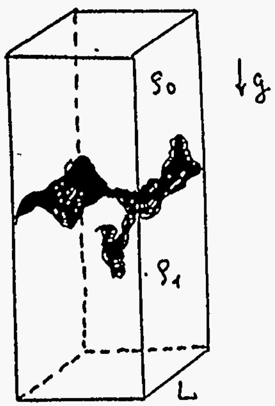

$$S_{turb} = S_e \, f_1(\alpha, F_r)$$
$$= \sqrt{gL} \, f_2(\alpha, F_r)$$

LIMIT $F_r \to 0$

BYOUANCY DOMINATES

$$\boxed{S_{turb} = C \sqrt{gL} \;\; f(\alpha)}$$

- C - ?
- $f(\alpha) = \frac{\alpha-1}{\alpha+1}$ - ?

- Surface $A \propto \frac{1}{S_e}$ - ?

Experimental calibration

(Khokhlov, Oran, Wheeler, 1994)
Combustion & Flame

▲ - SN

● - experiment : $L = 50 cm$, $H = 4 m$
methain
$\phi = 0.6$
$\delta = 0.1$ mm
$g = 980 \frac{cm}{s^2}$
$S_{lam} = 10$ cm/s

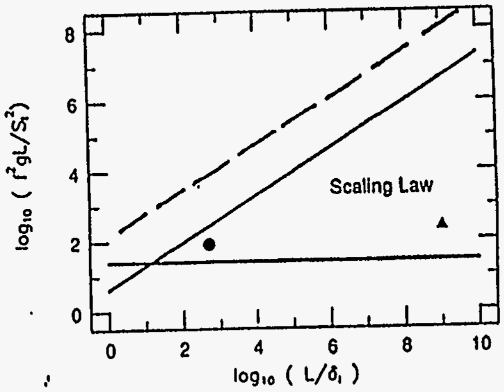

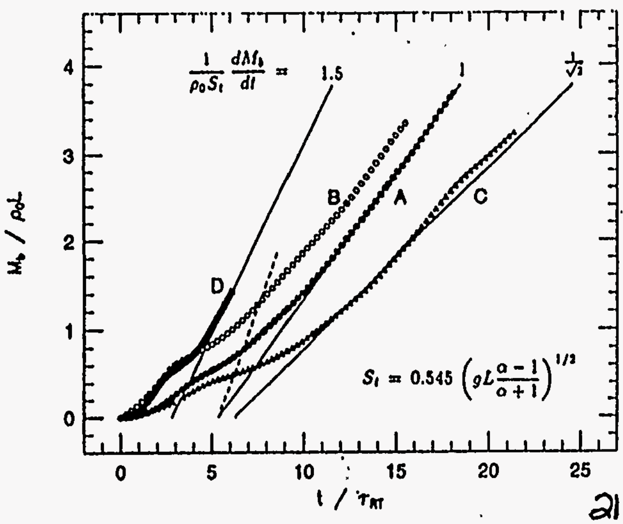

214

Laser-Generated High Mach-Number Shocks in Lab Simulations of Astrophysical Phenomena

Jacob Grun
Naval Research Laboratory

Laser-Generated High Mach-Number Shocks in Lab Simulations of Astrophysical Phenomena

by Jacob Grun

Naval Research Laboratory

Outline

how lasers generate shocks and turbulence

shock wave instability experiment

shock-turbulence interaction experiment

Colleagues:

A. Buckingham, R. Burris, J. Crawford, C. Manka, B.H. Ripin, J. Stamper

---

Laser as a source of shocks, blast waves and turbulence

little mass to obscure hydro
energy density = kjoule/μgram

Naval Research Laboratory

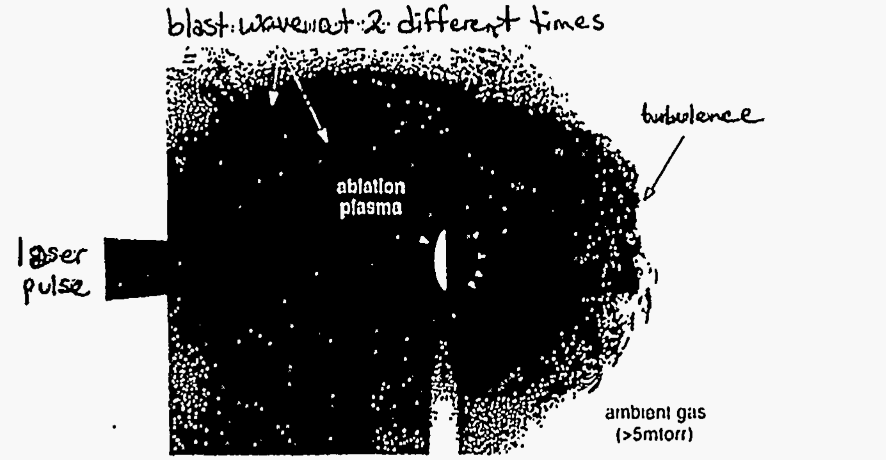

Blast waves in a uniform ambient gas
Are they stable?

Naval Research Laboratory

relevance to astrophysics (from Mac Low and Norman, Astr. J.407, pg. 207 (1993))

filamentary structures in older supernovae

initial conditions for star formation

formation of globular clusters

some theoretical work

Insenberg (1977), Cheng (1979), Book (1980)

Newman (1980), Vishniak (1983), Gaffet (1984)

Bertschinger (1986), Ryu and Vishniak (1987)

Kohberg (1989), Mac Low and Norman (1993)

Typical scales

Naval Research Laboratory

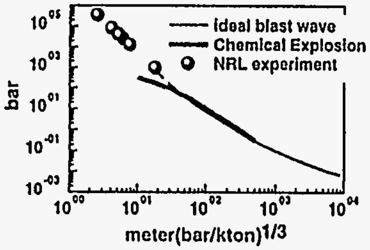

- blast radius: 1cm
- shock width: 100 microns
- Mach number: few hundred

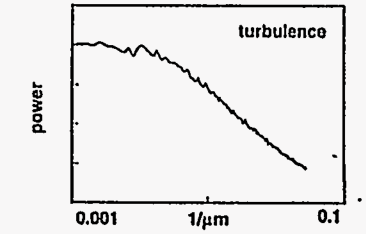

- Kolmogoroff scaling
- flow speed: 10^6 cm/sec
- Reynolds number: 10^6

Setup of experiment

Naval Research Laboratory

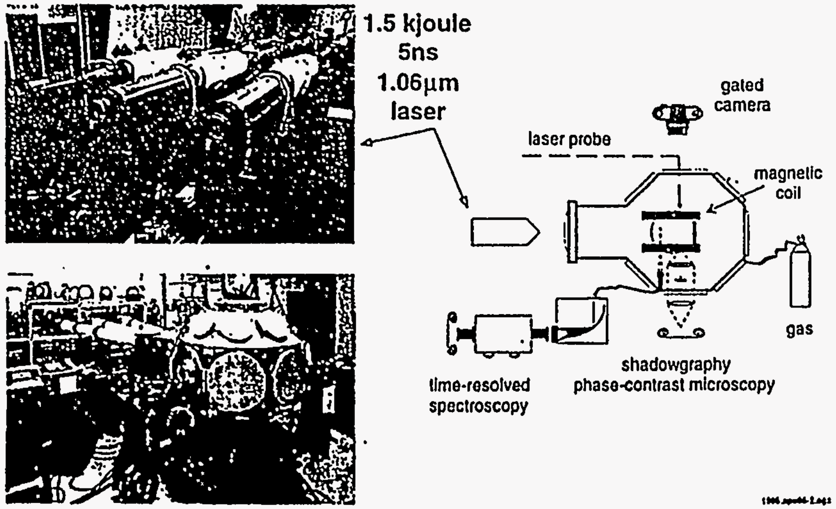

1.5 kjoule
5ns
1.06μm
laser

gated camera

laser probe

magnetic coil

gas

shadowgraphy
phase-contrast microscopy

time-resolved spectroscopy

Blast waves in a low γ gas are unstable

Naval Research Laboratory

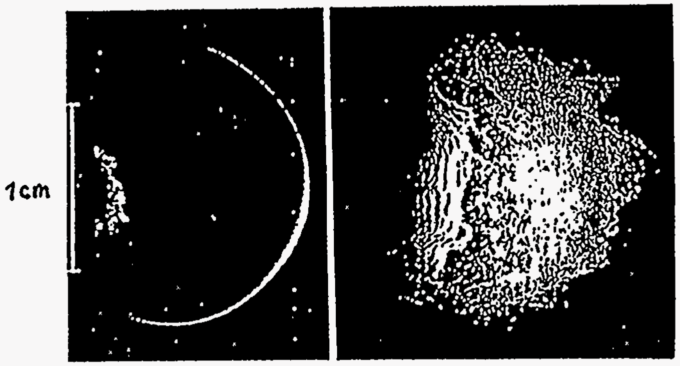

in nitrogen ($\gamma \cong 1.4$)

in xenon ($\gamma < 1.1$)

Progression of perturbation growth

Naval Research Laboratory

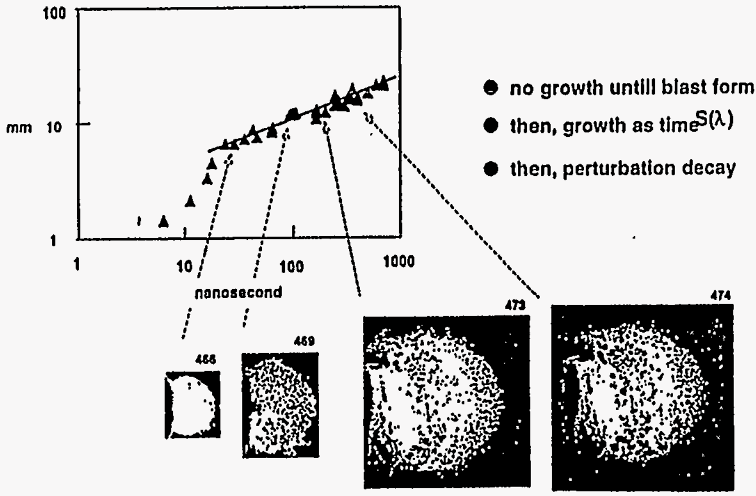

- no growth untill blast formed
- then, growth as time$^{S(\lambda)}$
- then, perturbation decay

1/2

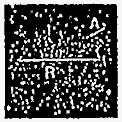

A/R ∝ time$^{S(\lambda)}$

Naval Research Laboratory

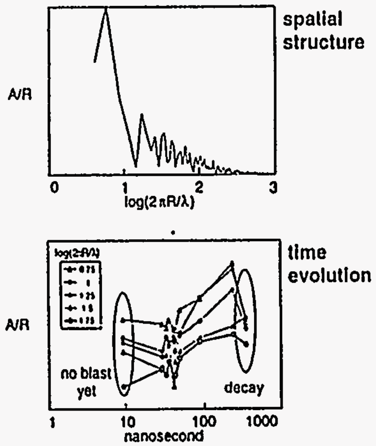

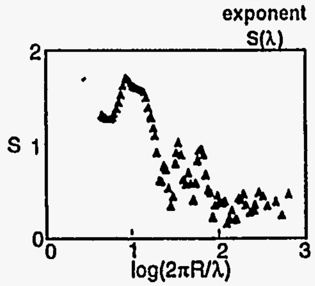

γ of Xenon inferred from Taylor-Sedov solution

Naval Research Laboratory

$$Radius=\left(\frac{(\gamma-1)(\gamma+1)^2}{(3\gamma-1)}E\frac{M_{N_2}}{M}\right)^{1/5}time^{0.4}$$

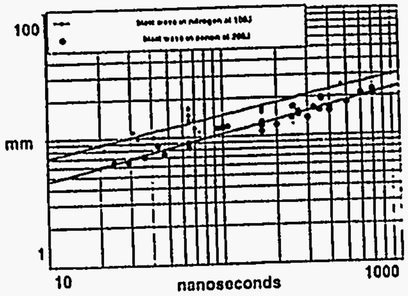

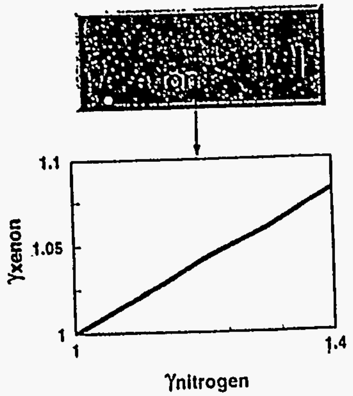

113

γ of xenon lowered by copious emission

Naval Research Laboratory

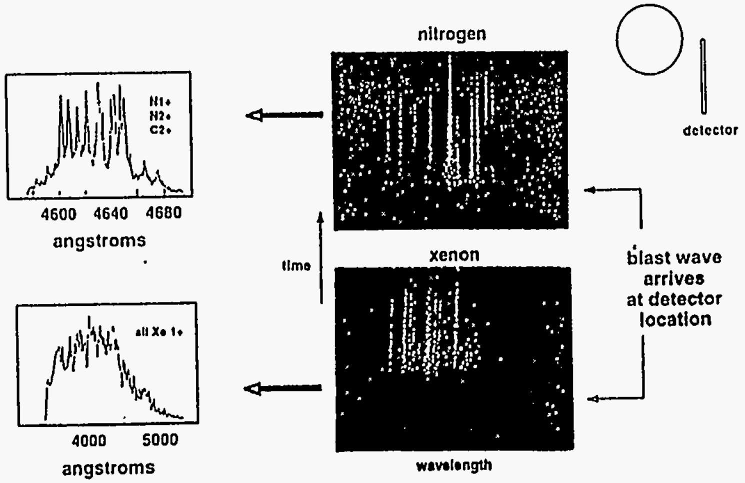

Comparison to theory

source
Linear:Ryu and Vishniac, Astrophys. J., 368, pg. 411 (1991)
Non-linear:Mac Low and Norman, Astrophys. J., 407, pg. 207 (1993)

- experiment confirms Vishniac's prediction of overstability when $\gamma<1.2$
- timeS(λ) growth agrees with linear theory
- But, experimental S(λ) is ~ 2 times larger then predicted

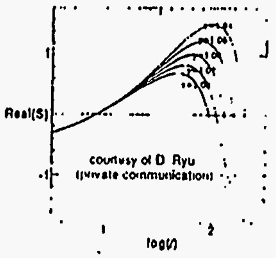

courtesy of D. Ryu
(private communication)

- observed saturation explained by nonlinear theory

Instability mechanism*

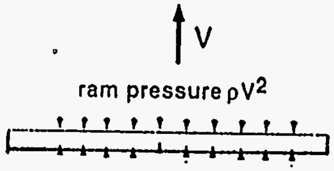

$V >> C_S$

$V < C_S$

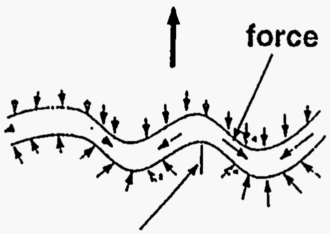

$\delta \propto t^S Y_{lm}$

lighter peak slows faster
occilation produced
growth if $\gamma < 1.2$

---

[*] from E.T. Vishniac, Astr. J. 274, pg. 152 (1983)

Turbulence appears altered by Blast-Wave

Weak-shock theory predicts turbulence amplification & PSD changes

There is no strong-shock theory

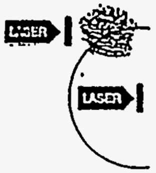

shot 91-518

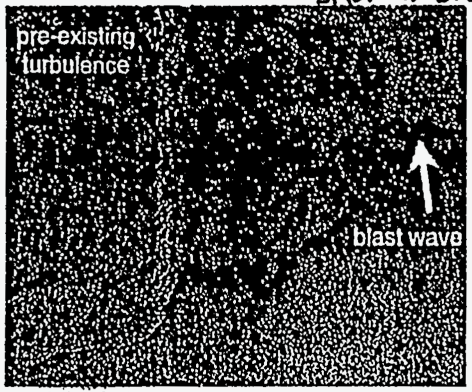

2 cm

NRL Space Plasma

Turbulence amplifcation in nitrogen gas

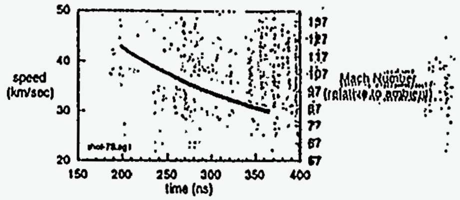

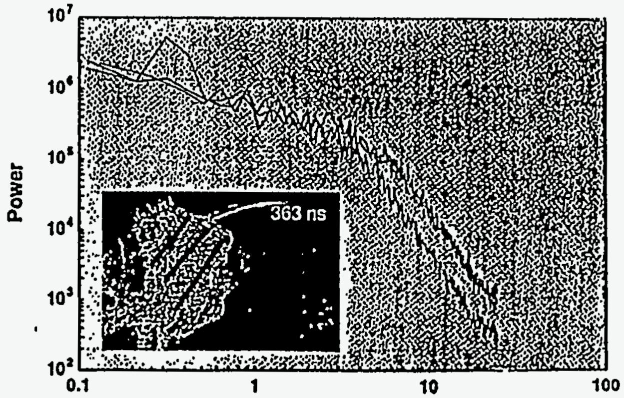

Colliding blast-waves experiment

Scaling: two explosions, 45km apart,
100 kinetic kilotons each, at 150 km altitude

Shot 91-337 (dark-field shadowgraph)

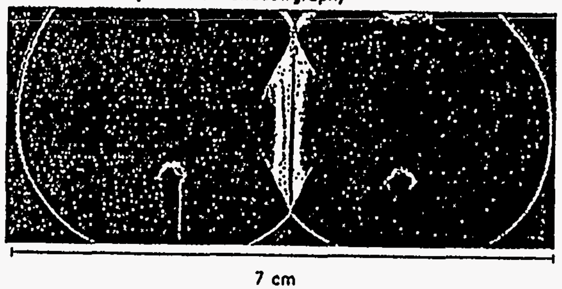

Measurements
- visible emission (gated photography)
- density gradients (darkfield shadowgraphy)
- density profiles (interferometry)
- densities and temperatures (visible spectroscopy)
- source temperatures (x-ray spectroscopy)
- IR emission

HAN9103

NRL space plasma

Some Publications

Spectroscopic Diagnostics in a Colliding-Blast-Wave Experiment
R C Elton, D M Billings, C.K. Manka, H.R. Griem, J Grun, B H. Ripin, and J Resnick
Physical Review E 49, pg 1512 (1994)

Space Plasma Physics in the Laboratory
B.H. Ripin, J. Grun, C K Manka, J. Resnick, and H.R. Burris
Research Trends in Physics: Nonlinear Space Plasma Physics , pg 449- 463, H. Alven, R Bingham, K Quest, and R Z. Sagdeev, editors (AIP Press, NY, 1993)

Numerical Simulations and Experiments on Physics of High Mach Number Shockwave-Turbulent Flow Interactions
A C. Buckingham and Jacob Grun
Proc 4th International Workshop on the Physics of Compressible Turbulent Mixing, eds P. Linden, D Youngs, Cambridge Univ Press (1993).

Instability of Taylor-Sedov Blast Waves Propagating in a Uniform Atmosphere.
J Grun, J. Stamper, C Manka, J Resnick, R. Burris, J Crawford, Phys Rev Lett 66, pg 2738 (1991)

Laboratory Laser-Produced Astrophysical-Like Plasmas
B H Ripin, C.K Manka, T A Peyser, E.A. McLean, J A Stamper, A N Mostovych, J Grun, K Kearney, J R Crawford, J.D Huba, Laser and Particle beams , Vol 8, pg 183 (1990)

Laboratory Laser-Produced Astrophysical-Like Plasmas
B H Ripin, C K Manka, T A Payser, E.A McLean, J. Stamper, A N Mostovich, J Grun, K Kearny, J R Crawford, J.D Huba, pg 196-199, Laser Interaction with Matter, G Velarde, editor (World Scientific, Singapore, 1989)

Progress in Understanding and Modeling of Hydro Instabilities and the Construction of a Turbulent Mixing Model

Dov Shvarts
Nuclear Research Center Negev

Progress in understanding and modeling of hydro instabilities and the construction of a turbulent mixing model

D. Shvarts, U. Alon, D. Ofer

Phys. department
N.R.C.N
ISRAEL

- The basic physics of the mixing zone growth
  → large structures (bubbles) inverse-cascade and not turbulence
- Models to describe the late nonlinear evolution of the instability
  → • bubble-merger model
  • modal model
- Construction of an effective 1D mix model based on the large

---

- Freed, Ofer, Shvarts, Orszag – Phys. Fluids A, 1991
  [illegible] phase flow [illegible]
- Ofer, Shvarts, Zinamon, Orszag – Phys. Fluids B, 1992
  [illegible] late nonlinear stage
- Alon, Mukamel, Shvarts – Phys. Rev E, 1993.
  [illegible] mechanic. models for [illegible]
- Alon, Hecht, Shvarts – Phys Fluids, 1994.
  [illegible] model for 1, 2 modes
- Alon, Hecht, Mukamel, Shvarts – PRL, 1994.
  [illegible] bubble front [illegible]
- Alon, Hecht, Ofer, Shvarts – PRL, 1995.
  [illegible] and bubble scaling law
- Shvarts, Alon, Ofer, McCrory, Verdon – Phys. Plasmas, 1995.
  [illegible] bubble model + modal model in [illegible]
- Hecht, Ofer, Alon, Shvarts, McCrory, Orszag – Laser & Particle Beams, 1995.
  [illegible] modes in planar and sph[illegible] geometry.

<u>submitted:</u>

- Ofer, Alon, Shvarts, McCrory, Verdon – to Phys plasmas (1996)
  2[illegible] modal model
- Alon, Shvarts – to Phys of Fluids (1996).
  [illegible] model

<u>in preparation:</u>

- Ofer, Alon, Shvarts, McCrory, Verdon – 3D [illegible]

Classical experiments can be used to study aspects of the Rayleigh-Taylor and Richtmyer-Meshkov instabilities

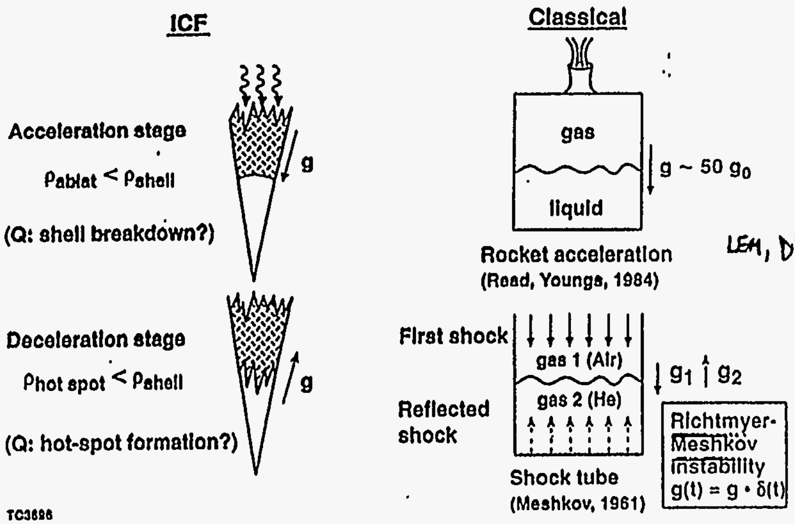

ICF

Acceleration stage

$\rho_{ablat} < \rho_{shell}$

(Q: shell breakdown?)

Deceleration stage

$\rho_{hot\ spot} < \rho_{shell}$

(Q: hot-spot formation?)

Classical

Rocket acceleration
(Read, Youngs, 1984)

LEM, Dimonte

First shock

Reflected shock

Shock tube
(Meshkov, 1961)

Richtmyer-Meshkov instability
$g(t) = g \cdot \delta(t)$

TC3686

The Rayleigh-Taylor (RT) instability

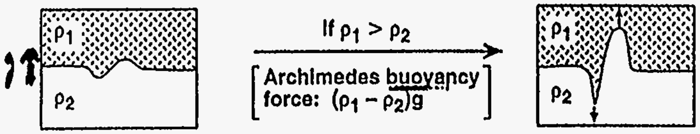

If $\rho_1 > \rho_2$

[Archimedes buoyancy force: $(\rho_1 - \rho_2)g$]

- Linear theory: $a(x,t) = a_k(t) \cdot \cos(kx)$ $(k = 2\pi/\lambda)$

$$\ddot{a}_k = \gamma_k^2 \cdot a_k$$

with $\gamma_k = \sqrt{A \cdot k \cdot g}$ $\left(A = \frac{\rho_1 - \rho_2}{\rho_1 + \rho_2}, \text{ Atwood number}\right)$

$$\longrightarrow a_k(t) = a_k(\bullet) \cdot e^{\gamma_k \cdot t}$$

- Nonlinearity: when $a/\lambda \gtrsim 0.1$ $(ka \gtrsim 1)$ – kinematic drag becomes important

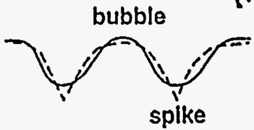

$\longrightarrow$ growth slowing down (saturation)
$\longrightarrow$ rounding of bubble tips
$\longrightarrow$ appearance of higher harmonics
$\longrightarrow$ bubble/spike structure

TC3691

Richtmyer-Meshkov Modeled by Initial Velocity and g=0

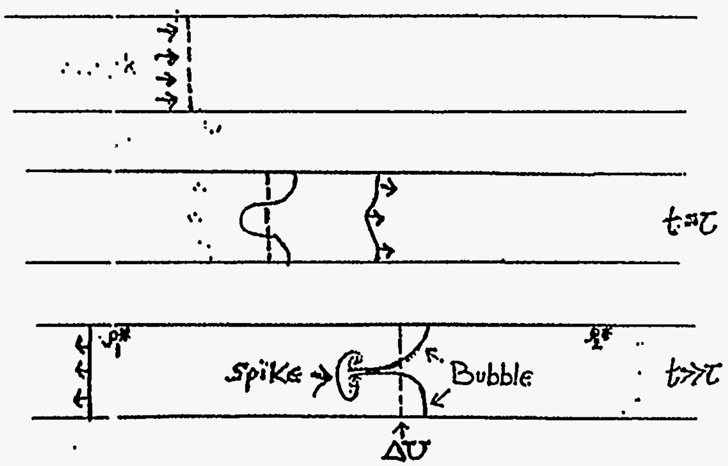

- Shocks don't interact with interface after
  $\tau \sim \lambda / \mathit{Shock\ Speed} \sim \lambda / \Delta U$
- Initial velocity from linear theory
  $u_0 = \tilde{a}_0 k \tilde{A} \Delta U$ · $a_0 k << 1$

[Richtmyer (60), Meyer-Blewett (72), Holmes-Grove-Sharp (94), Yang-Zhang-Sharp (94)]

Scaling from Simple Buoyancy and Drag Considerations

[Youngs (89), Takabe,Yamamoto (91), Alon,Hecht,Ofer,Shvarts (95)]

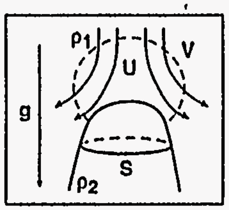

$S \sim \lambda^2,\ V \sim \lambda^3$

- In the bubble Frame:

$$\underbrace{\rho_1 V \frac{dU}{dt}}_{\text{"}na\text{"}} \sim \underbrace{-\rho_1 S U^2}_{drag} + \underbrace{(\rho_1 - \rho_2) g V}_{buoyancy}$$

- Drag/Buoyancy $\sim S / V \sim 1/\lambda$

$\boxed{\text{Large structures rise faster} \longrightarrow \text{Inverse cascade}}$

$\longrightarrow$ rounded tips

- RT (drag $\underset{\dot{v}=0}{\approx}$ buoyancy) : $\boxed{U \sim \sqrt{g\lambda}} \cdot \sqrt{\frac{2A}{1+A}}$
- RM (no buoyancy, only drag): $\boxed{U \sim \lambda / t}$ no A dependence.

  $\dot{U} \sim U^2/\lambda$

Late stage mixing zone structure for a
2-D random initial perturbation (A=0.5)

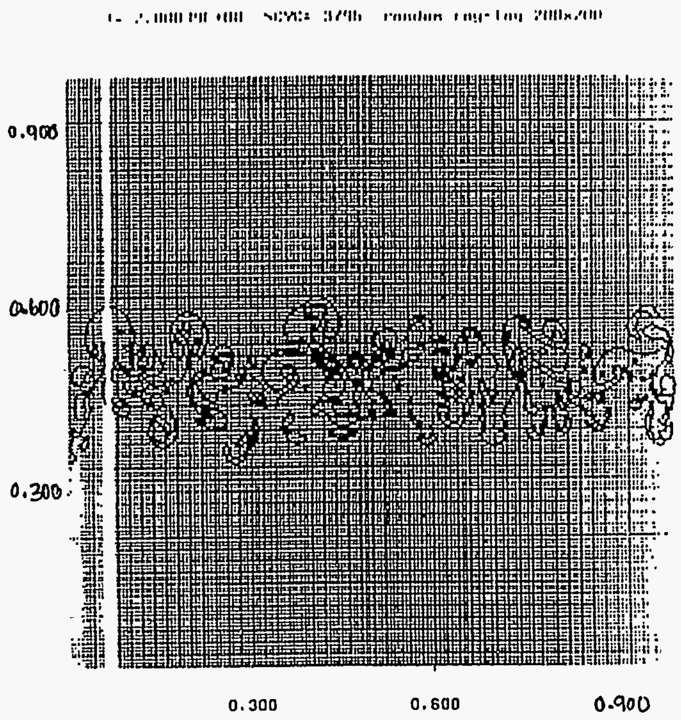

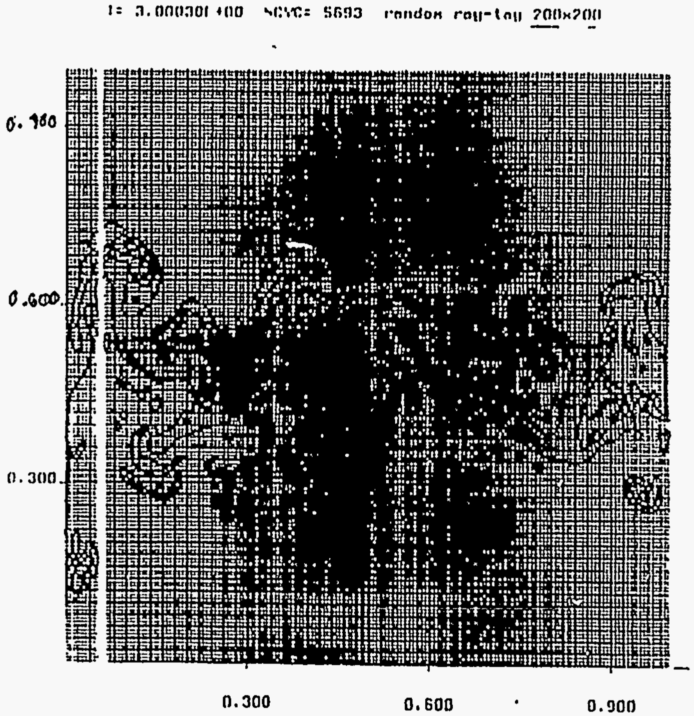

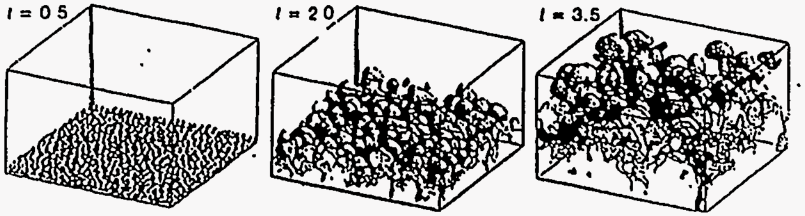

FIGURE 1. Iso-surfaces of $f_1 = 0.99$ for the three-dimensional Rayleigh-Taylor calculation in the region $x < 0$. Gravity acts vertically downward.

D. Youngs (1995)

Rayleigh-Taylor growth at the ablation front is see both from the surface finish and from laser imprinting

Indirect drive

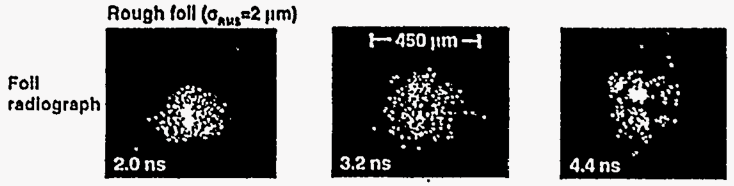

Remington *et al.*, Phys. Fluids B 5, 2589 (1993)

Direct drive (0 bandwidth)

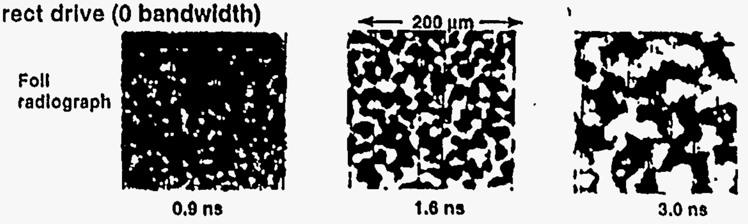

Glendinning (LLNL), Knauer (LLE)

Large structure dominates the late time flow even with no initial long-wavelength perturbation

D. Ofer - LEEDR2D)

Classical RT (A = 0.5)

initial spectrum: ℓ = (40 - 80)

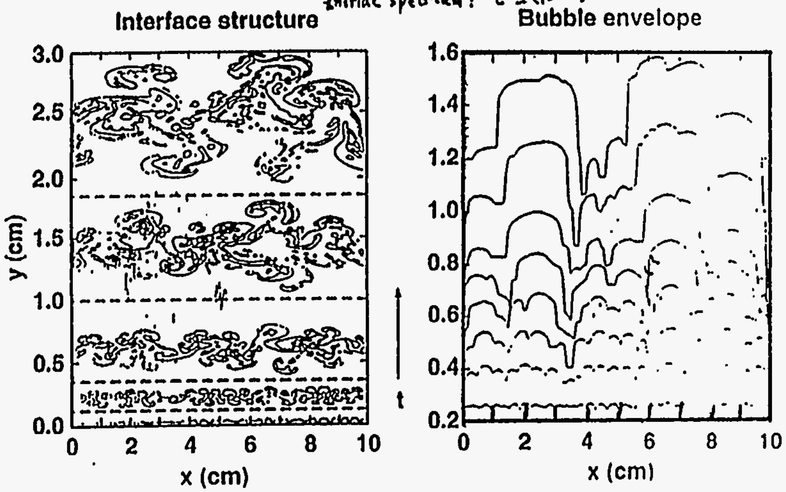

TC3679

Simulation of multimode Richtmyer-Meshkov instability shows bubble competition

(A = 0.98)

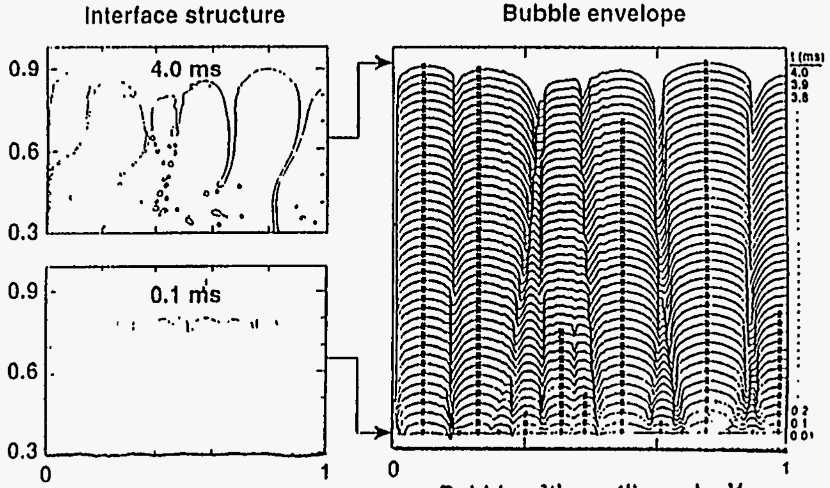

- Bubble with positive velocity

Early-stages evolution of a random initial mass perturbation (rms = 2 µm) under ablation condition ($I \cdot 10^{14}$ W/cm^2, τ_{rise} = 1 ns, λ_L = 0 53 µm, Δ_{CH_2} = 20 µm)

(Density contours)

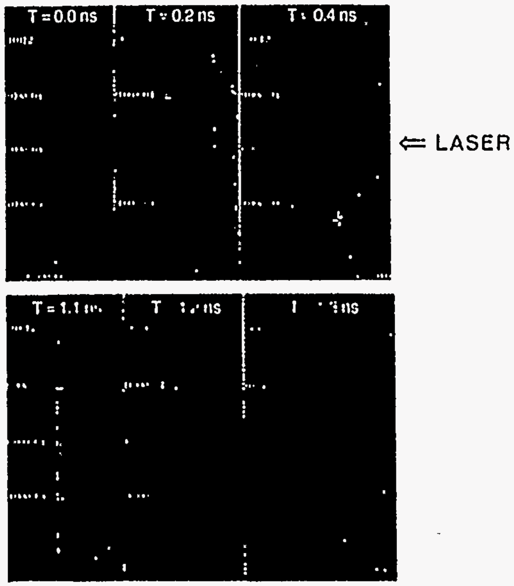

FC3701

Bubble dynamics and competition are clearly seen while spikes are washed downstream

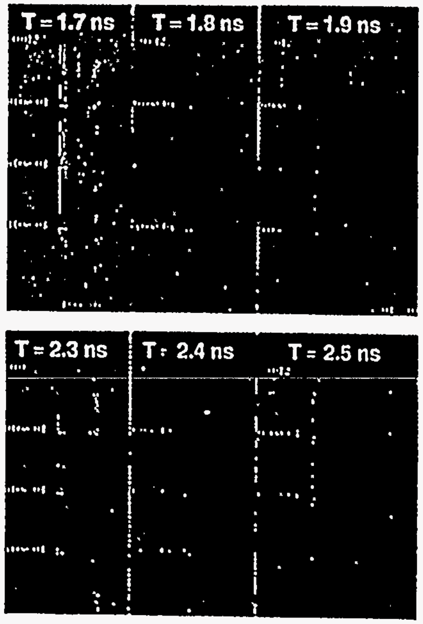

At late stage, few bubbles are controlling the front evolution and punching the shell

UR LLE

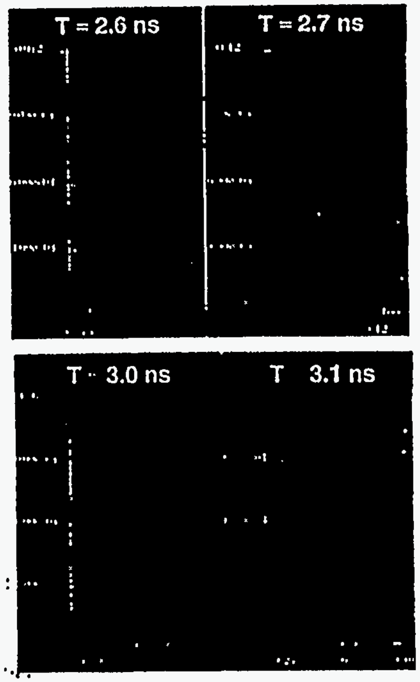

TC3703

3-D bubble competition is clearly seen for a 3-D isotropic short-wavelength initial perturbation

UR LLE

(D. Ofer - LEEOR3D)

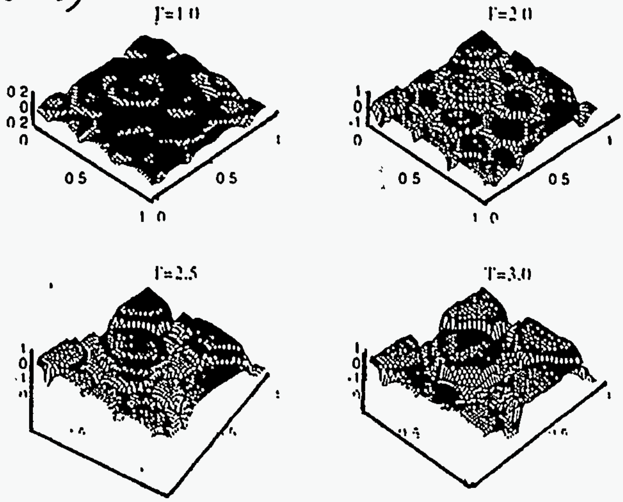

In the multimode case nonlinearity is leading to the creation of large structures together with the saturation of small structures

UR LLE

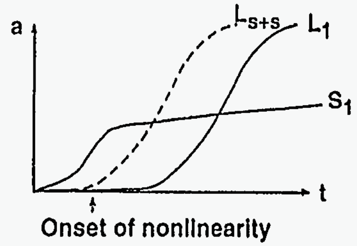

Onset of nonlinearity

[illegible]

S_1 - [illegible] 1-mode growth

L_{s+s} - long w.l. growth from short mode-coupling

Mode coupling:

- Generation of higher harmonics ($k_1, k_2 \rightarrow \underline{k_1 + k_2}$)
  → saturation of small structure (decreasing S/V by rounding the tips)
- Generation of long wavelengths ($k_1, k_2 \rightarrow \underline{k_1 - k_2}$)
  → large-structure seeding and growth (decreasing S/V by increasing λ)

1C3097

Two approaches to overcome the divergence problems

The Modal Approach

(K-space)

- **Use the basic modes—cos(kx)**
- **Take only 1,2 mode interaction into account**
- **Use a mean-field approach for all higher-order contributions**
  - **a nonlinear closure**

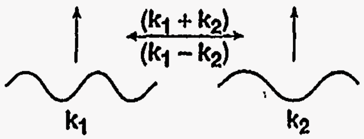

+ nonlinear closure

The Bubble Approach

(Physical space)

- Use late-stage "dressed" nonlinear elements—Bubbles (harmonic information already included)
- Write an evolution equation for ensemble of bubbles with an effective 1,2 bubble interaction

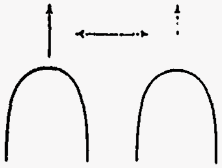

bubble bubble

TC3695

Bubble-Merger Model Gives Multi-Mode Evolution from 1 and 2 bubble physics

Sharp and Wheeler (61), Glimm, Sharp, Zhang (88-91)
Alon, Shvarts, Mukamel (93)

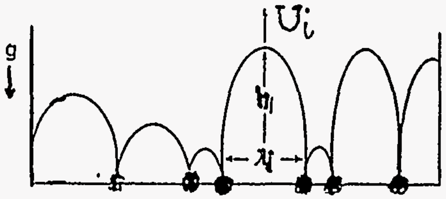

- Single-Bubble Velocity

$$\text{RT: } U_i = c_1\sqrt{g\lambda_i}$$
$$\text{RM: } U_i = c_1\lambda_i / t$$

- Two-Bubble Merger, $\omega(\lambda_i, \lambda_{i+1})$

$$\lambda_i, \lambda_{i+1} \xrightarrow[\omega]{} \lambda_i + \lambda_{i+1}$$

Mean-field model equation (no correlations) gives the main properties of the bubble distribution time evolution

$g(\lambda, t)$ – number of bubbles of size $(\lambda, \lambda + d\lambda)$

$N(t) = \int_0^\infty g(\lambda, t)\, d\lambda$ – total number of bubbles at time t

$$\boxed{\begin{aligned} N(t)\cdot\frac{\partial g(\lambda,t)}{\partial t} &= -2\cdot g(\lambda,t)\cdot\int_0^\infty g(\lambda',t)\cdot\omega_m(\lambda,\lambda')\,d\lambda' && \underline{\text{(Death)}} \\ &+\int_0^\lambda g(\lambda-\lambda',t)\cdot g(\lambda',t)\cdot\omega_m(\lambda-\lambda',\lambda')\,d\lambda' && \underline{\text{(Birth)}} \end{aligned}}$$

Basic features:

$$\frac{dN(t)}{dt} = -\langle\omega\rangle\cdot N(t) \rightarrow N(t) \quad \text{decreases}$$

$$\rightarrow \langle\lambda(t)\rangle \quad \text{increases}$$

$$\rightarrow \langle v(t)\rangle \sim \langle\sqrt{\lambda(t)}\rangle \quad \text{increases}$$

TC3574

Single-Model RM Bubble goes as $U \sim \lambda / t$

- At $A = 1$, Potential Flow model

[RT - Layzer (55), RM - Hecht, Alon, Shvarts (94)]

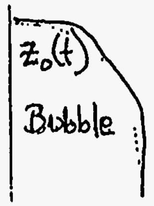

$\nabla^2 \phi = 0$

$\phi = a(t) \cos kx\, e^{-kz}$

$Z_0(t)$

RT: $U = 0.23\sqrt{g\lambda}$

Bubble velocity: dashed=simulation, full line=potential flow model

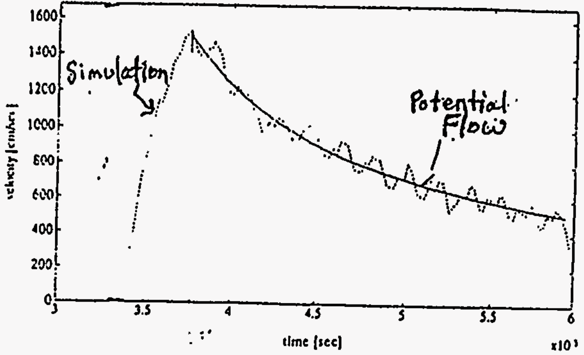

RM.

Bubble competition is described by the potential flow model

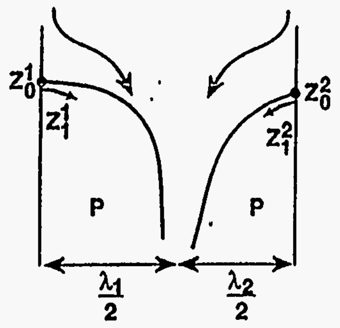

$$\phi(x,z,t)=\sum_{n=1}^{3} a_n(t)\cdot \cos(n\cdot k\cdot x)\cdot e^{-n\cdot k\cdot z}$$

$$k=\frac{2\pi}{(\lambda_1+\lambda_2)}$$

$$+\begin{cases}\phi+\frac{1}{2}v^2+gz=\text{const}\\ v_z=\frac{DZ}{Dt}\Big|_{\text{Interface}}\end{cases}$$

Linearizing the equations near the tip

⇓

7 ODE's for: z_0^1, z_0^2, z_1^1, z_1^2

a_1, a_2, a_3

TC3577

Dynamics of two-bubble competition

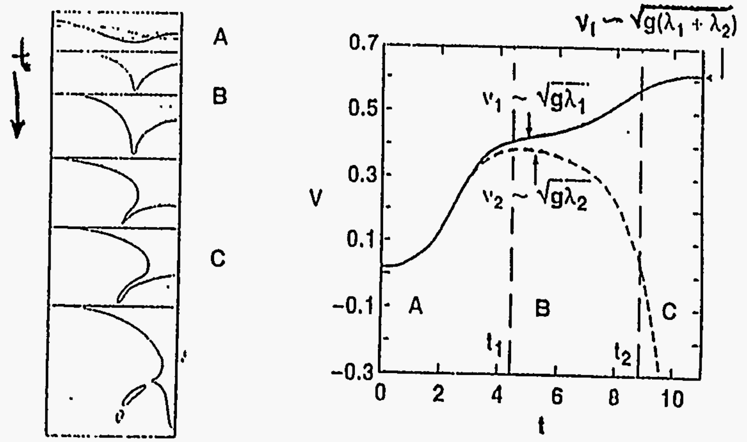

A. Exponential growth
B. Coexistence
C. Overtake

$$\Delta t_{merge}=t_2-t_1$$

$$\omega(\lambda_1,\lambda_2)=\frac{1}{\Delta t_{merge}}$$

Bubble Front Reaches Scale Invariant Regime, where $h/\langle\lambda\rangle$ is Constant

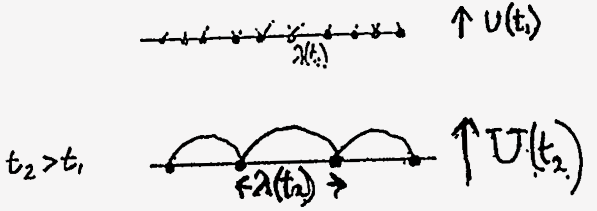

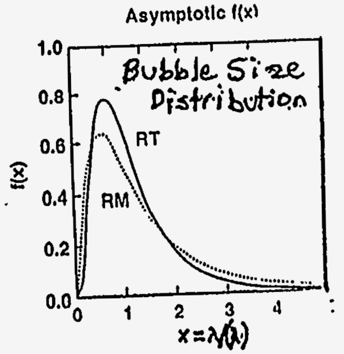

$$\frac{dh_B}{dt} = \langle u(\lambda)\rangle_f$$

- $f(\frac{\lambda}{\langle\lambda\rangle})$ independent of initial pertubation.

Using Single-Mode Velocities and Merger-Rates Yields Multi-Mode Scaling

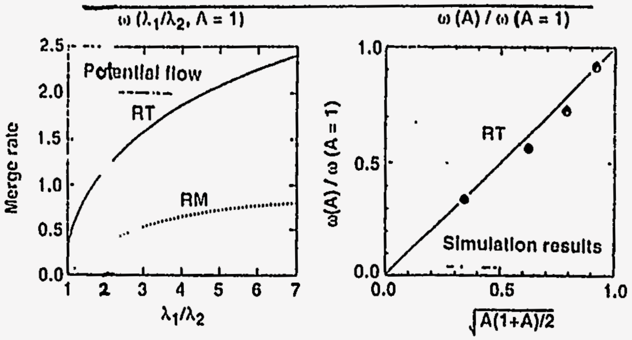

- Bubble penetration from mean velocity

$$\frac{dh_B}{dt} = \langle U(\lambda)\rangle_f$$

RT Bubble Front: $\boxed{h_B \cong \underline{0.05Agt^2}}$

New Power-Law Scaling for the RM Bubble Front

- RM bubble-front penetration

$$\boxed{h_B \cong a_B(u_o t / \lambda_o)^{0.4}}$$

- **Power law - "no gt^2"**

- **Depends on u_o, λ_o**

λ_o- initial mean wavelength

$$u_o \cong \underbrace{\tilde{a}_o}_{\substack{\text{initial}\\ \text{amp.}}} \frac{2\pi}{\lambda_o} \tilde{A} \Delta U$$

1- Bubble equation of motion :

$$V \rho_h \dot{U} = -S\rho_h \cdot U^2 + V(\rho_h - \rho_L) g$$

$$V/S \sim \lambda$$

$$\rho_h \dot{U} = - C_D \rho_h U^2/\lambda + C_B(\rho_h - \rho_L) g$$

Layzer 1955: in 2D, for $\rho_h >> \rho_L$:

$$C_D = \frac{1}{2} \quad , \quad C_B = 3\pi$$

asymptotic velocity:

RT: $U = \sqrt{\frac{1}{6\pi}} \sqrt{g\lambda}$

RM $U = \frac{1}{3\pi} \lambda/t$

The Multi-Bubble case.

from statistical model. $h_B(t) \sim \frac{1}{4} \lambda_{eff}(t)$

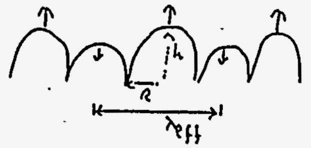

- for min (S/V) : $h \approx R$ (round tip)
- bubble competition: $\lambda_{eff} \approx 4R$

$$\Downarrow$$

$$\boxed{h_B \cong \frac{1}{4} \lambda_{eff}}$$

RT: $\dot{h}_B(t) = U(t) = \sqrt{\frac{1}{6\pi}} \cdot \sqrt{g \lambda_{eff}(t)} \cong \sqrt{\frac{4}{6\pi} \cdot g \cdot h_B}$

$$h_B = \alpha g t^2$$

$$\boxed{\alpha \approx 0.06}$$

RM: $\dot{h}_B(t) = U(t) = \frac{1}{3\pi} \cdot \lambda/t \approx \frac{4}{3\pi} \cdot h_B/t$

$$h_B \sim t^{\theta}$$

$$\boxed{\theta \cong 0.4}$$

The spike front evolution is determined by the dominant bubble structure at each time

Spikes have similar periodicity as bubbles

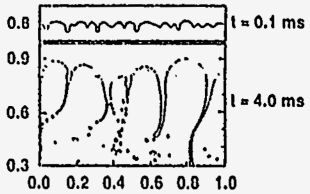

Single-mode spike/bubble structure at $h_B/\langle\lambda\rangle \cong 0.26$

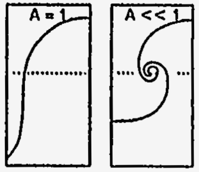

$\Longrightarrow$ $\boxed{dh_s/dt = \langle u_s(\lambda)\rangle \text{ when } h_B/\langle\lambda\rangle \cong 0.26}$

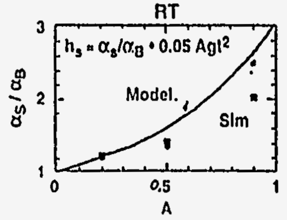

TC3697

$h_B, h_s \sim g t^2$

$$\Downarrow$$

$TMZ \sim g t^2$

RM Spike and Bubble Fronts have *Different* Power Laws

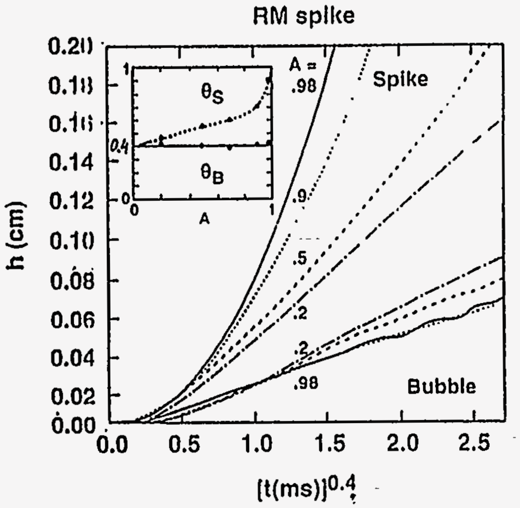

A=|postshock Atwood num.

RM:

$$h_s \sim t^{\theta s(A)}$$

$$\theta_S = \begin{cases} 0.4 & A \to 0 \\ 1.0 & A \to 1 \\ & \text{(free coast)} \end{cases} \Rightarrow TMZ = h_B + h_s \neq t^{\beta}$$

Experiments Welcome!

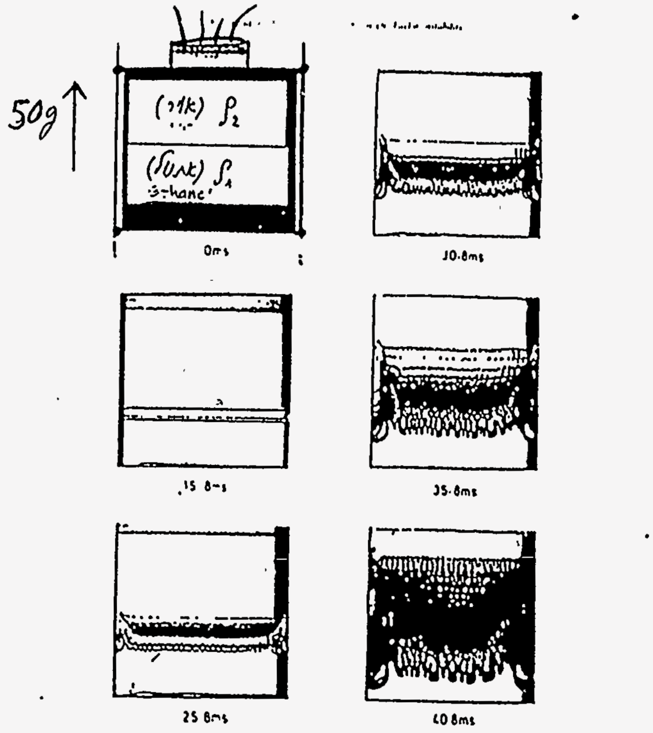

LEM Experiment Utilizes Modern Techniques & Reaches Turbulence Criterion

- **Linear electric motor (LEM)**
  - Variable acceleration
  - Deceleration for "de-mixing"
- **Laser Induced fluoresence (LIF)**
  - High resolution 2D images
  - No edge effects
- **Particle Imaging velocimetry (PIV)**
  - Measures turbulent energy
- **Radiography**
  - Turbulent mix distribution

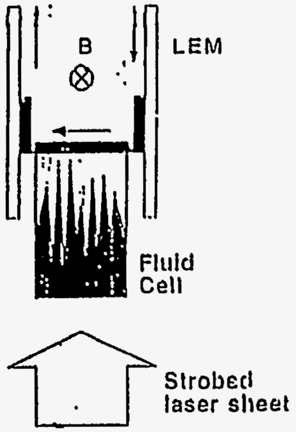

Displacement (250 cm) >> Fluid size (10 cm) >> Shortest scale (.05 cm)

- Multi-Mode Bubble Front Penetration

$RT \sim 0.05Agt^2, \qquad RM \sim (u_0t/\lambda_0)^{0.4}$

- Multi-Mode Spike Front Penetration

$RT \sim \alpha_S(A)Agt^2, \qquad RM \sim (u_0t/\lambda_0)^{\theta(A)}$

$TM\ z_{eT} \sim gt^2 \qquad TM\ z_{em} \neq t^{\beta}$

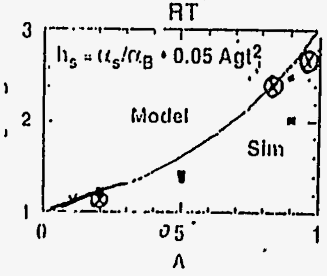

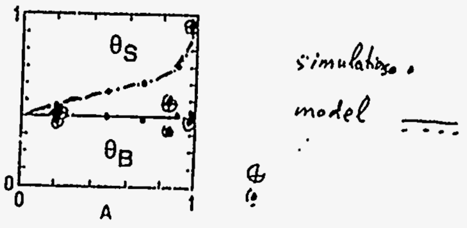

New nonlinear model accounts for mode generation via two-mode coupling and for mode saturation

- One- and two-mode interaction

$$\ddot{a}_{\underline{k}} = \gamma_{\underline{k}}^2 \cdot a_{\underline{k}} + A \cdot k \cdot \sum_{\underline{k}'} \left(\alpha_{\underline{k},\underline{k}'} \, \dot{a}_{\underline{k}'} \cdot \dot{a}_{\hat{\underline{k}}'} + \beta_{\underline{k},\underline{k}'} \, \ddot{a}_{\underline{k}'} \cdot a_{\hat{\underline{k}}'} \right)$$

$$\left(\hat{\underline{k}}' = \underline{k} \pm \underline{k}' \right)$$

(linear) (mode coupling)

- Nonlinear closure (Haan's saturation)

for $a_{\underline{k}} \geq a_{\underline{k}}^{sat}$ use $\dot{a}_{\underline{k}} \leq \dot{a}_{\underline{k}}^{sat}$

as an average description of all higher nonlinear contributions.

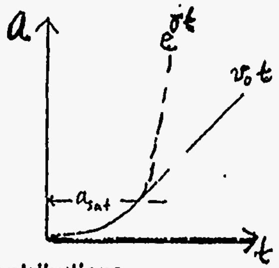

TC3669

Haan's band saturation model is a nonlinear closure that represents the average effect of all higher-order contributions

Initial mode spectrum: ℓ = 40–80 only

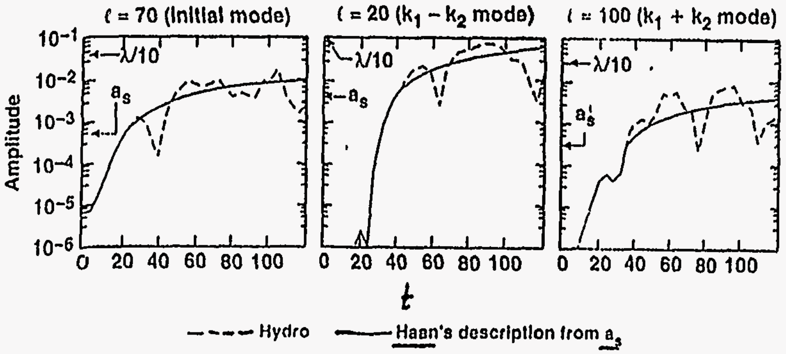

TC3680

The classical Rayleigh-Taylor case (Read & Youngs) is a mode-coupling (M.C.) dominated case—new model predicts both mode generation and saturation

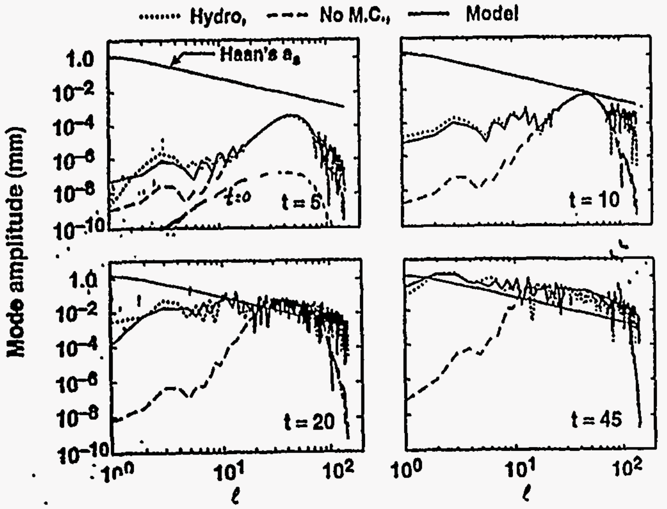

TC3676

The new model can reasonably predict the interface structure in late nonlinear stages

ICF case (A = 1)

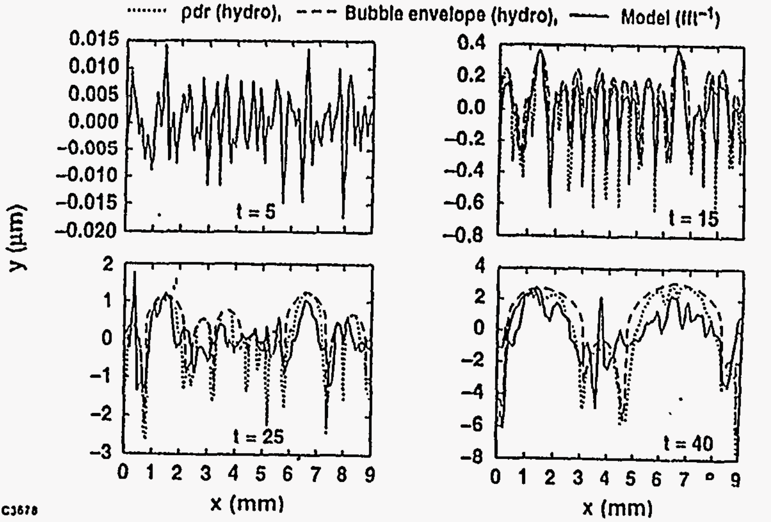

TC3678

Late time 3-D structure of an ICF Hot-Spot interface for a ($l=6$, $\cos(4\Phi)$) 10% initial velocity perturbation

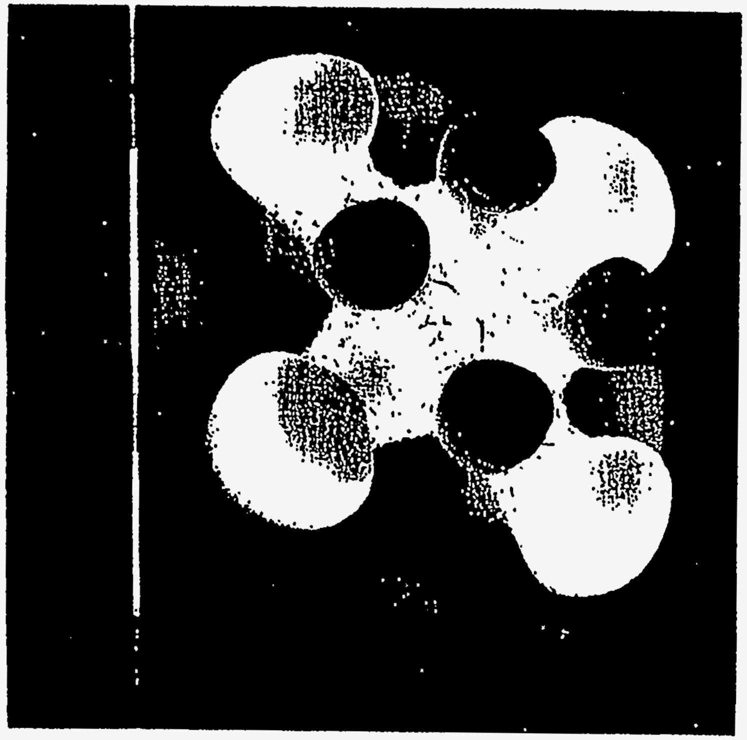

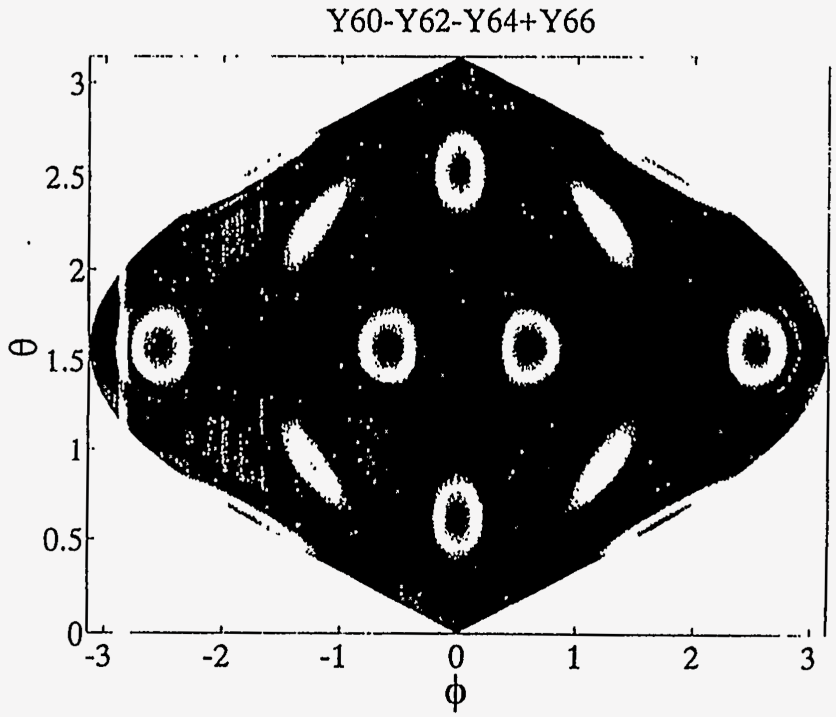

Late time 3-D structure of an ICF Hot-Spot interface for a (l=6, random m's) 10% initial velocity perturbation

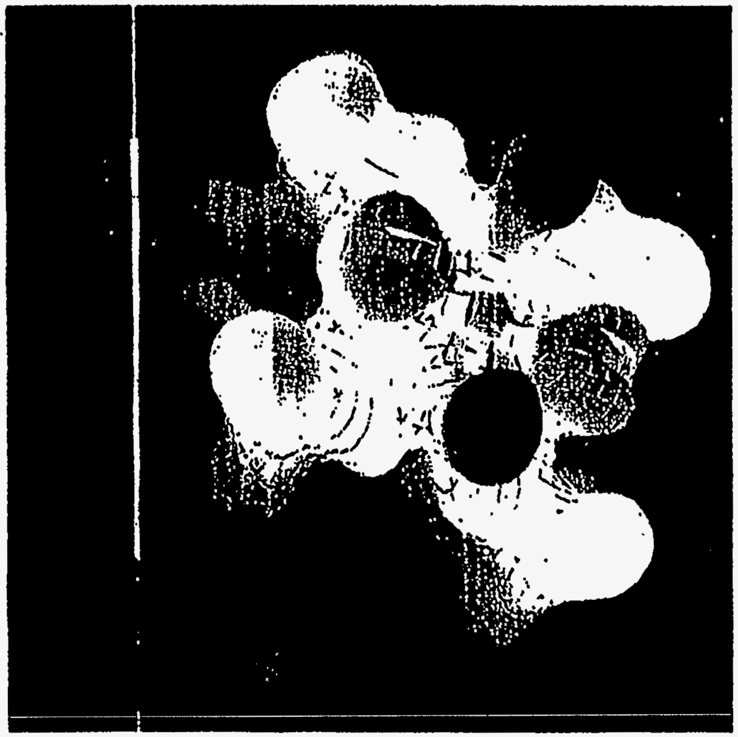

① Bubble and Spike fronts:

Large structure physics.

- bouyancy
- drag
- bubble merging

a 2 phase - flow description

$$\boxed{\frac{dU_i}{dt} = C_{B,i}(A) \cdot g(t) - C_{D,i}(A)\,\frac{U_i|U_i|}{L_i(t)}}$$

(i = bubble, spike)

- use Layzer's parameters:

$$C_{B,b} = C_{B,s} = 1/_2 \cdot A$$
$$C_{D,b} = 3\pi$$
$$C_{D,s} = \pi \cdot [4/F(A) - 1]$$

- use 2 scale length $L_b(t)$, $L_s(t)$

$$\boxed{\dot{L}_i = \beta\, U_i \quad \text{with } L_i(0) = \bar{\lambda}_0}$$

- $\beta = 0$ - 1-mode Layzer's result
- $\beta \cong 2\pi$ - bubble-merger Scaling laws for RT + RM bubble + spike fronts !!

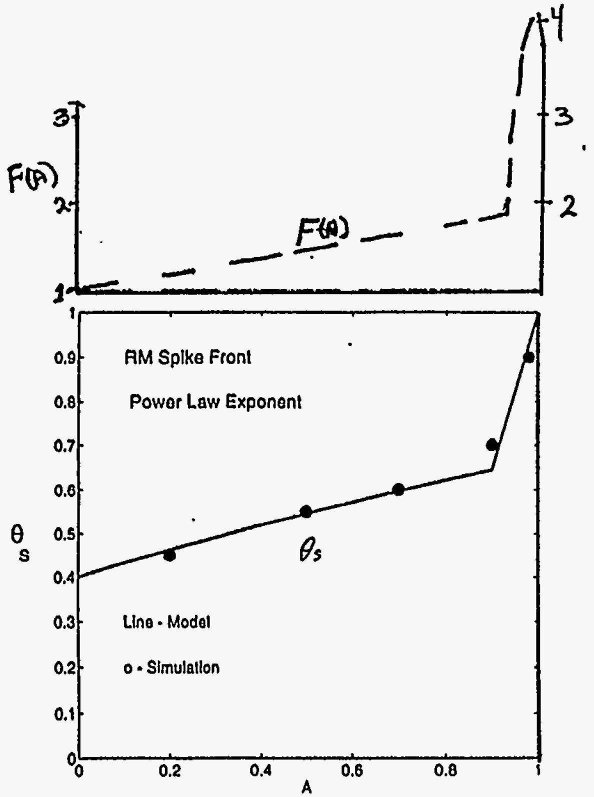

$$\text{Using}: F(A) = \frac{\alpha_s}{\alpha_b} = \begin{cases} 1+A & A \le 0.9 \\ 21(A-0.9)+1.9 & A > 0.9 \end{cases} \longrightarrow 4 \text{ for } (A=1)$$

$$\Downarrow$$

$$\theta_s \approx 0.4(1+A) \quad (A \le 0.9)$$
$$\rightarrow 1.0 \quad A > 0.9$$

② Mixing zone inner structure:

mass conservation eq:

$$\frac{\partial f_i}{\partial t} = \nabla(f_i u_i)$$
$$= \nabla(D \nabla f_i)$$

with $D(x) = \frac{u_i f_i}{\nabla f_i}$

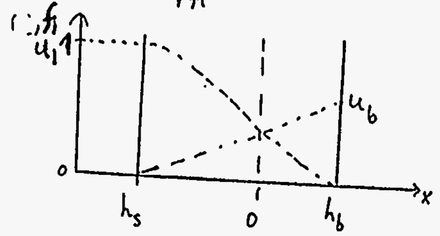

for $A \ll 1$: f_i, u_i are linear and $h_b \approx h_s$

$\Rightarrow D(x)$ is parabolic.

we try to use parabolic (asymetric) for all A's and $g(t)$

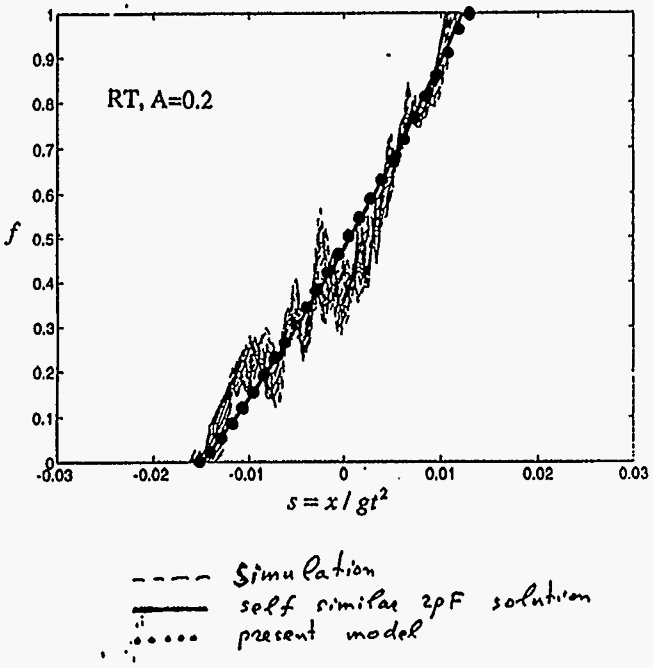
RT, A=0.2
f
1
0.9
0.8
0.7
0.6
0.5
0.4
0.3
0.2
0.1
0
-0.03
-0.02
-0.01
0
0.01
0.02
0.03
$s = x / gt^2$
Simulation
self similar 2pF solution
present model

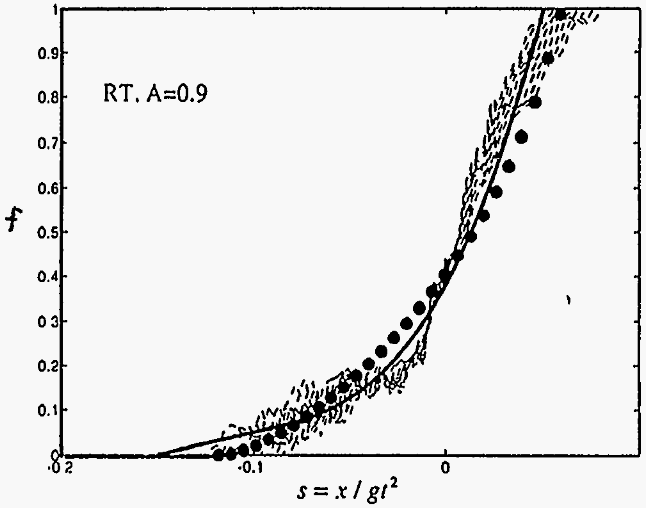
RT. A=0.9
f
1
0.9
0.8
0.7
0.6
0.5
0.4
0.3
0.2
0.1
0
-0.2
-0.1
0
$s = x / gt^2$

276

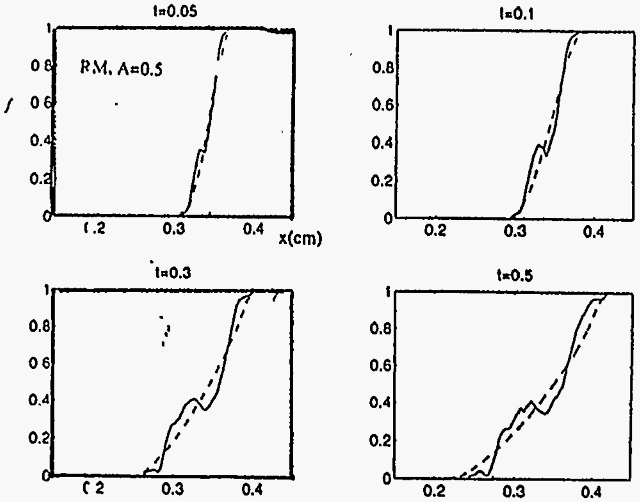
t=0.05
t=0.1
t=0.3
t=0.5
RM, A=0.5
f
1
0.8
0.6
0.4
0.2
0
0.2
0.3
0.4
x(cm)

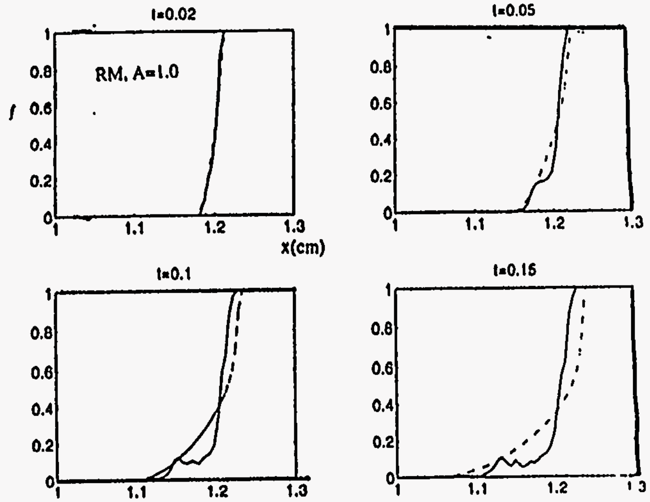

What is still missing: (work in progress)

- Compressibility effects

  ($C_s \cdot t$ is an additional scale-length)

- Non planar geometry

  (R is an additional scale-length

  and is important when:

  $\lambda_{dominant} \sim L \sim TMZ \sim R$)

- Multiple shock treatment

  (Is the $t^{0.4}$ ok. for a shock hiting a turbulant region?)

- The eq's for L_s and L_b in the mix model are good for early ($L \sim \lambda_0$) and late ($L \sim U$) stages. What happens at intermidiate stages? (use of modal-model to predict h_B, h_s, L_B, L_s)

- 2/3D effects — Lateral mixing — the transition from "ordered" to "disordered" flow

Two Laser-Plasma Experiments of Astrophysical Interest

Guy Dimonte
Lawrence Livermore National Laboratory

Two laser-plasma experiments of astrophysical interest

Guy Dimonte

Lawrence Livermore National Laboratory

Phys. Rev. Lett. 67, 1755 (1991)
Rev. Sci. Inst. 63, 5151 (1992)
Phys. Rev. Lett. 70, 1806 (1993)
Phys. Rev. Lett. 74, 4855 (1995)
Phys. Plasma 3, 614 (1996).

Two laser-plasma experiments of astrophysical interest

- Dynamics of exploding plasma in a magnetic field
  - Model Very High Altitude Nuclear Explosions (VHANE)
  - Structure and size of diamagnetic cavity
  - Compare with dispersion relation of lower-hybrid drift instability
  - Janus laser - 100 J in 25 ns
- Richmyer-Meshkov instability with high Mach ~ 15 shocks
  - Radiatively driven shocks
  - Linear growth of single modes at high compression
  - Turbulent growth due to 3D random perturbations
  - Nova laser - 30 kJ in 3 ns

Basic Issues Associated with Exploding Magnetized Plasmas

- What is plasma containment radius ?

$$\frac{m}{2}V_o^2 \sim \frac{B^2}{2\mu}\frac{4\pi}{3}R_b^3$$

- Is ion magnetization important ?

$$\frac{\rho_i}{R_b} \sim \frac{V_o}{\Omega_i R_b}$$

- What is instability and dominant scale of plasma structure ?

$$k_{max} \sim \frac{\Omega_{LH}}{\sqrt{gL}} \qquad g \sim \frac{V_o^2}{2R_b}$$

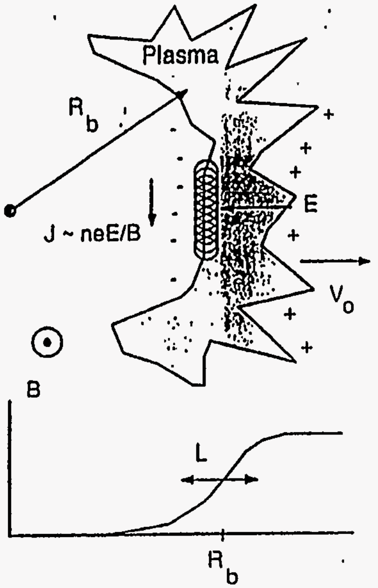

UNCLASSIFIED

Scaled laser experiments benchmark key physics

- 400 shots on Janus laser
  - Magnetic containment of plasma
  - Plasma instability structure
  - Multiple bursts
- Constructing "Space Chamber"
  - MHD-EMP generation
- Benchmark simulation codes
  - Collaborate with D-Division

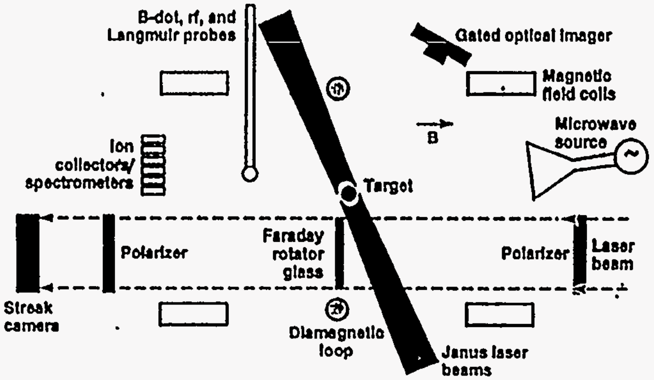

UNCLASSIFIED

UNCLASSIFIED

Lab experiments match scaled VHANE parameters

	STARFISH	LLNL
Total plasma energy (J)	~10^{15}	~100
Altitude (km)	400	—
Number of ions	10^{28}	~2 10^{17}
Atomic mass	55	6
Directed speed-v (10^7 cm/s)	15	2–4
Magnetic field (G)	0.3	2000
Larmor radius ρ_i (cm)	2 10^6	1
Bubble radius R_b (cm)	3 10^7	5

[redacted]

Expanding plasma
- Many ions
- Light ions
- Large magnetic field

Plasma structure caused by magnetic field

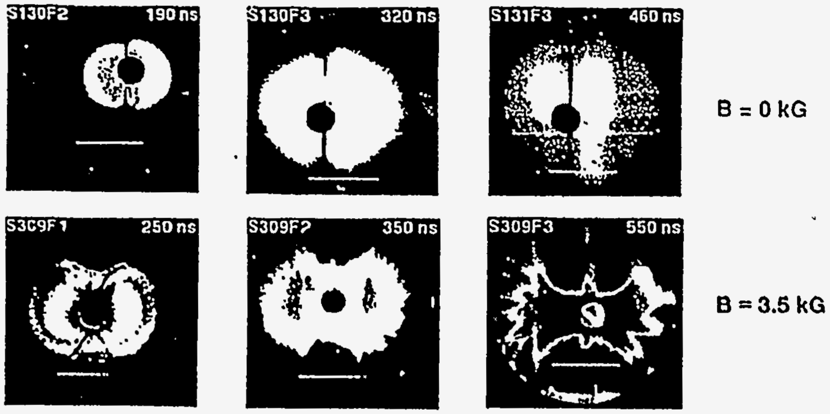

Magnetic compression magnifies small asymmetries
Instabilities evolve toward longer wavelengths

Magnetic Profile of Expanding Plasma Cavity

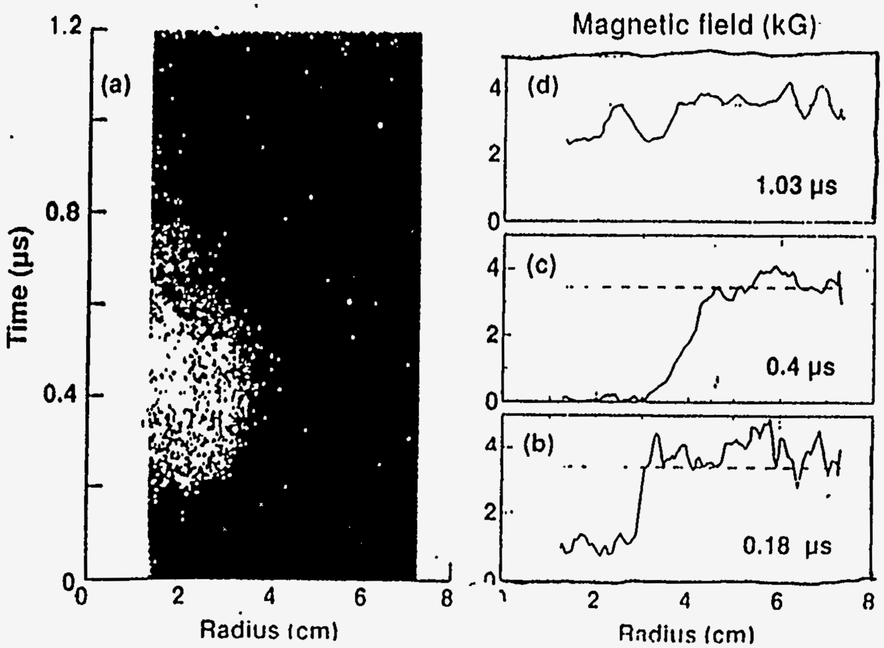

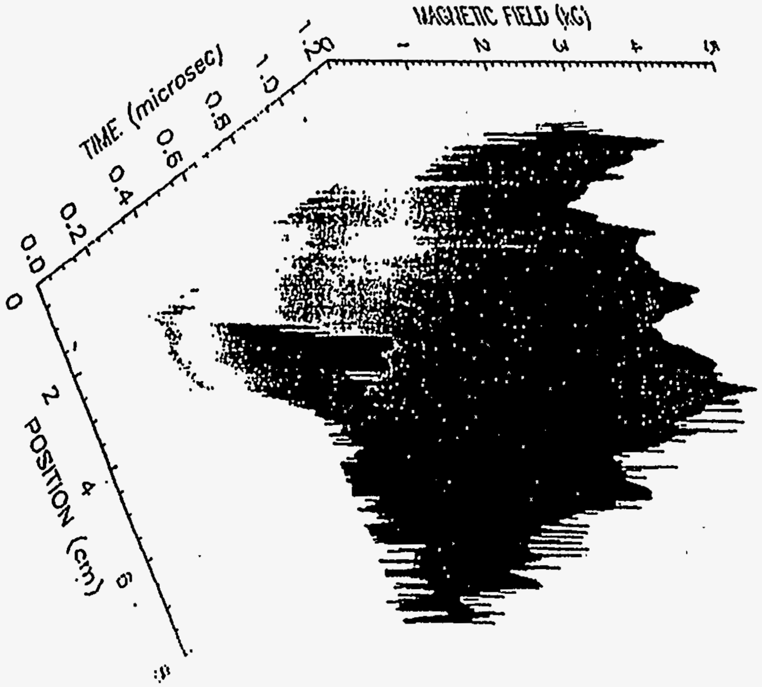

Plasma Radius Increases With Classical Bubble Radius

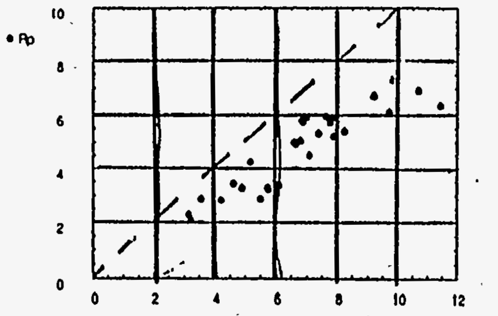

$\sim (E_k / B^2)^{1/3}$

Plasma radius decreases weakly with ion magnetization

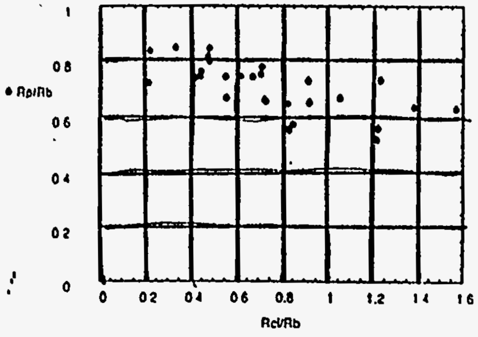

Plasma Structure Obtained by Fourier Analyzing Edge Contour of Optical Plasma Image

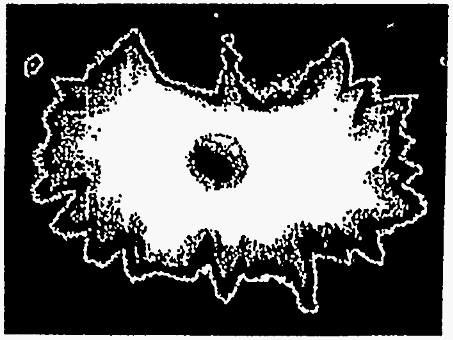

B = 3.5 KG
E = 100 J
Dia = 3.2 mm
CH
500 ns

Spectral Amplitude (mm) vs Mode Number (N) .... B = 0

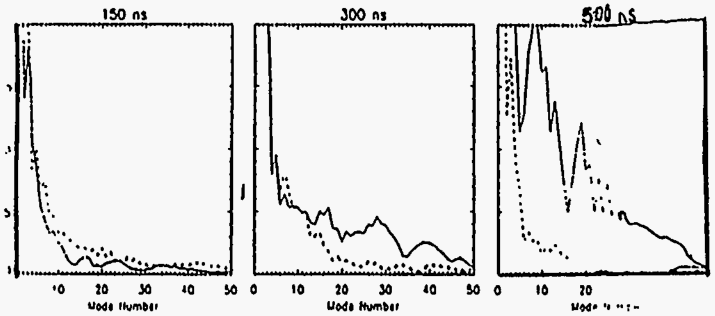

Linear theory predicts $N_{max} \sim 500$

$\gamma t = 200$

Nova laser produces strong shocks to investigate compression, but mainly in weakly nonlinear regime

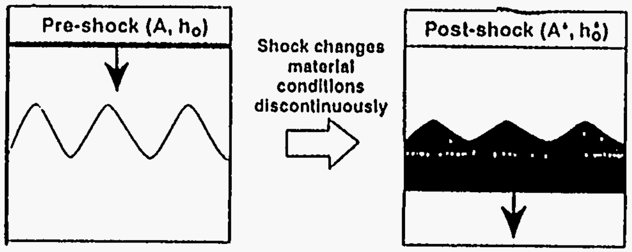

- Strong compression effects exhibited in linear regime

$$\frac{dh}{dt} \sim k\, U\, A_{eff}\, h_{eff} \qquad h_{eff} \overset{?}{=} \begin{cases} h_o \\ h_o^* \\ \frac{h_o + h_o^*}{2} \end{cases}$$

- Compression makes A_{eff} and h_{eff} ambiguous
- Pre- and post-shock parameters are easily distinguishable on Nova experiments

UNCLASSIFIED

Configuration for Nova Richtmyer-Meshkov Experiments

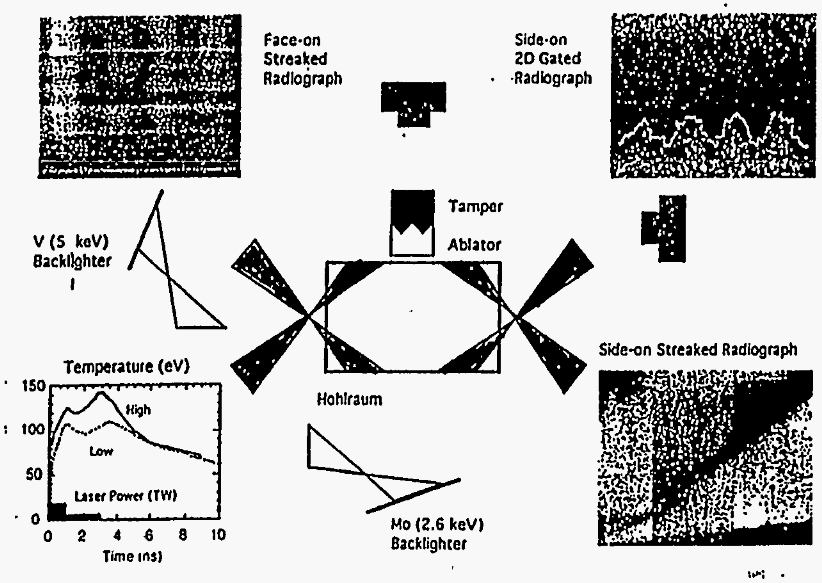

CALE simulations (2-D) reproduce measured growth of single mode

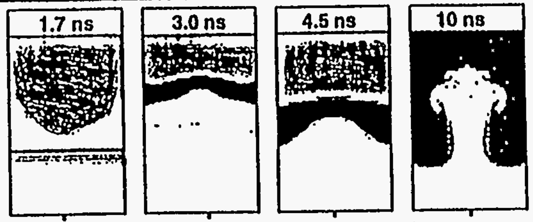

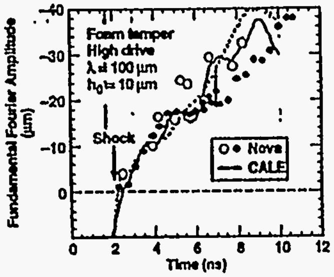

Physics of Plasma (in press)

Growth rates from Nova single mode experiments agree with simulations and models over wide variation in A, k, U, h_0

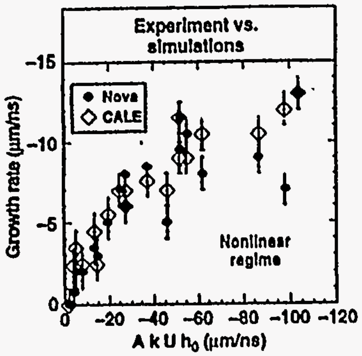

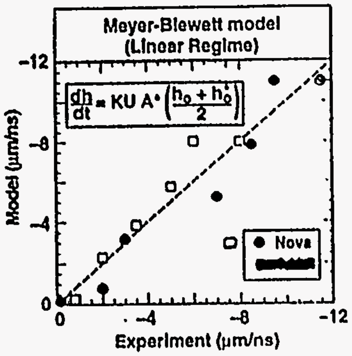

- Linear and nonlinear growth rates agree with CALE simulations
- Compression described by average of pre- and post-shock parameters

Compressible turbulence experiments performed on Nova with random 3D interfacial perturbations

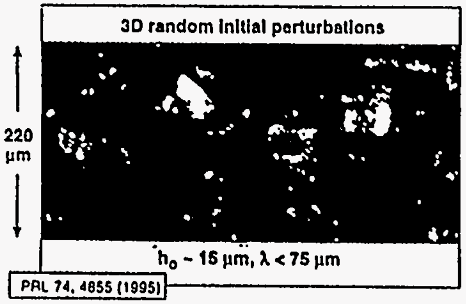

PRL 74, 4855 (1995)

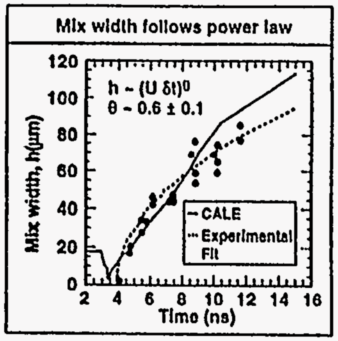

Experimental limitations

— Large initial amplitude required because experiment duration is short
— Feature size not discernable with radiography

Summary

- Dynamics of exploding plasmas (Janus laser)

  Maximum radius ~ $(E_k / B^2)^{1/3}$ insensitive to ion magnetization
  Magnetic structure measured with Faraday rotation
  Observed wavelengths larger than most unstable lower hybrid drift modes
  Instability nonlinear - many e-foldings during stagnation

- Richtmyer-Meshkov instability with high Mach shocks (Nova laser)

  Single modes obey Meyer-Blewett model for A < 0 $\boxed{\frac{d\eta}{dt} \sim A^* k U \frac{\eta_o + \dot{\eta}_o}{2}}$

  3D random modes obey power l $\boxed{h \sim t^{\beta}}$ $\beta \sim 0.6 \pm 0.1$

Pair Production by Ultra-Intense Lasers

Edison Liang
Rice University

PAIR PRODUCTION BY ULTRA-INTENSE LASERS

Edison P. Liang
Summer Faculty Fellow, University of California, Lawrence Livermore National Laboratory, Livermore, CA 94550
and
Department of Space Physics and Astronomy, Rice University, Houston, TX 77251*
and
S.C. Wilks
University of California, Lawrence Livermore National Laboratory, Livermore, CA 94550

ABSTRACT

We consider the production of electron-positron pairs by the interaction of relativistic superthermal electrons generated by ultra-intense laser pulses with high-Z material. We discuss the laser and target parameters required in order to optimize the pair production rate. We explore the regime when the pairs, if sufficiently confined, can start to exponentiate in number and the feasibility of ultimately achieving a pair-dominated plasma: a plasma in which the pairs outnumber the target background electrons.

PACS numbers: 52.40.Nk, 52.35.Nx, 52.60.+h

The pending development of ultra-intense laser pulses will allow the study of new regimes of laser-matter interaction[1]. Experiments are now being designed[2] which will eventually lead to laser intensities such that $I\lambda_\mu^2 > 10^{19}$ W $\mu m^2/cm^2$. Here I is laser intensity and λ_μ the wavelength in microns. At such intensities the electron jitter velocity in the laser electric field becomes relativistic: $p_o/mc > 1$ where p_o is jitter momentum, m is electron rest mass, and c is light speed. When such lasers interact with an overdense plasma it is known to produce relativistic superthermal electrons. Numerical simulations with the Particle-In-Cell (PIC) codes[3] show that as much as half of the absorbed laser energy goes into superthermal electrons whose characteristic kinetic energy E_{hot} is roughly given by:

$$E_{hot} \sim ((1+ I\lambda_\mu^2/1.4x10^{18})^{1/2} - 1) mc^2 \qquad (1)$$

Hence $E_{hot} > mc^2$ for $I\lambda_\mu^2 > 4x10^{18}$. In addition extremely intense magnetic fields with B up to 250 MG are observed to form in the overdense plasma. Such strong fields help to confine the superthermal electrons in the lateral directions. For even higher $I\lambda_\mu^2$ we expect E_{hot} to exceed the pair production threshold. It is the purpose of this letter to explore the physics of this regime and consider the prospects of creating a copious pair source and ultimately a pair-dominated plasma in the laboratory, in which the pair density outnumbers the background electron density.

Nonthermal electron-positron plasmas are known to be abundant in many astrophysical environments from pulsars to quasars. In the last few years discoveries of intense broadened 511 keV annihilation features lasting from days to weeks from several Galactic black hole candidates[4] in our own Galaxy suggest that steady state thermal pair plasmas also exist. Since pairs annihilate on very short time scales, to maintain a steady state plasma over such long times the pairs need to be created prolifically to balance the annihilation rate. Such thermal plasmas represent a new state of matter with unique thermodynamic and radiative properties drastically different from ordinary plasmas[5]. If we define "compactness"[5] roughly as the total plasma heating rate divided by its physical size, then for high compactness the pairs are primarily created by gamma ray (photon-photon) collisions. For low compactness cases the pairs are primarily created by charged particle (lepton-ion) interactions whose cross section goes up as the square of Z, the ion nuclear charge. Whereas in the astrophysical contexts we are often dealing with the high compactness case[5], in the laboratory simple estimates show that we will always be dealing with the low compactness case even for micron size laser spots. Hence in the following we will concentrate on pair production with high Z targets (e.g. Au, Z=79). For low compactness and a confined thermal plasma, Bisnovaty-Kogan, Zeldovich and Sunyaev (BKZS)[6] first show that there exists a fundamental limiting temperature above which there is no pair equilibrium since the pair production rate will always exceed the annihilation rate. This limiting temperature was found to be about 20 mc^2 for pure hydrogen. For high Z or high B plasma[7] it is expected to be lower but above the pair production threshold of $2mc^2$. If we use Eq.1 as a measure of the superthermal electron temperature we find that formally, above a laser intensity of ~ $10^{20}W/cm^2$, the superthermal temperature would exceed the BKZS limit. In reality the BKZS limit does not apply due to the short duration of a laser pulse since it assumes a steady state. What all these mean is that above a certain laser intensity pair processes must become important. We need to perform a time-dependent kinetic calculation to estimate the correct pair density development.

Consider a situation in which a significant fraction of the superthermal electrons and pairs are confined and reaccelerated to relativistic energies according to Eq.1. In practice this can be accomplished by using a double-sided laser illumination so that the superthermal electrons and pairs are confined by the laser pondermotive pressure in the front and back and by the strong magnetic fields on the side. In the limit of low annihilation rates the pair density grows according to:

$$n_+ = n_{ei} + n_{ee} + n_{e\gamma} + n_{\gamma\gamma} + n_{\gamma i} \qquad (2)$$

where the first term is the lepton-ion pair production rate, the second term the lepton-lepton pair production rate, the third term lepton-photon pair production rate, the fourth term the photon-photon pair production rate and the fifth term the photon-ion pair production rate (here photons include bremsstrahlung and Compton upscattered gamma rays). We have estimated in detail the relative magnitudes of the five terms in Eq.2. It turns out that for typical laser target environments the first term is by far the dominant term, at least until the pair density starts to dominate the ion density. Hence in the pair deficient regime Eq.2 reduces to:

$$n_+ = n_{ei} = (n_+ + n_-) < n_i f v \sigma_{ei} > \qquad (3)$$

where n_i is ion density, $n_- = n_+ + Zn_i$ is total electron density, v is relative velocity between ions and leptons and σ_{ei} is cross-section for pair creation in the ion rest frame. The bracket deontes averaging over the normalized lepton distribution function f. At lepton energies much above threshold the cross section assumes the form[8]

$$\sigma_{ei} = 1.4x10^{-30} Z^2 (\ln \gamma)^3 \qquad (4)$$

where γ is the lepton Lorentz factor. Eq. 3 can be integrated to give the pair growth rate:

$$n_+ = Zn_i [\exp(\Gamma t) - 1] / 2 \qquad (5)$$

where the pair growth rate Γ is given by the integral:

$$\Gamma = 2\, n_i\, c \int d\gamma\, \sigma_{ei}\, f\, (1 - \gamma^2)^{1/2} \qquad (6)$$

As we will see below, Γ is of the order of $0.1(n_{Au})$/ns where n_{Au} is the gold atomic density in units of normal solid density of 6×10^{22} ions/cm^3, for laser intensity exceeding a few times 10^{19} W.cm^{-2}.

Using the PIC codes we have run a number of 2-sided illumination of Au targets for various laser intensities. Fig.1 shows the superthermal electron distributions for sample cases generated by such 2-sided laser heating. Using the superthermal electron distribution f generated by these PIC simulations in Eq.6 we find the pair growth rate as a function of the laser intensity. This is plotted in Fig.2. As we anticipated, Γ rises with laser intensity rapidly near threshold. But above a laser intensity of a few times 10^{19} W/cm^2, Γ increases only slowly with laser intensity due to the log dependence of the cross-section. An important implication of this result is that for a laser of given total energy, to optimize the pair production one should make the laser pulse as long as possible provided the intensity stays above ~ 10^{20} W/cm^2. A collorary is that the smaller the laser spot size the better. From Fig.2 we see that for a 10^{20}W/cm^2 laser lasting 10 ps (such as that proposed for the faster ignitor at LLNL), $\Gamma t \sim 2\times10^{-3}$ and the pair density can in principle reach ~ 0.1% of the target electron density. Since Γ is linearly proportional to n_i one obvious way to increase the pair creation rate is to precompress the target to densities much higher than solid density (e.g. with another laser) prior to hitting it with the high intensity laser.

Another relevant issue is the maximum number of pairs one can hope to achieve for a given laser pulse energy and whether we can ever reach a pair-dominated state, as in the case of BKZS[6]. Assuming that a typical pair carries a total (rest plus kinetic) energy of ~ 4mc^2, we find that a kJ of laser energy, if 50% converted to superthermals and then a fraction p of that converted to pairs, will give rise to a total of $p\times10^{14}$ pairs. This is to be compared to the total number of Au ions in a 10 μm diameter target spot of 1μm thickness ≈ 5×10^{12} and the total number of background electrons ≈ 4×10^{14}. Hence to reach a truly pair-dominated state we will need a laser energy of more than a kJ, independent of pulse duration and target density.

In addition to the confinement and reacceleration of the superthermal electrons and secondary pairs, we also need to consider their radiative cooling. These include bremsstrahlung and synchrotron cooling. If these are much shorter than the laser pulse then the above discussions on pair density evolution needs to be amended. For a typical field of a few hundred megagauss and Lorentz factor of 10, we find that the synchrotron cooling time[9] is ~ 10 ns, whereas the bremsstrahlung cooling time[9] is ~ ns. Hence they are longer than the laser pulse if we are dealing with sub-ns pulse. But if we eventually go to a much longer laser pulse scheme then the radiative losses must be included in estimating the pair production. In any case we find that the energy loss by the superthermals to bremsstrahlung will always be at least a factor of 10 or more larger than the loss to pair production. Hence the factor p in the above paragraph will always be less than 0.1. However, at sufficently high compactness (large photon density) some of the bremsstrahlung gamma rays will be reconverted back to pairs via gamma-gamma collisions. Accurate estimates can only be calculated via detailed numerical simulations.

How does one diagnose the pairs and superthermals? The direct method is to measure the prompt bremsstrahlung and annihilation gamma ray fluxes and spectra. However, many of the pairs will escape from the production region and annihilate in the surroundings (e.g. target chamber walls), likely after the laser pulse is over. Hence to estimate the total number of pairs produced we need to integrate the total 511 keV flux over durations comparable to positron flight times to the target chamber walls. On the other hand, the prompt bremsstrahlung gamma rays from the superthermals provide diagnostics about the superthermal flux and energies during the laser irradiation. Hence together they will serve to calibrate the above estimates of the pair production efficiency.

In summary, we expect that the next generation of ultra-intense lasers such as the one under development for the fast ignitor at LLNL, will be able to generate significant density of pairs under optimal conditions. A 10ps, 10^{20}W.cm^{-2} laser hitting solid-density gold foils on both sides can in principle produce peak pair density of the order of 10^{-3} of the target elecctron density. To go much beyond that we need to either consider much more powerful lasers with longer pulses, or precompressed targets with much higher than solid density or both.

We thank M. Tabak, W. Kruer, R. More and J. Woodworth for valuable discussions. This work is performed under the auspices of the US DOE by the Lawrence Livermore National Laboratory under contract W-7405-ENG-48. EPL is also supported in part by NASA NAG 5-1547.

→Permanent Address.

1. M. Chaker et al. Phys. fluids B 3, 167 (1991); H. Milchberg et al. Phys. Rev. Lett. 61, 2364 (1988); G.L. Landen, D.G. Stearns and E.M. Campbell, Phys. Rev. Lett. 63, 1475 (1989).
2. M. Perry and G. Mourou, Science ------ (1994).
3. S.C. Wilks, W.L. Kruer, M. Tabak and A.B. Langdon, Phys. Rev. Lett. 69, 1383 (1992).
4. For review, see articles in AIP Conf. Proc. No. 280, ed.M. Friedlander et al. (AIP, NY, 1993).
5. R. Svensson, Mon. Not. Roy. Ast. Soc.209, 175 (1984); A. Zdziarski, Astrophys. J. 283, 842 (1984).
6. G.S. Bisnovaty-Kogan, Y.B. Zeldovich and R. Sunyaev, Sov. Ast. J. 15, 17 (1971).
7. M. Kusunose and F. Takahara, Pub. Ast. Soc. Jap. 40, 435 (1988).
8. W. Heitler, Quantum Theory of Radiation (Oxford, London, 1954).
9. G.B. Rybicki and A.P. Lightman, Radiation Processes in Astrophys. (Wiley, NY, 1979).

15a

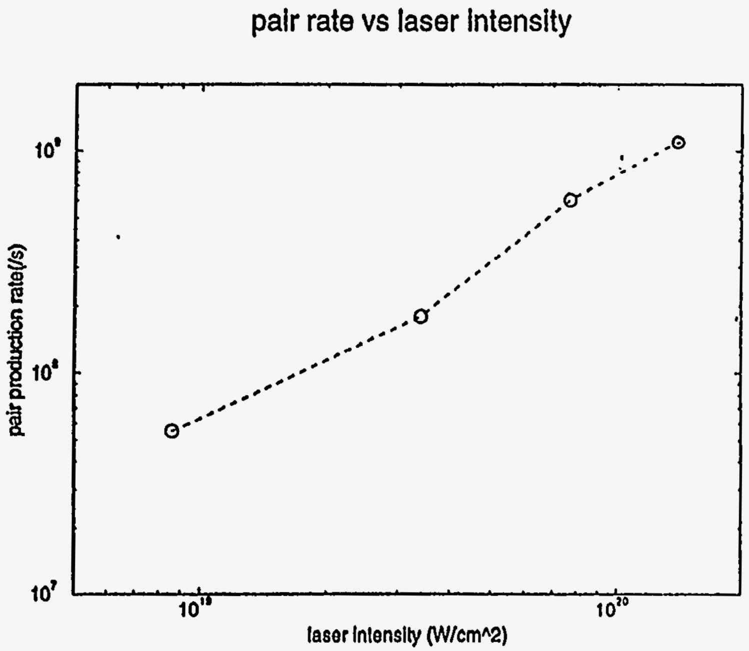
pair rate vs laser intensity
pair production rate(/s)
10^9
10^8
10^7
10^19
10^20
laser intensity (W/cm^2)

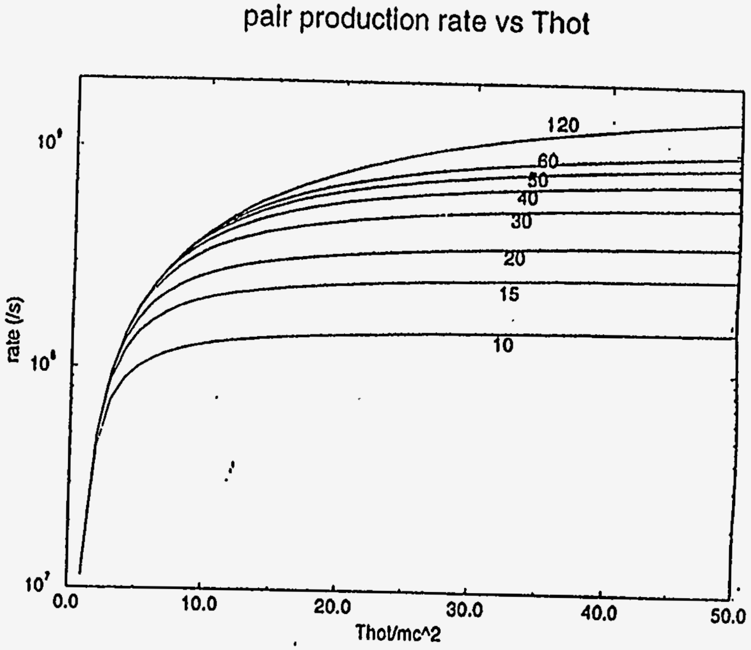
pair production rate vs Thot
rate (/s)
10^9
10^8
10^7
0.0
10.0
20.0
30.0
40.0
50.0
Thot/mc^2
120
60
50
40
30
20
15
10

Nova Experiments to Study the Interactions of SN1987A with Circumstellar Matter

Edison Liang
Rice University

NOVA EXPER... ENTS TO STUDY THE INTERACTIONS OF SN1987A WITH CIRCUMSTELLAR MATTER

Edison P. Liang

Summer Faculty Fellow, X-Division, LLNL, Livermore, CA 94551
and
Rice University, Houston, TX 77251-1892

ABSTRACT

This report summarizes the results of 1-dimensional numerical simulations of the interaction of NOVA laser target blowoffs with low density foams. Such experiments are explored to see if they can simulate some aspects of the interaction of Supernova (SN)1987A with circumstellar matter (CSM) and the anticipated x-ray emissions when the supernova shock wave reaches the high density circumstellar ring around the year 2000. We focus on (a) the most important astrophysics issues that may be addressed with such NOVA experiments; (b) the optimal experimental design parameters.

1. INTRODUCTION AND ASTROPHYSICS BACKGROUND

The sunpernova SN1987A was one of the most spectacular and important astronomical events of this century (see Chevalier 1992, McCray 1993 for reviews). At a distance of 55 kpc in the Large Magellanic cloud, a satellite of our own Milky Way, it was the nearest and brightest supernova in modern times. In addition, its progenitor star had the unusual property of going through both a red and blue supergiant phase before the final explosion, creating a multilayered circumstellar environment for the supernova ejecta to interact with. The earlier red supergiant progenitor had a slow, higher density stellar wind while the later blue supergiant had a faster, lower density stellar wind (see, e.g. Chevalier and Liang1989). The interaction of the fast wind with the slow wind created a cocoon of high density shell, which is conjectured to have a peanut or hourglass shape (Fig.1a, see Luo and McCray 1991, Panagia et al 1991, Wang and Mazzali 1992). When this peanut-shaped cocoon was lit up by the light of the supernova itself, it was observed as a spectacular triple ring system by the Hubble Space Telescope (Fig.1b). The middle ring of the three rings likely defines the "neck" of the cocoon which is the part of the high density shell closest to the supernova. Based on current estimates of the SN shock wave velocity the forward shock should impact this equatorial high density ring sometime near the year 2000. At that point it will drive a shock into the high density material, resulting in strong x-ray and other frequency emissions for the next twenty years or more (Luo and McCray 1991, Suzuki et al 1993). The anticipated x-ray luminosity of $\sim 10^{38}$ erg/s, even at a distance of 55 kpc, should be easily detectable by the next generation of x-ray satellites, such as the NASA AXAF observatory to be launched in 1999.

There are however several important uncertainties with the predicted scenario. One is the density of the blue supergiant wind (BSW) and of the equatorial high density ring (HDR). They will affect the arrival time of the SN shock wave and the resultant evolution and x-ray emissivity of the shocked ring material. The other is the effective thermal conductivity (e.g. Liang and Chevalier 1984, Band 1988) of the circumstellar matter (CSM), which will greatly affect the strength and structure of the shock wave and the density and temperature of the post-shock material. The third is the possible effects of hydrodynamic instabilities and their growth rates (e.g. Chevalier and Blondin 1995). These are some of the uncertainties the effects of which we hope to address with NOVA laser target experiments.

The idea is to use laser target blowoff material (rarefaction wave) to simulate the SN ejecta, and foam layers of different densities to simulate the BSW and HDR. Of course most physical parameters such as the distance and time scales, densities and pressures of the laboratory experiments will be many orders of magnitude different from those of SN1987A (cf. Sec.3). The key question is: is there any relevant parameter of the two phenomena which may have similar values. As we will demonstrate below, it turns out that the *velocities and temperatures* of the two cases can be quite similar. These are the similarities that we plan to exploit, and hope to learn something relevent to the actual astronomical scenarios with NOVA experiments.

We first briefly review the physics of SN interactions with its CSM. To highlight the basic physics of such interactions we first ignor the 2-and 3-diminsional nature of the SN ejecta and its CSM and idealise them as 1-dimensional spherical shells. Based on the works of Chevalier (1982), Dickel and Jones (1985), Liang and Chevalier (1984) and Band and Liang (1988), the evolution of the interaction zone of the SN ejecta with the low density BSW can be approximated by self-similar solutions. The contact surface is sandwiched between a forward shock propagating into the BSW material and a reverse shock propagating into the SN ejecta (Fig.2). In the adiabatic limit (zero thermal conductivity) the density peaks at the two shock fronts and goes to zero at the contact surface, where the temperature profile has a sharp narrow spike. This whole interaction zone moves outward at the same rate as the expansion of the SN ejecta. The shocked ejecta layer is Rayleigh-Taylor (RT) unstable since the pressure and density gradients are pointing in opposite directions (Chevalier and Blondin 1995).

The adiabatic assumption is usually made in SN shocks since we know little about astrophysical thermal conductivity or the interstellar magnetic field topology. If, on the other hand, we assume as in laboratory laser plasmas that flux-limited Spitzer conductivity (Spitzer 1967, Max 1982, Fechner et al 1984) applies, then the SN-CSM interaction zone takes on a rather different structure (Liang and Chevalier 1984, Band 1988). The efficient thermal conduction makes the interaction zone close to be isothermal at all times. The shock interaction region then consists of only a single density plateau sandwiched between the forward and reverse shocks. (Fig.2). The profile is narrower and manifestly RT stable at all times. The shocks also propagate faster in this case due to thermal wave preheat. These differences potentially lead to rather different x-ray emission temperatures and profiles and arrival times at the HDR.

Based on the adiabatic simulations, the forward shock in the BSW is expected to reach the HDR around 1999 to 2002 (Luo and McCray 1991, Suzuki et al 1993), at which point the equatorial section of the front will drive a slower shock in the HDR, while the rest of the shock front in the BSW will continue to propagate at higher speed, graduately wraping around the HDR and eventually evaporating it. These results are suggested by 2-dimensional numerical simulations (Fig.3, Suzuki et al 1993). While such 2-dimensional details will be important in later phase studies, many of the critical questions can still be addressed in the context of 1-dimensional models. Moreover, since the size of the HDR is small compared to the curvature of the SN shock, to first order we can ignor the spherical divergence of the SN ejecta and approximate the interaction with planar SN ejecta and CSMs. Hence we will first explore 1-dimensional plane geometric laser experiments.

Since it is obviously impossible to reproduce the density and pressure of the SN ejecta or CSM (<10 particles/cm^3 for BSW and $\sim 10^4$ particles/cm^3 for the HDR) in a laboratory laser experiment, we concentrate on exploring the temperature and velocity of the shock achievable in the laser experiments. Using standard NOVA laser intensities ($\sim 10^{14}$W.cm^{-2}), we find that it is easy to achieve blowoff velocities $\sim 10^3$ km/s when the density rarefies to $\sim$ mg/cm^5, a density that can be almost matched to the lowest density foams. The above velocity is only a factor of ~ 10 below that of the real SN forward shock velocity ($\sim 10^4$ km/s). Since in the SN case the density jump between the BSW and the HDR is ~10^3 the velocity drop from the BSW to the HDR is ~ 30, resulting in a shock in the HDR of only ~few x 10^2 km/s and a temperature of ~ keV. To achieve a similar shock velocity and temperature we therefore propose the use of two foam layers with a density jump of 10, so that the velocity drop is only ~3. In the numerical simulations reported below, we will assume that the low denisty (LD) foam layer representing the BSW has a density of 1-5 mg/cm³ and the high density (HD) foam layer representing the HDR has a density of 10-50 mg/cm³.

2. PHYSICS OF LASER TARGET BLOWOFF INTERACTION WITH STANDOFF FOAM LAYERS.

To first order we can assume that the laser energy is deposited in a thin layer at the critical density surface (where laser frequency equals plasma frequency). From this layer outward temperature rises quickly to a constant asymptotic value via thermal conduction and the (planar) blowoff is adequately represented by an isothermal rarifaction wave with linear velocity and exponential density profiles. Inward from the critical density surface the density rises rapidly to solid density and temperature drops off quickly. The thermal diffusion front eventually drives a weak shock wave into the target whose momentum is balanced by that of the blowoff. In the isothermal limit the asymptotic blowoff at distance z is well described by a self-similar solution (e.g. Schmalz 1985):

$$v = z/t + c_s \text{ and } \rho = \rho_0 \exp(-z/c_s t) \qquad (1)$$

where c_s is the isothermal sound speed and ρ_0 is an initial value somewhere between the critical density and quarter critical density. When the leading edge of this blowoff hits the low-density (LD) foam at a fixed standoff distance (the gap is needed for the laser beams to get in without preheating the foam layers), it generates a forward shock into the LD foam and a reverse shock in the blowoff material. The strength of the shocks depend on the velocity and density of the blowoff reaching the standoff distance. According to Eq.(1) we see that the higher c_s and ρ_0 the better. From the literature (e.g. Max 1982) we have .

$$c_s=(ZkT_e/m_i)^{1/2} \sim 750 \text{ km/s } (Z/A)^{1/2}(I_{14}\lambda_\mu^2)^{1/3};\ \rho_0\sim\rho_c = 1.8\times10^{-3}\text{g/cm}^3(A/Z)\lambda_\mu^{-2} \qquad (2)$$

where Z is mean atomic number, A is mean atomic weight (A/Z~2 for most materials), $I_{14}=I/(10^{14}\text{W.cm}^{-2})$ and λ_μ is laser wavelength in microns. Hence the higher the laser intensity the better. But c_s and ρ_0 have opposite dependences on laser wavelength. It turns out that the sound speed plays a more dominant role than the critical density since it sits in the exponent, and numerical simulations confirm that *longer laser wavelength indeed generates stronger shocks in the foam layers.*

Eqs (1) and (2) show that for NOVA laser pulse durations, wavelengths and intensities and realistic standoff distances, to get a good density match we need to use foams in the mg/cc range for the LD layer. One of the goals of our simulation is to see the effects of varying the foam densitiy. Another goal is to see the effects of varying the thermal conductivity. In practice the thermal conductivity may be varied by doping with high Z material or applying strong transverse magnetic fields.

3. COMPARSION OF SN1987A AND NOVA EXPERIMENT PARAMETERS

In Table I we compare the physical parameters of SN1987A with that of the proposed NOVA experiments to illustrate the drastic differences of the scales. We see that the only similarity is in the shock velocity and temperature of the HD foam. Note also that in both cases the coulomb mean free paths are >> the interaction region size but the cyclotron radius is << the interaction region size.

Table I.

	SN1987A	NOVA experiments
Distance to HD ring/foam	6×10^{17}cm	1mm
Shock arrival time at HD ring/foam	12-15 yr	1.2-1.5 ns
Density of preshock BSW/LD foam	~10 atoms/cc	1 - 5 mg/cc
Density of preshock HD ring /foam	~10^4atoms/cc	10 - 50 mg/cc
Pressure in shocked BSW/LD foam	~10^{-6} erg/cc	~10^{13} erg/cc
Pressure in shocked HD ring/foam	~10^{-5} erg/cc	~10^{13} erg/cc
B-field	~μG	10MG
Electron cyclotron radius	~10^9 cm	10^{-4} cm
Coulomb mean free path in HD ring/foam	~1.5×10^{18} cm	4.5 cm
Coulomb mfp/interaction zone size	~10	150
Shock velocity in BSW/LD foam	~6000 km/s	~500 km/s
Shock velocity in HD ring/foam	~200-400 km/s	~150-300 km/s
Shock electron temperature in BSW/LD foam	4-6 keV	2-3 keV
Shock electron temperature in HD ring/foam	0.7-1 keV	0.6-2 keV

4. 1-DIMENSIONAL NUMERICAL SIMULATION RESULTS

We have performed a large number of 1-dimensional (plane geometry) numerical simulations with LASNEX to explore the interactions of laser target blowoffs with different density foams at a standoff distance realistic for actual laser experiments. The sample results reported here compare the runs of (a) 1mg/cc LD plus 10mg/cc HD foam densities versus 5 mg/cc LD plus 50mg/cc HD foam densities; (b) thermal conductivity on versus off (adiabatic); (c) $2\omega_0$ (green) versus $3\omega_0$ (blue) laser light. Except for the above differences, the assumptions and parameter settings for everything else are the same for all runs and are summarized here:

1) The laser intensity is assumed to be 10^{14} W.cm^{-2} normal incidence, all absorbed at the critical surface; the laser is left on for the duration of the entire run (~3-3.6 ns).
2) The LD foam is located at 0.05 cm from the laser target. Its thickness is taken to be 0.06 cm in the low (1mg/cc) density runs and 0.05 cm in the high (5mg/cc) density runs.
3) The HD foam lying beyond the low density foam is taken to be ten times denser than the LD foam and its thickness is set to be 0.09 cm.
4) Both the laser target and the foams are assumed to be 50% C and 50% H in composition; the target is assumed to be at solid density (1.1gm/cm³) initially.
5) Artificial linear and quadratic viscosities are turned on to their default values to control any numerical ringing from shock interactions.
6) When thermal conductivity is on, the flux limiter parameter f is always set equal to 0.03 as is customary in laser target calculations.

The initial geometry setup of the numerical runs is illustrated in Fig.4. We now summarize the results of the different runs.

A. Benchmark run: $2\omega_0$ laser light, conduction on, low foam densities (1 mg/cc LD plus 10 mg/cc HD foams):

Fig.5 gives the density profile snapshots at sample times. At 1 ns the forward shock in the LD foam has not yet reached the HD foam boundary, and the interaction region bounded by the forward and reverse shocks in the LD foam has a standard "plateau" structure similar to the conductive SN runs made by Liang and Chevalier (1984.

cf. Fig.2)... Notice the exponential density profile of the blowoff and the width of the interaction region (~.015cm, much larger than typical foam cell size). The forward shock hits the HD foam at around 1.2 ns. This produces a forward shock in the HD foam and a reflected shock in the LD foam. (see e.g. profile at 1.5 ns). Eventually, however, the *reflected and reverse shocks merge into a single reflected shock in the blowoff material.* There is no evidence of any "reverberation" of the reflected shock between the reverse shock and the forward shock as claimed by Luo et al (1994).

Fig.6 gives the pressure profile snapshots at various times. The development of the forward and reflected shocks when the HD foam is first hit and the subsequent merging of the reflected and reverse shocks are more clearly illustrated in this picture. Fig.7 gives the velocity profile snapshots and Fig.8 gives the bremsstrahlung emissivity profile ($\sim n^2T^{1/2}$) snapshots. Note that the latter profile broadens with time as the shock advances. Note also that since the above emissivity function is dominated by the density peak and not the temperature, this profile need not represent the picture seen by x-ray detectors of a narrow band pass. Fig.9 gives a sample temperature profile at t=3.0ns. The temperature is in fact quite low near the forward shock where density peaks and rises slowly to a plateau of 2.8 keV only near the rear of the density profile. Hence the spectrum of x-ray emissivity is very soft at the shock front and gets harder only near the contact surface. Fig.10 gives the transverse optically thin x-ray intensity spectrum just to the left of the density peak at t=3 ns. We see that even though the spectrum above ~2 keV is close to that of thermal bremsstrahlung, at lower frequencies it is still dominated by the bound-bound and bound-free opacities of carbon. Doping the foam with higher Z tracers will be very useful in mapping the density and temperature profiles of the shock interaction region.

Note also from the pressure and density profiles that since both of their gradients point in the same direction, the shock interaction regions are RT stable, thanks to the effects of thermal conduction. At 3 ns the shock has reached the outer edge of our HD foam at 0.2 cm.

B. High density run: the densities of both the LD and HD foams are 5 times higher than in A, all other parameters remain the same as in A; conduction is turned on.

Fig.11-14 give the density, *pressure*, velocity and temperature profile snapshots. Note that the shocks are now propagating much more slowly than in case A. It does not reach the LD-HD foam interface until 1.5 ns. Even before the shocks reach the HD foam, the density profile is sharply forward peaked, unlike the flat plateau of the lower density run. When the shock hits the HD foam, it generates a very sharp forward density peak. This peak also propagates much more slowly than in the lower density case. The reflected shock also propagates more slowly. It has not yet caught up with the reverse shock by the end of the run at 3.6ns. *Note also that the density jump at the forward shock* reaches a factor of ~50, much higher than the factor of ~3 reached in case A. Fig.15 shows the late-time bremsstrahlung emissivity profiles which trace the density profiles. They are much narrower than those in case A. These results suggest that the width and amplitude of the x-ray emission profile may serve as a diagnostic of the density of the foam, and by analogy, the density of the CSM around SN 1987A.

In Fig.16 we compare the forward shock trajectories of case A versus case B after the shock penetrates the HD foam. We see that A propagates much faster than B. In Fig.17 we compare the forward shock peak density of case A versus case B. We see that B is shocked to much higher density than A. From the velocity profiles of runs A and B we see that the late time shock velocity amplitudes in the HD foam are in the range of 150-300 km/s, similar to those expected when SN1987A hits the high density ring.

C. Adiabatic *run: conductivity is set equal to 0;* all other parameters remain the same as in A.

Fig.18-21 give the density, pressure , velocity and temperature profile snapshots of the shock interaction regions. Note that before the forward shock hits the HD foam (t< 1.3 ns), the interaction region has the classical double density peak structure with a sharp temperature spike at the contact surface, well known in adiabatic SN runs (cf. Fig.2). Despite the differences between our laser blowoff and SN ejecta cases (exponential instead of power-law density profile, and plane instead of spherical geometry), the shock interaction structures in both cases are almost identical in the adiabatic limit. This gives us some confidence that the laser experiments can reproduce some of the important *aspects of the SN interactions with the CSM.*

After the shock hits the LD-HD foam interface, it generates a forward shock into the HD foam and a reflected shock in the LD foam which propagates toward the blowoff-LD foam contact surface. This reflected shock interacts with the contact surface and at late times produces a sharp density spike situated between the forward shock and the contact surface. Hence we see that *the density is highest not at the forward or reflected shock but at somewhere in between.* The overall density profile is clearly narrower than the conductive case. Whether the density peak here is caused by the reverberation effect discussed by Luo et al (1994) remains to be seen. Fig.22 gives the thermal bremsstrahlung emissivity profile snapshots. Again it traces mainly the density profile. The sharp temperature spike at the target blowoff-LD foam contact surface does not lead to much x-ray emission since it coincides with a density dip. Note also that at all times the pressure and density gradients point in opposite directions in at least part of the forward shock interaction region, suggesting that it is RT unstable, similar to the adiabatic SN cases.

D. $3\omega_0$ run: laser frequency set equal to $3\omega_0$; all other parameters remain the same as in A.

In Fig.23-26 we compare the density, pressure, velocity and temperature profiles of the $2\omega_0$ versus $3\omega_0$ runs at 1ns, just before the shock reaches the LD-HD foam interface. By integrating the density x velocity profile we find that in the $3\omega_0$ case the blowoff delivers to the foams only about 60% of the shock momentum of the $2\omega_0$ case. Hence from the point of view of generating the stronger shock, a $2\omega_0$ laser is definitely better than the $3\omega_0$ laser.

5. PROPOSED NOVA EXPERIMENTS

Based on the results of above numerical simulations, we propose a series of NOVA experiments using 5 NOVA $2\omega_0$ beams of 0.7 terawatt each incident at 50° from normal and a foam standoff distance of 0.5mm. Based on the design calculations by Gail Glendinning the 5 beams should be able to avoid the foams and produce an average *projected intensity of 10^{14} W.cm^{-2} lasting about 3.5 ns. The footprint of the 5 beams is* reproduced in Fig.27. The circular region has a diameter of 0.15 cm which should deliver a plane target blowoff covering an effective area of at least 0.1 cm diameter. Even though the laser intensity in the footprint appears quite nonuniform over the circular region, based on past experience the resultant blowoff should quickly homogenize itself.

For the first experiment we should start with the *lowest density* foam available since lower density should lead to higher shock velocity and temperature, and study the effects of increasing foam density in later shots. To simulate the transition from the BSW to the HDR in SN1987A we suggest using a density jump of a factor of 10 between the LD and HD foams. But the thickness of the LD foam depends on the foam density. For an LD foam density of ~1mg/cc a thickness of 0.6mm is recommended but if the LD foam density goes as high as 5mg/cc its thickness should be reduced to 0.5mm or even less, since the shock speed decreases with increasing density. We should try to observe the propagation of the shock profile in both x-ray emission and absorption. In particular, time-and space-resolved x-ray spectral measurements will be useful in studying the evoluton of the output x-ray spectrum as a function of the foam densities. The use of laser probe beams and high-Z tracers in the foam should also be considered.

Once the above benchmark experiments prove successful, we should consider follow-up experiments aimed at (a) studying the effects of reduced thermal conductivity, (b) 2-dimensional effects. Two methods of inhibiting the plasma thermal conductivity should be explored: (a) doping the target and foam materials with high Z atoms (since Spitzer resistivity goes up as Z) and (b) application of transverse magnetic fields. In order to freeze the external magnetic flux into the blowoff and foams we may explore preheating the materials to ionizing temperatures for long enough so that the fields can fully diffuse into the plasma before the blowoff begins. To study 2-dimensional effects we may first try various rod or ring shaped HD foam geometries to simulate the HD ring or shell.

E.L. gratefully acknowledges the hospitality and support of X-Divison , LLNL for this work. He also thanks Rich London, Bruce Remington and John Castor for valuable discussions. The LASNEX generator decks are adapted from input.decks provided by Rich London.

6. REFERENCES

Band, D. 1988, Ap. J. 332, 842.
Band, D. and Liang, E. 334, 266.
Chevalier, R. 1982, Ap. J. 258, 790.
Chevalier, R. 1992, Nature 355, 691.
Chevalier, R. and Blondin, J. 1995, Ap. J. 444, 312.
Chevalier, R. and Liang, E. 1989, Ap. J. 344, 332.
Dickel, J. and Jones, E. 1985, Ap. J. 288, 707.
Fechner, W. et al 1984, Phys. Fl. 27, 1552.
Liang, E. and Chevalier, R. 1984, Annals N.Y. Acad. Sci. p.233 (NYAS, NY).
Luo, D. and McCray, R. 1991, Ap. J. 379. 659.
Luo, D. et. al. 1994, Ap. J. 430, 264.
Max, C. 1982, Laser-Plasma Interaction, XXXIV Les Houches Proc. p.302 (North Holland, Amsterdam).
McCray, R. 1993, Ann. Rev. Ast. Ap. 31, 175.
Panagia, R. et al. 1991, Ap. J. 380, L23.
Schmalz, R. 1985, Phys. Fl.28, 2923.
Spitzer, L. 1967, Physics of Fully Ionized Gases (Wiley, NY).
Suzuki, T. et al. 1993, Ast. Ap. 274, 883.
Wang, L. and Mazzali, P. 1992, Nature 355, 58.

Fig.1 (a) Artist conception of the peanut-shaped cocoon of low density BSW surrounded by a high density shell formed by the interaction of the BSW with the RSW. The ejecta of SN1987A is represented by the central sphere; (b) triple ring system observed by the NTT compared with a simulated image of the rings, which are formed by limb brightening when the cocoon of (a) is viewed at 43° from the symmetry axis (from Wang and Mazzali 1992).

Fig.2 Sample density and temperature profiles of the interaction zone between the SN ejecta and the CSM. NC denotes the adiabatic case and C denotes the conducting case with flux-limited Spitzer thermal conduction (from Liang and Chevalier 1984).

Fig.3 2-dimenisonal numerical simulation of the SN1987A shock interaction with the equatorial high density ring (from Suzuki et al 1993).

Fig.4 Sketch of the initial geometry of the laser target and the foam layers.

Fig.5 Density profile snapshots of the benchmark run (caseA) with LASNEX.

Fig.6 Pressure profile snapshots of the benchmark run.

Fig.7 Velocity profile snapshots of the benchmark run.

Fig.8 Bremsstrahlung emissivity profile snapshots of the benchmark run.

Fig.9 Temperature profile of the benchmark run at 3.1 ns.

Fig.10 Transverse x-ray flux spectrum near the density peak at 3 ns for the benchmark run.

Figs.11-15 Density, pressure, velocity, temperature and bremsstrahlung emissivity profile snapshots of the high foam density run (case B).

Fig.16 Comparison of the forward shock trajectories after the shock hits the HD foam between (a) case A and (b) case B

Fig.17 Comparison of the peak shock density as a function of time after the shock hits the HD foam between (a) case A and (b) case B.

Figs.18-22 Density, pressure, velocity, temperature and bremsstrahlung emissivity profile snapshots of the adiabatic run (case C).

Figs. 23-26 Comparison of the density, pressure, velocity and temperature profiles at 1ns between the benchmark $2\omega_0$ and the $3\omega_0$ runs (case D).

Fig.27 Combined footprints of 5 NOVA beams incident at 50° from normal (from Glendinning 1995).

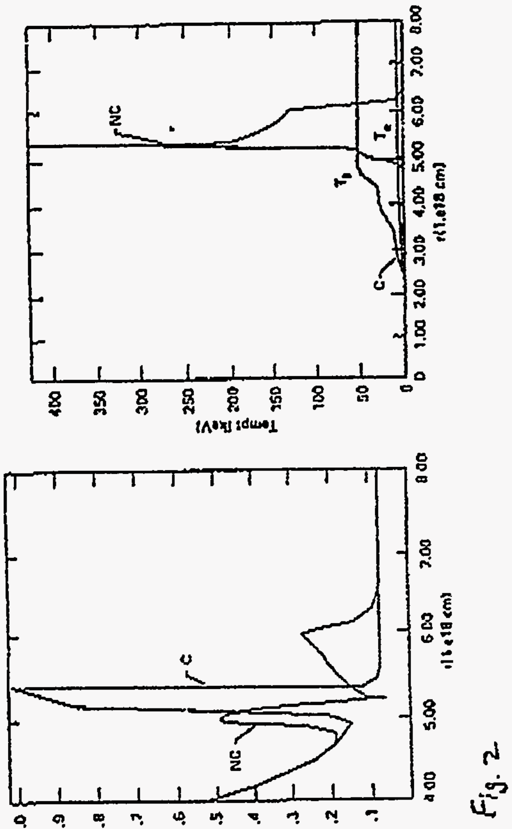

Fig. 2

Fig.2

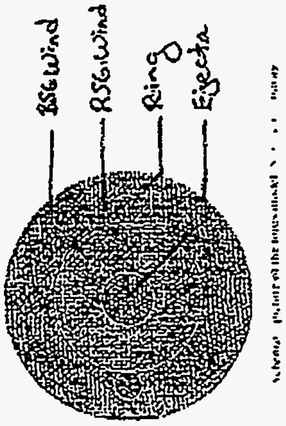

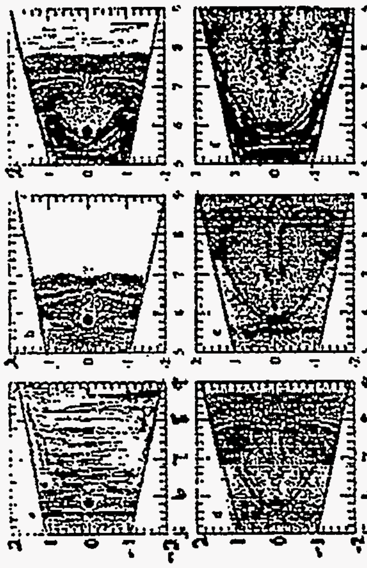

Fig. 3

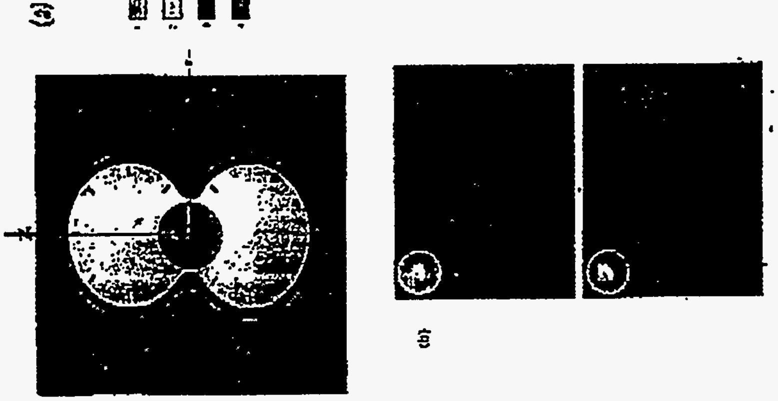

Fig. 1

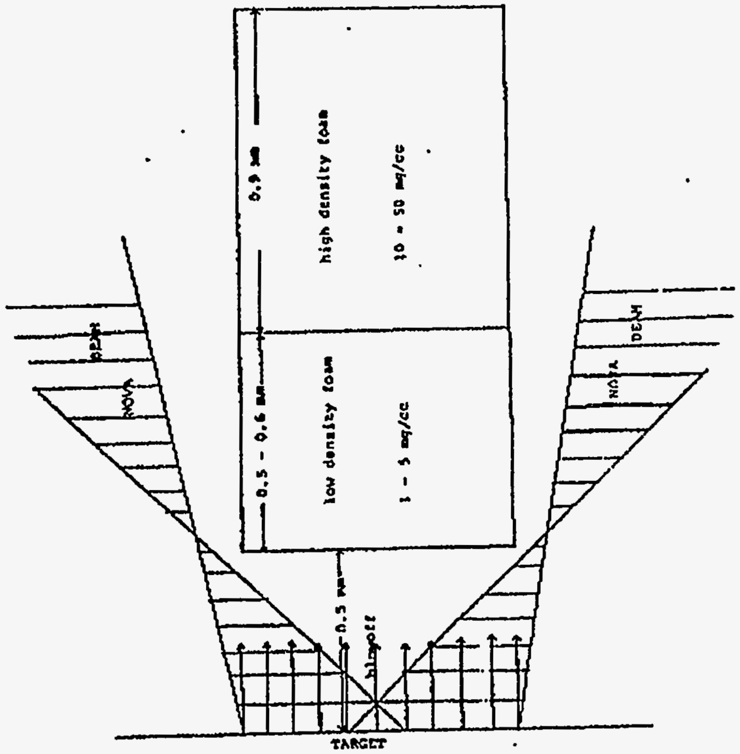
0.9 mm
high density foam
10 - 50 mg/cc
0.5 - 0.6 mm
low density foam
1 - 5 mg/cc
0.5 mm
blowoff
TARGET
NOVA
DEAM
NOVA
DEAM

Fig. 4

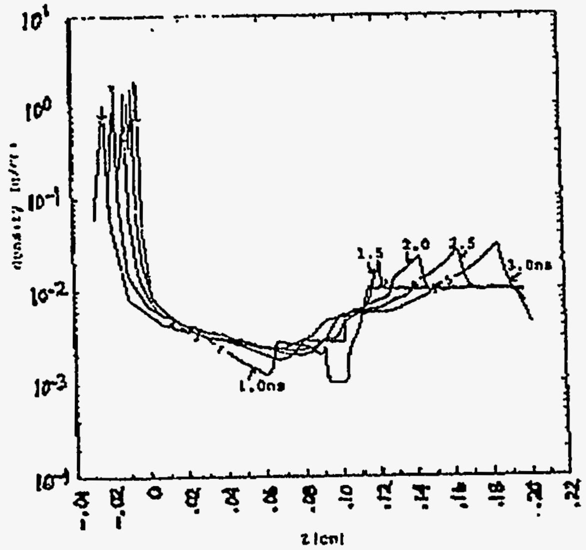
density (g/cc)
10¹
10⁰
10⁻¹
10⁻²
10⁻³
10⁻⁴
-.04
-.02
0
.02
.04
.06
.08
.10
.12
.14
.16
.18
.20
.22
z(cm)
1.0ns
1.5
2.0
2.5
3.0ns

Fig. 5

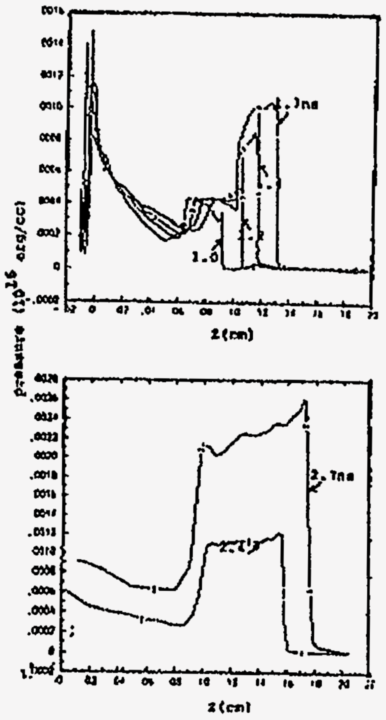

Fig.6

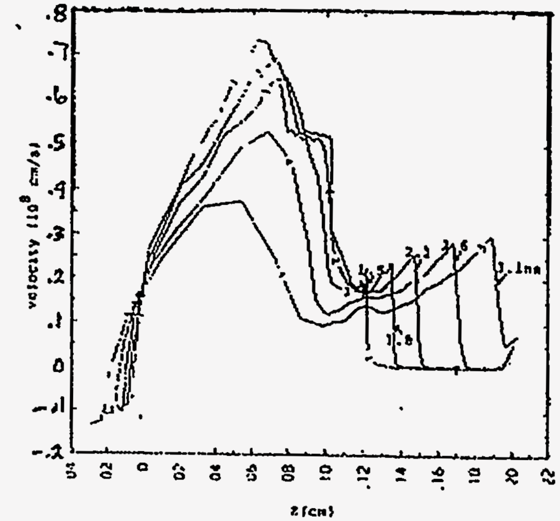

Fig.7

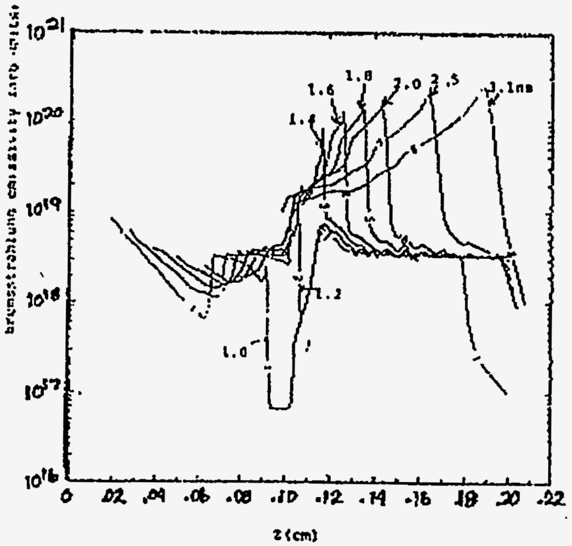

Fig.8

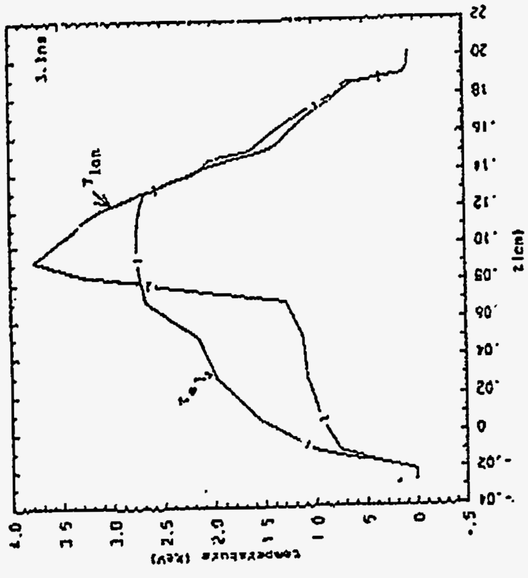

Fig. 9

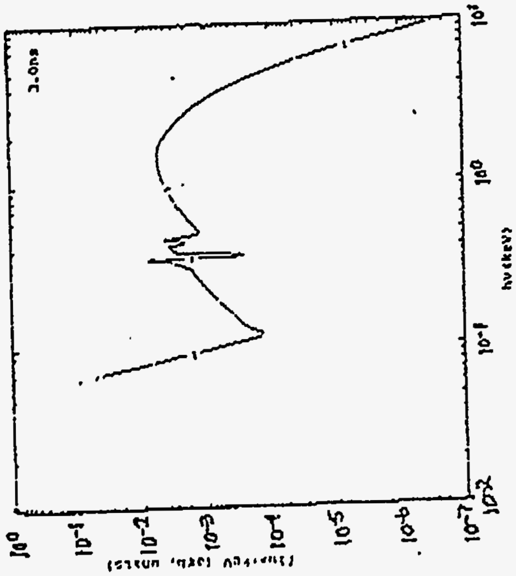

Fig. 10

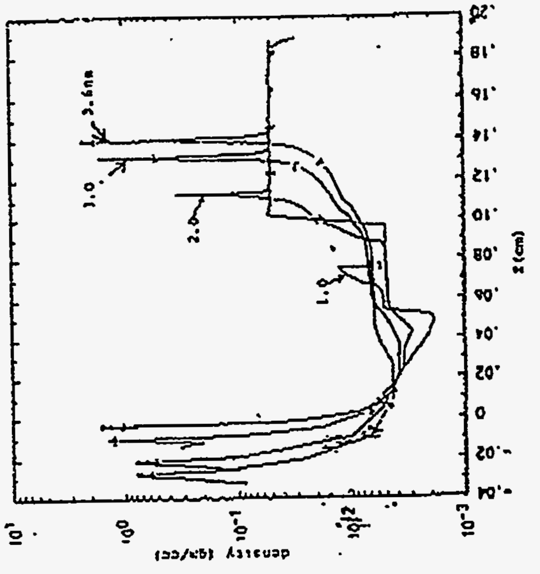

Fig. 11

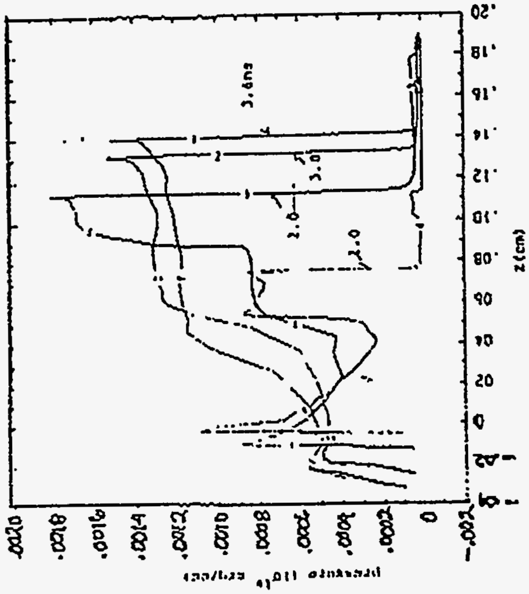

Fig. 12

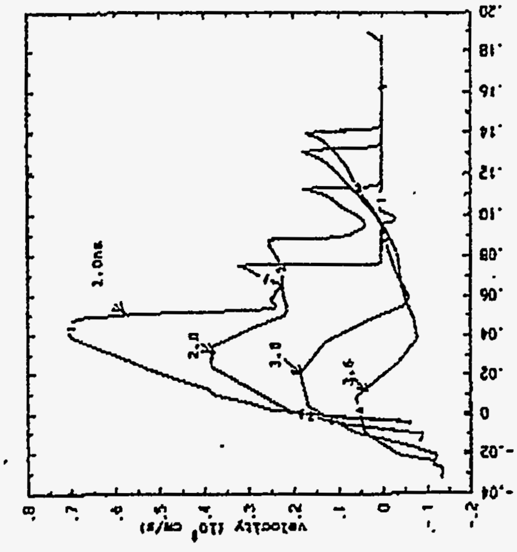

Fig.13

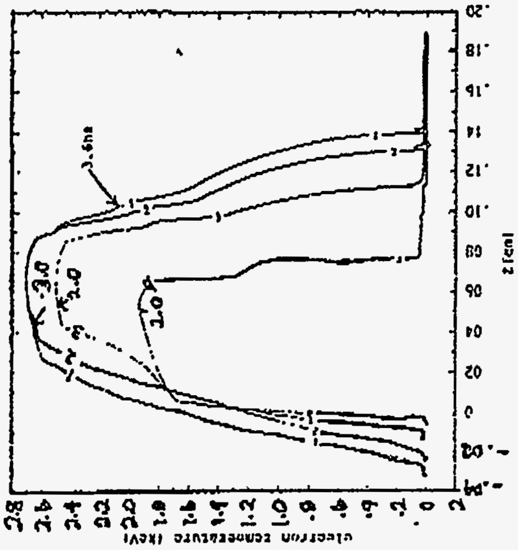

Fig.14

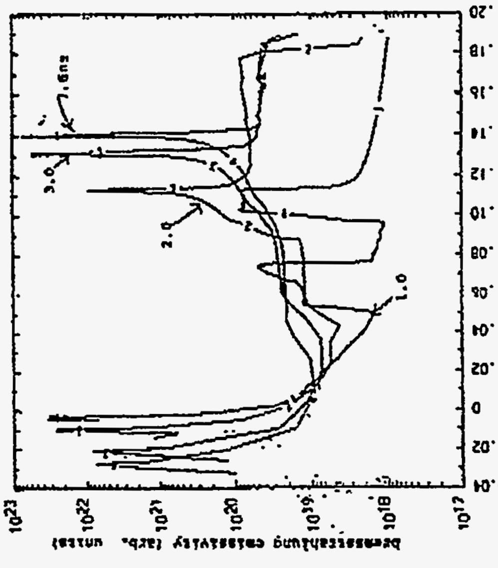

Fig.15

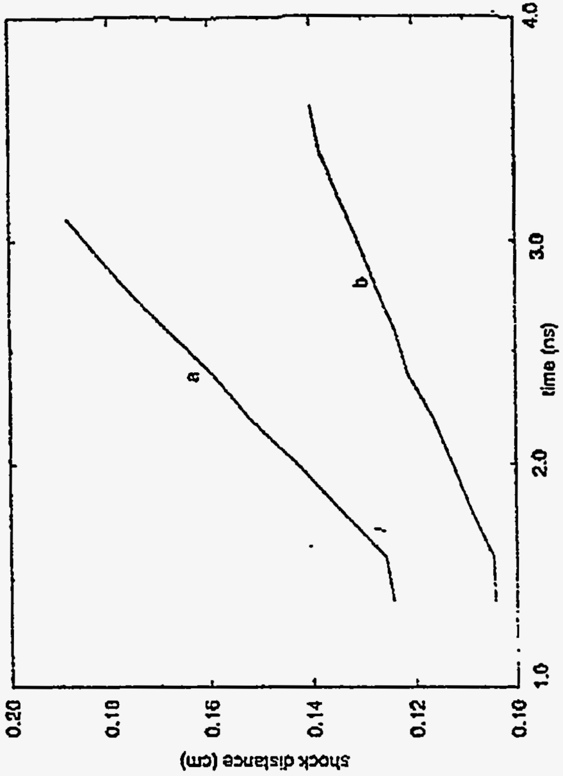

Fig.16

Fig.16

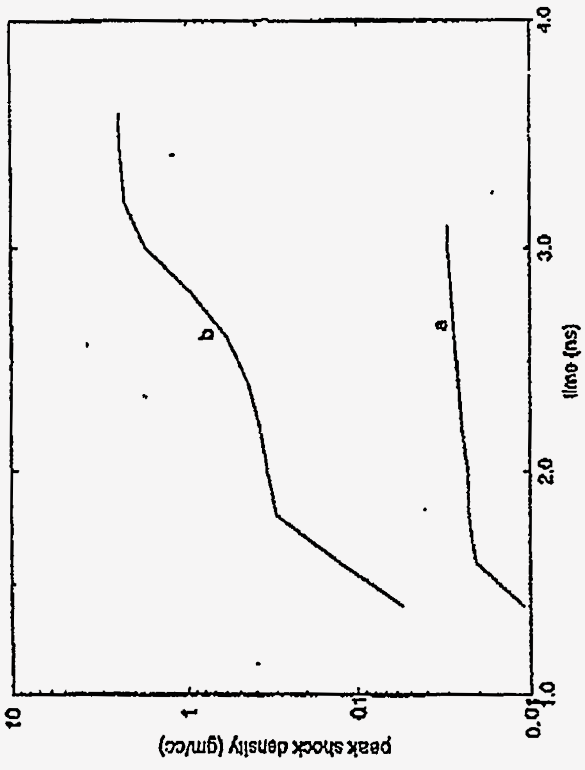

Fig. 17

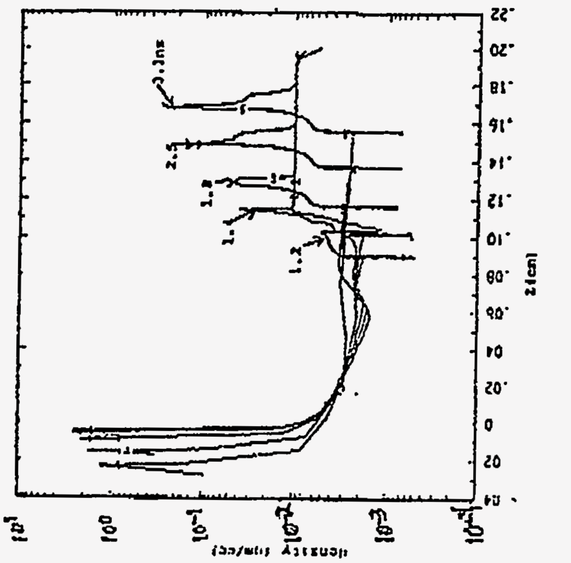

Fig 18

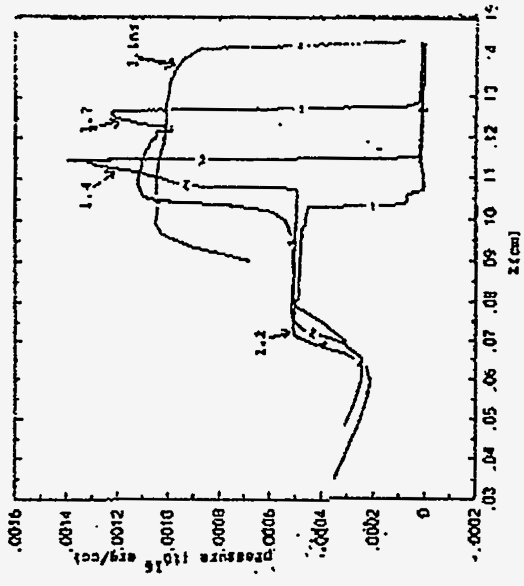

Fig. 19

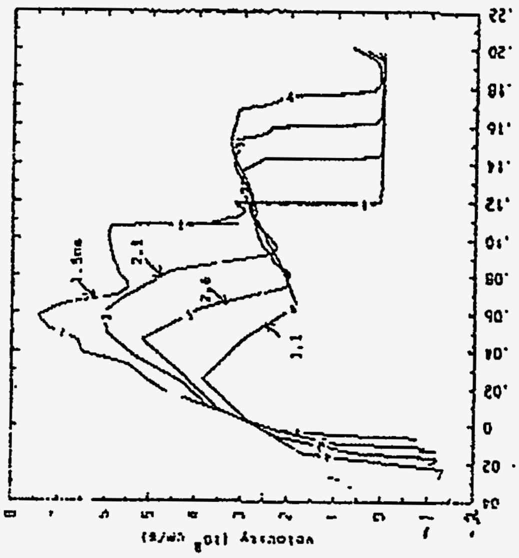

Fig. 20

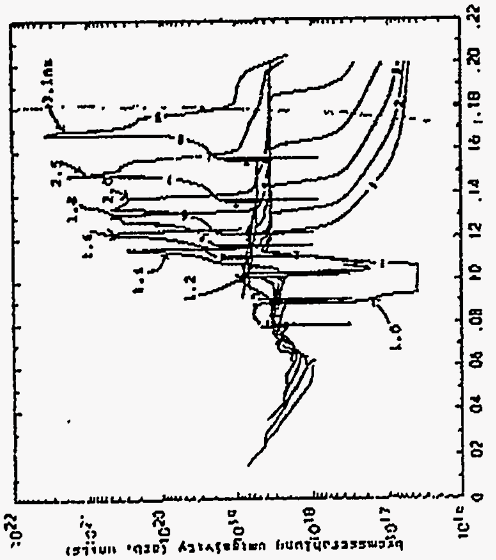

Fig.22

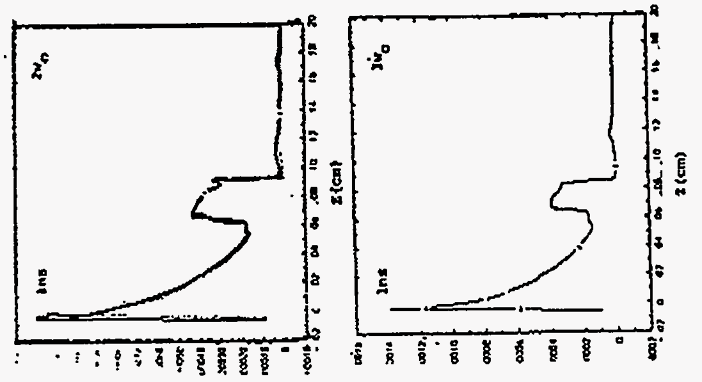

Fig.24

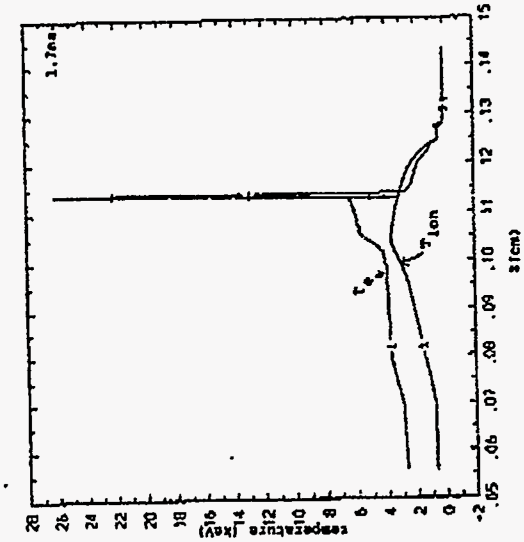

Fig.21

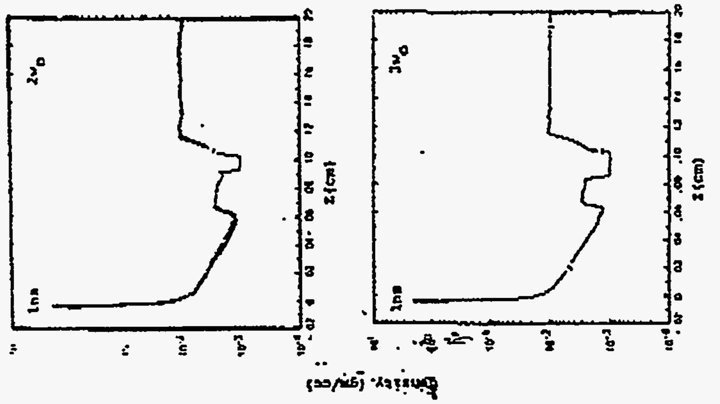

Fig.23

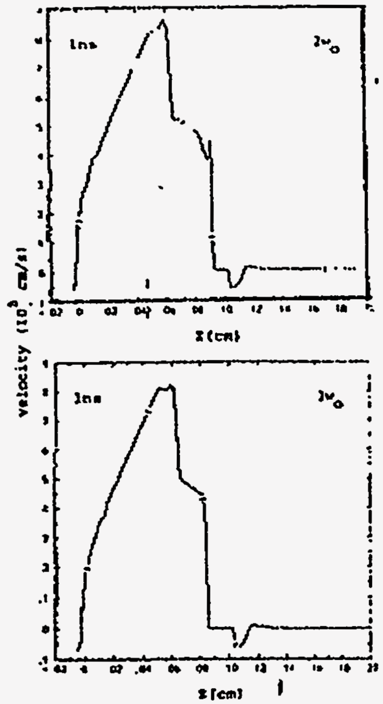

Fig 25

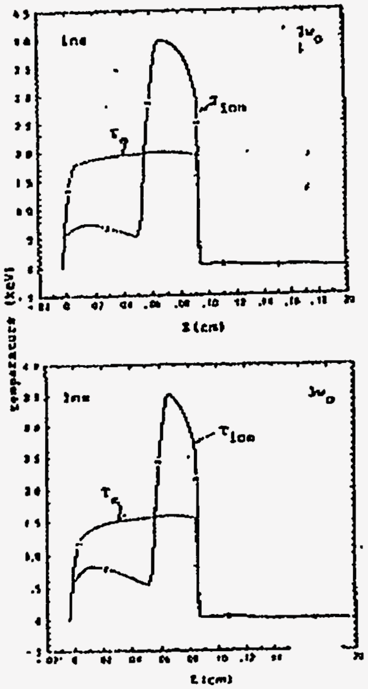

Fig 26

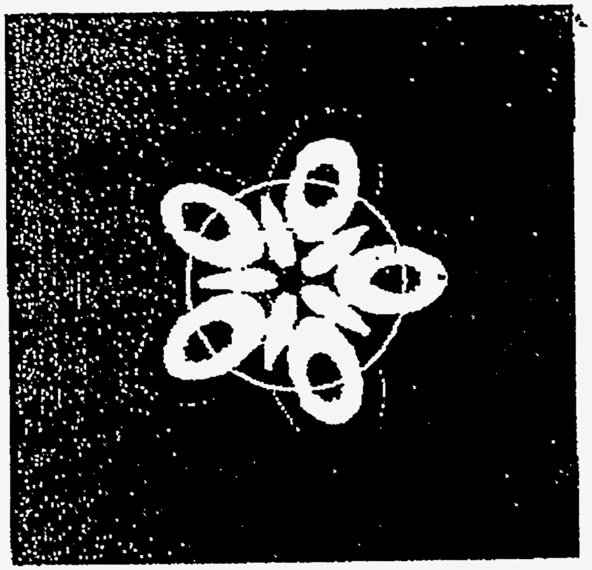

The circle is a 1500 μm diameter target, a fair amount of energy is outside the circle [illegible] to make the regions between the beams not go to [illegible] within the circle the average intensity is about [illegible] per input [illegible] beam of laser light and the standard deviation is about [illegible] W/cm². [illegible] TW/beam we can run Nova for about 3.5 ns, about 4 ns with [illegible]

Fig 27

Results from a Recent Shock Wave Experiment on Trident

Gottfried Schappert
Los Alamos National Laboratory

Results from a recent Shock Wave Experiment on Trident

i.e.

the Vishniac Instability

Gottfried T. Schappert , Robert D. Fulton and David M. Oro

Los Alamos

Blast Wave in 5 torr Helium (d05)

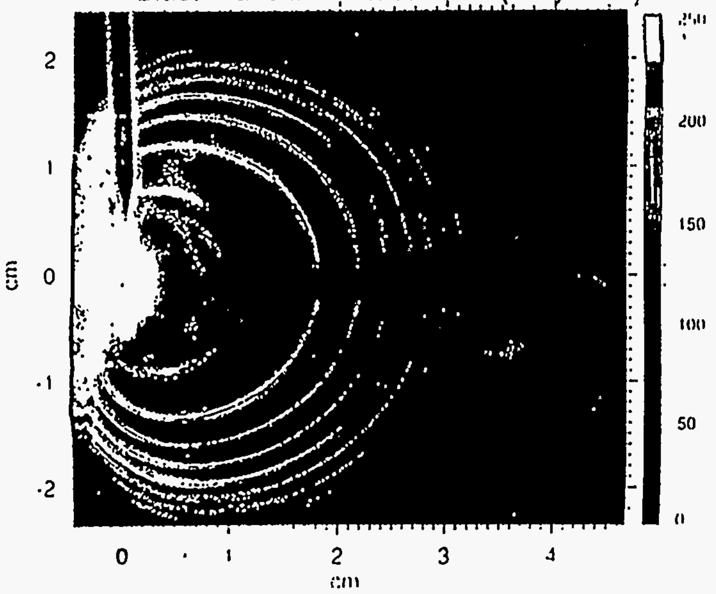

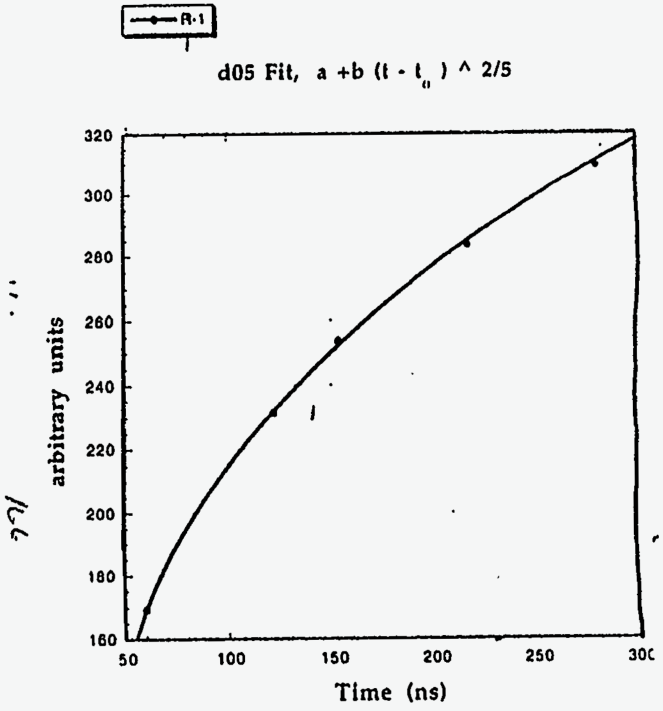

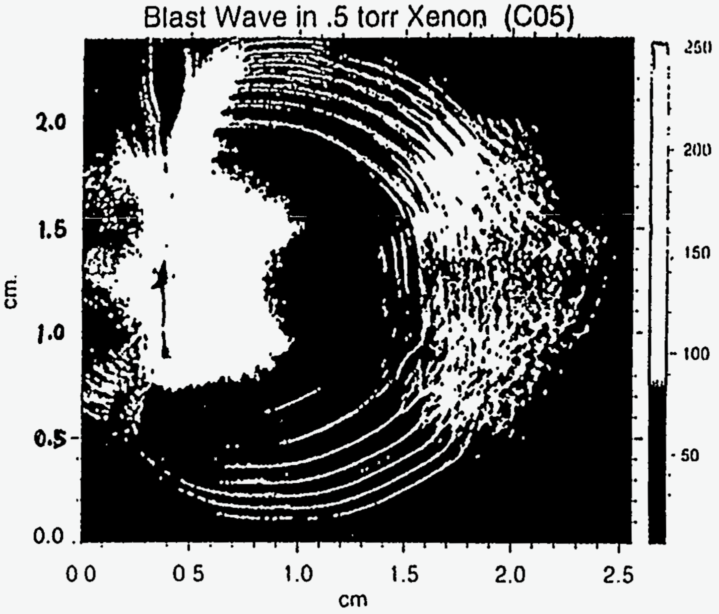

The Growth of Linear Perturbations of Adiabatic Shock Waves

D. Ryu and E. Vishniac, The Astrphysicsal Journal, 313: 820-841, Feb. 1987

The Perturbed radius of a spherical wave is

$$R \sim t^{2/5} \left(1 + b \times t^{S} \times Y_l^m(\Theta, \phi) \right)$$

The growth rates S for various values of l are:

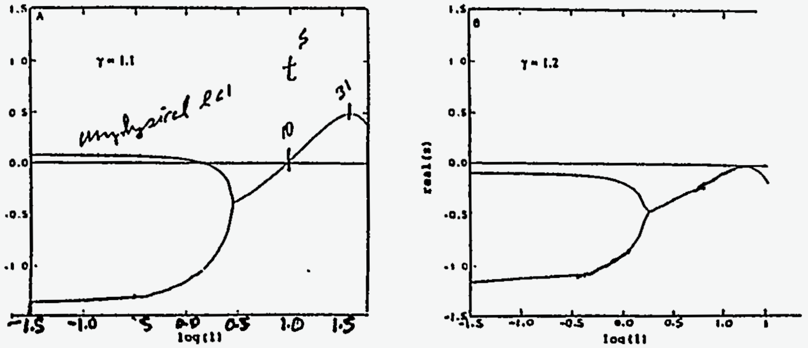

γ : the ratio of specific heats c_p / c_v

In statistical mechanics γ = (degrees of freedom + 2) / (degrees of freedom)

Xe : $\gamma = 5/3$

N_2 $\gamma = 7/5 - 9/7$

For non-ideal gases, under conditions of dissociation, excitation and ionization the blast wave model uses the relationship between pressure, energy density, and density

$P = (\gamma - 1) E \rho$

which we can get from equation of state tables.

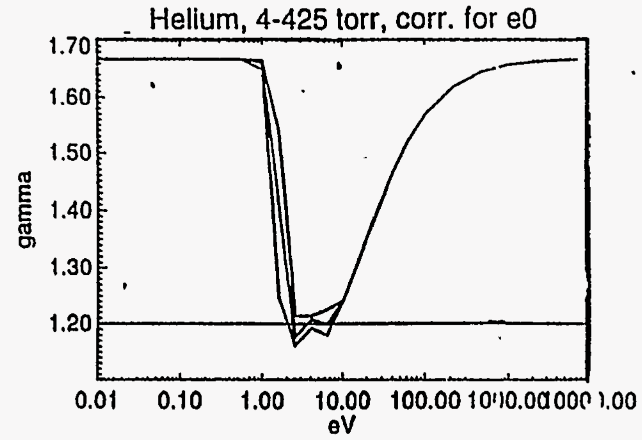

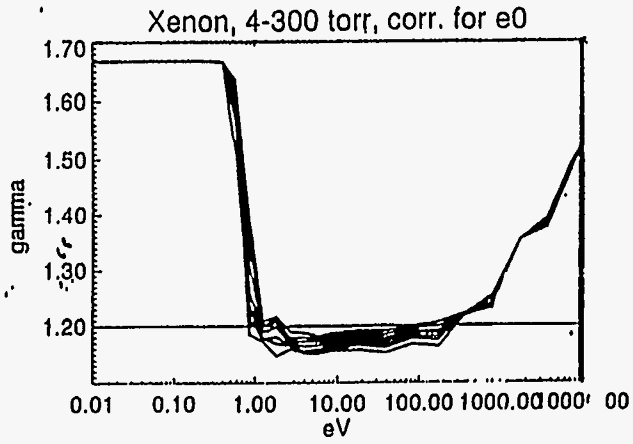

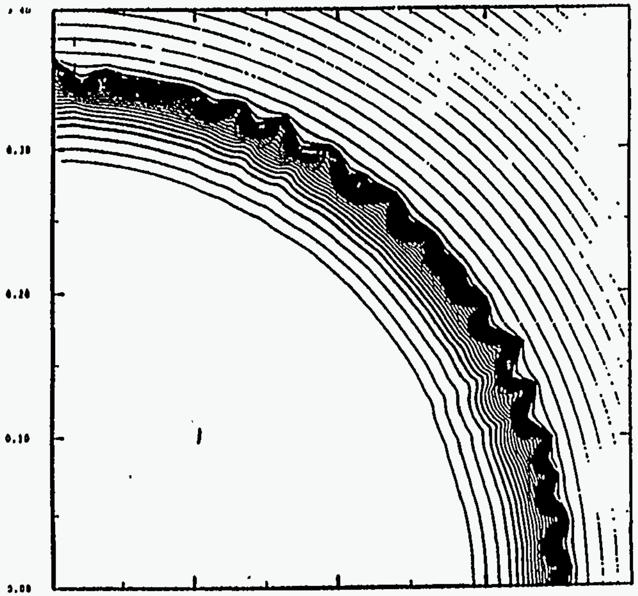

LASNEX calculation of a sherical Taylor-Sedov blast wave in a gas with a $\gamma = 1.06$ and a perturbation of 10^{-4} $P_{l=30}$

Top View of Layout for Trident Blast Wave Experiment

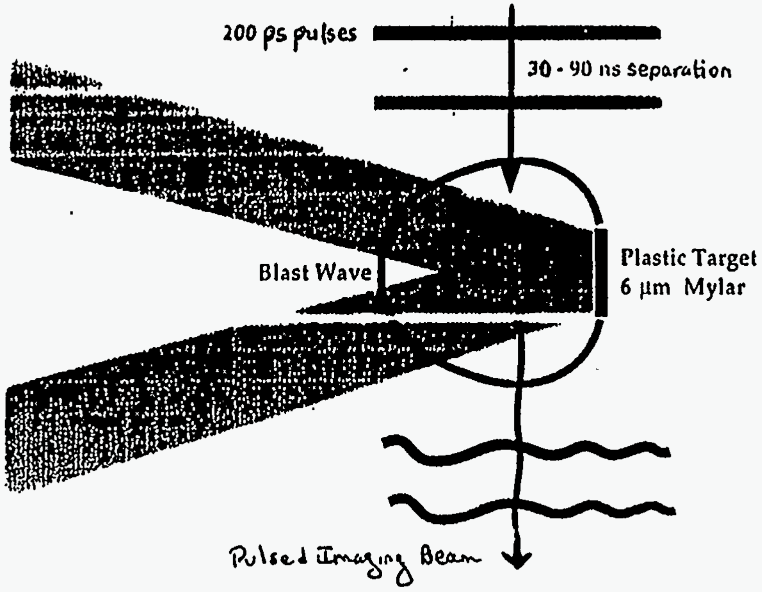

Imaging and Interferometry layout

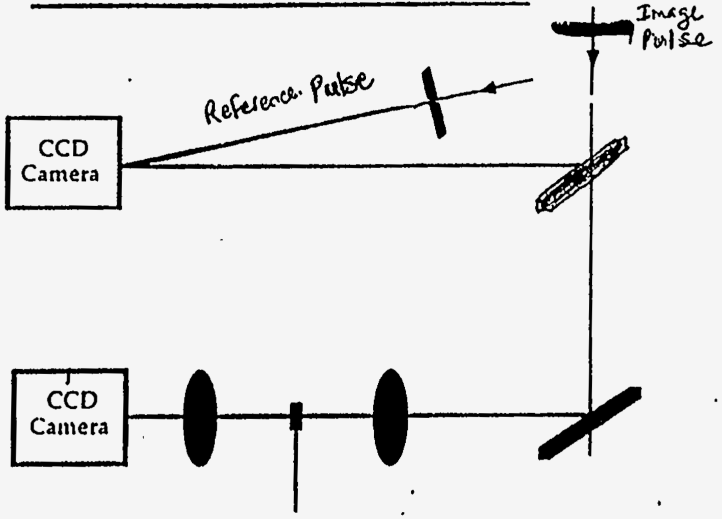

Los Alamos

Image and Interferogram of Blast Wave in Helium

5 torr He
138 J
Time 52.6 ns

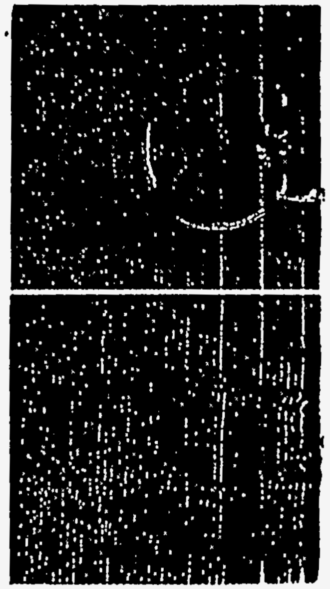

Image and Interferogram of Blast Wave in Xenon

1 torr Xe
118 Joules
Time 52.9 ns.

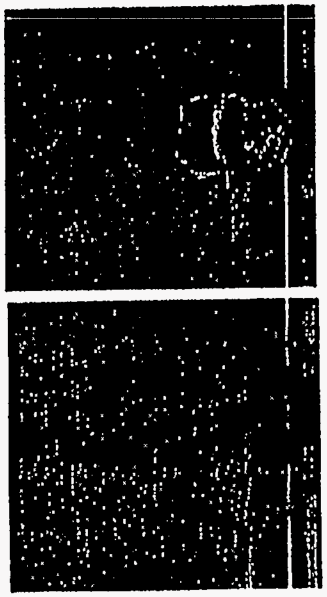

Los Alamos

Soda Straw

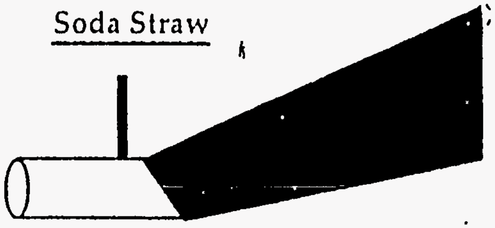

25 torr Xe
47 J

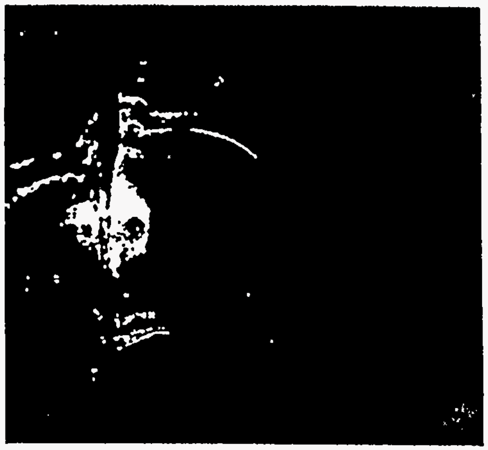

P105

Conclusion:

This is fun stuff

More modeling with complete hydro, atomic and
radiation physics needs to be done

Even small laser systems can still contribute

Instabilities, Convection and Smoke Rings

Stirling Colgate
Los Alamos National Laboratory

INSTABILITIES, CONVECTION AND SMOKE RINGS

Stirling Colgate, T-6, LANL

2/26/96

Why a dynamo?

Why an accretion disk?

Why a sodium explosion?

Why a hurricane?

Why a supernova; 1A?

Why a supernova; II

Why a thunderstorm?

Why a tornado?

Why a plume?

Why a mixing length?

why a mixing layer?

why a smoke ring?
in a non-smoking environment.

An answer to all, even a few of these would more than scratch the surface of the problem of instabilities, convection, and smoke rings, but such a big scratch deserves a big itch. : A unifying principle is needed:

The principle of maximal dissipation.

If it can, it will.

Or a scratch dissipates an itch.

Convection dissipates Free Energy
e, g, negative, gravity

Entropy. S $dS/d(z,R)$ negative

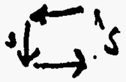

$\Longrightarrow$ free energy

Reed and Young

a = constant

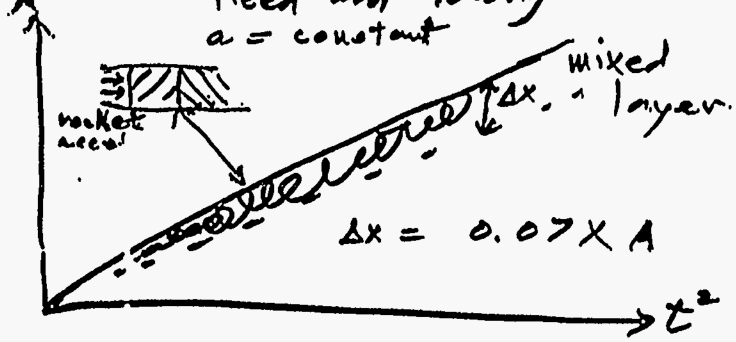

$\Delta x = 0.07 X A$

A = Atwood number - density contrast

$\frac{\rho_1 - \rho_2}{\rho_1 + \rho_2} \longrightarrow 1$

$\Delta x / x$ independant of a, acceleration

If gases are reactive

ie $\left\{ \begin{array}{c} Na + H_2O \\ C, O \Rightarrow Si \Rightarrow Fe \\ Lava + H_2O \end{array} \right\}$

S_0 original entropy

Then $\Delta x = .07 X (S_1/S_0)^?$

if $(.07\ S_1/S_0) \gtrsim 1$ then a flame

if $(\quad) >> 1 \Rightarrow$ explosion,

$$\Delta x = \Delta_0 \exp\left[(2\pi A a/\lambda)^{1/2} t \right]$$

$$x = (1/2)\, a t^2$$

$$\Delta x = \Delta_0 \exp\left[\left(4\pi A \frac{x}{\lambda}\right)^{1/2} \right]$$

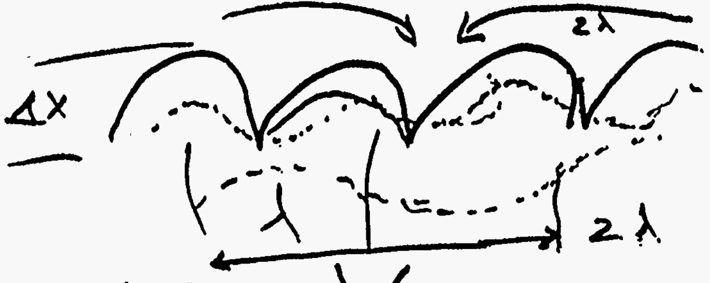

$$\Delta X = \lambda/2$$

Then $\exp\left(4\pi A\, x/\lambda\right)^{1/2}$

$$\simeq \exp\left[9\, A^{1/2} \right]$$

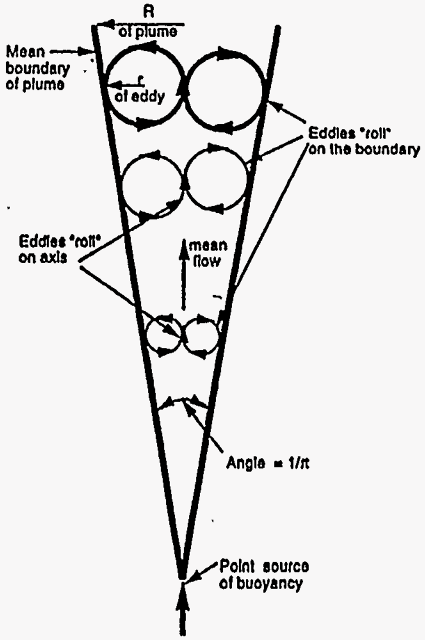

Plume: Steady State Structure of Convection

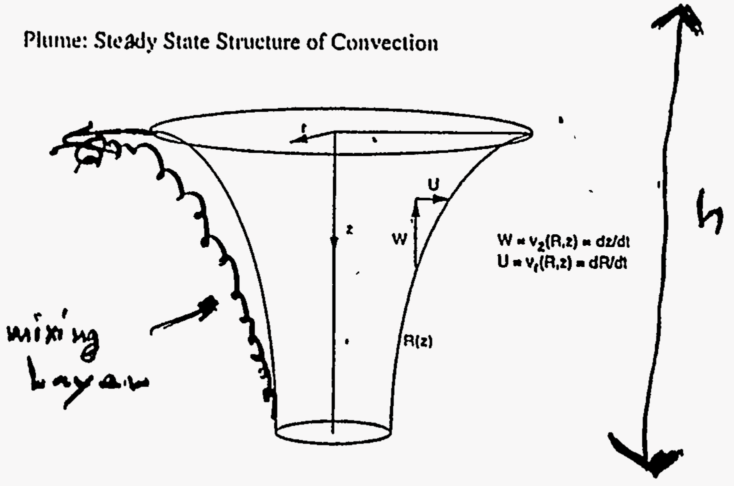

h = scale height

Plume Convection:
Equation for Radius W/O Entrainment

Greg Willette

$$\frac{d^2R}{dz^2}=\frac{1}{R}\left(\frac{z}{z_0}\right)^{2m}\left(\frac{R}{R_0}\right)^4-\frac{1}{R}+\frac{2}{\Im R z_0}\left(\frac{z}{z_0}\right)^{2m}\left(\frac{R}{R_0}\right)^4(z_0-z)+\frac{m}{z}\frac{dR}{dz}+\frac{2}{R}\left(\frac{dR}{dz}\right)^2+\left(\frac{z}{z_0}\right)^{2m}\frac{\Omega_0{}^2R}{\Im\varepsilon gz}$$

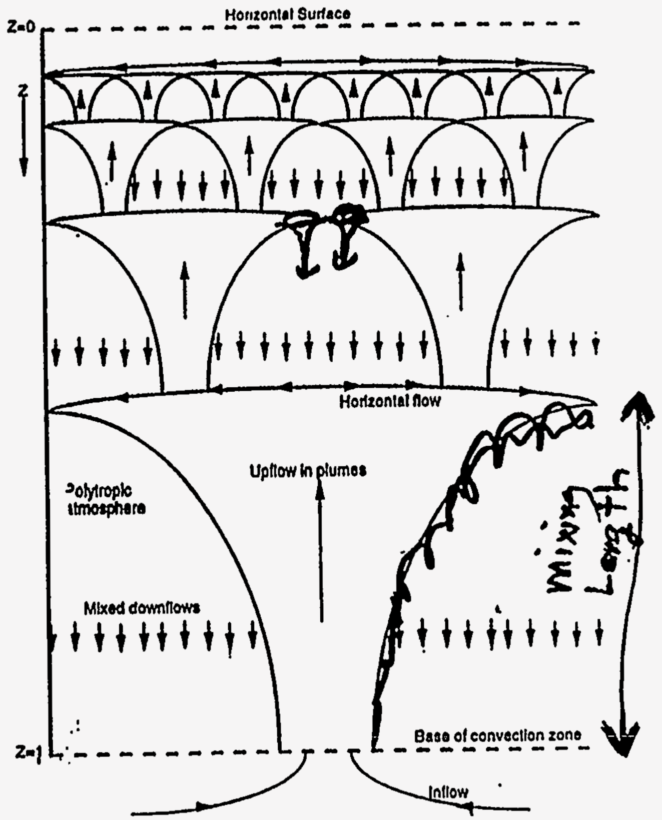
Horizontal Surface
Z=0
z
Horizontal flow
Polytropic atmosphere
Uplflow in plumes
Mixed downflows
Mixing Length
Base of convection zone
Z=1
Inflow

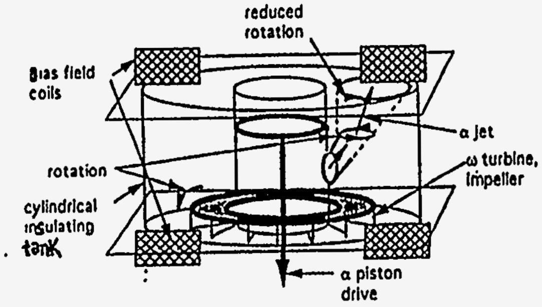
reduced rotation
Bias field coils
α jet
rotation
ω turbine, impeller
cylindrical insulating tank
α piston drive

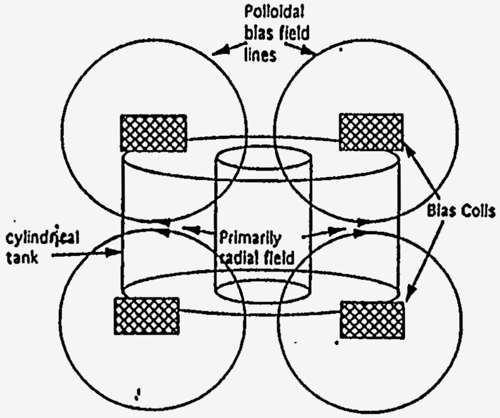
Polloidal bias field lines
Bias Coils
cylindrical tank
Primarily radial field

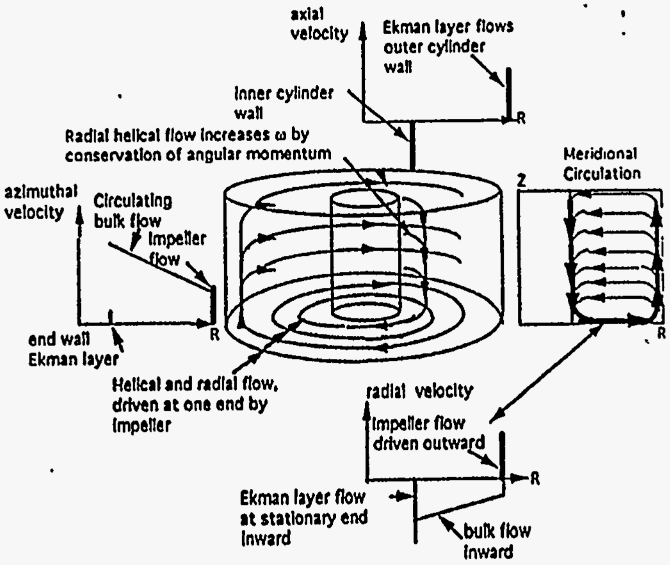
axial velocity
Ekman layer flows outer cylinder wall
R
Inner cylinder wall
Radial helical flow increases ω by conservation of angular momentum
azimuthal velocity
Circulating bulk flow
Impeller flow
R
end wall Ekman layer
Helical and radial flow, driven at one end by impeller
Z
Meridional Circulation
R
radial velocity
Impeller flow driven outward
R
Ekman layer flow at stationary end inward
bulk flow inward

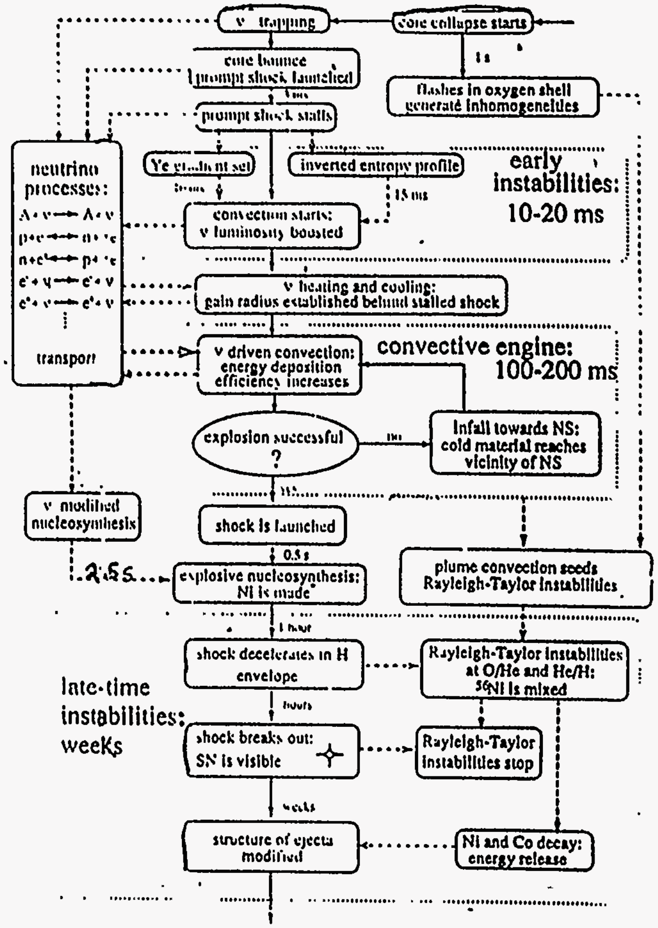
core collapse starts
1 s
flashes in oxygen shell generate inhomogeneities
ν trapping
core bounce
prompt shock launched
prompt shock stalls
Ye gradient set
inverted entropy profile
15 ms
convection starts:
ν luminosity boosted
early instabilities: 10-20 ms
neutrino processes:
A+ν ⟷ A+ν
p+e ⟷ n+ν_e
n+e⁺ ⟷ p+ν̄_e
e⁺+ν ⟷ e⁺+ν
e⁺+ν ⟷ e⁺+ν
⋮
transport
ν heating and cooling:
gain radius established behind stalled shock
ν driven convection:
energy deposition
efficiency increases
convective engine: 100-200 ms
explosion successful ?
Infall towards NS:
cold material reaches vicinity of NS
ν modified nucleosynthesis
shock is launched
0.5 s
2.5s
explosive nucleosynthesis:
Ni is made
plume convection seeds Rayleigh-Taylor instabilities
1 hour
shock decelerates in H envelope
Rayleigh-Taylor instabilities at O/He and He/H:
56Ni is mixed
late-time instabilities: weeks
hours
shock breaks out:
SN is visible
Rayleigh-Taylor instabilities stop
weeks
structure of ejecta modified
Ni and Co decay:
energy release

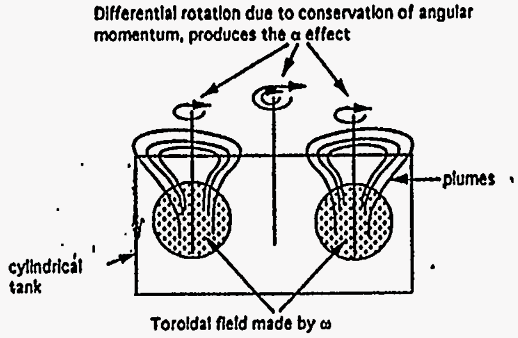
Differential rotation due to conservation of angular momentum, produces the α effect
plumes
cylindrical tank
Toroidal field made by ω

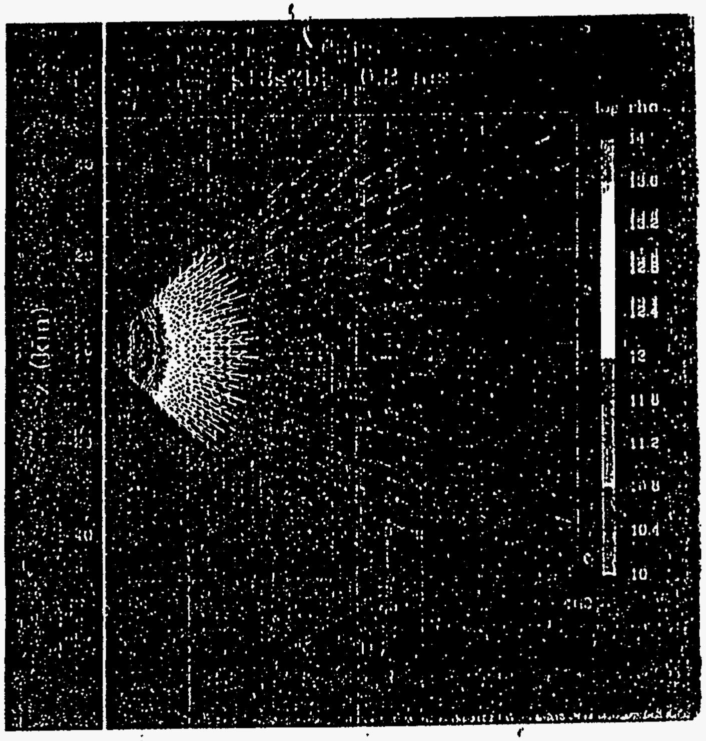
log rho
14
13.6
13.2
12.8
12.4
12
11.6
11.2
10.8
10.4
10
z (km)
20
40

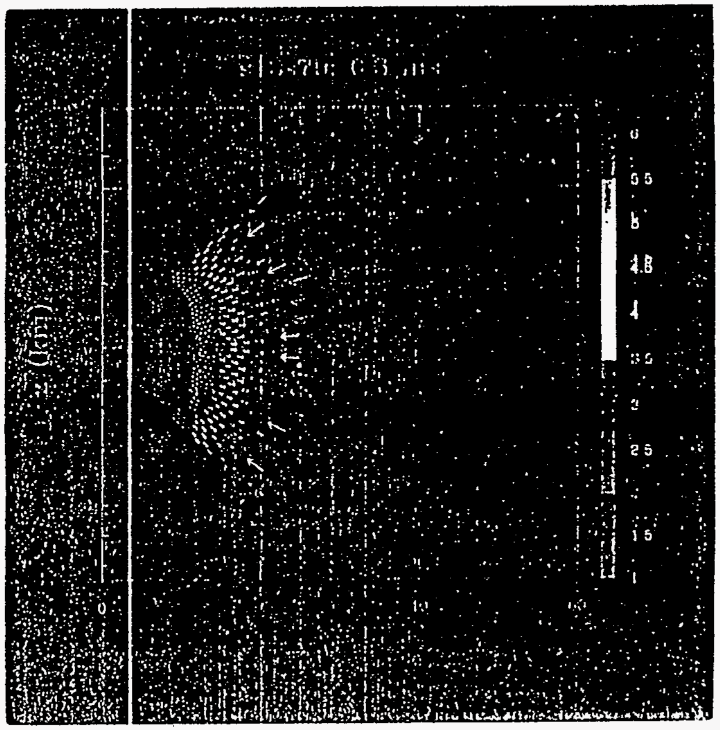
6
5.5
5
4.5
4
3.5
3
2.5
1.5
1
z (km)
0
10

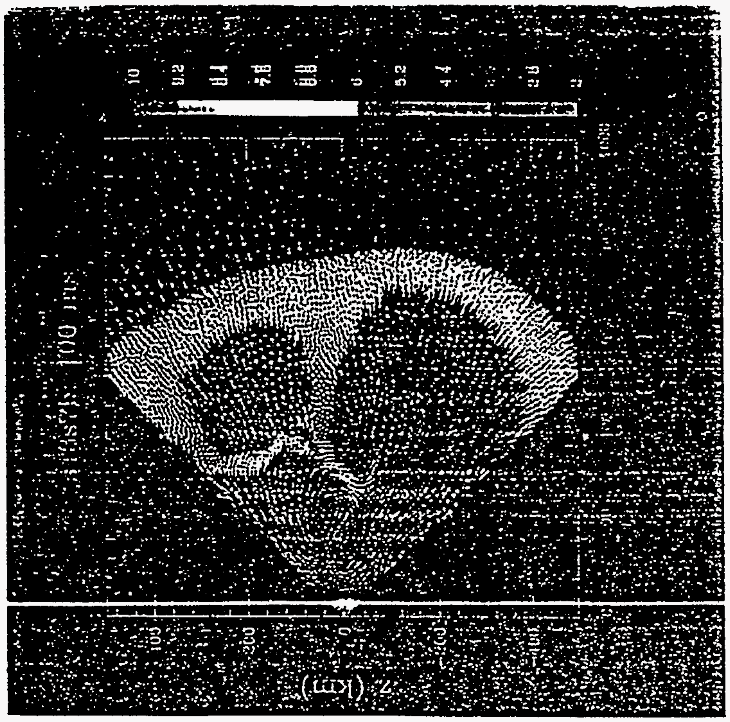
z (km)
100 ms
10
9.2
8.4
6.8
6
5.2
4.4
2.8
2

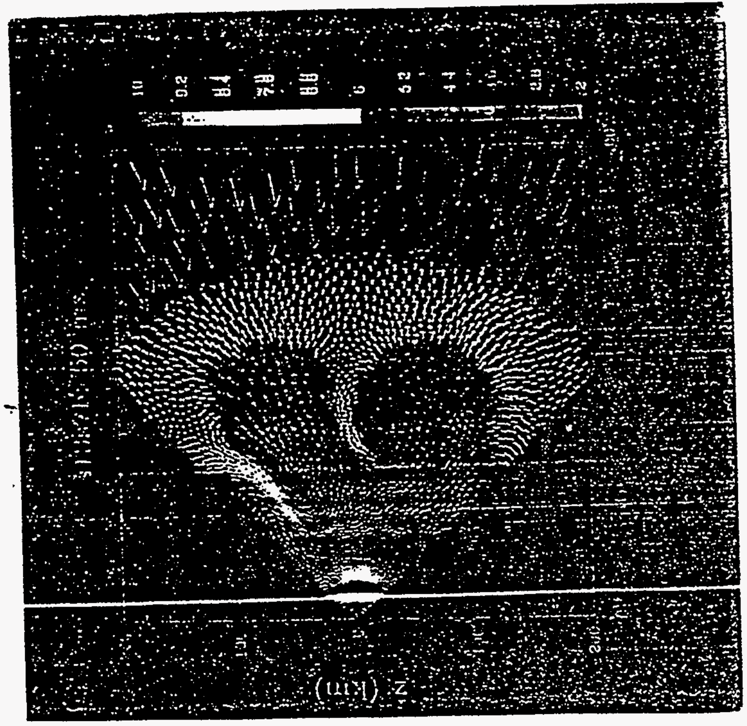
z (km)
50 ms
10
9.2
8.4
6.8
6
5.2
4.4
2.8
2

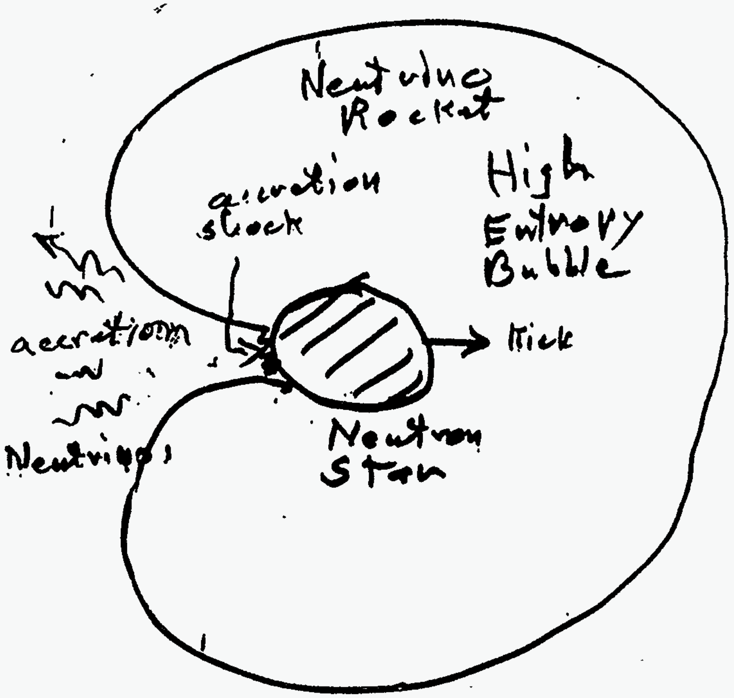
Neutrino Rocket
High Entropy Bubble
accretion shock
kick
accretion
Neutrinos
Neutron Star

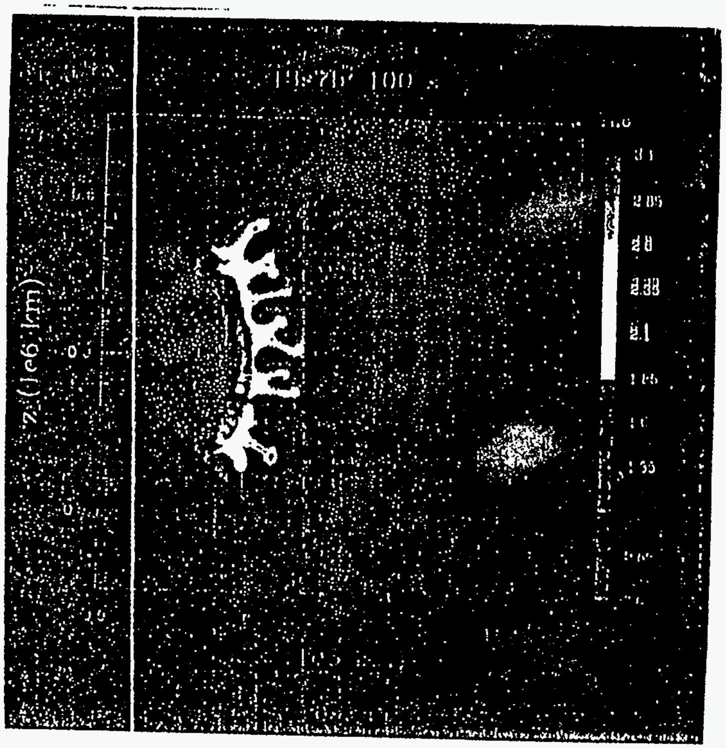
100 s
z (1e6 km)
2.05
2.1

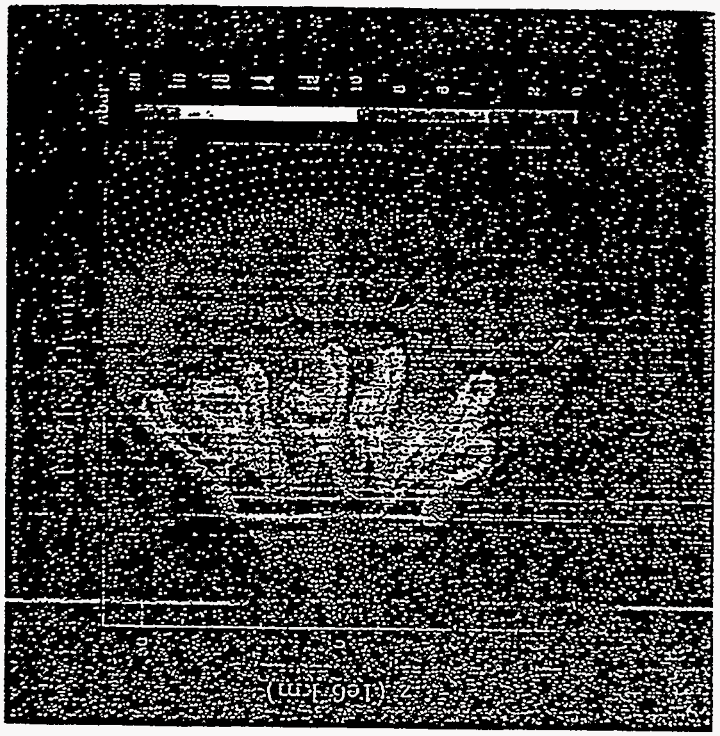
z (1e6 km)

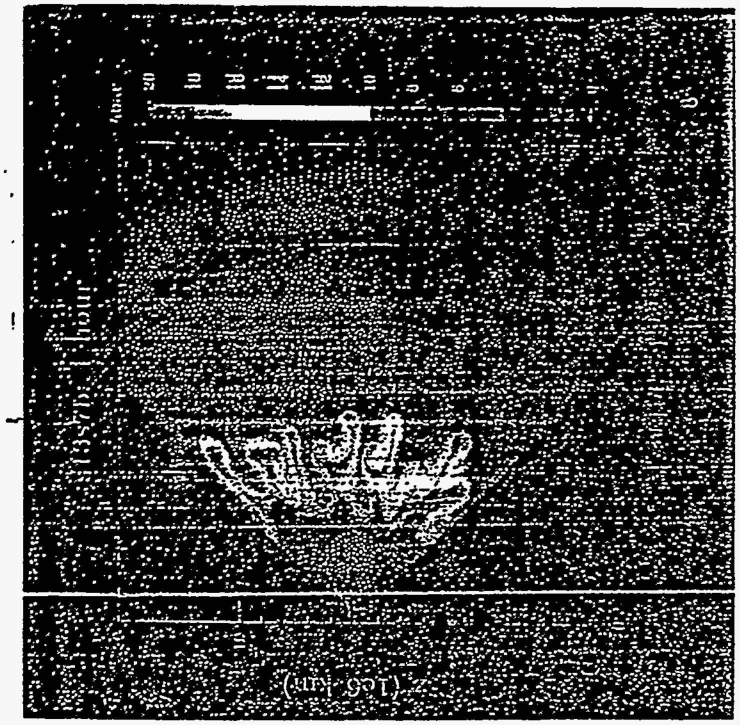
z (1e6 km)
hour

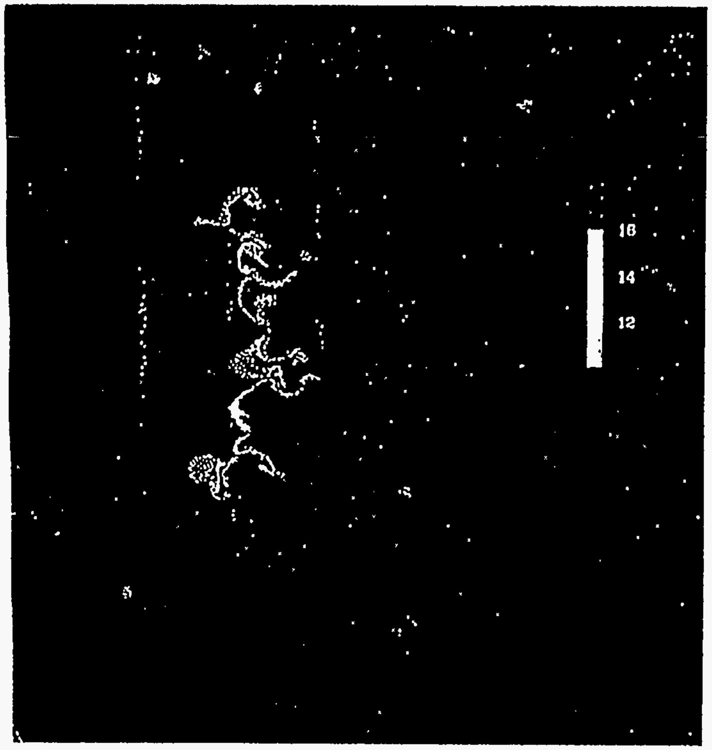
16
14
12

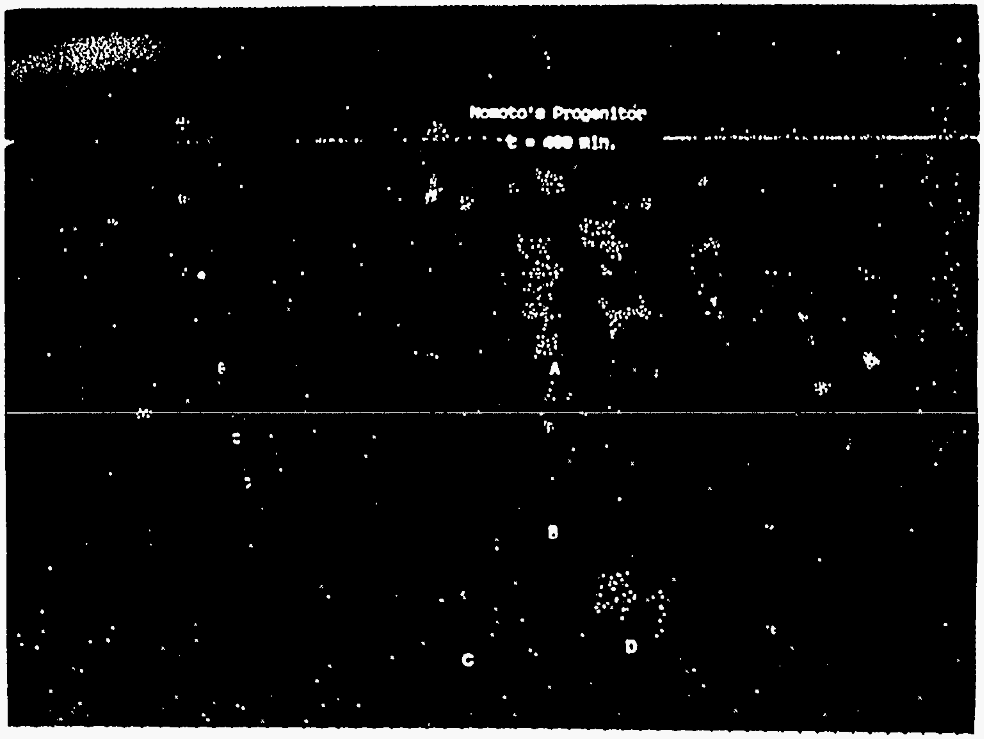
Nomoto's Progenitor
t = 400 min.
A
B
C
D

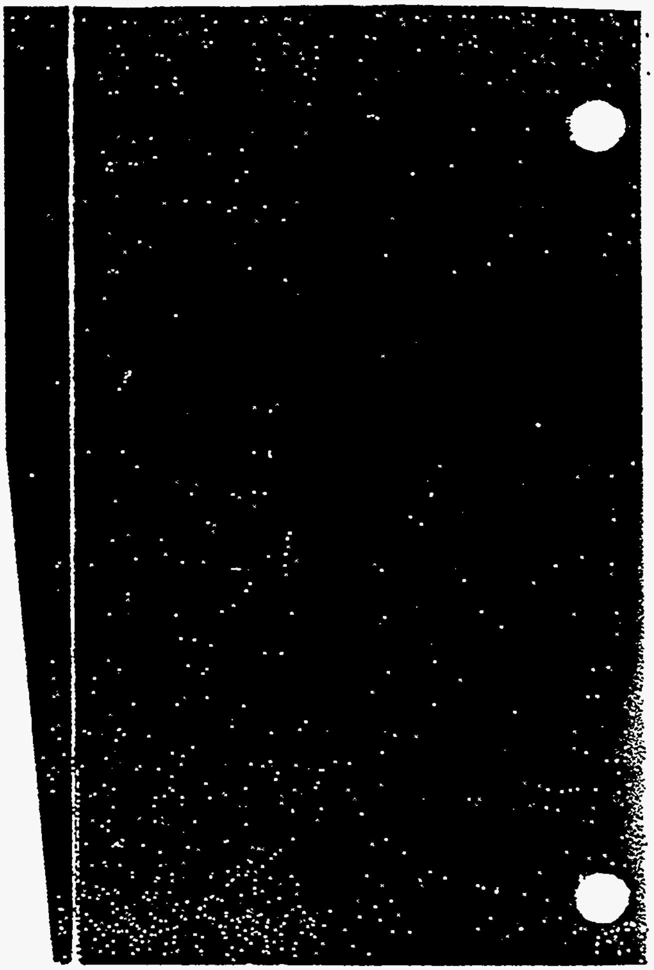

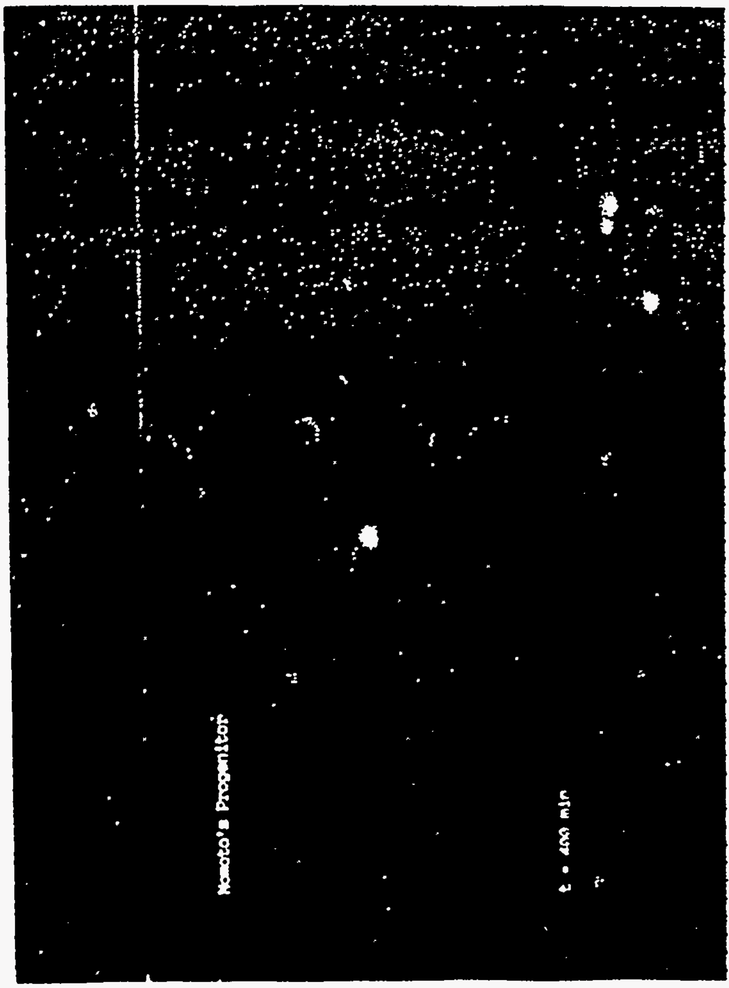
Nomoto's Progenitor
t = 400 min

Convection-Driven Turbulence

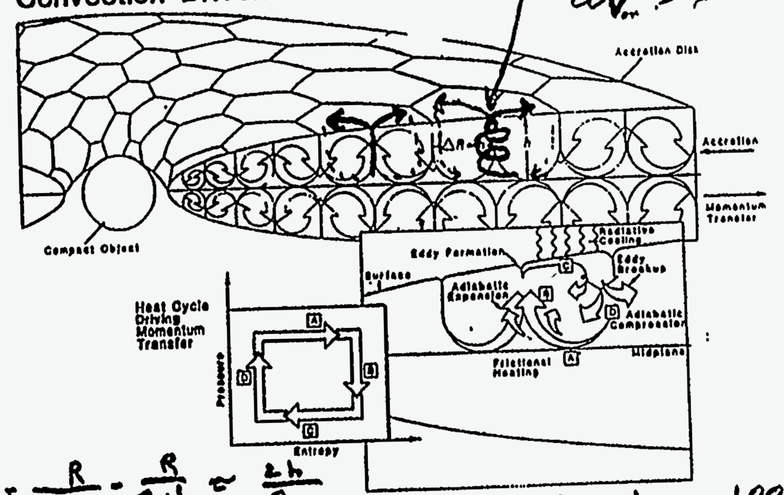

suction vortex
$\omega_{Vor} >> \omega_{Disk}$

$$\Delta V_{Kep}^2 = \frac{R}{R-h} - \frac{R}{R+h} \simeq \frac{2h}{R}$$

$$\Delta V_J^2 = \frac{R^2}{(R-h)^2} - \frac{R^2}{(R+h)^2} = \frac{4h}{R}$$

$$\Delta u^2 - \Delta V^2 = 2h/R = \Delta V_{Kep}^2$$

∴ Requires 100% efficiency

cannot with $\frac{T_{ambient}}{T_{..}} \to 0$

Car Engines, Hurricanes, suction vortex

Car Engine starts only for

$\omega_{starter} \gtrsim \frac{1}{10}\,\omega_{run}$

very non-linear instability

Hurricane = same starting condition

$\omega_{run} \simeq 100\,\omega_{earth}$

---

suction Vortex same starting

$\omega_{run} \simeq 10\,\omega_{Disk}$

Multiple Vortices act like un-meshed gears

$\omega_1 > \omega_2$

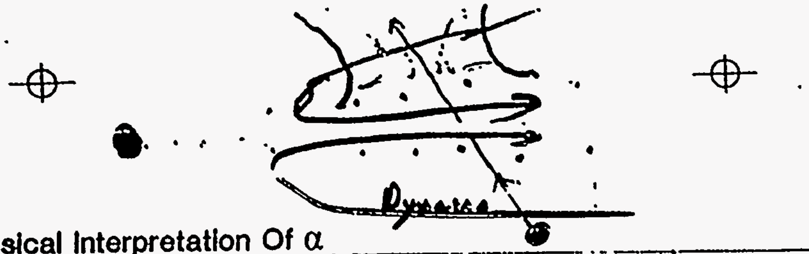

Physical Interpretation Of α

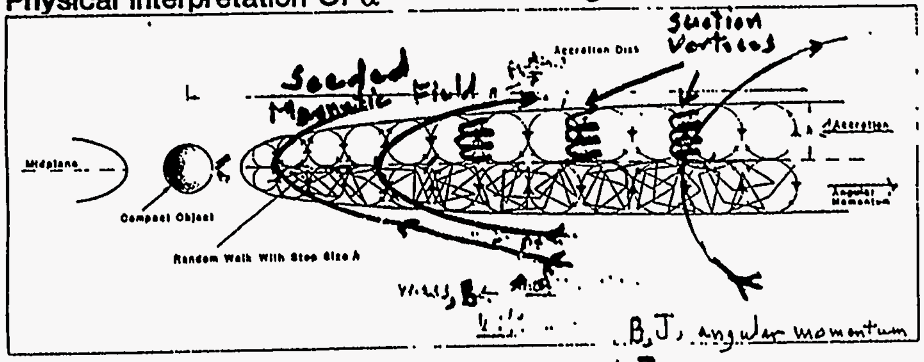

Diffusion of B ⇒ Diffusion of J, Angular momentum.

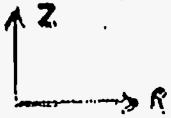

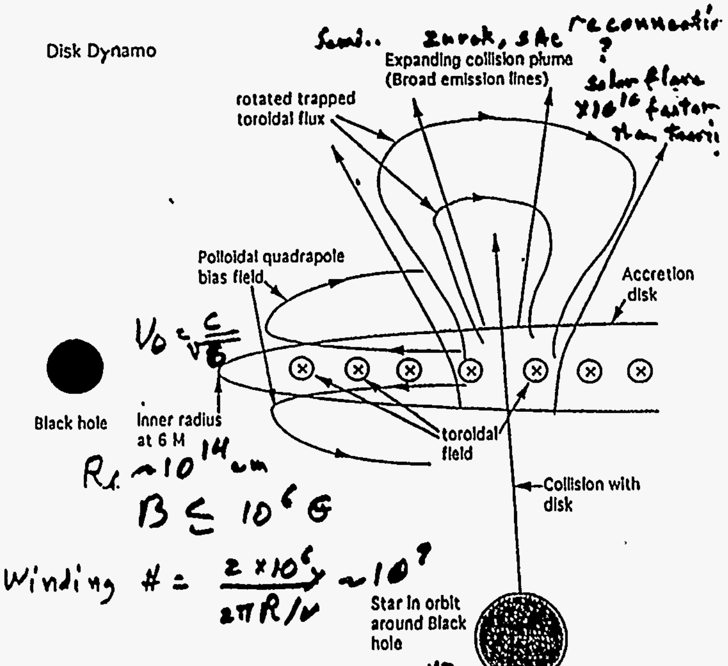

$V_0 \approx \frac{c}{\sqrt{6}}$

$R_i \sim 10^{14}$ cm

$B \leq 10^6$ G

Winding # $= \frac{2\times10^6 y}{2\pi R/v} \sim 10^9$

$\Phi_{gm\,Disk} \lesssim$ area × B × $\#_t = 10^{43}$ gauss cm^2

$\Phi_{galaxy} \sim B \times (10\,kpc)^2 = 10^{40}$ gauss cm^2

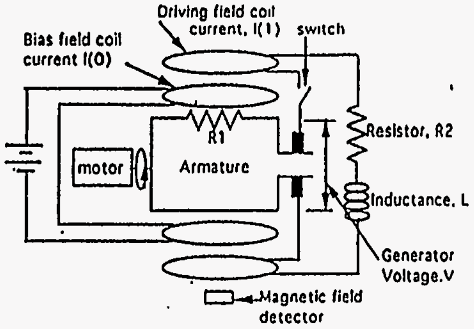

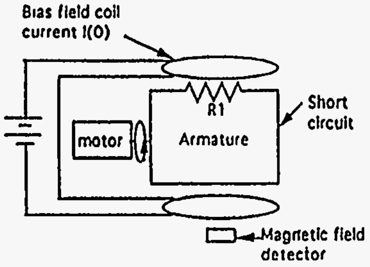

Recollections and Overview of Opacities for Stellar Astrophysics

Arthur N. Cox
Los Alamos National Laboratory

RECOLLECTIONS AND OVERVIEW OF OPACITIES FOR STELLAR ASTROPHYSICS

ARTHUR N. COX

LOS ALAMOS NATIONAL LABORATORY

Los Alamos
NATIONAL LABORATORY

Useful Opacity Tables for Stellar Structure in 1964

Vitense, Erika, Der Aufau der Sternatmospharen IV Teil: Kontinuierliche Absorption und Streuung als function von Druck und Temperatur.
1951,ZsAp,28,81

Stromgren, B., Unpublished hydrogen opacities including ionized H molecules.

Keller, G. and Meyerott, R. E., The Ionization of Gas Mixtures in Stellar Interiors.
1952,Argonne National Laboratory Report ANL-4771

Keller, G. and Meyerott, R. E., The Ionization of Gas Mixtures in Stellar Interiors. II. The Average Number of Electrons in Various Shells.
1952,Argonne National Laboratory Report ANL-4856

Keller, Goeffrey and Meyerott, Roland E., A Table of the Radiative Opacities of a Number of Gas Mixtures.
1955,ApJ,122,32

Zirin, Harold, The Calculation of Opacities for Stellar Interiors.
1958,ApJ,128,342

Los Alamos
NATIONAL LABORATORY

Useful Opacity Tables for Stellar Structure in 1990

Cox, A.N. and Stewart, J.N., Radiative and Conductive Opacities for Twenty Three Stellar Mixtures.
1969, Sci. Inform. Astron. Council USSR,15,1 and Nauch. Info. 15,3

Cox, A.N. and Stewart, J.N., Rosseland Opacity Tables for Population I Compositions. 1970,ApJS.,19,243

Cox, A.N. and Stewart, J.N., Rosseland Opacity Tables for Population II Compositions. 1970,ApJS.,19,243

Cox, A.N. and Tabor, J.E., Radiative Opacity Tables for 40 Stellar Mixtures. 1976,ApJS.,31,271

Huebner, W. F., Atomic and Radiative Processes in the Solar Interior. Physics of the Sun, eds. P.A. Sturrock, T. E. Holtzer, D. Mihalas, and R.K. Ulrich (Dordrecht: D. Reidel) vol. 1, p. 33

Weiss, Achem, Keady, J.J., and Magee, N.H., A Collection of Los Alamos Opacity Tables for all Temperatures.
1990,At. Data Nucl. Data Tables,45,209

Los Alamos
NATIONAL LABORATORY

Current Useful Opacity Tables for Stellar Structure

Iglesias, C. and Rogers, F.J., Opacities for the Solar Radiative Interior. 1991,ApJ,371,408

Lenzuni, P., Chernoff, D.F. and Salpeter, E.E., Rosseland and Planck Mean Opacities of a Zero Metallicity Gas. 1991,ApJS,76,759

Sharp, C.M., Molecular Opacities for Solar and Enchanced CNO Abundances: Relevence for Accretion Disks. 1992,A&AS,94,1

Rogers, F.J. and Iglesias, C., Radiative Atomic Rosseland Mean Opacity Tables. 1992,ApJS,79,507 (OPAL)

Iglesias, C. and Rogers, F.J., Spin-Orbit Interaction Effects on the Rosseland Mean Opacity. 1992,ApJ,397,717 (OPAL)

Iglesias, C. and Rogers, F.J., Radiative Opacities for Carbon and Oxygen Rich Mixtures. 1993,ApJ,412,752

Seaton, M.J., Yan, Y., Mihalas, D., Pradhan, A.K., Opacities for Stellar Envelopes. 1994,MNRAS,266,805 (OP)

Alexander, D.R. and Ferguson,J.W., Low Temperature Rosseland Opacities. 1994,ApJ,437,879

Los Alam
NATIONAL LABORA

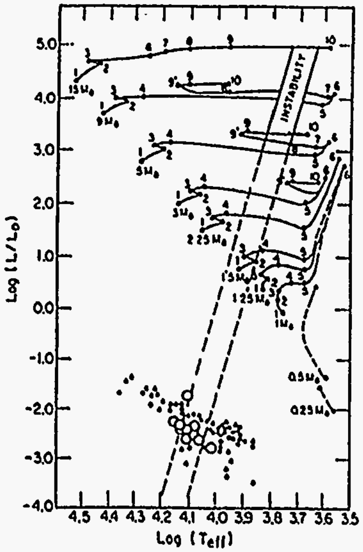

Figure 3. The instability strip in the H-R diagram. The upper portion of the figure showing the theoretical evolutionary tracks and the location of the Cepheids is adapted from Figure 1 of Henden and Cox (1976). The instability strip has been extrapolated linearly along the dashed lines into the region occupied by the white dwarfs. The locations of the variable white dwarfs are shown by the large open circles.

Los Alamos

NATIONAL LABORATORY

JOHN P. COX

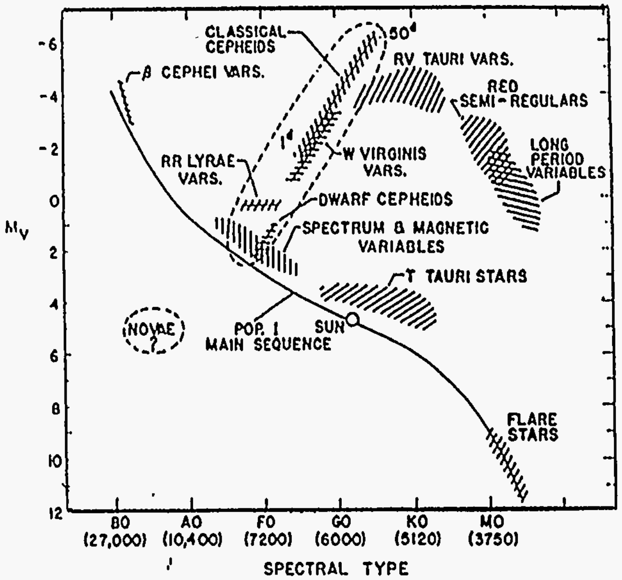

FIG. 1 Location of various types of intrinsic variables on the Hertzsprung-Russell diagram

Los Alamos

NATIONAL LABORATORY

Areas Recently Affected by Improved Opacities

- Double-Mode Cepheid Masses
- Double-Mode RR Lyrae Variable Masses
- Delta Scuti Variable Period Ratios and Masses
- Solar p-Mode Oscillation Frequencies
- OB Star Pulsational Instability
- Massive Star Instabililities and the Upper Mass Limit
- Hyades G Star Lithium Depletion
- Overshoot from Massive Star Convective Cores
- Enhanced Mass Loss from Wolf-Rayet Stars

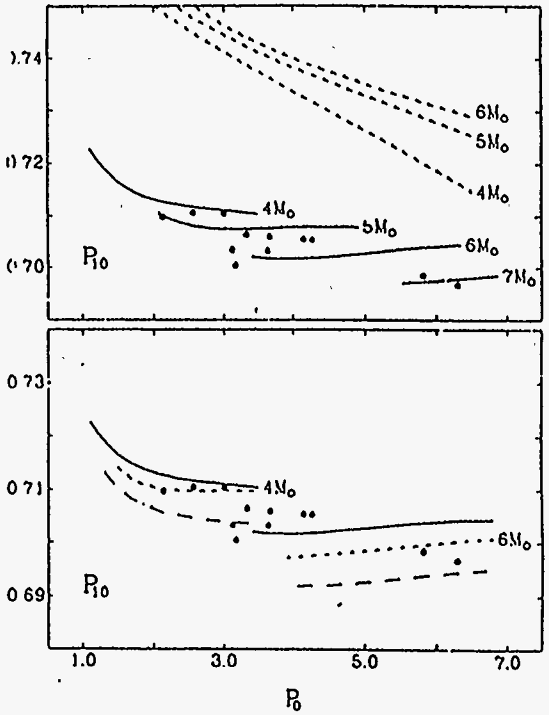

FIG. 1.—*Top*: Period ratio P_{10} vs period P_0. *Solid lines*: I-R opacities; *dashed lines*: LA opacities, both with BIT $M - L$ relation; *dots*: observed beat Cepheids. *Bottom*: Period ratio P_{10} vs. P_0 with I-R opacities. *Solid lines*: BIT $M - L$ relation with $Z = 0.02$; *dashed lines*: enhanced $M - L$ relation (with $Z = 0.02$). *Dash-dotted lines*: BIT $M - L$ relation with $Z = 0.03$ (AG mixture); *dots* observed beat Cepheids.

Quantitatively, our postulates of local thermodynamic equilibrium and almost equal matter and radiation temperature can be expressed by assuming an intensity given by the blackbody function reduced slightly or,

$$I_\nu(s) = B_\nu(T) - \frac{1}{\rho(\kappa_\nu' + \sigma_\nu)} \frac{\partial B_\nu(T)}{\partial s}, \qquad (4)$$

The definition of the monochromatic radiative flux in direction x is given by

$$F_{\nu,x} = \int I_\nu(s) \cos\theta \, d\omega, \qquad (11)$$

where $\cos\theta$ is now the projection factor for the intensity on to the direction x at angle θ from direction s. Insertion of the expansion of I_ν yields the expression

$$F_{\nu,x} = -\int_0^\pi \int_0^{2\pi} \frac{1}{\rho(\kappa_\nu' + \sigma_\nu)} \frac{\partial B_\nu(T)}{\partial x} \cos^2\theta \sin\theta \, d\theta \, d\phi, \qquad (12)$$

where the first isotropic term in the intensity vanished due to the symmetry of the integral. The integral is thus

$$F_{\nu,x} = -\frac{4\pi}{3\rho(\kappa_\nu' + \sigma_\nu)} \frac{\partial B_\nu(T)}{\partial x}. \qquad (13)$$

Now the total flux at all frequencies in direction x is

$$\begin{aligned} F_x &= \int_0^\infty F_{\nu,x} \, d\nu \\ &= -\frac{4\pi \partial T}{3\rho \partial x} \int_0^\infty \frac{1}{(\kappa_\nu' + \sigma_\nu)} \frac{\partial B_\nu(T)}{\partial T} \, d\nu \qquad (14) \\ &= -\frac{4\pi \partial T}{3\rho \kappa \partial x} \int_0^\infty \frac{\partial B_\nu(T)}{\partial T} \, d\nu, \end{aligned}$$

defining κ as a harmonic mean of $(\kappa_\nu' + \sigma_\nu)$ (see eq. [62]). Thus,

$$\begin{aligned} F_x &= -\frac{4\pi}{3\rho\kappa} \frac{\partial}{\partial x} \int_0^\infty B_\nu(T) \, d\nu \\ &= -\frac{4\pi}{3\rho\kappa} \frac{\partial}{\partial x} \frac{\sigma}{\pi} T^4 \qquad (15) \\ &= -\frac{ac}{3\rho\kappa} \frac{\partial T^4}{\partial x}, \end{aligned}$$

which is our desired result. Here $\sigma = ac/4$, where σ and a are radiation constants and c is the velocity of light. The derivation is originally due to Rosseland (1924). Another early derivation was given by Eddington (1926, chap. V)

We have seen (eq. [14]) that the average absorption, according to Rosseland, is given by

$$\frac{1}{\kappa} = \frac{\int_0^\infty \frac{1}{(\kappa_\nu' + \sigma_\nu)} \frac{\partial B_\nu(T)}{\partial T} \, d\nu}{\int_0^\infty \frac{\partial B_\nu(T)}{\partial T} \, d\nu}. \qquad (62)$$

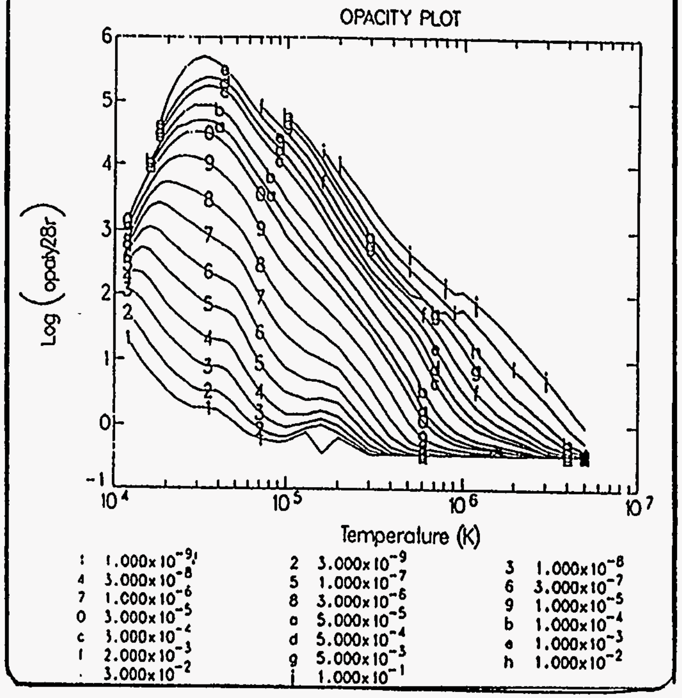

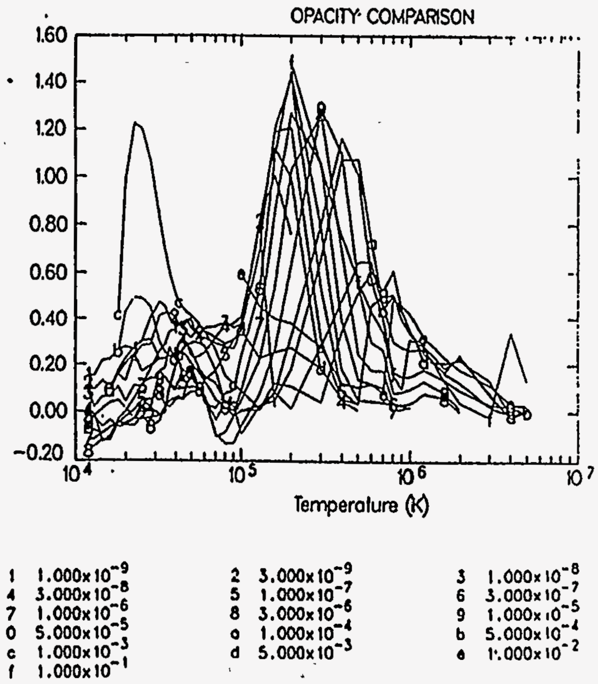

Los Alamos
NATIONAL LABORATORY

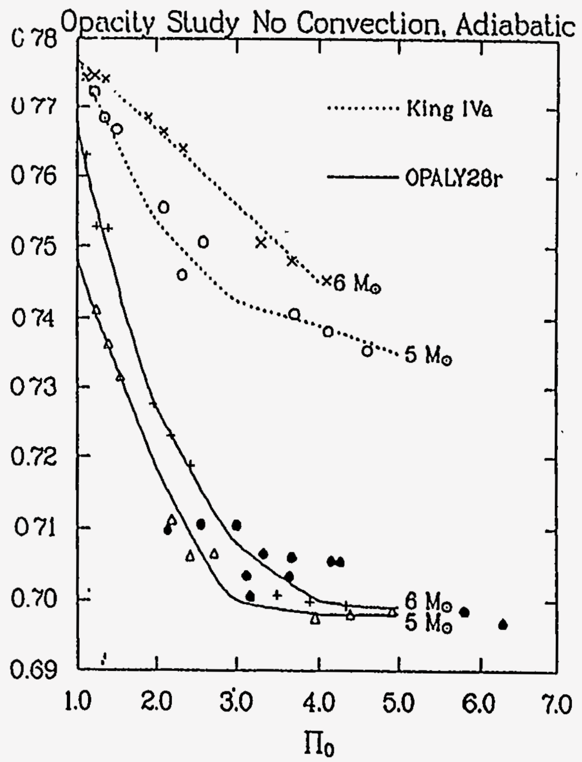

Los Alamos
NATIONAL LABORATORY

192

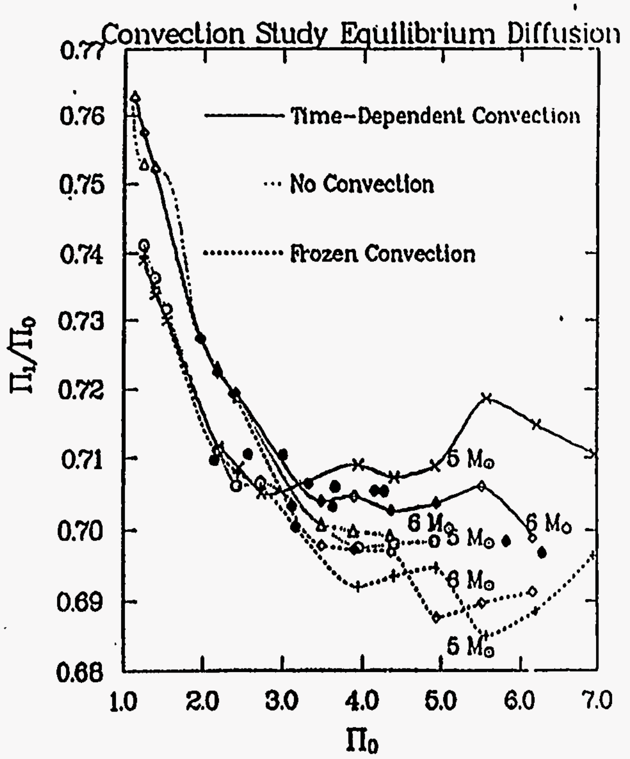

Los Alamos
NATIONAL LABORATORY

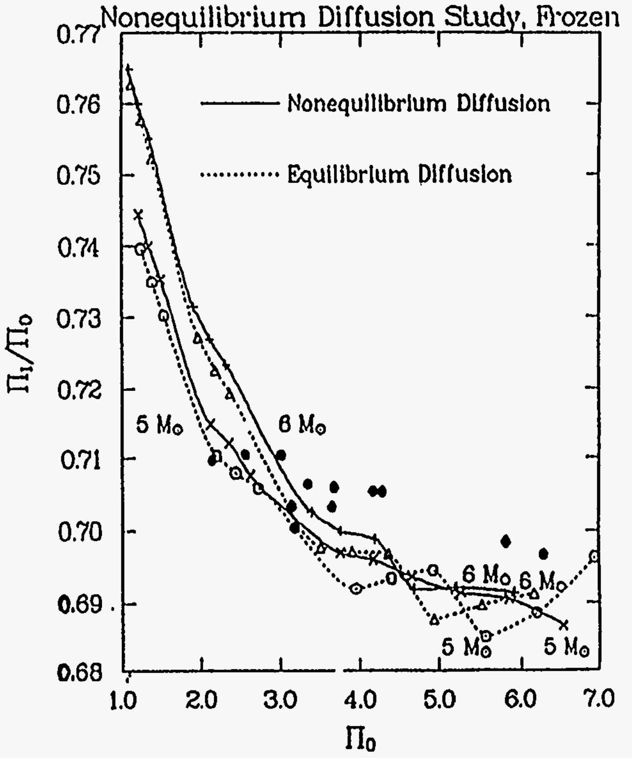

Los Alamos
NATIONAL LABORATORY

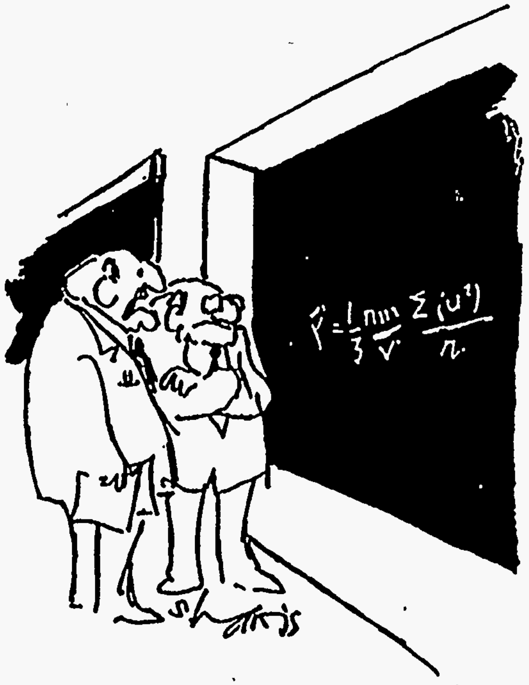

"What's most depressing is the realization that everything we believe will be disproved in a few years."

CONCLUSIONS

1. The appearance of the Los Alamos opacities in 1965 to 1970 caused a great expansion of studies of stellar structure, evolution, and stability.

2. The appearance of the Livermore (OPAL) and United Kingdom (OP) opacities in 1989 to the present have allowed explanations of many previous problems, mostly in stellar pulsation theory.

3. The double-mode Cepheids can be interpreted with standard masses and luminosities from evolution theory, but the early simple interpretations with OPAL opacities did not reveal the whole complicated situation.

Opacity and Radiative Transfer Experiments Using High-Power Lasers

Steven J. Rose
Rutherford Appleton Laboratory

Opacity and radiative transfer experiments using high-power lasers

S J Rose

Rutherford Appleton Laboratory
and
Department of Physics and Space Science, University of Birmingham,
U K

Outline

- Opacity experiments
- Dense plasma experiments
- Line transfer experiments
- Accretion plasmas
- Future opportunities

Absorption spectroscopy opacity experiment

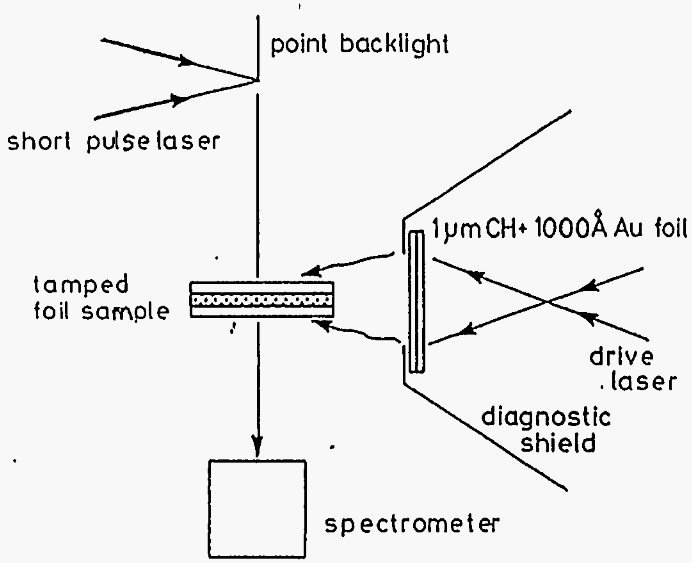

Comparison between IMP and experiment for germanium at 76eV and 0.054 gcm-3

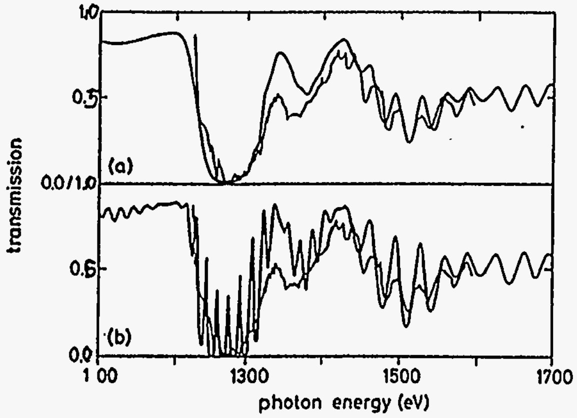

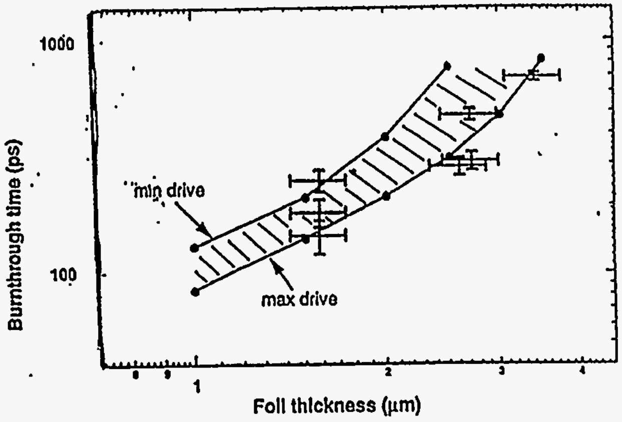

Radiation wave opacity experiment

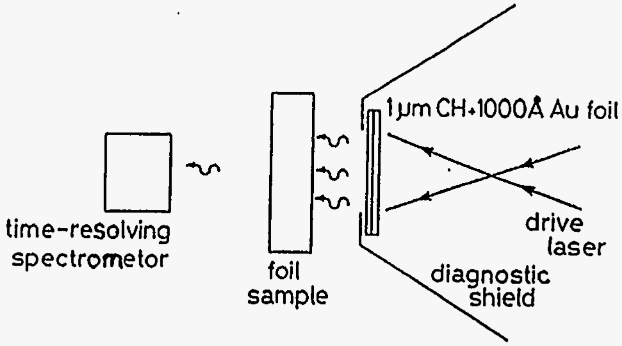

Supersonic radiation wave opacity experiment

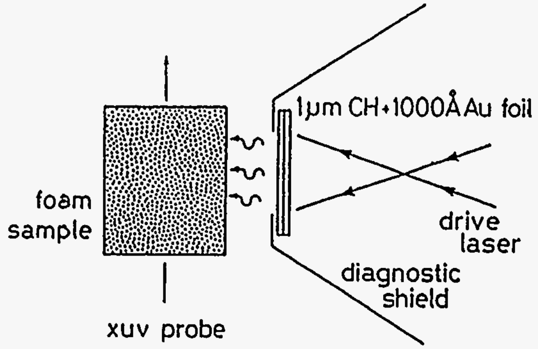

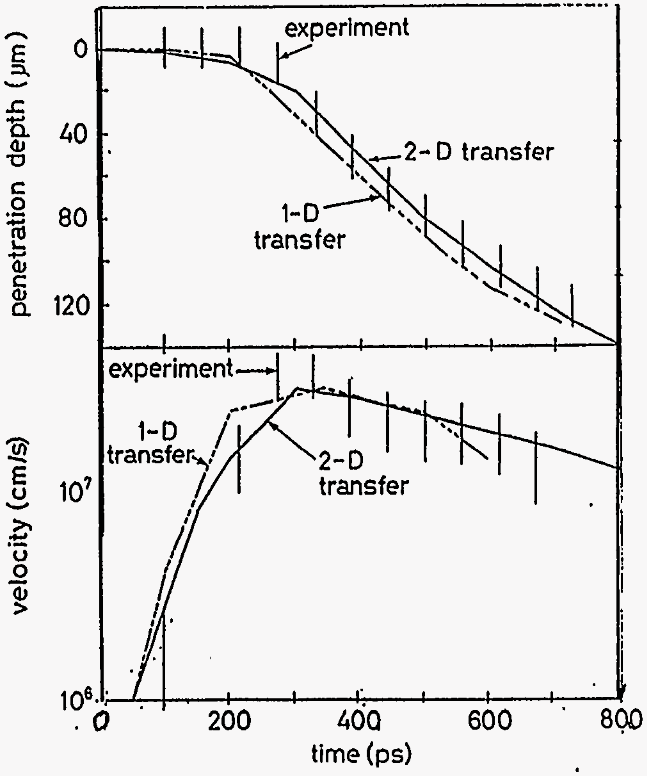

Opacity and dense plasma experiments

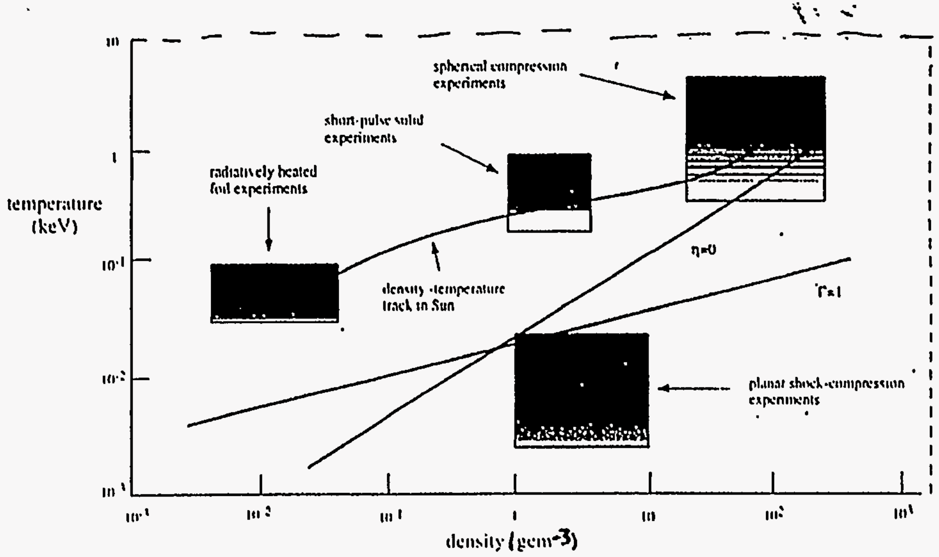

Short-pulse experiments

- Our understanding of the physics of short-pulse interaction with solid targets is still incomplete.

- Temperatures of a few hundred eV is possible with present lasers.

Short-pulse emission experiment to measure opacity

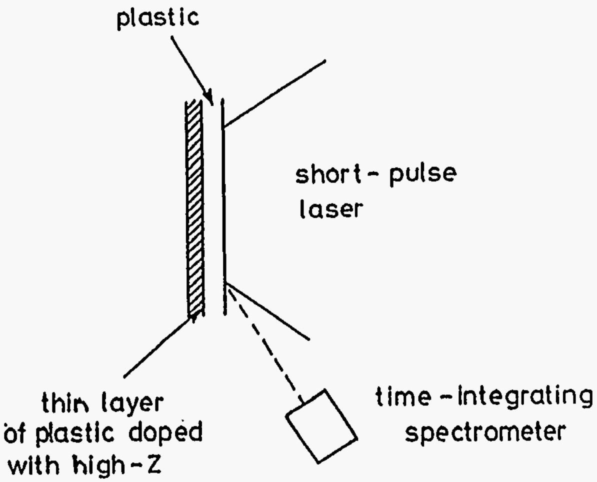

Variation with time of average electron temperature over iron layer

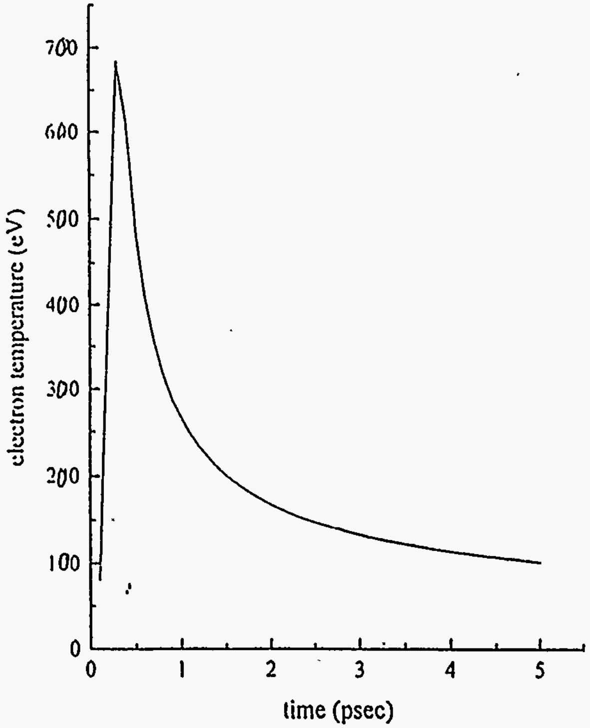

Variation with time of average density over iron layer

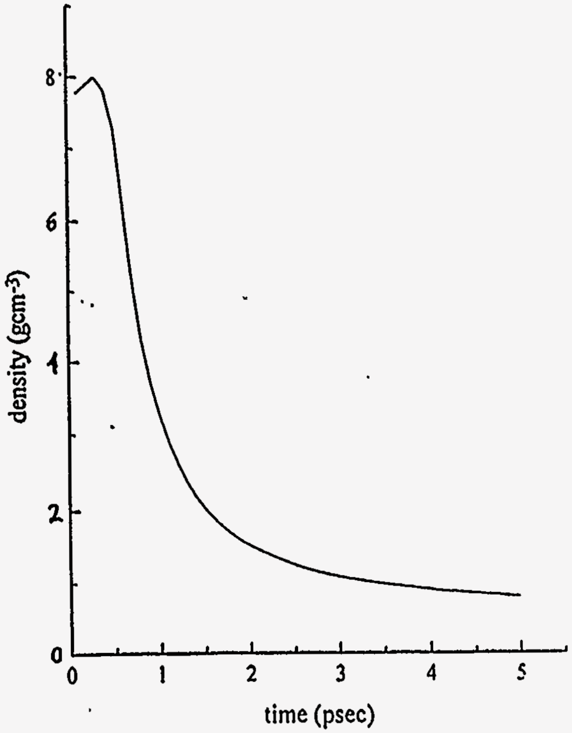

Variation with time of average Z* over iron layer

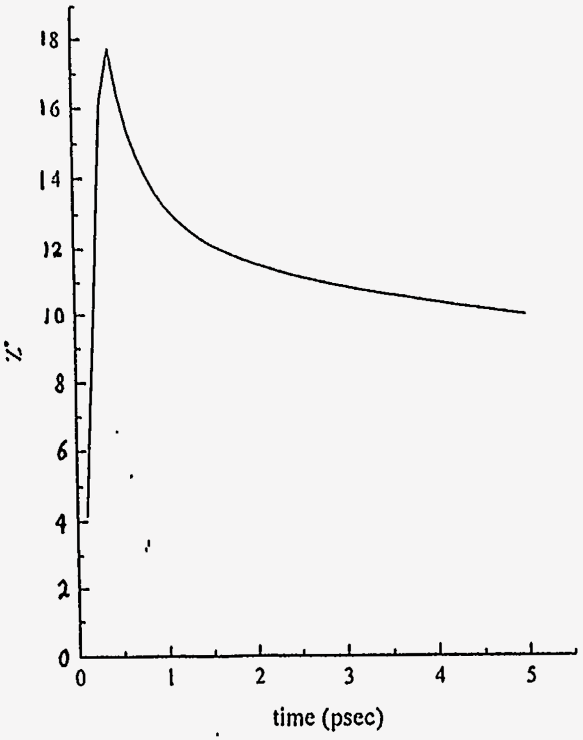

Short-pulse iron opacity experiment

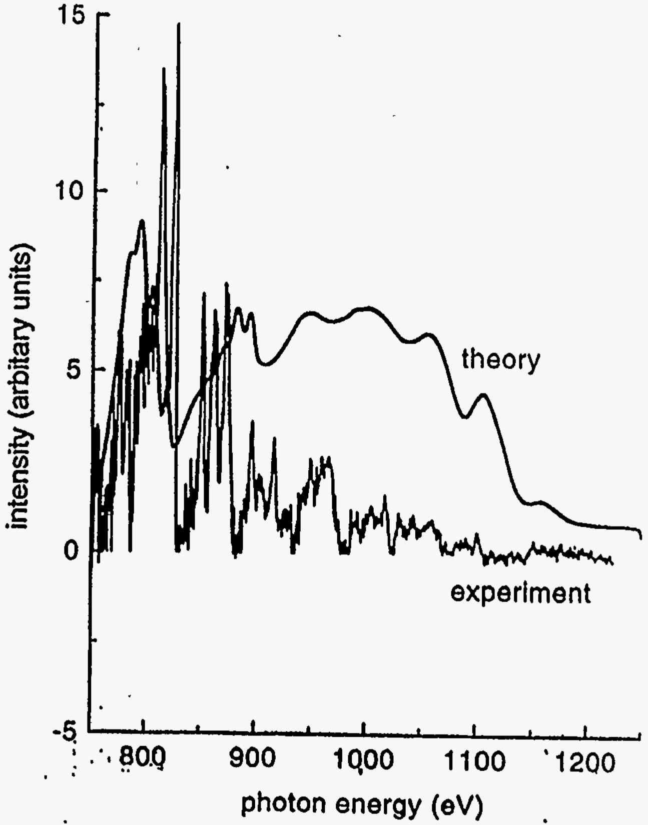

Line-transfer experiments

- Line radiation transfer in large velocity gradients is very important in certain astrophysical plasmas (Sobolev theory). Laser-plasma measurments have tested our understanding of this process.

- Resonance fluorescence is an important mechanism in planetary nebulae. Laser-plasma experiments test our understanding of radiation transport in overlapping lines.

Measurement of line radiation in a velocity gradient

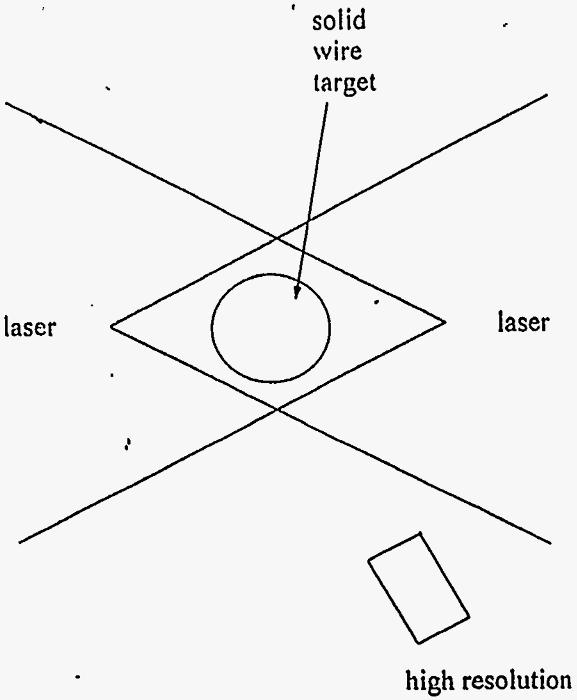

Line radiation transport in a velocity gradient - comparison of theory and experiment

Irradiance 4×10^{14} Wcm^{-2}

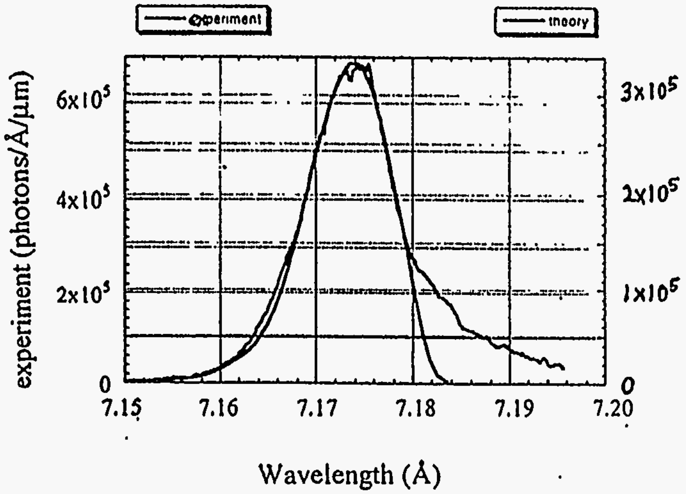

Accretion-powered objects

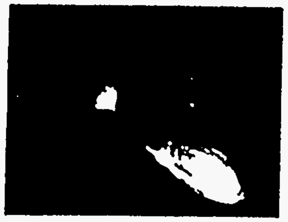

X-ray binaries, active galactic nuclei and cataclysmic variables are the dominant sources of energy in the observable universe

- Radiation domination of excitation and ionisation
- Inelastic Compton scattering

Compton scattering energy exchange

- Compton scattering from a stationary electron moves energy from radiation to electrons. But scattering from moving electrons moves energy both ways.

- In a plasma with high T_e and low radiation field

electrons → radiation

In a plasma with low T_e and high radiation field

radiation → electrons.

Simplified model of radiation evolution in DT plasma ball

$$\mathcal{I}(\varepsilon)=\frac{2\varepsilon^3}{h^2c^2}n(\varepsilon)$$

intensity

modal photon density

$$\frac{\partial n(\varepsilon)}{\partial t}=$$

$$\frac{n_e\sigma_T}{m_e c}\frac{1}{\varepsilon^2}\frac{\partial}{\partial \varepsilon}\left\{\alpha(\varepsilon,kT_e)\varepsilon^4\left(kT_e\frac{\partial n(\varepsilon)}{\partial \varepsilon}+n(\varepsilon)+n(\varepsilon)^2\right)\right\}$$

$$+c\rho\kappa(\varepsilon,T_e)(1+n(\varepsilon))\left[\frac{1}{\exp(\varepsilon/kT_e)-1}-n(\varepsilon)\right]$$

$$-\frac{n(\varepsilon)}{(R/c)}$$

scattering

absorption /emission

loss from plasma

Comparison of radiation intensity with and without Compton scattering

DT ball, R=0.005cm, ρ=500gcm-3

.... with Compton scattering

———— without Compton scattering

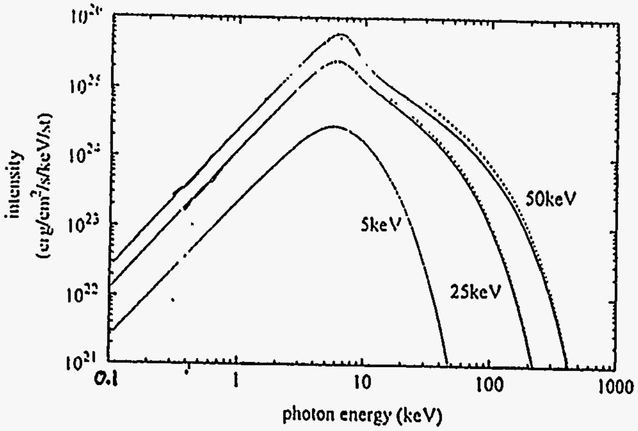

The effect of Compton scattering on line radiation transport

$D_{0.495}T_{0.495}Xe_{0.01}$ ball, R=0.005cm, ρ=500gcm^{-3}

┈┈┈┈┈ with Compton scattering

——— without Compton scattering

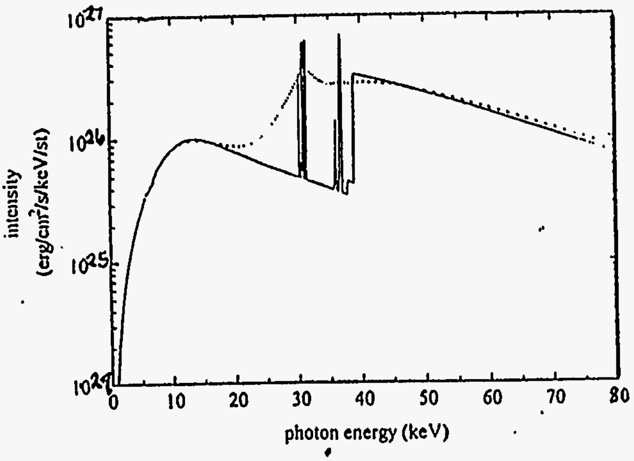

Future Opportunities

- High B-field physics studies
- Thermonuclear reaction rate measurements
- Electron-positron plasma studies
- Particle acceleration in plasmas

Conclusions

- The values of plasma temperature, density, radiation field, ionisation stage, velocity and velocity gradient etc. which can be achieved with high-power lasers are comparable to values found in certain astrophysical plasmas.

- Complex laser experiments are now being performed in which the plasma conditions can be controlled to investigate specific physical processes. Measurements are starting to be made.

- Further work is underway to investigate other effects and to produce more exotic plasmas.

Opacity Measurements for Stellar Atmospheres

Paul T. Springer
Lawrence Livermore National Laboratory

Opacity Measurements for Stellar Atmospheres

Paul T. Springer, J.H. Hammer, A. Toor,
B.G. Wilson, C.A. Iglesias, W.H. Goldstein,
F.J. Rogers, and R.E. Stewart

Workshop on Laboratory Astrophysics
Experiments with Large Lasers

February 26-27, 1996

Modern opacity models solve long-standing puzzles in stellar pulsation: Experimental validation is required

Locations of types of variable stars on Hertzsprung-Russell diagram

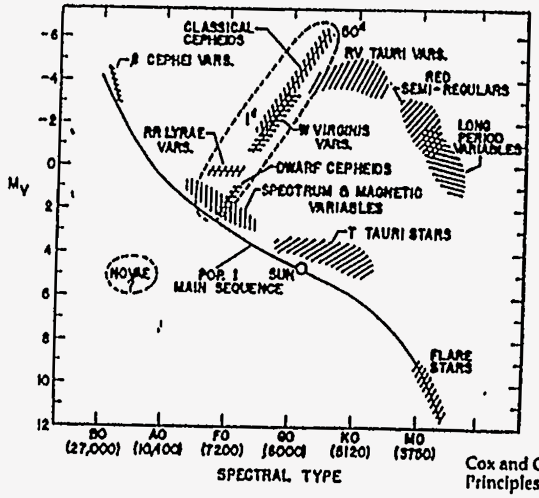

Problems:

- Cepheid Masses
  - Pulsation models
  - Evolution models
  - Blue loop excursions
- β Cephei pulsation

Cox and Giuli
Principles of Stellar Structure (1968)

Modern opacity models solve long-standing puzzles in stellar pulsation

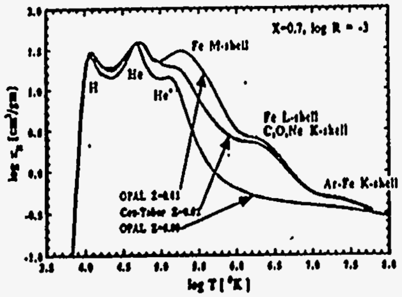

Stellar mixture opacity versus temperature along track of constant R = 10^{-3}

- Fe M-shell bump due to δn=0 transitions
- Provides mechanism for β-Cephei pulsation

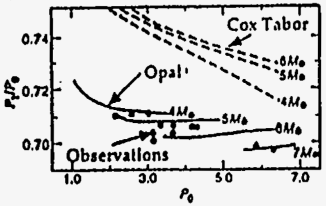

Ratio of first harmonic P_1 to fundamental P_0 determines masses for Cepheid variable stars.

- Masses from stellar evolution models
  - Inconsistent with Cox-Tabor opacities
  - Blue loop excursions -> M > 3 solar masses
- Opal resolves mass puzzle

Opal is only indirectly tested by complex stellar models
Experimental benchmarking at relevant conditions is needed

Plasma conditions for stellar atmospheres can be achieved in the laboratory

Stellar structure models with $R = \rho / T_6^3$

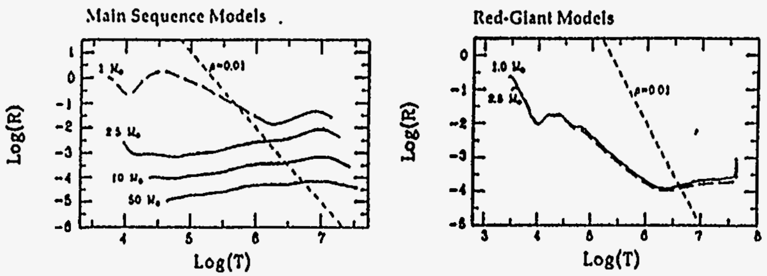

Fe contribution maximized at Log(T)=5.4, Log(R)=-3

T= 20 eV, Rho= 2 x 10^{-6} g/cc

Seaton et al. Not. R. Astron. Soc. 266 (1994)

Experimental setup and data

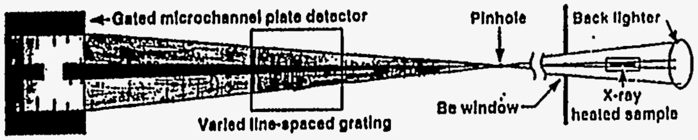

Fe + NaF data and theory, Te = 59 +/- 3 eV and ρ = 0.0113 +/- 0.001 g cm^{-3}

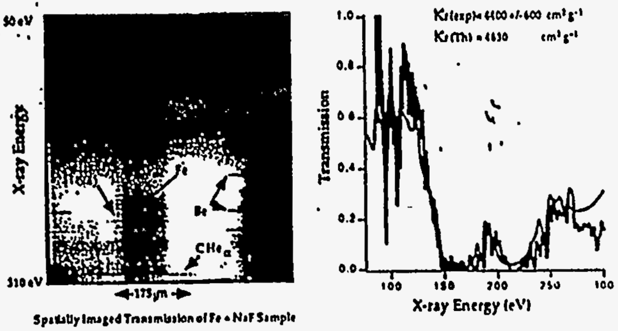

Spatially Imaged Transmission of Fe + NaF Sample

Iron opacity measurements at Nova have provided astrophysically relevant data at densities ~ .01 g/cc

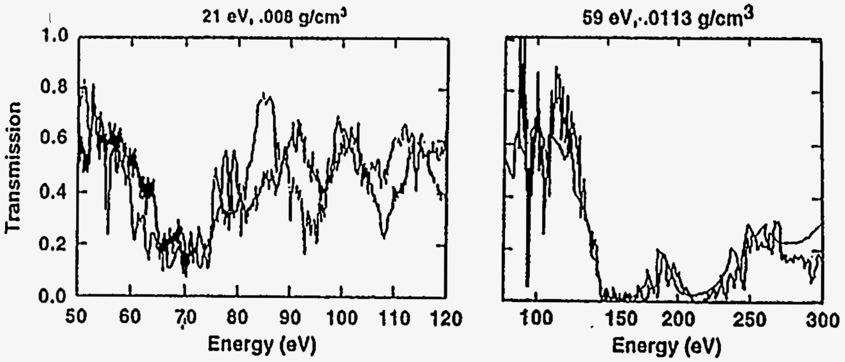

Science 263, 50 (1994)
PRL 69, 438 (1992)

experiment
OPAL opacity

PRL 69, 3735 (1992)

Rosseland mean opacities for iron are strongly model-dependent for ρ < 10–2 g/cc

Tests of line shape theories and the accuracy of statistical methods are important for stellar opacities

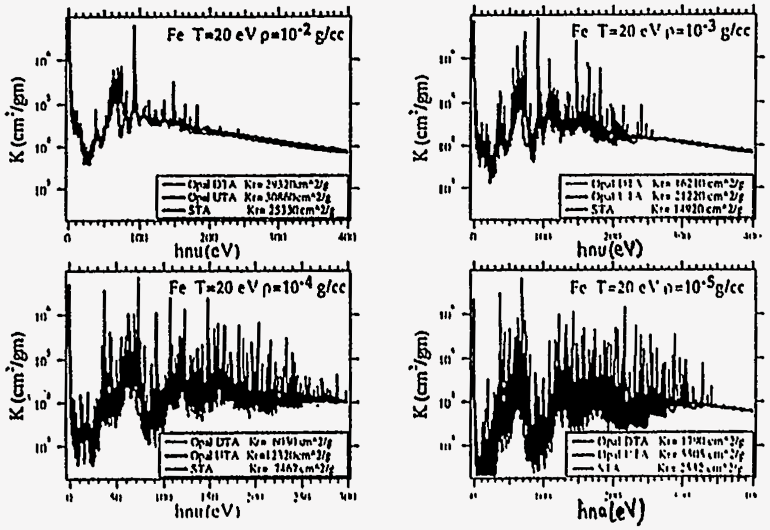

37448 ps u-12

Long-lived hohlraums are required to establish equilibrium at low density

Time dependent ionization for Iron

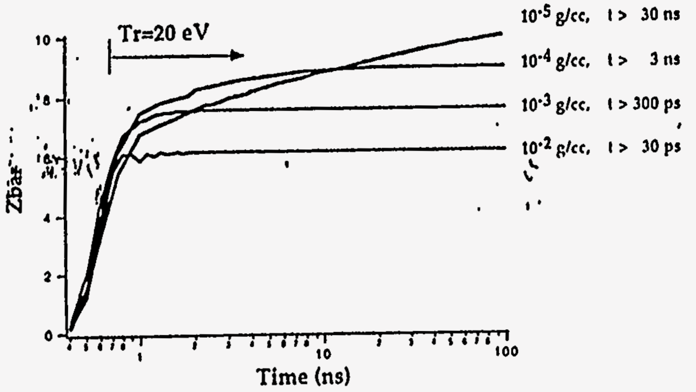

Low density experiments require radiative equilibrium, Planckian spectra, and large plasma volume

LTE and NLTE iron opacity models at varied densities

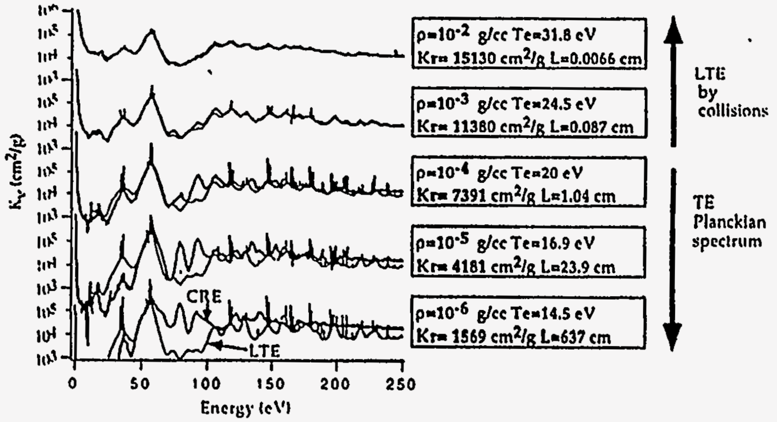

High spectral resolution is required to accurately measure UTA breakup

Simulated absorption spectrum for 1 cm path length

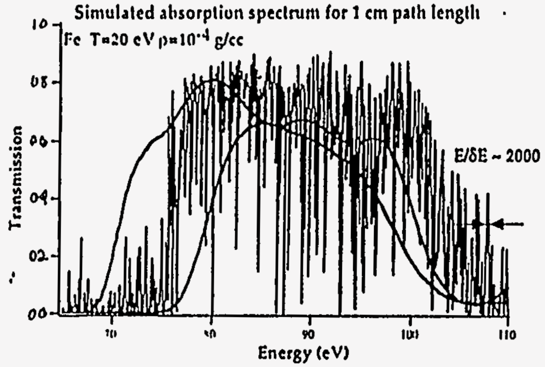

Theories require accurate treatments of line shapes
- Natural width
- Collisional broadening
- Residual configuration and term broadening
- Stark broadening
- Doppler broadening
- Line wings

Experimental setup for laser-driven hohlraum

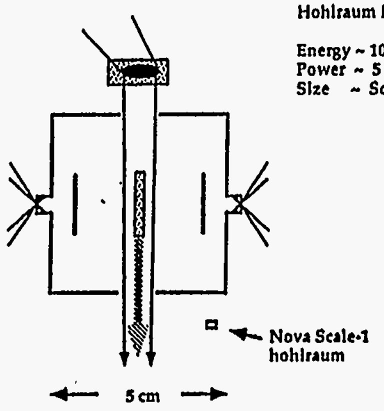

Hohlraum Parameters

Energy ~ 100 kJ
Power ~ 5 TW
Size ~ Scale 30

Issues:
- Sample conditions
  - -Density < 10^{-4}
  - -Temperature ~ 20 eV
  - -Equilibrium rad-driven LTE
  - - Gradients
- Backlighting
  - - Intensity
  - - Sample emission
- Characterization

Experimental Setup

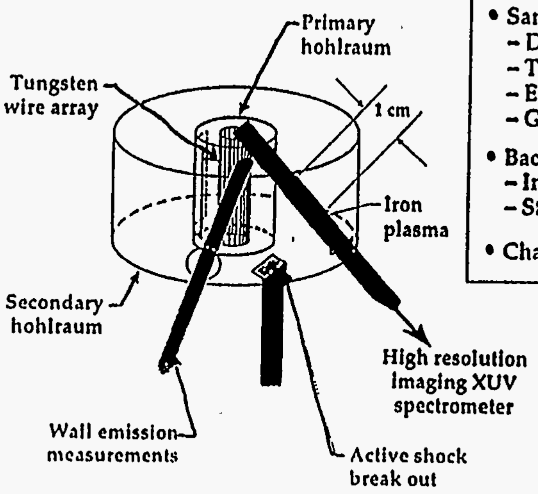

Issues:
- Sample conditions
  - – Density < 10-4
  - – Temperature ~ 20 eV
  - – Equilibrium rad-driven LTE
  - – Gradients
- Backlighting
  - – Intensity
  - – Sample emission
- Characterization

Experimental design has begun using using 2d radiative hydrodynamic models

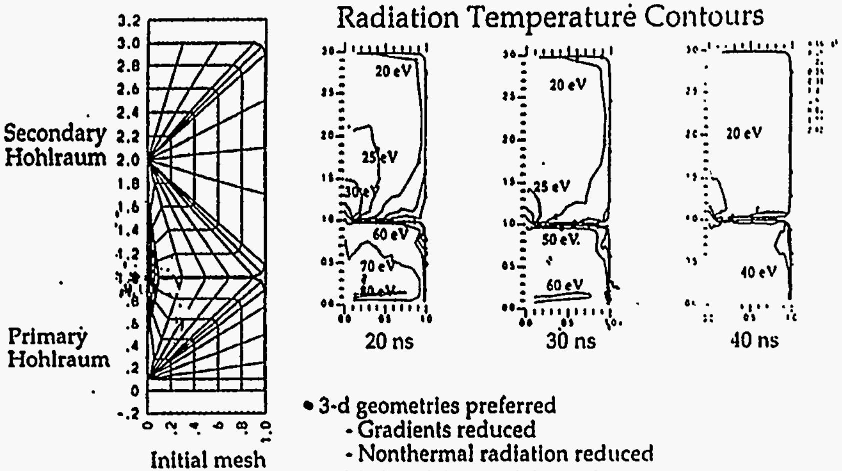

- 3-d geometries preferred
  - - Gradients reduced
  - - Nonthermal radiation reduced
- 2-d R-Z and R-θ models used
- Experimental control and characterization required

#11
37448-05-u-09

Primary hohlraum heats secondary target to desired conditions, and provides backlighting source

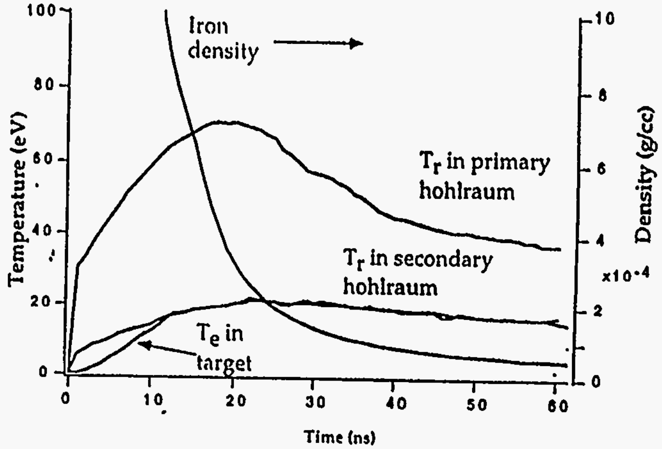

The required thermal radiation spectra are produced following initial heating

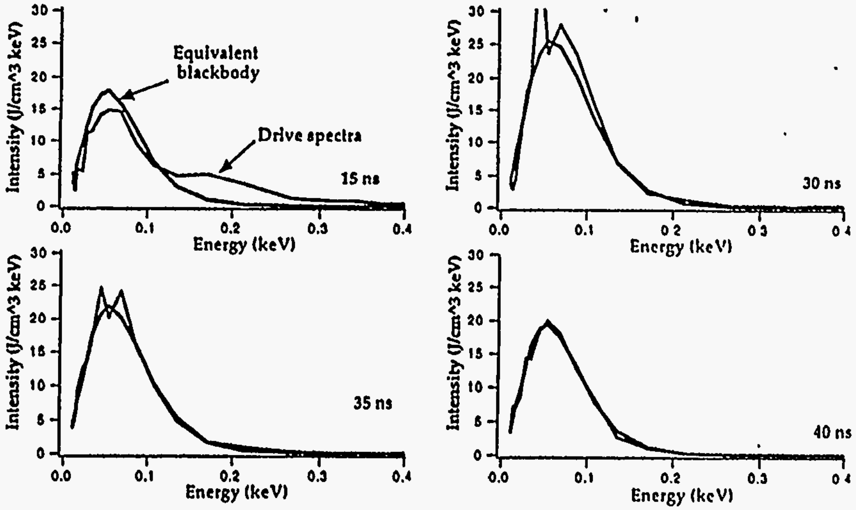

The crucial low density regime ($10^{-5} \lesssim \rho \lesssim 10^{-3}$ g/cc) has not been experimentally explored

Individual line-shapes and merging into UTA's and quasi-continua are important for $\rho < 10^{-2}$ g/cc

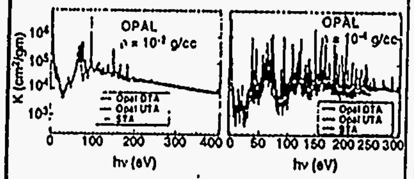

Rosseland mean opacities of iron became strongly model-dependent for $\rho < 10^{-2}$ g/cc

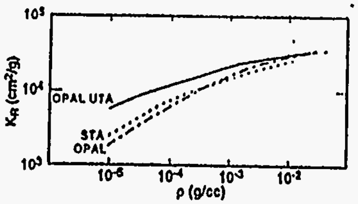

Time dependent ionization for iron

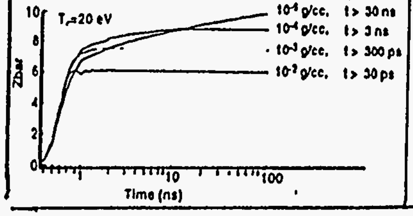

- Hohlraum requirements

T_e=T_r=20 eV Planckian
Lifetime > 40 ns
Sample length > 4 cm

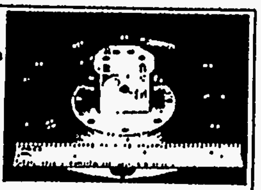

- Evaluate 200 kJ Saturn facility
- Experimental benchmarking with high resolution
- Accurate characterization of conditions

Uncertainties in Stellar Opacities

Carlos A. Iglesias
Lawrence Livermore National Laboratory

UNCERTAINTIES IN STELLAR OPACITIES

Carlos A. Iglesias
LLNL

1) Stellar Envelopes

2) Solar Radiative Interior

DEFINITIONS:

X = hydrogen mass fraction
Y = helium mass fracton
Z = metal mass fraction
[C, N, O, Ne, Na, Mg, Al, Si, S, Ar, Ca, Fe]

$R = \rho / T_6^3$ where ρ = mass density [g/cm³]
T_6 = million degrees [°K]

Typical Stellar Conditions:

Solar radiaive interior	X= 0.35-0.7,	Z=0.02,	logR=-1.5
Classical Cepheids	X=0.7,	Z=0.02,	logR=-3.5
Hot variable stars	X=0.7,	Z=0.02,	logR=-5.5
RR Lyrae	X=0.7,	Z=0.001,	logR=-4

R & T as independent variables:

$R = \rho / T_6^3$ where ρ = mass density [g/cm³]
T_6 = million degrees [°K]

Examples of Stellar Conditions:

Solar radiaive interior	X= 0.35-0.7,	Z=0.020,	logR=-1.5
Classical Cepheids	X=0.7,	Z=0.020,	logR=-3.5
Hot variable stars	X=0.7,	Z=0.020,	logR=-5.5
RR Lyrae	X=0.7,	Z=0.001,	logR=-4

"Phrenology"

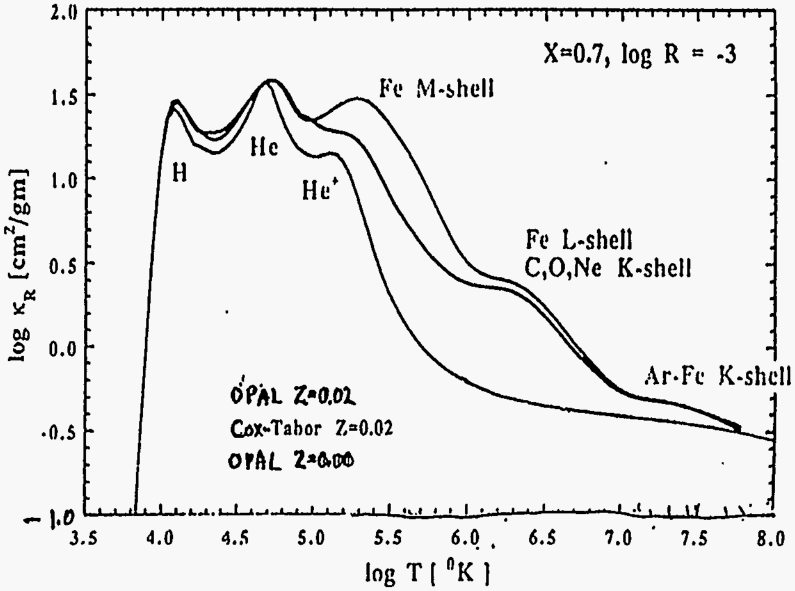

RESOLUTION OF BEAT MASS ANOMALIES WITH OPAL OPACITIES

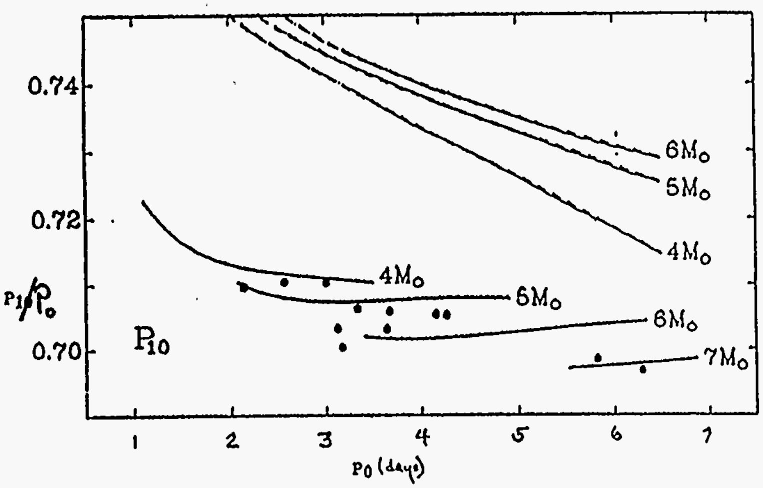

- • Observations (Szabados 1988)
- — Cox & Tabor, *ApJS* 31, 271(1976)
- — Iglesias & Rogers, *ApJ* 371, L73(1991)

From Moskalik *et al.*, *ApJ* 385, 685(1992)

Fe Experiment: Da Silva et al. Phys.Rev.Lett. ~~64~~ 69, 438(1992)

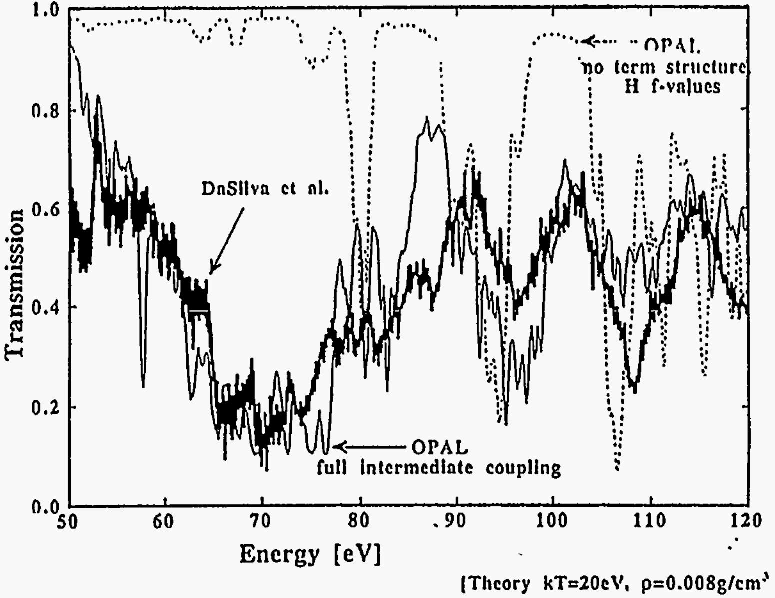

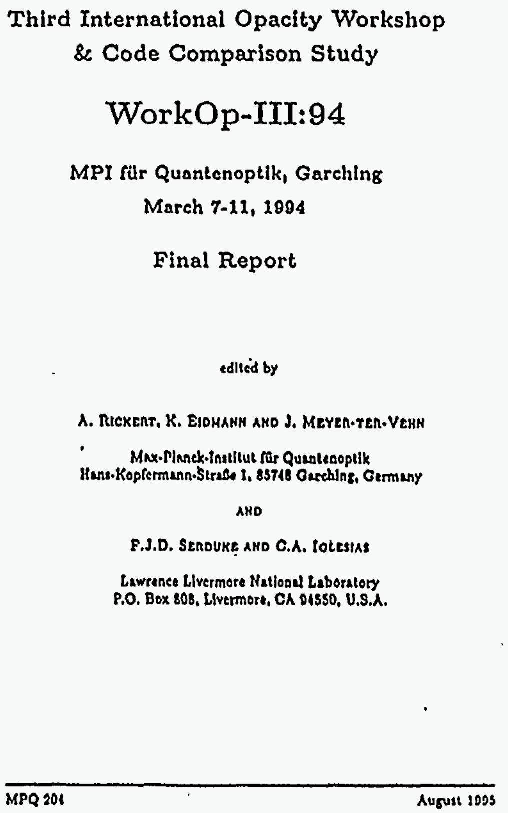

Third International Opacity Workshop
& Code Comparison Study

WorkOp-III:94

MPI für Quantenoptik, Garching
March 7-11, 1994

Final Report

edited by

A. RICKERT, K. EIDMANN AND J. MEYER-TER-VEHN

Max-Planck-Institut für Quantenoptik
Hans-Kopfermann-Straße 1, 85748 Garching, Germany

AND

F.J.D. SERDUKE AND C.A. IGLESIAS

Lawrence Livermore National Laboratory
P.O. Box 808, Livermore, CA 94550, U.S.A.

MPQ 204 August 1995

Fe κ_R COMPARISONS AT T = 20 eV (~230,000 °K):

Code	$\rho = 0.01$ g/cm^3	$\rho = 0.0001$ g/cm^3
LANL'77	1.04×10^4 [cm^2/g]	0.15×10^3 [cm^2/g]
HOPE	1.37×10^4	1.40×10^3
STA	2.58×10^4	0.76×10^3
OPAL	2.93×10^4	6.03×10^3
LANL'94	3.07×10^4	6.75×10^3
IMP	3.14×10^4	10.80×10^3

κ_R COMPARISONS FOR ASTROPHYSICAL MIXTURE 'KING4a' AT T = 20eV & $\rho = 1.2 \times 10^{-6}$ g/cm^3:

Code	κ_R [cm^2/g]
LANL'77	1.76
HOPE	5.10
OPAL	5.47
STA	8.40

Fe κ_R COMPARISONS AT T = 20 eV (~230,000 °K):

Code	$\rho = 0.01$ g/cm³	$\rho = 0.0001$ g/cm³
LANL'77	1.04 x 10⁴	0.15 x 10³ [cm²/g]
HOPE	1.37 x 10⁴	1.40 x 10³
STA	2.58 x 10⁴	0.76 x 10³
OPAL	2.93 x 10⁴	6.03 x 10³
LANL'94	3.07 x 10⁴	6.75 x 10³
IMP	3.14 x 10⁴	10.80 x 10³

κ_R COMPARISONS FOR ASTROPHYSICAL MIXTURE 'KING4a' AT T = 20eV & $\rho = 1.2 \times 10^{-6}$ g/cm³:

Code	κ_R [cm²/g]
LANL'77	1.76
HOPE	5.10
OPAL	5.47
STA	8.40

COMPARISONS TO Fe EXPERIMENT: T = 20 eV $\rho = 0.01$g/cm³

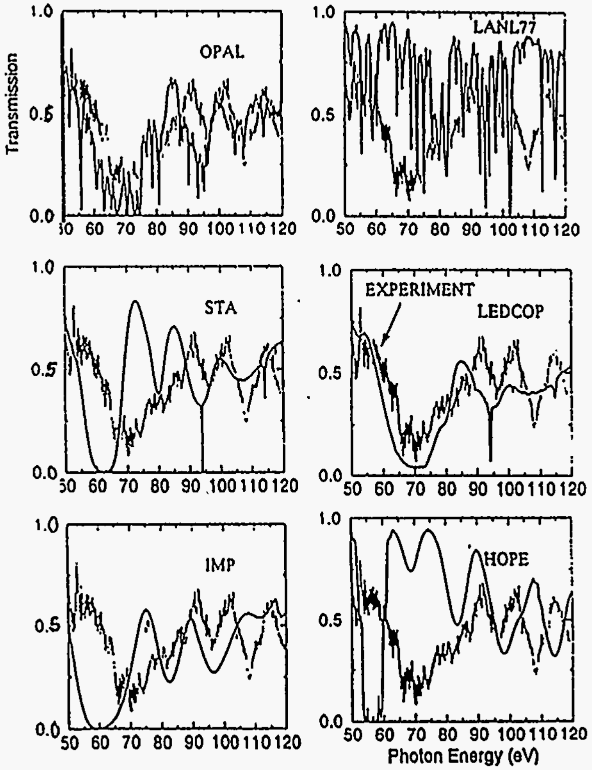

κR COMPARISONS OF OPAL & OPACITY PROJECT (OP):

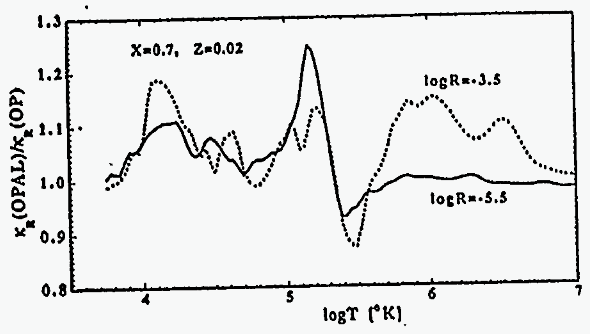

OP results from Seaton et al., *MNRAS* 266, 805(1994)

OPAL & OP COMPARISONS FOR DOUBLE-MODE CEPHEIDS:

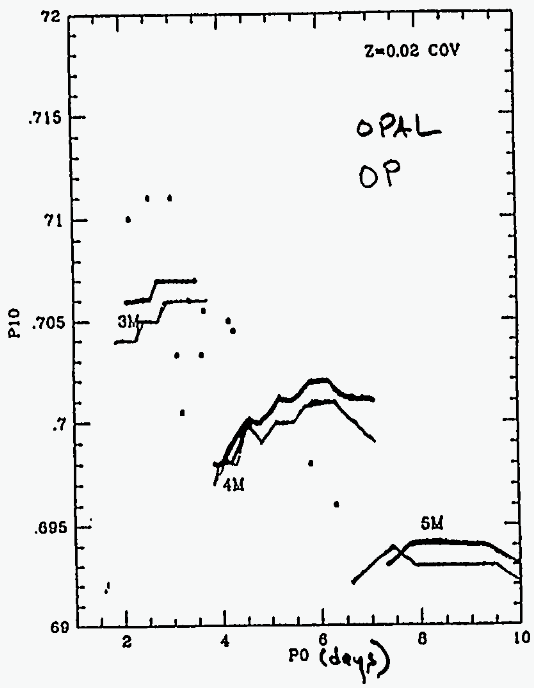

From Simon & Kanbur, *ApJ* 429,772 (1994)

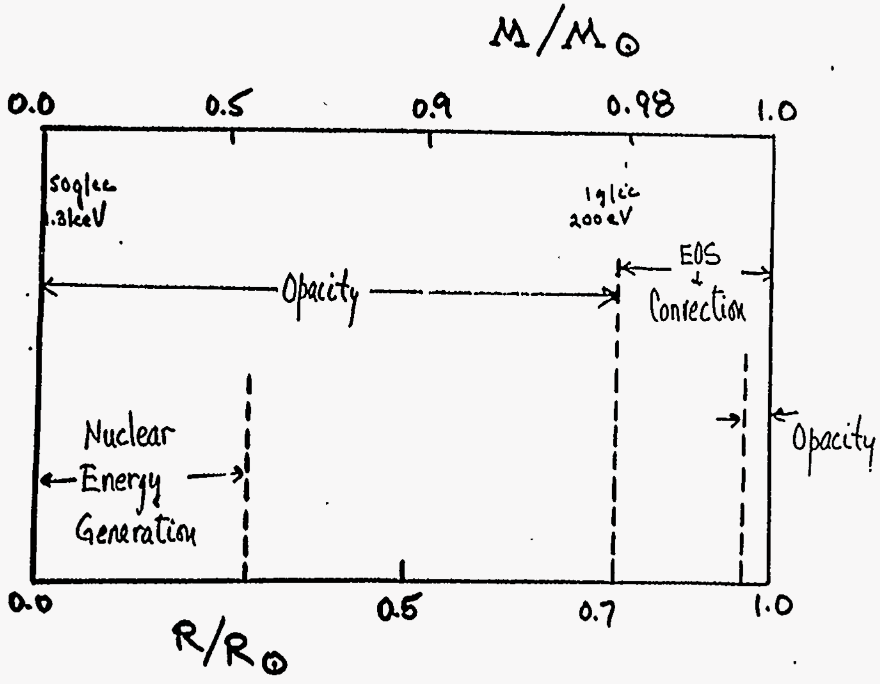

Comparisons of κ_R in Solar Radiative Interior:

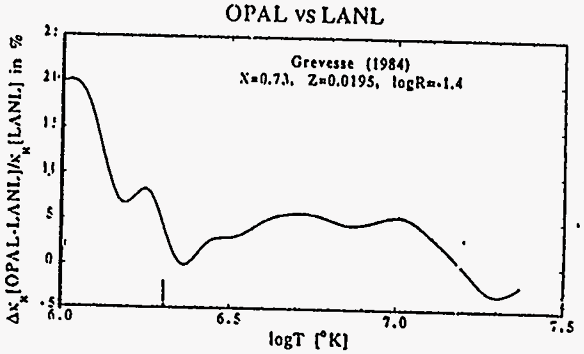
OPAL vs LANL

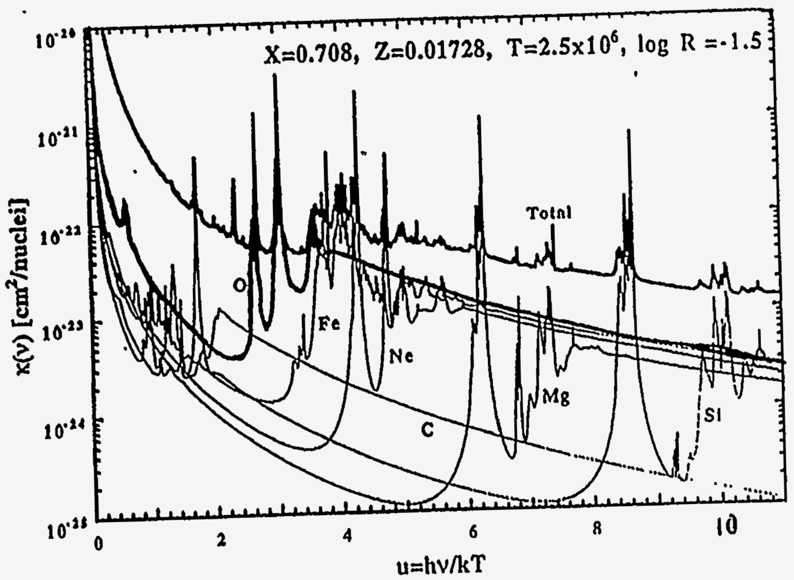

EOS COMPARISONS OPAL VS LANL:

Oxygen in an astrophysical mixture at
$\rho = 1.38 g/cm^3$, T_6=3.264, X= 0.73, Z = 0.0195

	LANL'77		OPAL		OPAL w/LANL EOS
Element	<Z>	κ_R	<Z>	κ_R	κ_R
O	7.406	7.14(-21)	7.187	8.69(-21)	7.04(-21)

From Iglesias & Rogers, *ApJ* 371, 408(1991)

COMPARISONS OF κ_R IN SOLAR RADIATIVE INTERIOR:

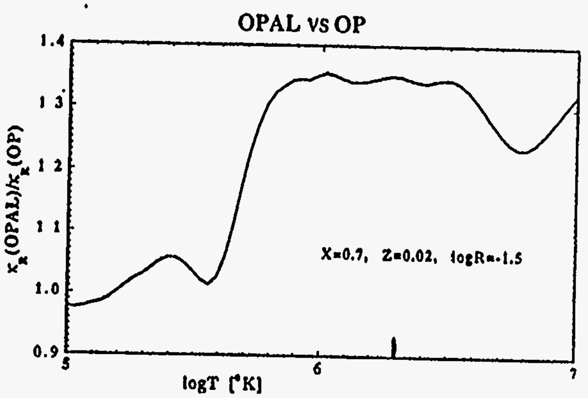

OP results from Seaton et al., *MNRAS* 266, 805(1994)

EOS COMPARISONS OPAL vs OP:

Hydrogenic Carbon "dissolution" in an astrophysical mixture at $\rho = 0.01 g/cm^3$, $T_6=1$, $X= 0.7$, $Z = 0.02$

n	OP	OPAL
1	1.00	1.00
2	0.991	0.996
3	0.906	0.995
4	0.495	0.995
5	0.0362	0.914
6	6.33(-6)	0.527
7	2.96(-16)	0.162
8	4.76(-41)	0.01237
9	1.06(-94)	0.00223

From Iglesias & Rogers, *ApJ* 443, 460(1995)

$T = 49\,\text{eV}$
$\rho = 0.026\ \text{g/cm}^3$

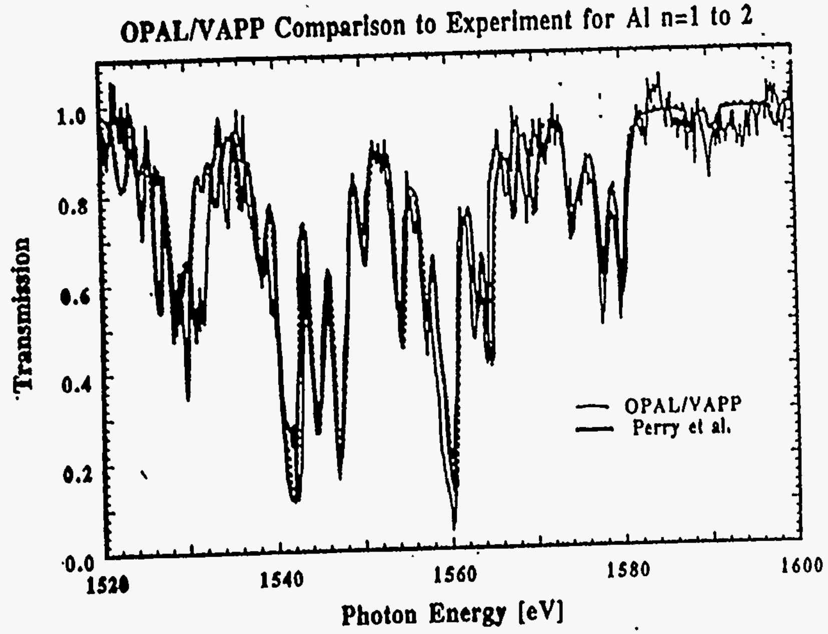

From Iglesias et al JQSRT 51, 125 (1994)

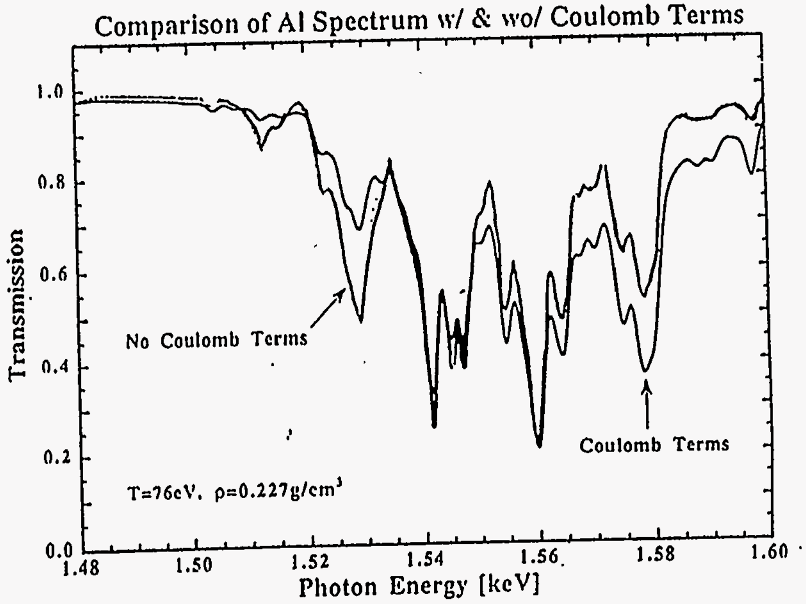

Comparison of Al Spectrum w/ & wo/ Coulomb Terms

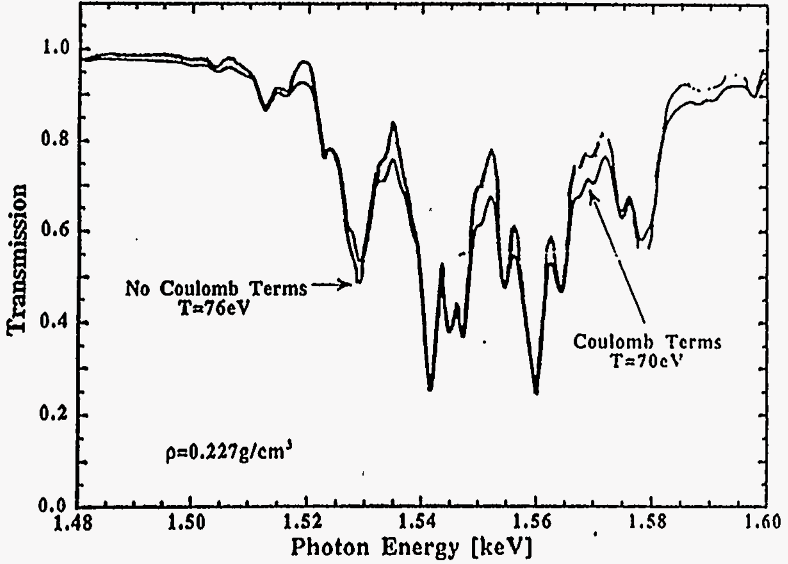

COMPARISONS OF OPAL & NOVA SHOCK EXPERIMENT:

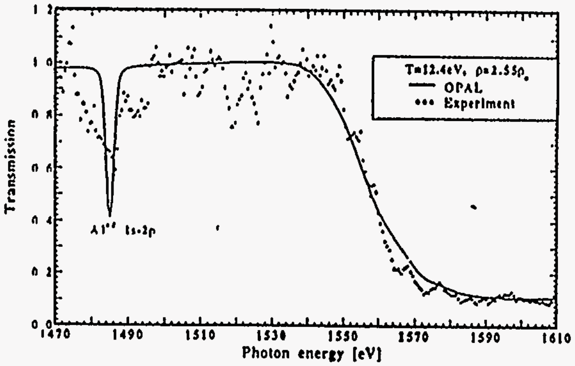

Data rom Celliers et al. (private communication)

COMPARISONS OF OPAL & STA:

T = 40eV
ρ = 3.7 ρo

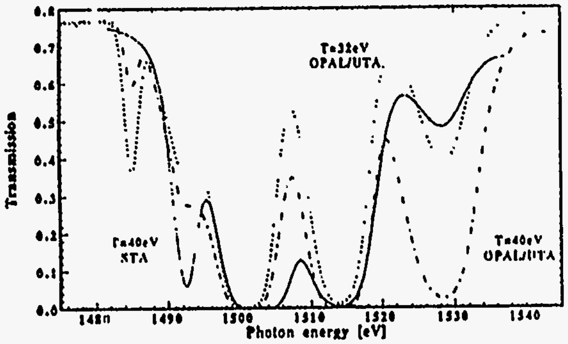

Ionization Balance

Charge	T=40eV OPAL	T=40eV STA	T=32eV OPAL
+7	0.056	0.005	0.011
+6	0.256	0.097	0.117
+5	0.406	0.418	0.377
+4	0.244	0.406	0.394
+3	0.037	0.073	0.102
<Z>	5.05	4.56	4.84

CONCLUSION:

1) Experiments relevant to stellar envelopes are welcomed in order to study details in opacity calculations

2) Ionization balance experiments are necessary to:

- a) Reduce uncertainties in solar opacities
- b) Fundamental issue in plasma physics!

Type Ia Supernova Lightcurves and Spectra

Phil A. Pinto
University of Arizona

Type Ia Supernova Lightcurves
& Spectra

or

Radiation Transport in Flows with Large Velocity Gradients & Dominated by Line Opacity

P.A. Pinto
Steward Observatory
U. of Arizona

R.G. Eastman
LLNL

(... a couple of theorists in need of an experiment...)

Type Ia Supernovae

For our purposes here, they are explosions w/

$E_{kinetic} \sim 10^{51}$ erg , $M_{tot} \sim 0.8$ to $1.4\ M_\odot$

$\langle v_{exp} \rangle \sim 7 \cdot 10^{8}$ cm s^{-1} $(v_{max} > 0.1c)$

homologous expansion , $\rho(v) \propto e^{-4v/v_{max}}$

radioactivity-powered by $\sim 0.5\ M_\odot$ of ^{56}Ni

$L_{peak} \sim 10^{43}$ erg s^{-1} 15^d past explosion

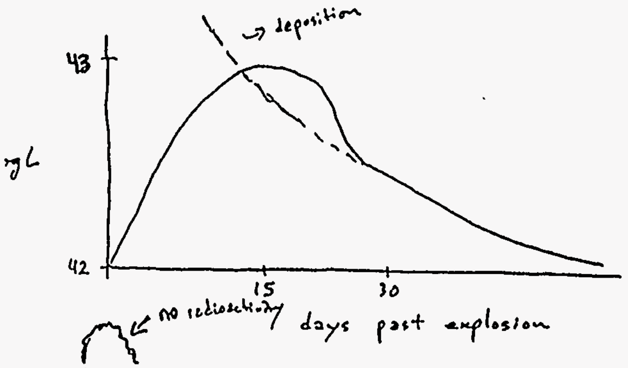

Lightcurve is the most basic diagnostic & is a competition between:

- Energy deposition by radioactive decay
  $^{56}Ni \xrightarrow[6.6^d]{} {}^{56}Co \xrightarrow[77^d]{} {}^{56}Fe$
- Adiabatic decompression (PdV work)
- Radiative transport to surface

Exponentially-falling deposition rate ⇒

Peak luminosity occurs when radiation has half a chance to escape: $\tau_{diff} \approx \tau_{exp} = t_{elapsed}$

This is typically $\sim 15^d$

For $M = M_{ch}$, $\langle v \rangle \sim 7500$ km s^{-1}

$\Rightarrow \kappa \sim 0.1$ cm^2 g^{-1}

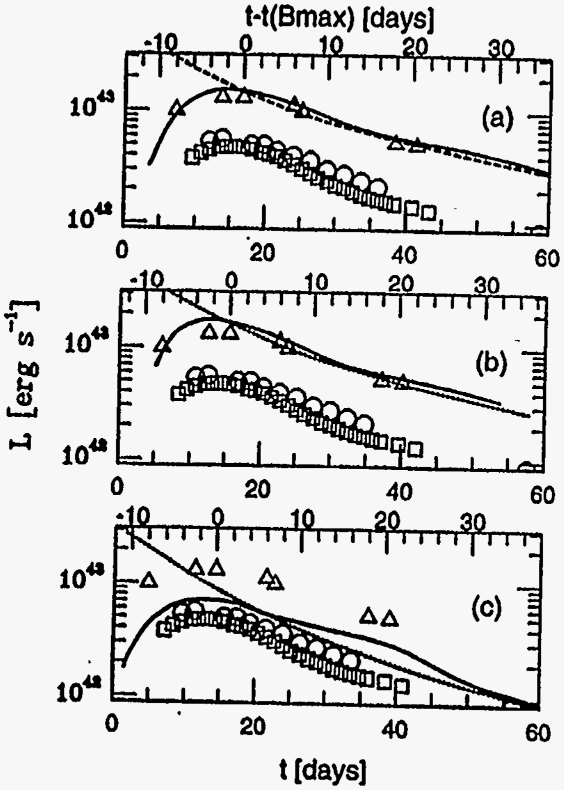

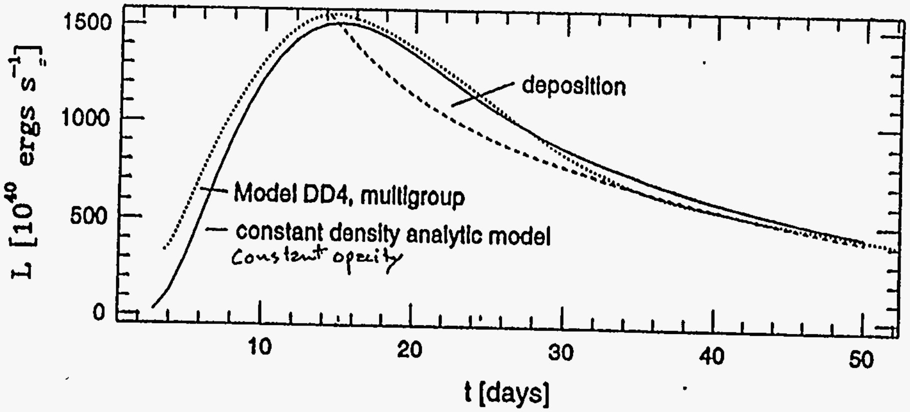

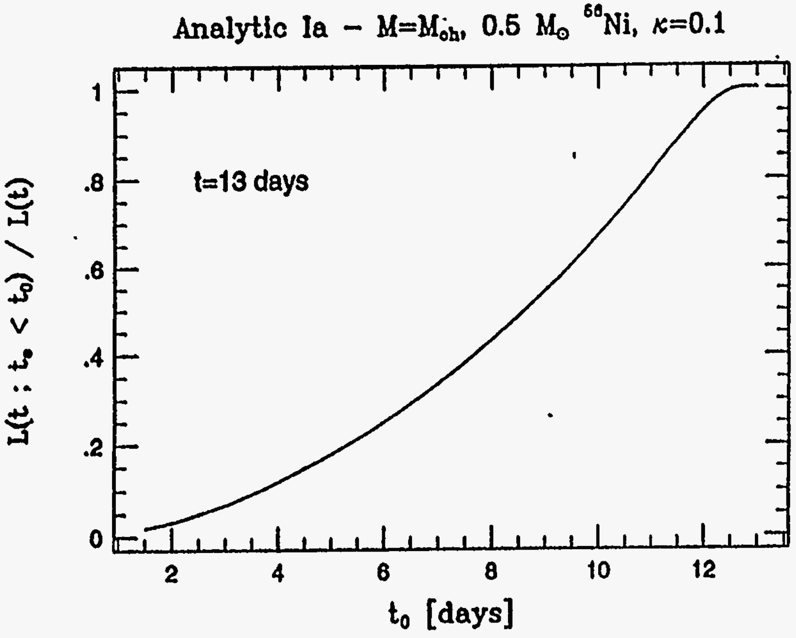
Analytic Ia – M=M$_{ch}$, 0.5 M$_\odot$ ^{56}Ni, κ=0.1
t=13 days
L(t ; t$_e$ < t$_0$) / L(t)
1
.8
.6
.4
.2
0
2
4
6
8
10
12
t$_0$ [days]

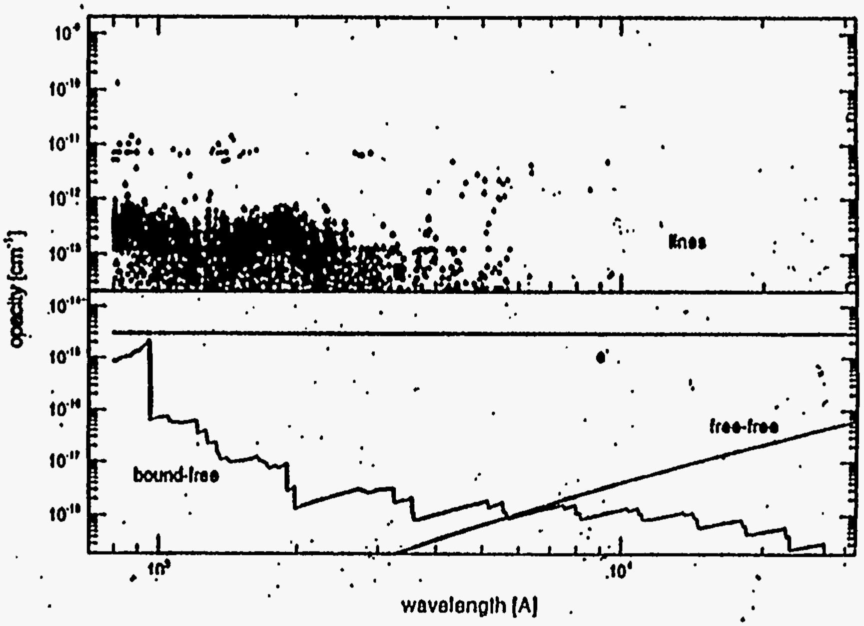
opacity [cm^{-1}]
10^{-9}
10^{-10}
10^{-11}
10^{-12}
10^{-13}
10^{-14}
10^{-15}
10^{-16}
10^{-17}
10^{-18}
lines
free-free
bound-free
10^3
10^4
wavelength [A]

- Opacity is dominated by line transitions
- large ∇v ⇒ Sobolev theory appropriate
- distance a photon travels while trapped in a line resonance region is

$$\frac{\langle \ell \rangle}{R_{max}} \approx \frac{4\, v_{th}}{v_{max}} \sim 10^{-3}$$

⇒ A photon spend virtually all of its time travelling <u>between</u> lines.

⇒ Each line acts as a single scattering event

The mean free path is thus the average distance between lines

$$\Rightarrow \tau_{SN} = \#\text{ of lines in } \left[\lambda, \lambda\left(1+\frac{v_{max}}{c}\right)\right]$$

$$\Rightarrow \text{“}\kappa_{lines}\text{”} \propto t^2 ,$$

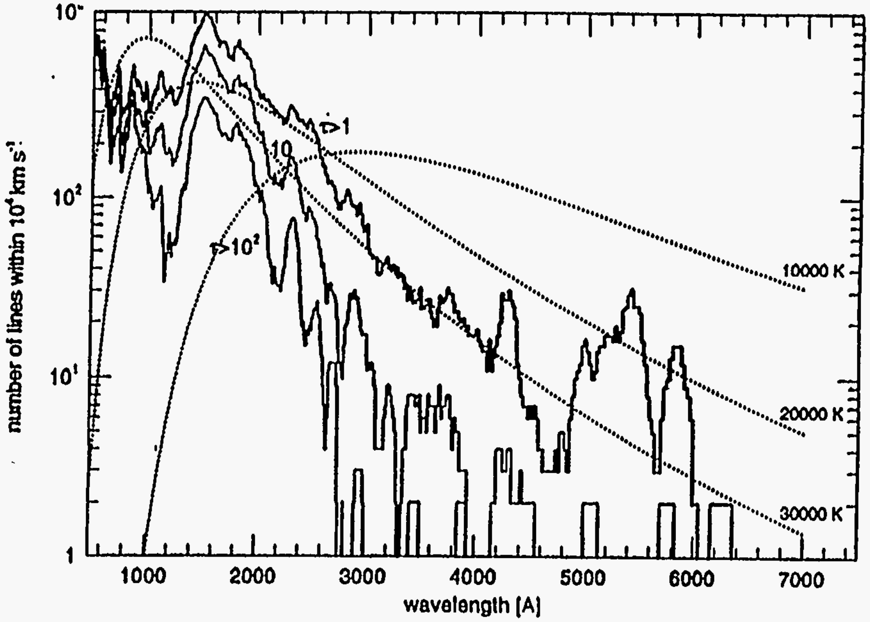

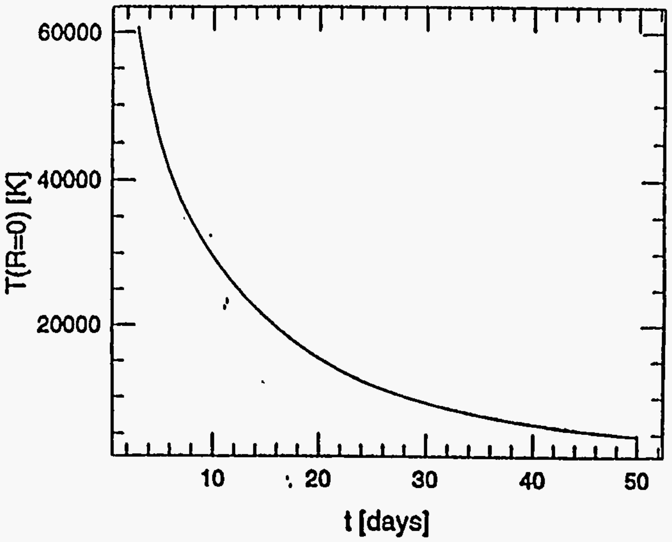

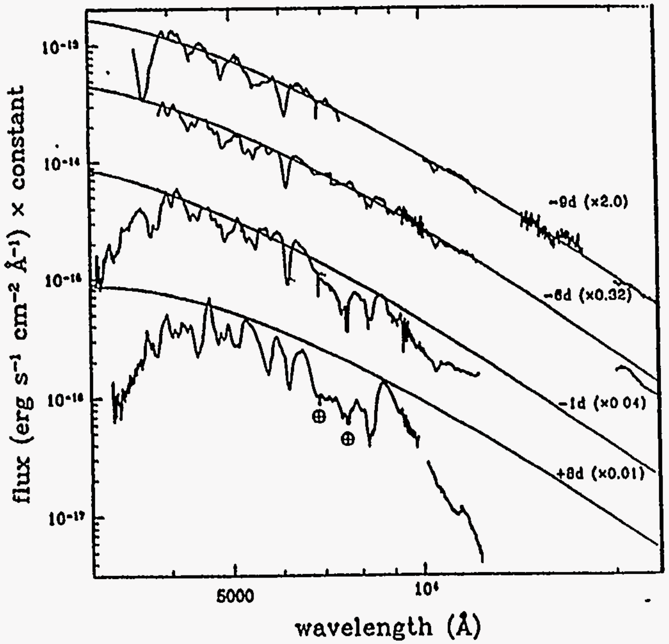
flux (erg s⁻¹ cm⁻² Å⁻¹) × constant
10⁻¹³
10⁻¹⁴
10⁻¹⁵
10⁻¹⁶
10⁻¹⁷
5000
10⁴
wavelength (Å)
−9d (×2.0)
−6d (×0.32)
−1d (×0.04)
+8d (×0.01)
⊕
⊕

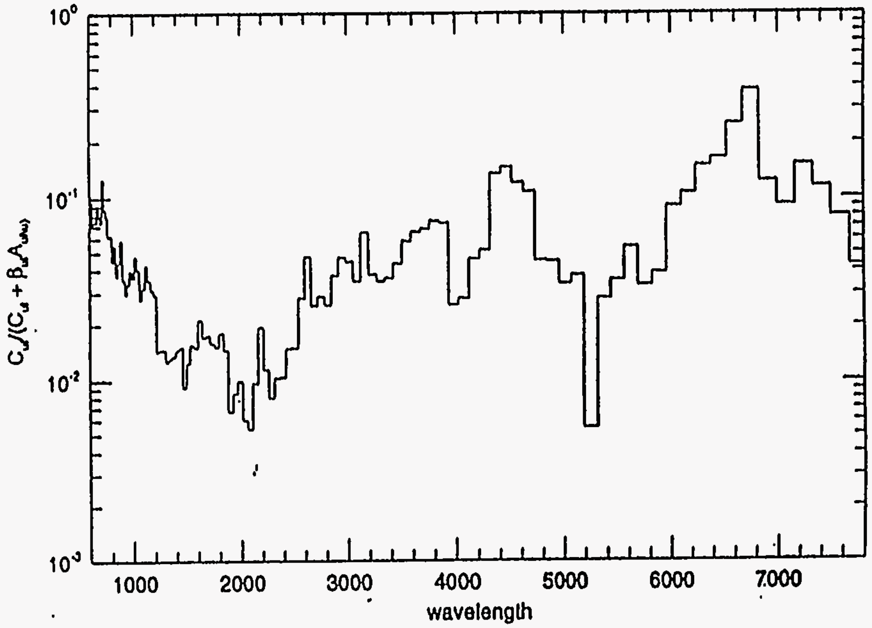
C_us/(C_us + β_us A_(uhu))
10⁰
10⁻¹
10⁻²
10⁻³
1000
2000
3000
4000
5000
6000
7000
wavelength

Energy Escape:

- As deposition falls faster than PdV, T drops & thermal emission shifts to longer λ, w/ lower τ $\Rightarrow$ escape.

- Since $\tau_{sH} = D$ lines/10^4 km s^{-1}, mfp $= \frac{R}{D}$ scatter τ^2 times to escape $\Rightarrow$ path length is DR $\Rightarrow$ total Doppler shift is $\frac{\Delta\lambda}{\lambda} \sim 1$.

Before this happens, photon falls in energy to region of lower τ & escapes.

- Photon "Splitting":

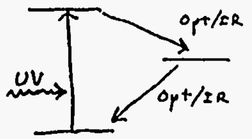

$$\sigma_{if} = (1 - e^{-\tau_i}) \frac{\beta_f A_f}{\sum_u \beta_u A_u}$$

β = escape probability

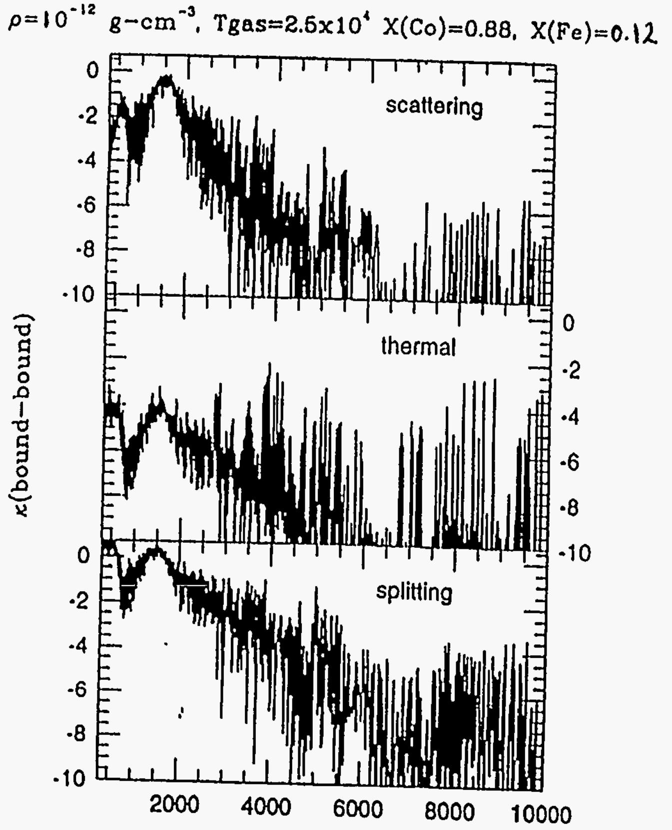

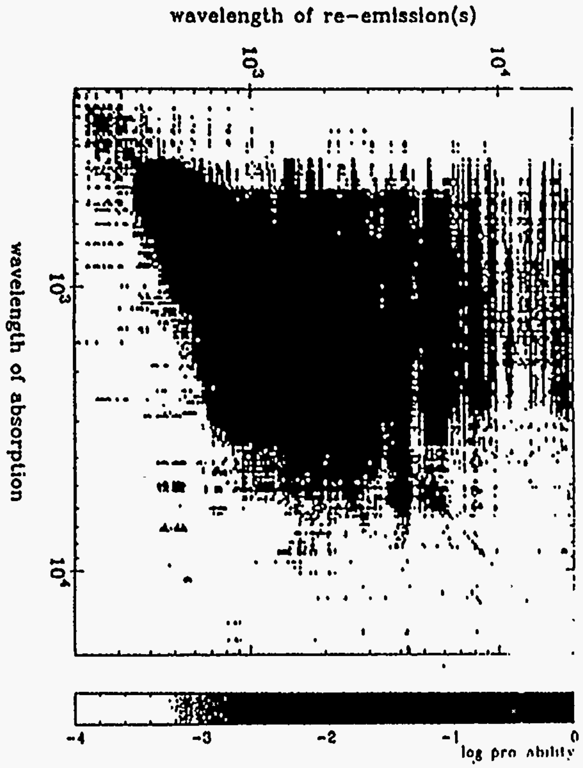

Using a multigroup, time-dependent, LTE calculation w/ Kurucz line list,

$\langle \kappa \rangle_F$ is nearly constant in time.

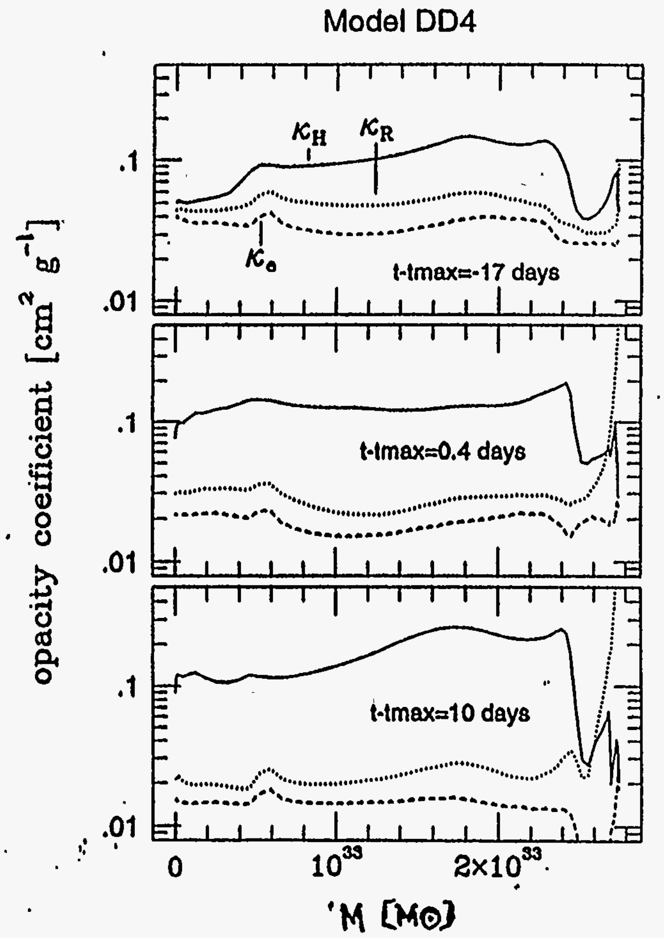

Help from Large Lasers

- "Expansion opacity" approximations
  How to take [line list, ρ, T_{gas}, T_{rad}]
  & get an appropriate $\langle \kappa \rangle$
- Tests of more detailed transport physics
  Model the experiment, don't try to
  make a SN in the lab.
- Possible test of Fe group atomic physics
  e.g. mean splitting probability as function
  of ρ, T

Photonization Modelling

Tim Kallman
NASA/Goddard Space Flight Center

Tim Kallman

Photoionization Modelling

i) Background

ii) Model ingredients

iii) Examples

with
D. Liedahl
S. Kahn
A. Osterheld
W. Goldstein
N. White
L. Angelini

and
S. Hatchett
R. McCray

[illegible]

[illegible]
[illegible]
[illegible]
[illegible]

[illegible]
[illegible]

[illegible]
[illegible] $\frac{F}{n}$ [illegible]

Why photoionization ?

- "Compact" astrophysical X-ray sources are among the brightest objects in the X-ray sky
  Also enigmatic : X-ray binaries, AGN
- Variability + large luminosities imply compact source
  $$\frac{\Delta t}{L} \sim \frac{\sigma_{th}}{m_H c^4} \sim \frac{0.5 \text{ m sec}}{10^{38} \text{ergs s}^{-1}}$$
- Lines & bound-free features formed in surrounding gas
  $t_{var} >> \Delta t_{cont}$??
- Continuum provides limited information about the conditions in the source

- What would we like to learn?
  - abundances processed material?
  - geometry heated disk? wind?
  - mass motions infall? outflow?
  - temperature heat source?
  - luminosity std. candles?
  - density
  - ⋮

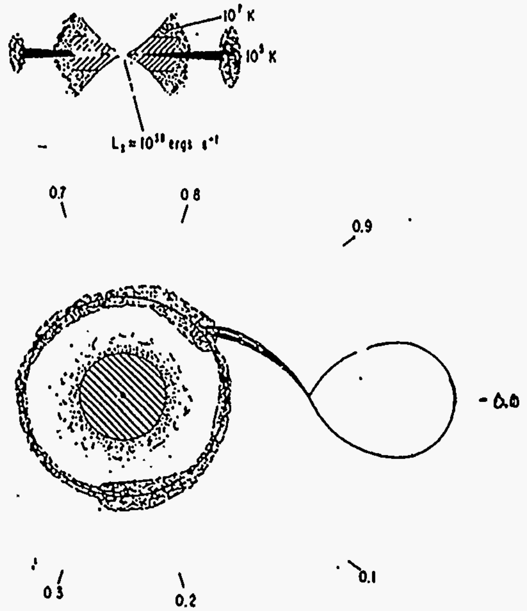

White & Holt 1982

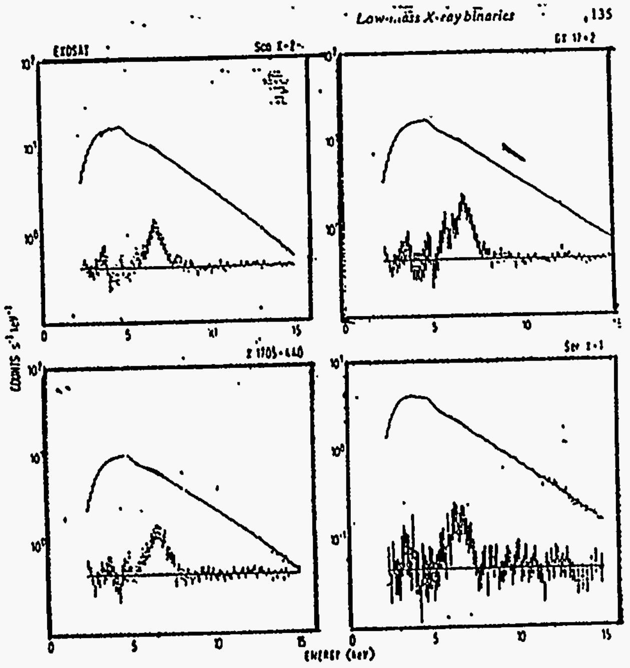

White et al. 1986

<u>Modelling</u>:

{ free parameters: "geometry", abundances, density, velocity, temperature } ⇒ { Calculate synthetic spectrum } ⇒ { Compare ⊗ observations }

<u>BUT</u> <u>this</u> <u>too</u> <u>hard</u>

X-ray opacity dominated by metals

Strategy: ignore: "geometry", velocity
other heat sources
time dependence

details: assume simple geometry (sphere or slab)
all heating & ionization from observed continuum
steady state
"coronal" excitation
simple R.T. (e.g. escape probability)

Try to treat the atomic microphysics as accurately as possible

More details

Assume "solar" abundances to start
$\gtrsim$ 10 most abundant elements

solve:

ionization = recombination
PI CI RR DI

heating = cooling
PI comp RR DI CX Comp brems

excitation = deexcitation
RR DI CX RX AD CX PI CI
"Collisional Radiative model"

"Radiation transfer
escape probability, 1 or 2 stream

Results

Scaling parameter:

"Ionization parameter"

$$\xi \sim \frac{\text{Radiation flux}}{\text{gas density}} \sim \frac{\text{Photoionization}}{\text{recombination}}$$

$$\frac{\text{heating}}{\text{cooling}}$$

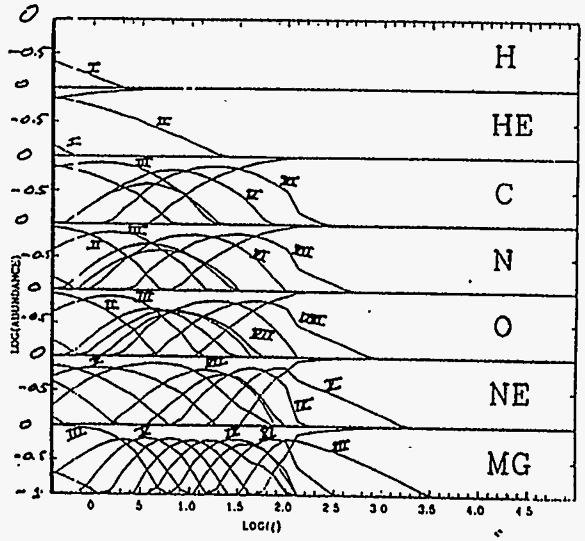

$$\xi \equiv \frac{4\pi F_x}{n}$$

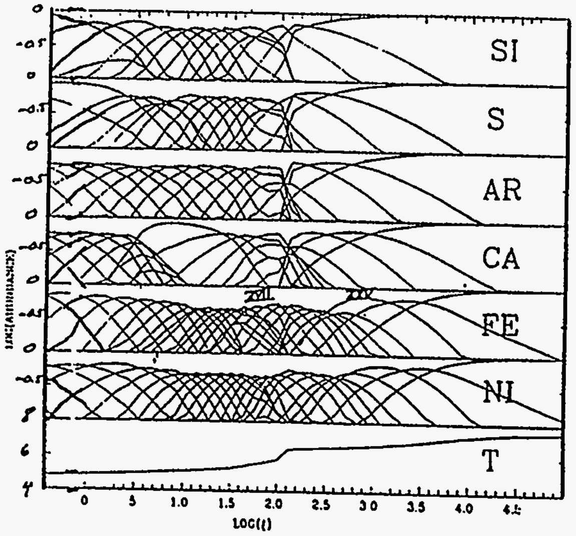

$$\xi \equiv \frac{4\pi F_x}{n}$$

Low (~1KeV) energy line modelling

- K lines of medium Z elements (~~N~~,O,Ne,Mg
  mostly from H & He -like ions Si,S)
  atomic physics is "simple": H-like scaling
  1 ⇒ Lα, Lβ, Lcontinuum
  lines are strongest due to abundances
  (n.b. O, Si, S)
  wide range of E for recombination
- L lines of iron ($n = 2 \rightarrow n = 3$)
  from Li − Ne like ions
  atomic physics is complicated:
  hundreds of levels thru $n = 3$
  need good model to do rec. cascade
  lines are weaker, lead to broad blends
  narrow range of E
  strongest are $2p - 3s$ not $2p - 3d$.

Iron L Line Spectra:
Recombination

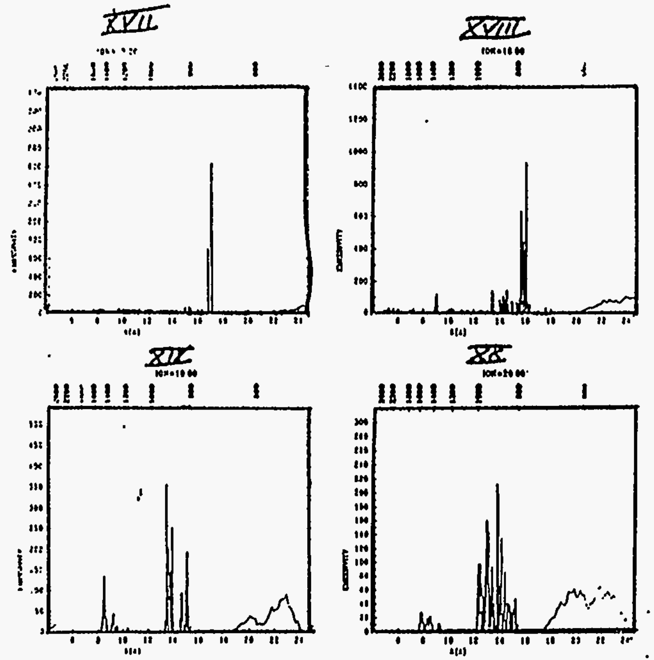

Iron L line spectra
Recombination

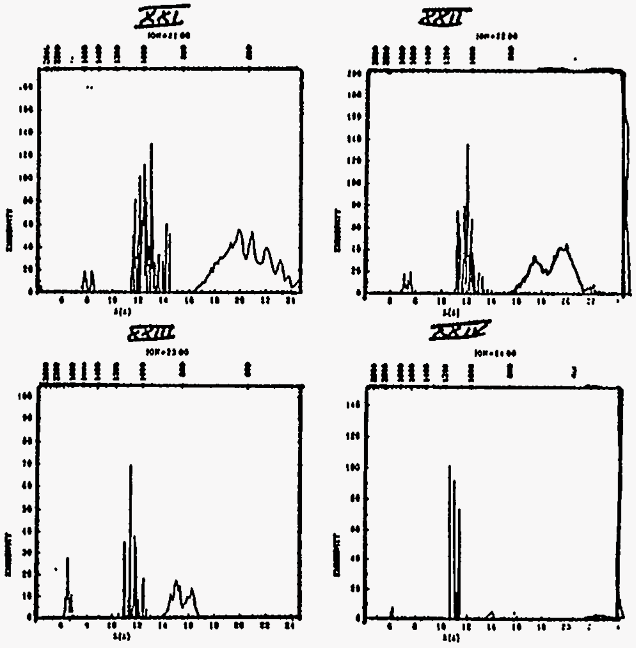

XXI XXII

XXIII XXIV

Iron L line spectra
Resonance scattering

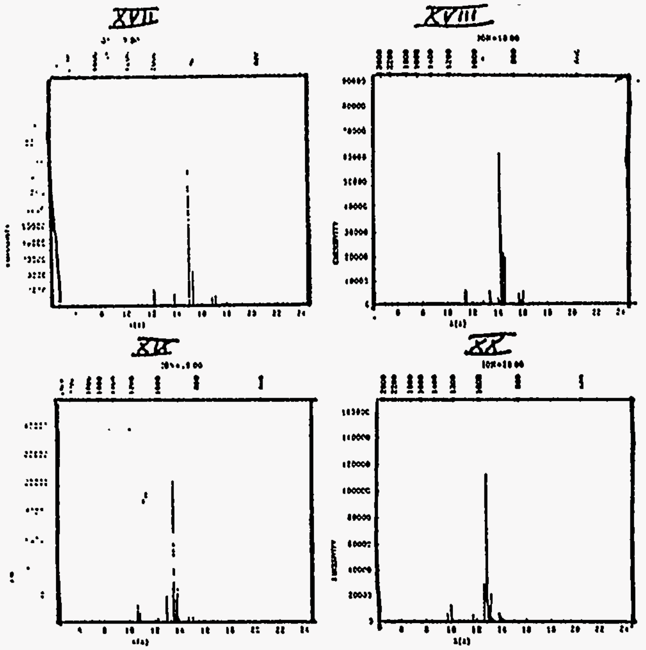

XVII XVIII

XIX XX

Iron L(1) line spectra
Resonance scattering

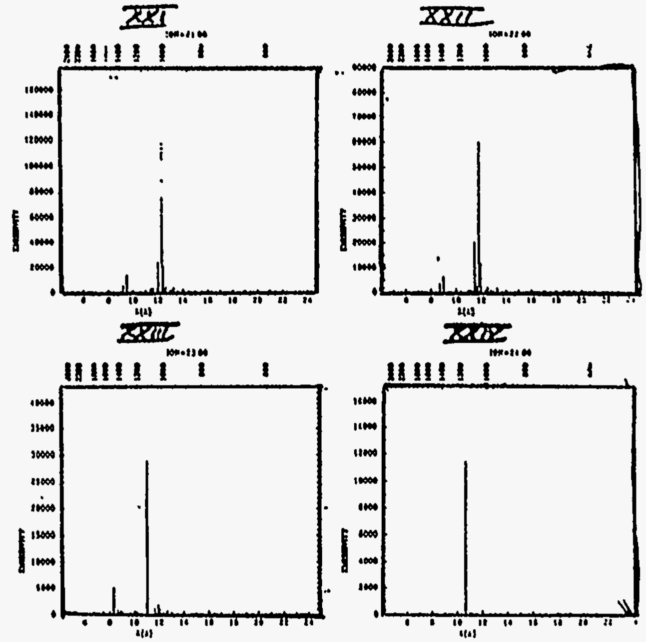

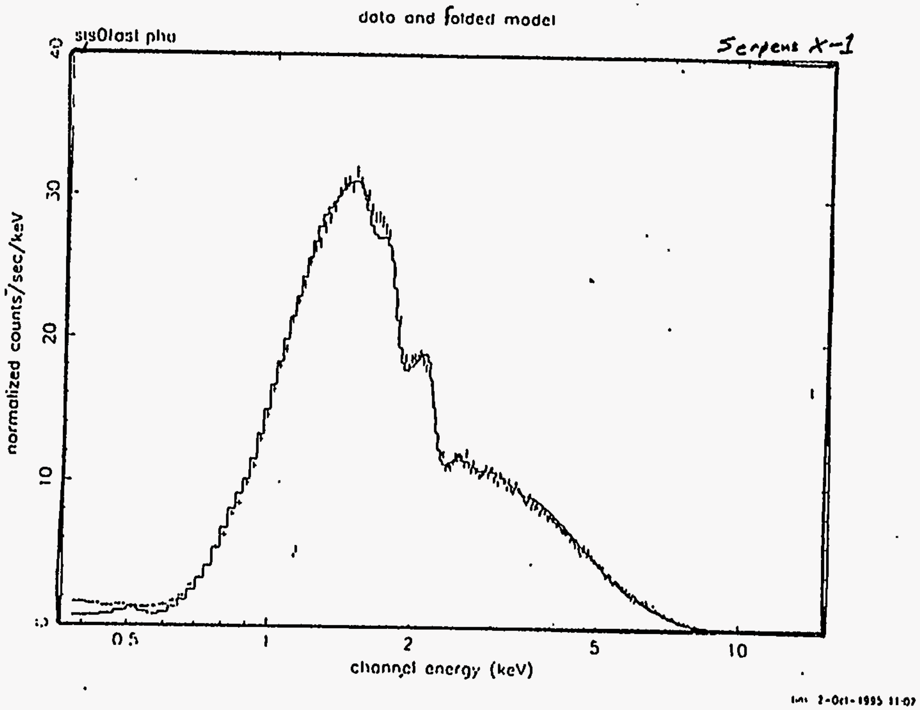

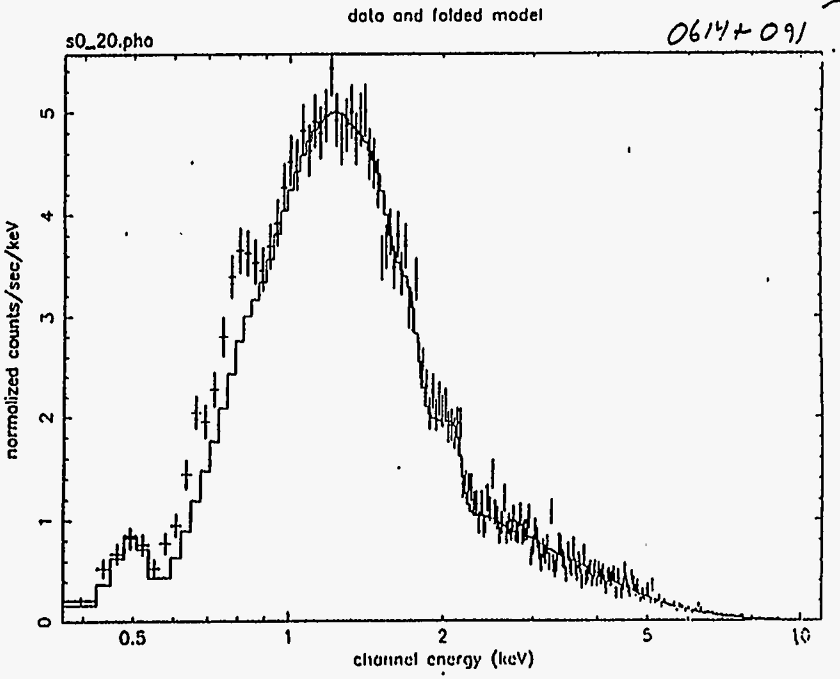

0614+091

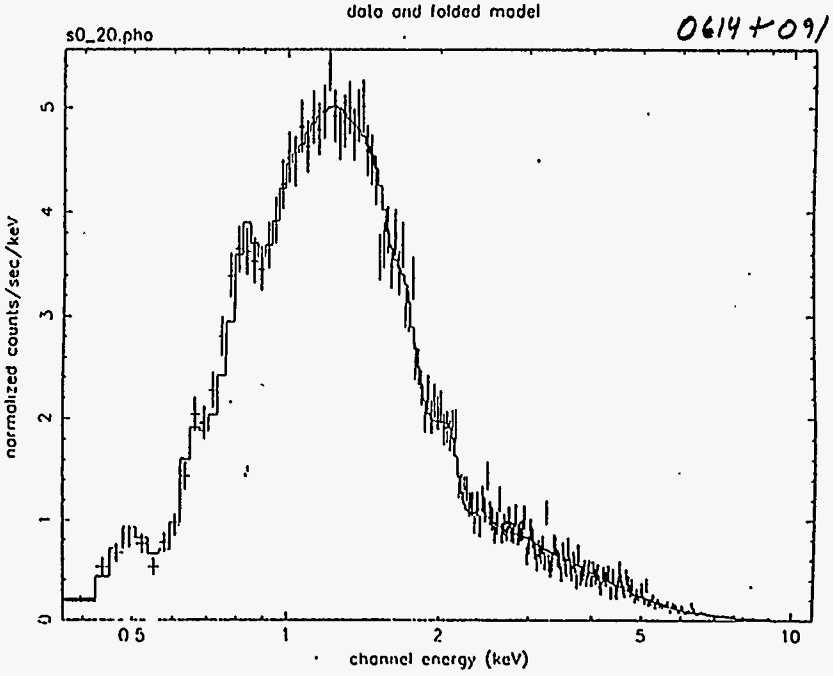

0614+091

10-Sep-1995 15:22

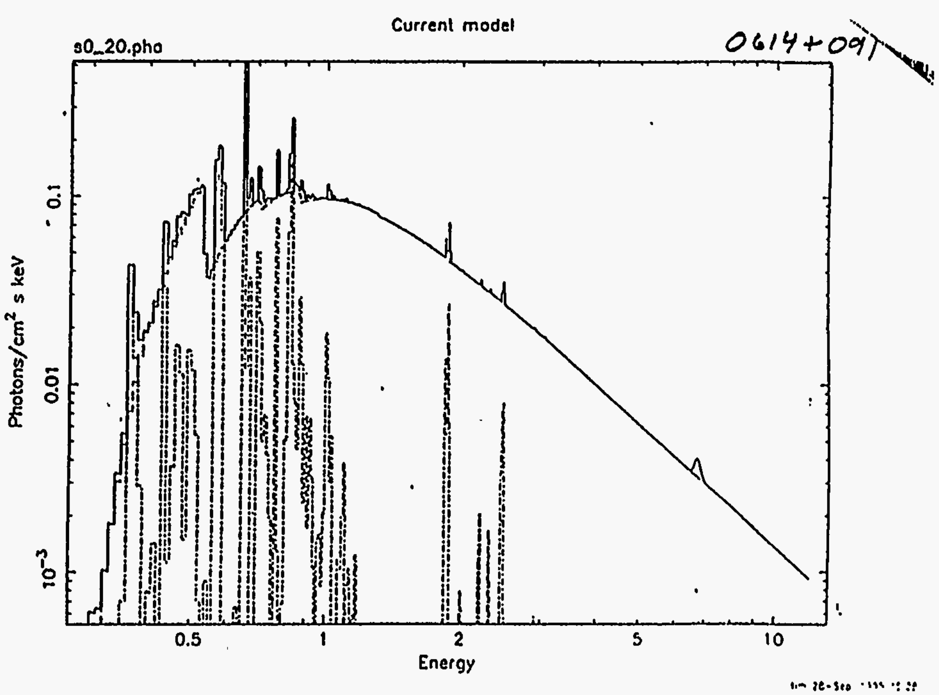

The ASCA spectrum 4U0614+091

- X-ray Burst source
- Continuum fits to absorbed power law
- Iron K line $\varepsilon = 6.75keV$ EW$\simeq$ 60 eV.
- Low energy line emission near 0.65 keV, 0.8 keV, EW$\simeq$125 eV.
- Best fit to [redacted] recomb. model, $\log(\xi) \simeq 2.8$,

  Abundances not strongly constrained.

  $\Longrightarrow$ solar abundances OK.

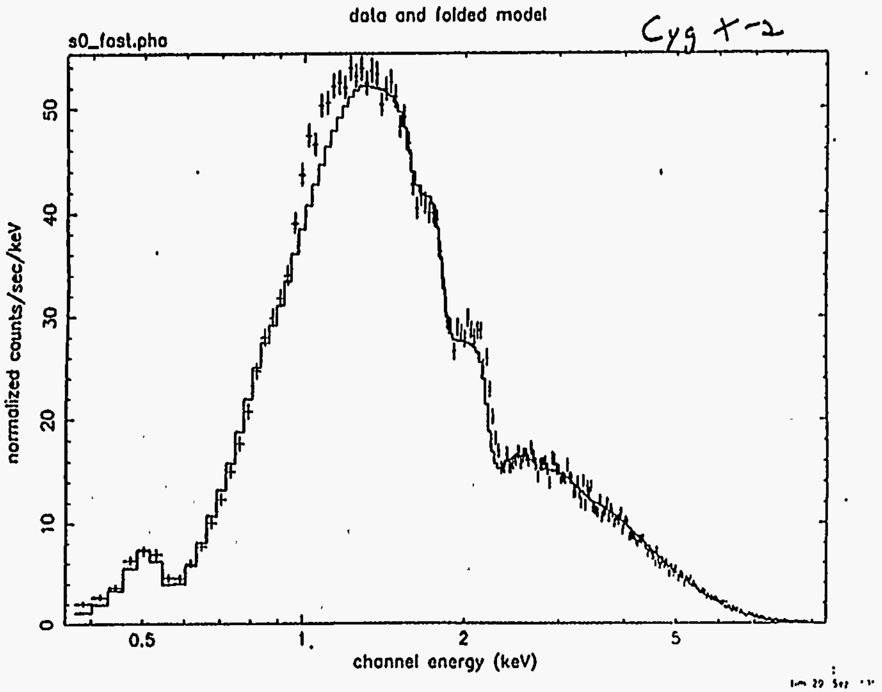
data and folded model
Cyg X-2
s0_fast.pha
normalized counts/sec/keV
0
10
20
30
40
50
0.5
1.
2
5
channel energy (keV)

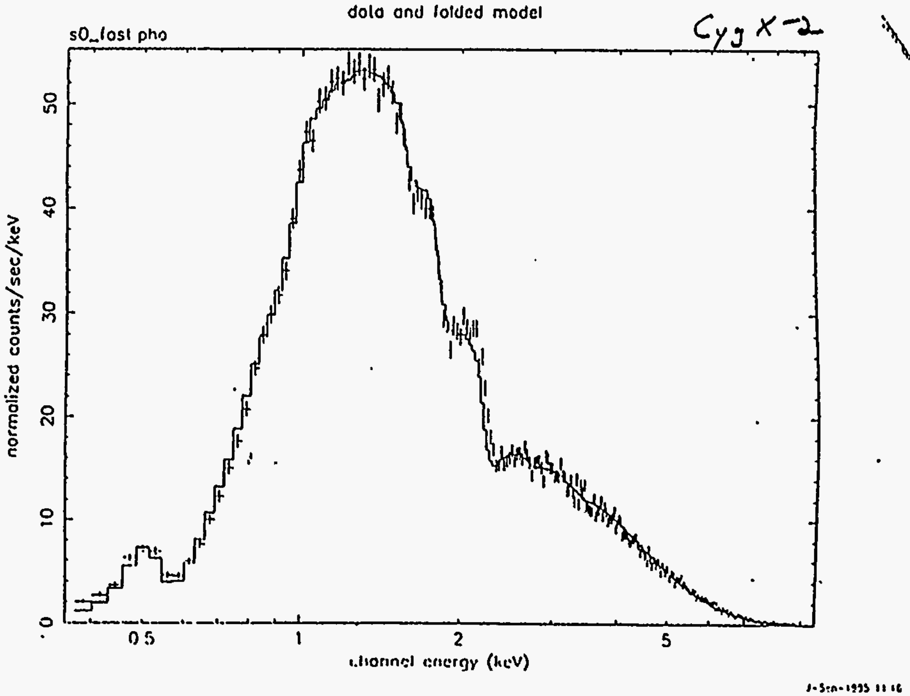
data and folded model
Cyg X-2
s0_fast pha
normalized counts/sec/keV
0
10
20
30
40
50
0.5
1
2
5
channel energy (keV)
J-Sep-1995 11:16

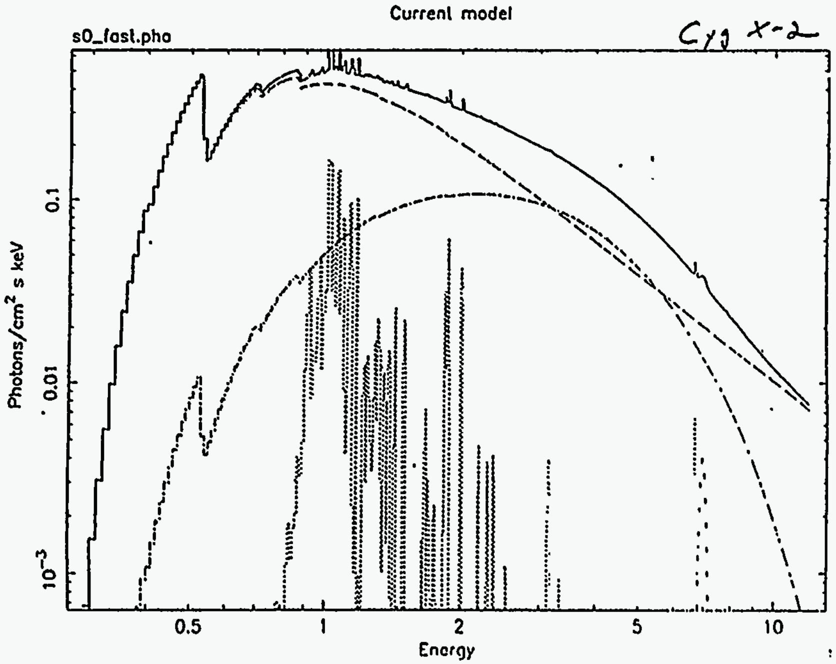

The ASCA spectrum of Cyg X-2

- well-known Z source, studied by all previous satellites.
- Continuum fits to absorbed power law.
- Iron K line $\varepsilon = 6.75keV$ EW≃ xx.
- Low energy line emission near 1 keV
- Best fit to *scattered* model, $\log(\xi) \simeq 2.8$, O/Fe≃ ~~10~~ 0.1 × solar.

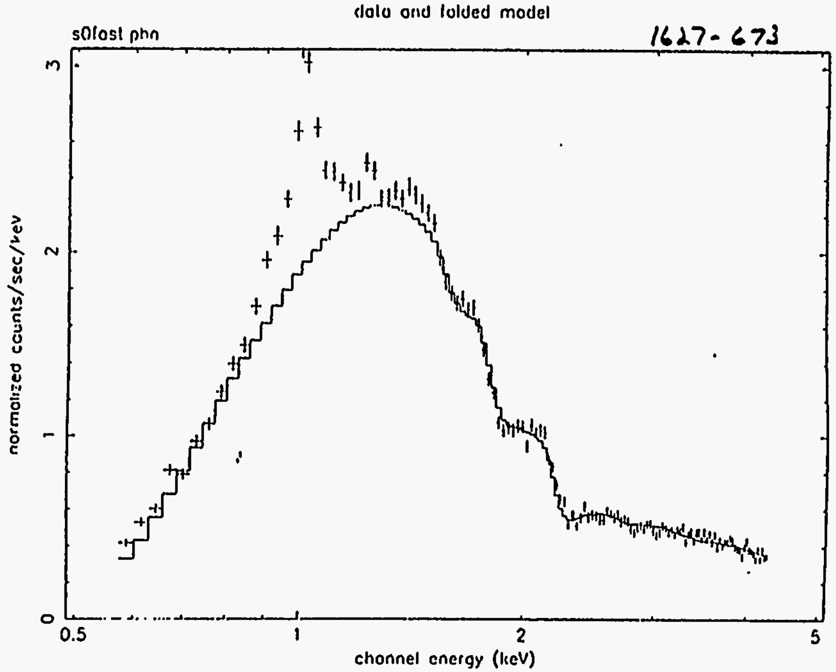

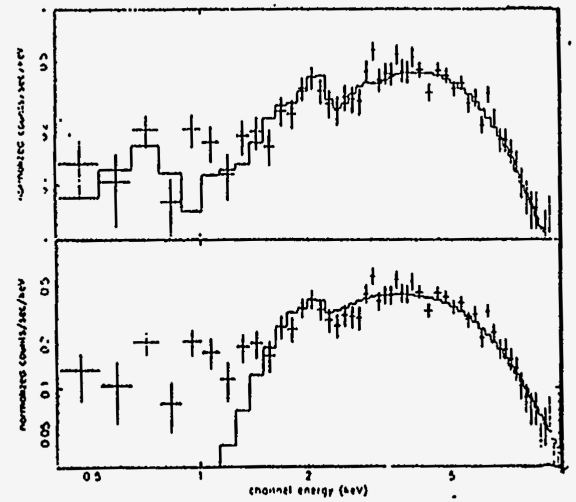

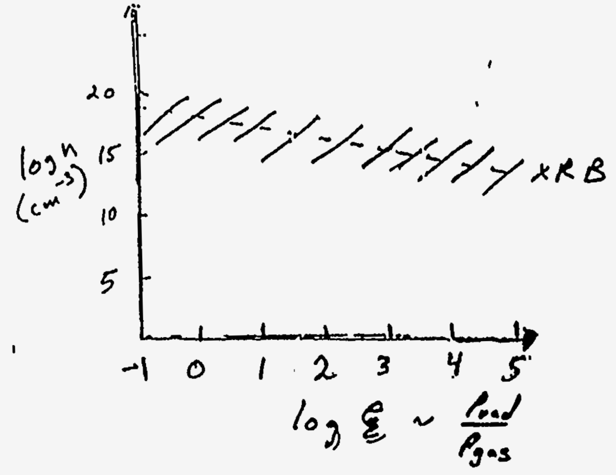

Issues

1) Atomic processes:
   DR, PI ....

2) Time dep.:
   is $F(\bar{\xi}) \approx \overline{F(\xi)}$?

3) other physics
   e.g. protons, non-maxwellian

4) Modelling (atomic model)
   & RT

5) Assumptions
   e.g. static

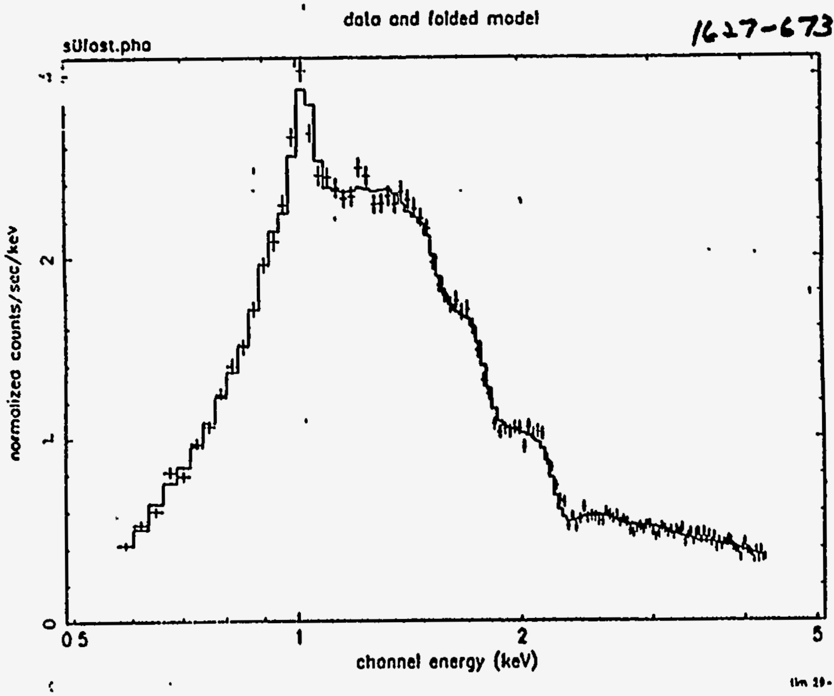
data and folded model
1627-673
sUlost.pha
normalized counts/sec/keV
0
1
2
3
0.5
1
2
5
channel energy (keV)
tim 29-Sep-1995 13:53

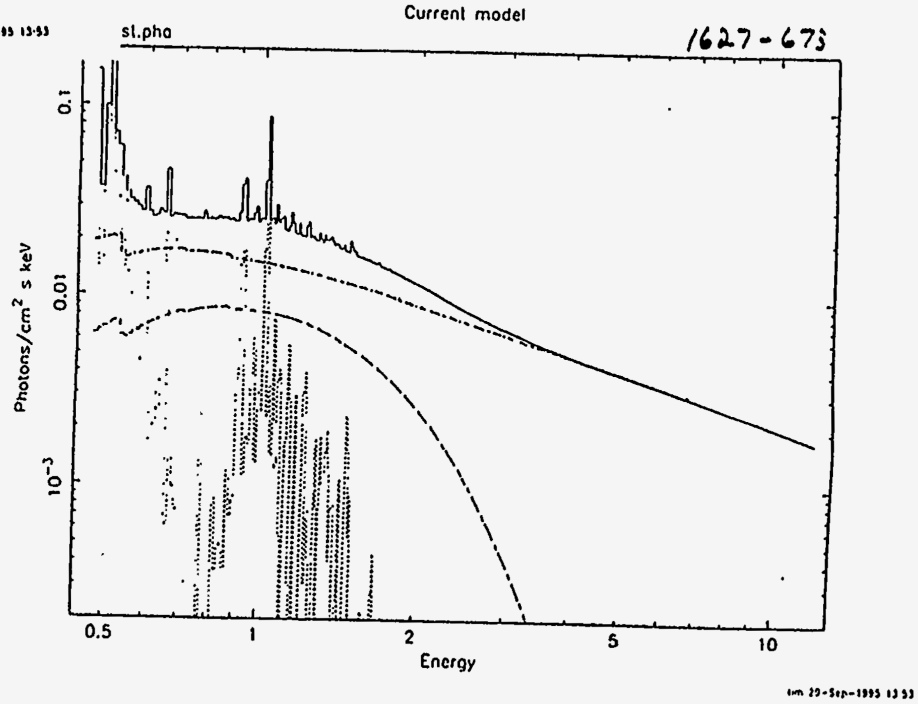
Current model
st.pha
1627-673
Photons/cm^2 s keV
0.1
0.01
10^{-3}
0.5
1
2
5
10
Energy
tim 29-Sep-1995 13:53

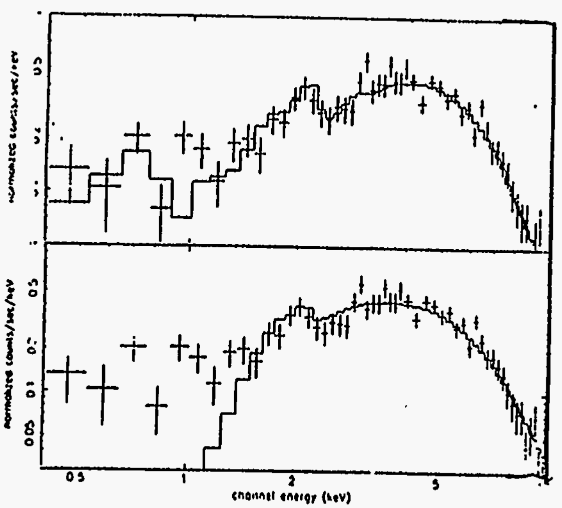

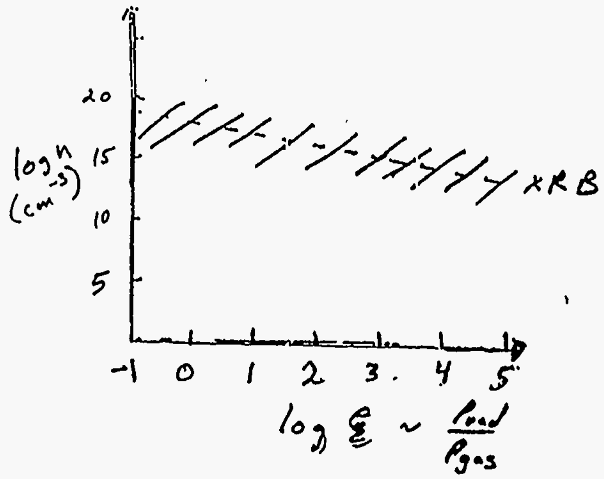

Issues

1) Atomic processes:

DR, PI ....

2) Time dep.:
Is $F(\bar{\xi}) \approx \overline{F(\xi)}$?

3) Other physics
e.g. protons, non-maxwellian

4) Modelling (atomic model)
& RT

5) Assumptions
e.g. static

Spectroscopy of X-ray Photonized Nebulae

Duane Liedahl
Lawrence Livermore National Laboratory

Spectroscopy of X-ray Photoionized Nebulae

Duane Liedahl
V-Division, LLNL

Collaborators:

James Dunn
William Goldstein
Albert Osterheld
Rosemary Walling
} LLNL

Tim Kallman - NASA/GSFC

Basic concept: create X-ray heated, photoionization-dominated plasmas in the laboratory that will allow the study of ionization/recombination, heating/cooling, and X-ray line formation as functions of ionization parameter ($\xi \sim F/n$), spectral shape, chemical composition, and density.

Motivation: launch of three facility-class X-ray satellite observatories with high-resolution spectrometers by 2000; complexity (micro & macro) of modeling spectra from X-ray photoionized plasmas; existence of suitable experimental facilities.

Presented at Workshop on Laboratory Astrophysics Experiments With Large Lasers 2/22/96, Pleasanton, CA

X-ray Spectral Bands for Cosmically Abundant Elements

Spectral Coverage of Future X-ray Observatories

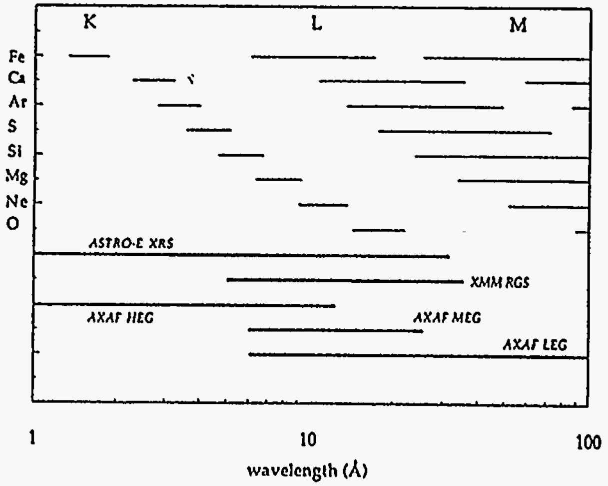

Contrast of Physical Processes in X-ray Emission-Line Regions

stellar coronae
supernova remnants
clusters of galaxies
interstellar medium
} hot, collisionally ionized

active galactic nuclei
X-ray binaries
cataclysmic variables(?)
} cool, photoionized

	Collisional equilibrium	*Photoionization equilibrium*
Ionization	electron-impact ionization	photoionization
Recombination	$\Delta n > 0$ DR	RR and $\Delta n = 0$ DR
Excitation	electron-ion impact	recombination, photoexcitation
Heating	mechanical	thermalization of photoelectrons
Characteristic temperatures	$10^6 - 10^7$ K	$10^5 - 10^6$ K
Radiative transfer	no	yes
Spectral quality	line-dominated	continuum-dominated
Fundamental parameter	T_e	ξ

Presented at Workshop on Laboratory Astrophysics Experiments With Large Lasers 2/22/96, Pleasanton, CA

Differences in the underlying population kinetics mechanisms leads to obvious differences in the resulting emission spectra. ***(Top)*** **F-like Ar X as it would appear in coronal ionization equilibrium.** ***(Bottom)*** **Ar X in photoionization equilibrium.**

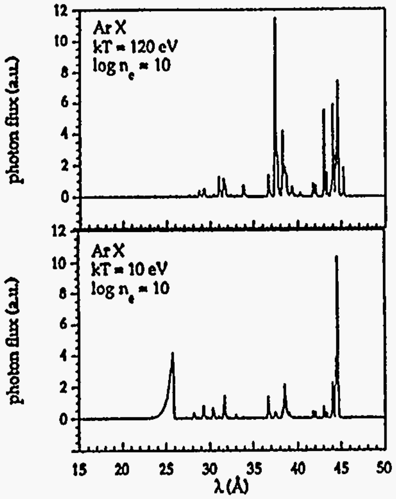

Presented at *Workshop on Laboratory Astrophysics Experiments With Large Lasers* 2/27/96, Pleasanton, CA

Different temperature dependences of RR and DR ($\Delta n = 0$) provide temperature diagnostics in L-shell ions. Shown here is the N-like Fe XX recombination spectrum, decomposed by process.

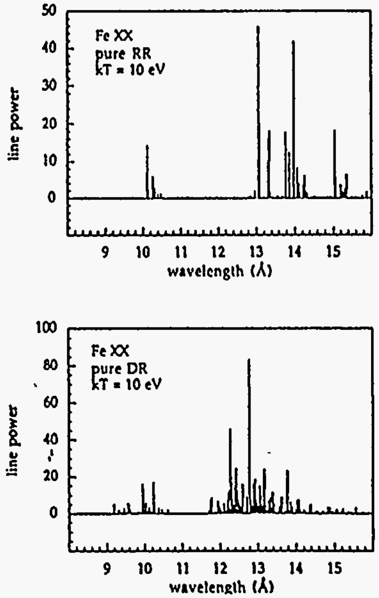

Mechanism providing density sensitivity in L-shell ions in X-ray photoionized plasmas

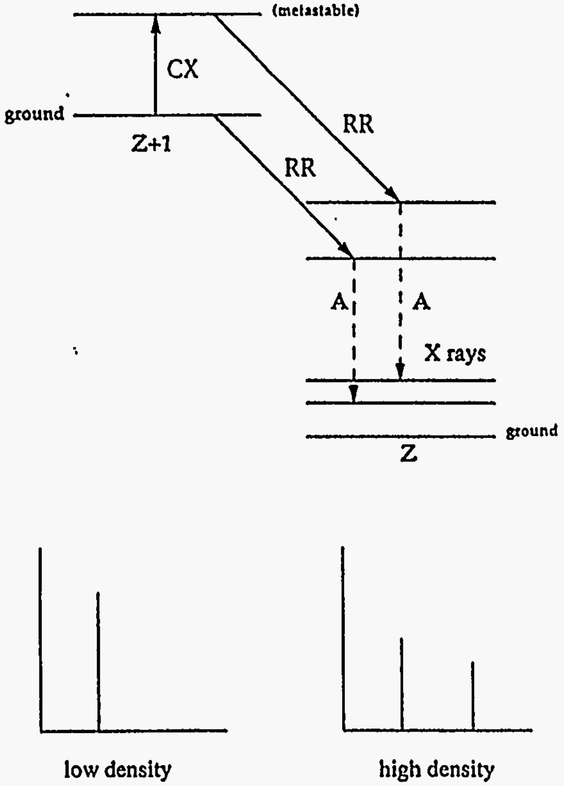

X-ray spectra of L-shell ions are sensitive to temperature and density. Shown here is F-like Ar X at two temperatures and two densities. Lines are from 3-2, 4-2, and 5-2 transitions. Features near 25 Å are radiative recombination continua, indicative of the low temperatures.

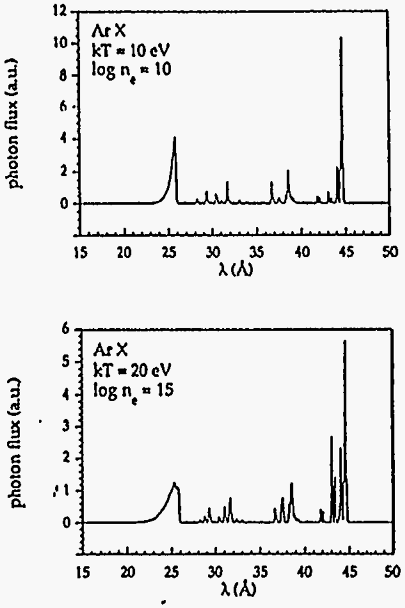

The gas cell experiment allows exceptional control over the target sample characteristics.

Total ion density known *a priori.*

Large range of ionization parameters are accessible

Elemental mixtures

No hydrodynamics

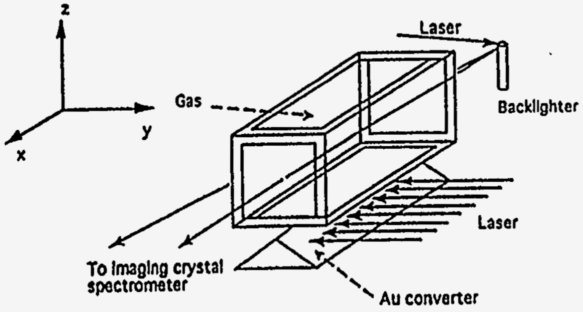

Gold converter spectra for two laser intensities (Carter *et al.* 1991).

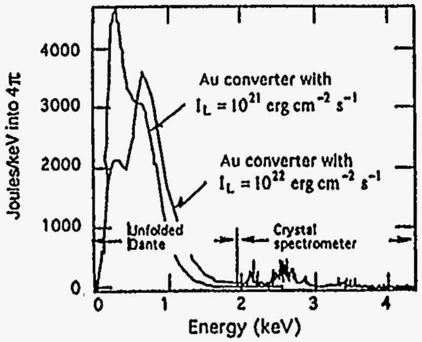

The converter flux has sufficient ionizing X rays to drive Ar (Z = 18) into the L shell, as shown here in a LASNEX simulation of the charge state distribution *vs.* time.

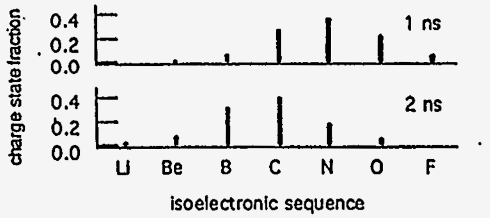

Ionization equilibrium in X-ray photoionized plasmas is characterized by the simultaneous presence of several charge states. Below is the Fe L-shell emission spectrum at two values of the ionization parameter, folded through the XMM RGS instrument response. Some of the brighter lines are labeled by their isoelectronic sequence. (Charge state distribution from Kallman & McCray 1982.)

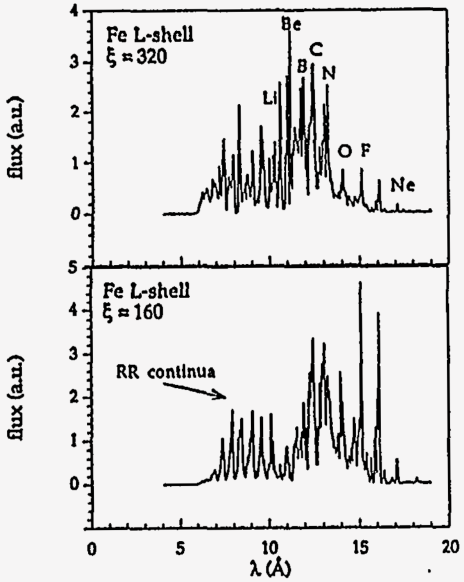

Presented at Workshop on Laboratory Astrophysics Experiments With Large Lasers 2/21/96, Pleasanton, CA

Model transmission spectra for two Ar ions, with column density $N_{ion} \approx 10^{16}$ cm^{-2}. Absorption structure results from Kα transitions ($1s \rightarrow 2p$). Adjacent charge states throughout the L shell can be easily separated. Assumed resolving power $\lambda / \Delta\lambda = 2000$. Models generated with HULLAC.

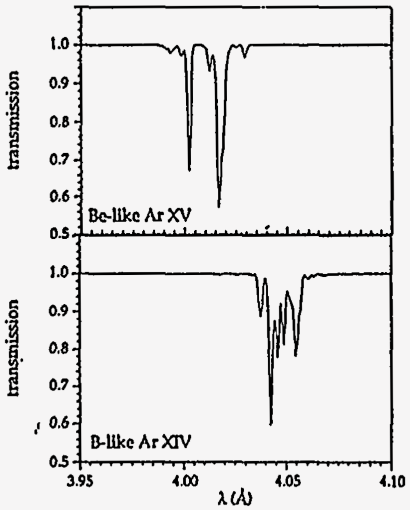

Future observations will allow high-resolution studies of accretion-powered X-ray sources. Shown here is a toy spectrum of a typical X-ray binary, convolved with the effective area and resolution of the *ASCA* Solid State Imaging Spectrometer *(red)* and the *XMM* Reflection Grating Spectrometer *(blue)*. Spectral model includes Fe L-shell ions overlying a central continuum. Assumed interstellar column density is $N_H = 4 \times 10^{21}$ cm^{-2}.

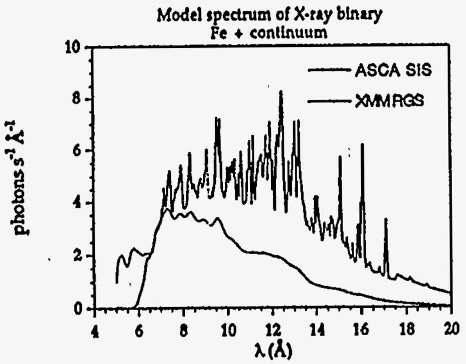

Concluding Remarks

Availability of high-quality spectroscopic data from hundreds of extrasolar X-ray sources provides major challenge to nebular modeling and atomic modeling.

X-ray spectra formed in photoionized plasmas are relevant to active galactic nuclei, X-ray binaries, and cataclysmic variables. Taken together these objects comprise >40% of pointed observations.

X-ray drives currently available on Nova are sufficient to study K-shell and L-shell physics of low-to-intermediate Z elements.

Spectral diagnostics in this regime have never been tested in the laboratory.

Effectiveness of point-projection backlighter technique has been demonstrated in other experiments.

Experiments on Nova can also help to lay the groundwork for larger scale experiments with NIF.

Hydrodynamic Instability Experiments at ILE

Hiroshi Azechi
Osaka University

Hydrodynamic Instability Experiments at ILE

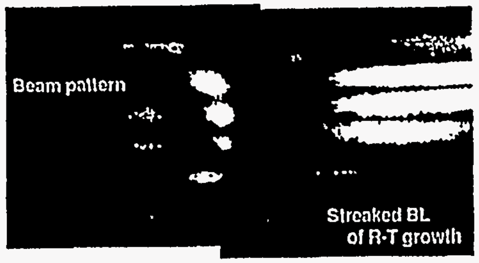

H. Azechi, K. Shigemori, M. Nakai, N. Miyanaga, H. Shiraga, K. Meguro, R. Kodama, M. Honda, H. Takabe, K. Mima

Institute of Laser Engineering, Osaka University

Introduction

Perturbation growth before the first-shock breakout gives initial conditions to the following Rayleigh-Taylor instability

ILE Osaka

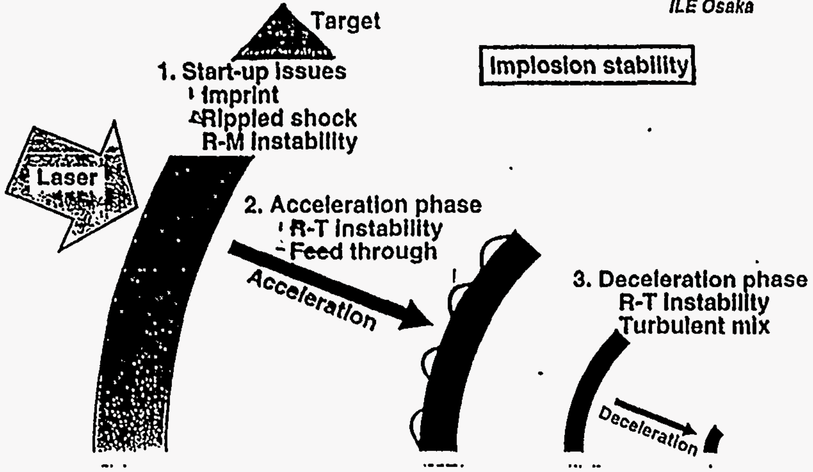

Implosion stability

1. Start-up issues
   - Imprint
   - Rippled shock
   - R-M instability
2. Acceleration phase
   - R-T instability
   - Feed through
3. Deceleration phase
   - R-T instability
   - Turbulent mix

Experimentals

Targets were irradiated by fiber-generated partially-coherent light.

ILE Osaka

- **Wavelength**
  $\lambda = 0.53\ \mu m$
- **Bandwidth**
  $\Delta\lambda = 0.2$nm (x470 transform limit)
- **Beam divergence**
  $\Delta\theta = 1.31\times10^{-4}$ rad. (64TDL)
- **Angular dispersion (1D)**
  $\Delta\theta / \Delta\lambda = 478\ \mu$rad. / nm
- **Smoothing characteristics**

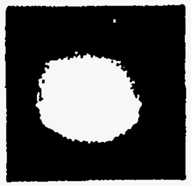

Time-integrated,beam pattern

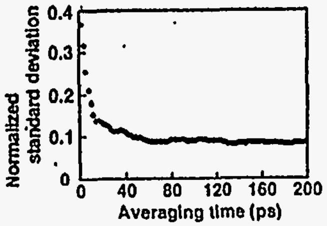

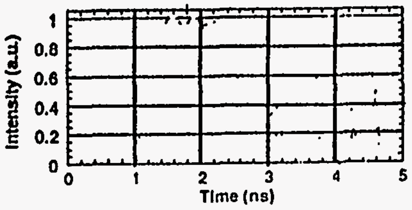

Pulse shape

Experimental

Experimental conditions on Rayleigh-Taylor / imprint experiments

ILE Osaka

Target	Flat CH (polystyrene) 16 μm Initial perturbation (R-T experiment) wavelength : 60 μm amplitude : 0.1, 0.3, 1 μm
Laser	PCL : flat top pulse (FWHM: 1.8 or 2.2 ns) Intensity modulation (imprint experiment) wavelength (on target) : 100 μm amplitude ($\Delta I/<I>$) : 10%, 40%

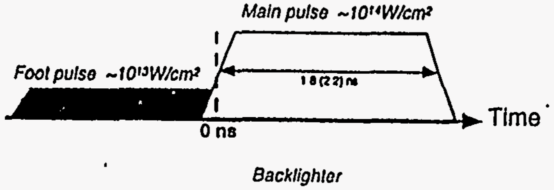

Foot pulse intensity was spatially modulated at the imprint experiment

Experimental

Perturbation growth was measured by face-on x-ray backlighting method.

ILE Osaka

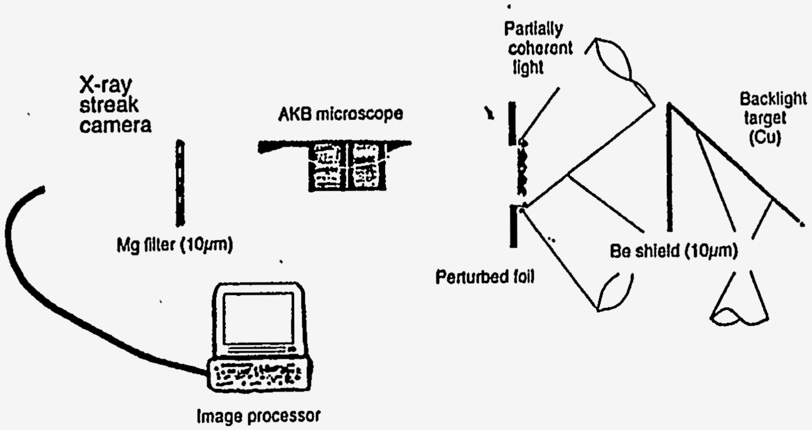

KS95A012 (APS)

Temporal evolution of backlit images due to R-T instability were obtained.

ILE Osaka

#17590 Initial amplitude : 1 μm

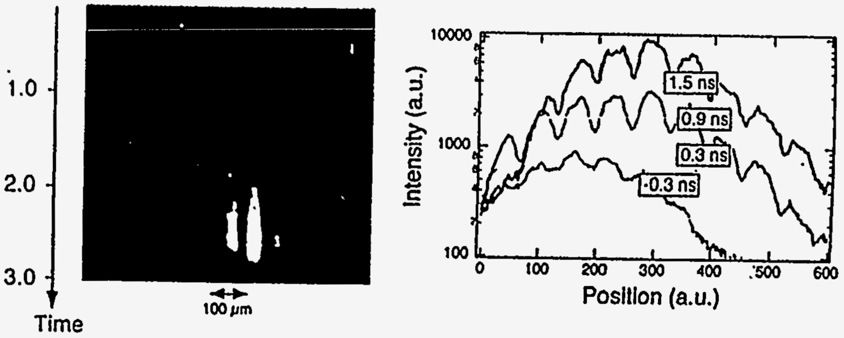

Results

Growth rate of R-T instability was evaluated from three target shots.

ILE Osaka

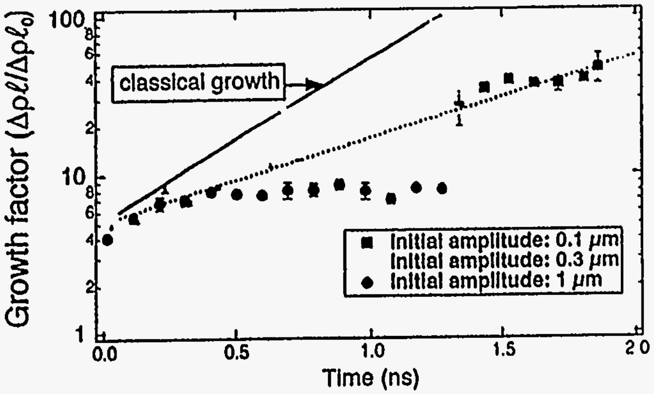

Simulation

to be revised!!

Experimental results were compared to calculations by ILESTA 1-D simulation.

ILE Osaka

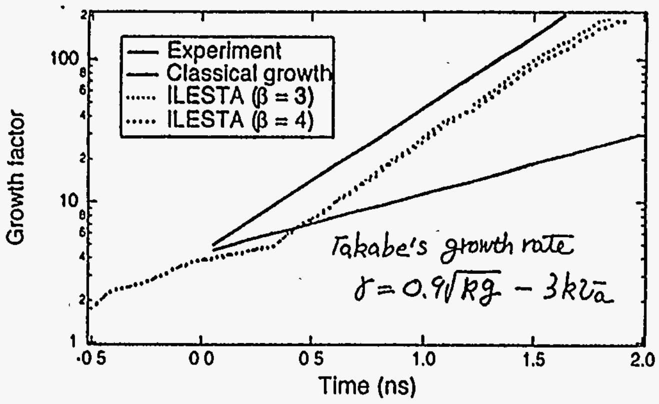

Takabe's growth rate

$\gamma = 0.9\sqrt{kg} - 3kv_a$

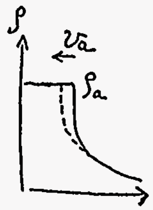

$v_a = \frac{\dot{m}}{\rho_a}$

Fokker-Planck simulations show that target preheating due to nonlocal electron thermal transport supresses Rayleigh-Taylor instability.

ILE OSAKA

R-T Insta. is supressed by
precursor thermal wave ?

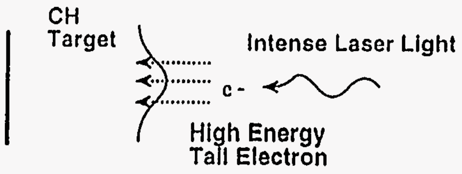

$$\ell_{\text{mf.p.at cutoff}} \approx 180\left(\frac{\lambda(\mu m)}{0.53}\right)^{14/3}\left(\frac{I(W/cm^2)}{10^{15}}\right)^{4/3}$$

R-T Insta. by FP 2d

Initial Temperature and Density Profiles for 2D Fokker-Planck Simulations

ILE OSAKA

Target Thickness : 32 [micron]

Laser Intensity : 1×10^{14} [w/cm^2]

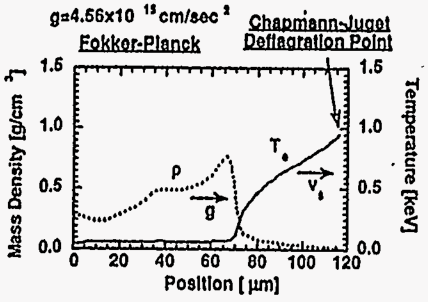

(by KEICO-1d FP Code)

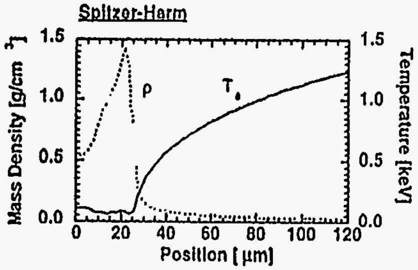

(by KEICO-1d SH Code)

R-T Insta. by FP 2d

Preheating due to nonlocal electron heat transport supresses the Reyleigh-Taylor instability

ILE OSAKA

RESULTS :

$\gamma_{classical}$ = 2.19×10^{9} [/s]

γ_{SH} = 2.04×10^{9} [/s]

γ_{FP} = 0.886×10^{9} [/s]

$V_{abl\ SH}$ = $(\rho v)_{C\text{-}J}/\rho_{abl}$

= 2.17×10^{5} [cm/s]

$V_{abl\ FP}$ = 3.22×10^{5} [cm/s]

β_{SH} = ?

β_{FP} = 3.51

for Wave Length : 60 micron,

Gravity Force : 4.56×10^{15} [cm/s^2]

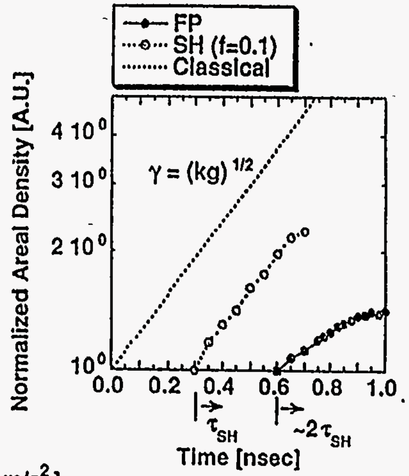

(by KEIC 'Code)

Sinusoidal intensity modulation was imposed by a opaque grating mask

ILE Osaka

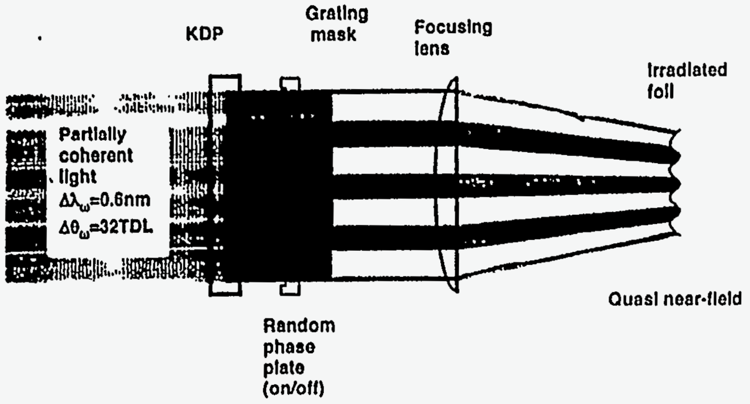

Intensity profile of the modurated prepulse on the target (without RPP)

ILE OSAKA

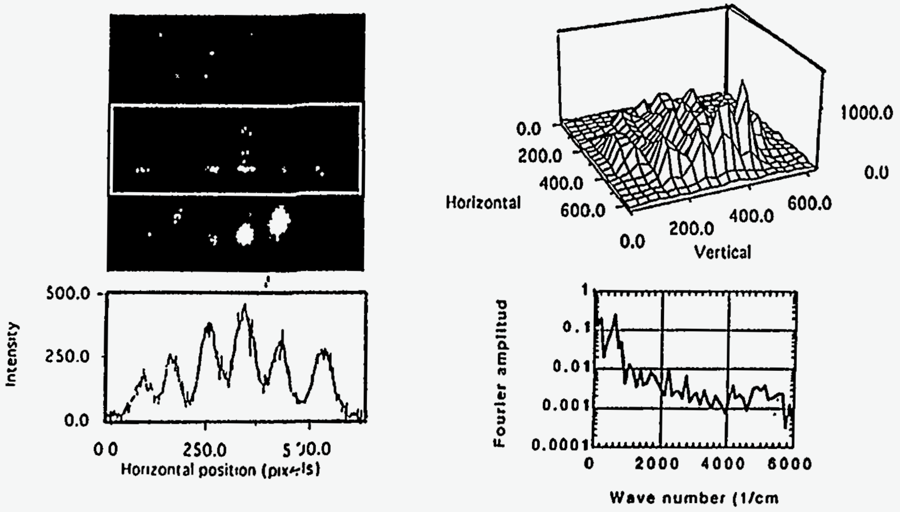

(Scale 1 15μ m/pixel)

Intensity profile of the modurated prepulse on the target (with RPP)

ILE OSAKA

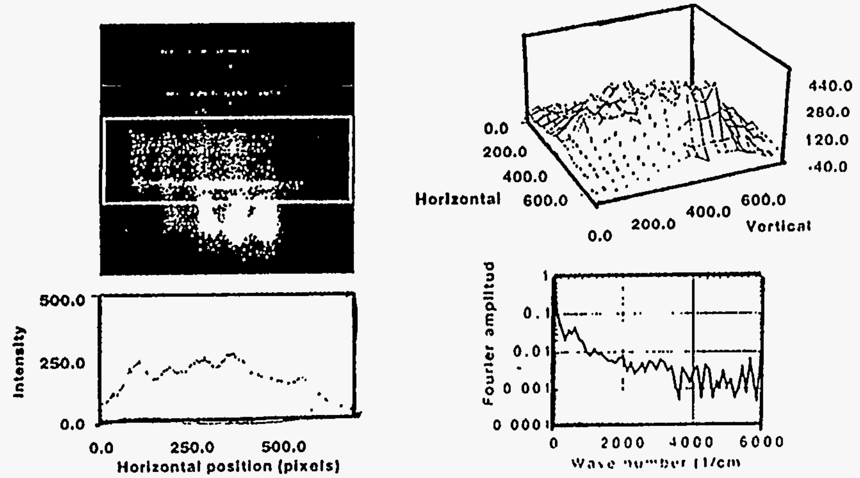

329

Areal density perturbation seeded by the initial imprinting increases with increasing imposed intensity modulation

ILE Osaka

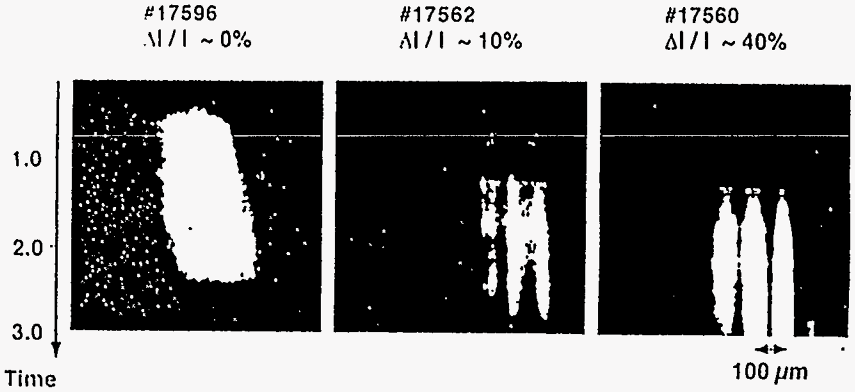

ΔI / I : modulation amplit

Initial imprinting perturbation is amplified by Rayleigh-Taylor instability

ILE Osaka

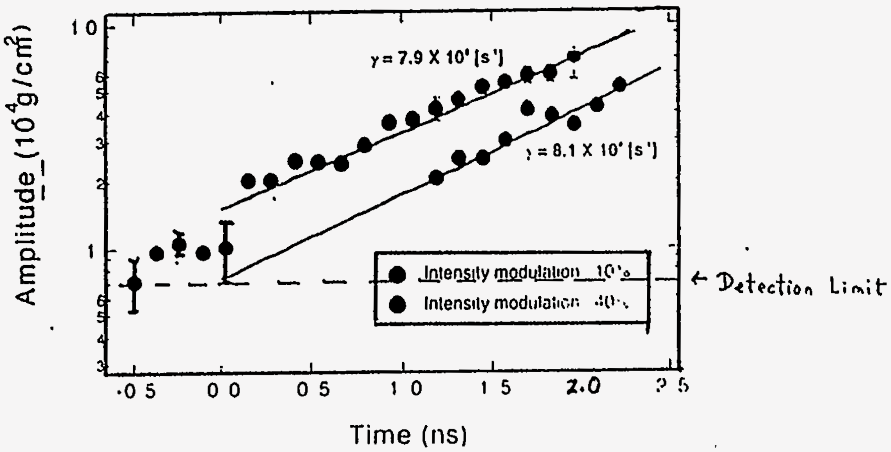

#17596 Intensity modulation : ~~8%~~ Δλ=6Å 32TDL

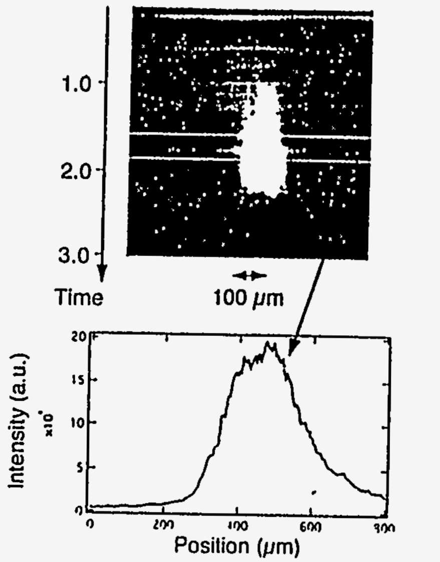

#17634 Δλ :3.5Å, 10TDL at ω_0

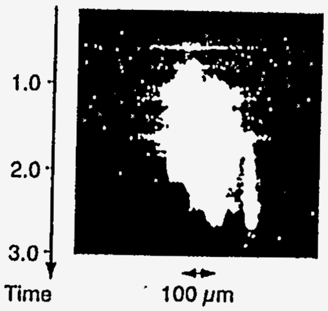

We used external x-ray source to suppress the initial imprinting

ILE Osaka

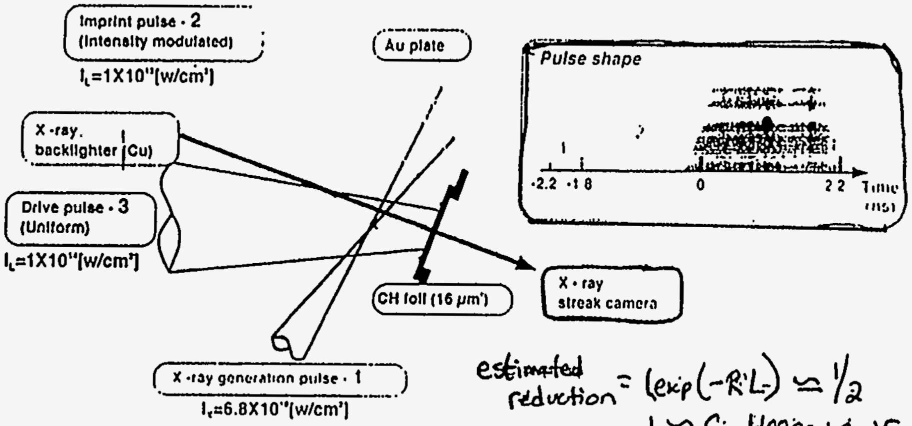

estimated reduction $= (\exp(-\dot{R}L) \simeq 1/2$

$L \simeq C_s\, 400\mathrm{ps} \simeq 15\,\mu m$

$\dot{R} = 2\pi/100\,\mu m$

Significant reduction of perturbation growth due to x-ray pre-irradiation was observed by face-on backlighting method

ILE Osaka

S.N. 17562

S.N. 17629

Intensity moduration ~10% without x-ray pre-irradiation

Intensity moduration ~10% With x-ray pre-irradiation

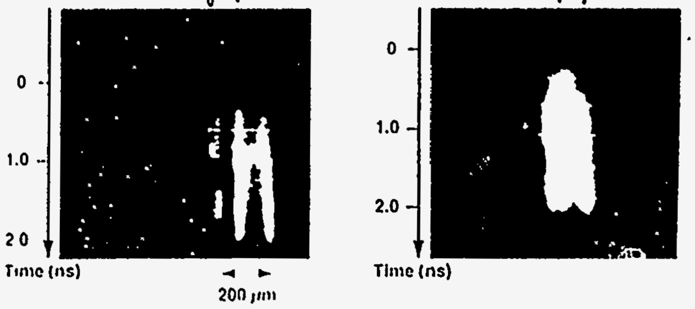

Perturbation growth was reduced to 65% of no x-ray pre-irradiation

ILE Osaka

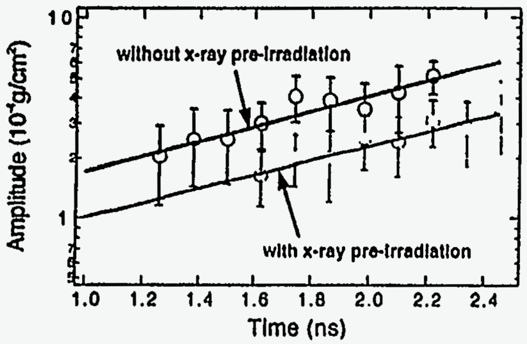

summary

A number of hydrodynamic perturbation growth crucial to ignition/burn has been clarified.

- *Ripple shock*
  Finding of damped oscillation.
  Areal-density-perturbations grow by a factor of ~4.
- *Initial imprinting*
  First observation of single-mode initial imprinting.
  ~~First~~ observation of laser coherency dependence.
  Initial imprinting is reduced by soft x-ray pre-irradiation.
- *Rayleigh-Taylor Instability*
  ~~First~~ observation of linear growth rate in direct-drive

Spectroscopy of Compressed High Energy Density Matter

Nigel Woolsey
Lawrence Livermore National Laboratory

263

Spectroscopy of Compressed High Energy Density Matter

N. C. Woolsey, B. A. Hammel, C. J. Keane,
A. Asfaw, C. A. Back, S. Glenzer,
B. Talin, R. Stamm, L. Godbert, C. Mossé,
L. S. Klein, J. S. Wark,
R. W. Lee

Lawrence Livermore
National Laboratory

Collaborations

N. C. Woolsey, B. A. Hammel, A. Asfaw, C. A. Back,
S. Glenzer, D. Kalantar, C. Keane, J. Koch, J. Moreno
LLNL, University of California, P.O. Box 808, Livermore, CA 94551, USA

B. Talin, R. Stamm, L. Godbert, C. Mossé
PIIMA, Centre St. Jerome Université of Provence, Marseille, Cedex 20 France

L. S. Klein
Department of Physics, Howard University, Washington, D.C. 20059, USA

J.S. Wark
Clarendon Laboratory, Department of Physics, University of Oxford, Parks Rd, Oxford OX1 3PU, UK

R. W. Lee
Department of Physics, University of California, Berkeley, CA 94720, USA

Lawrence Livermore
National Laboratory

Reasons to Develop Spectroscopy at High Energy Density

- Basic physics:
  1) Test physical models of the bound-bound and bound-free spectroscopy

  2) Investigate ion dynamic effects on the Ar XVII $1s^2$-$1s3p\,^1P$ emission line
- Radiation Transfer
- Reveals details of nature of the imploded core, e.g., gradients
- Applications
  Mechanisms involved are the same as those in ignition targets

Three points will be emphasized

- FWHM of the Ar K-shell 1 -3 lines are a robust N_e diagnostic
- Central region of the 1-3 lines are effected by ion-field fluctuations
- Dielectronic satellites of the 1-3 lines provide a T_e diagnostic

N_e Diagnostic

The FWHM of the 1 - 3 k-shell transitions shows it is a good density diagnostic

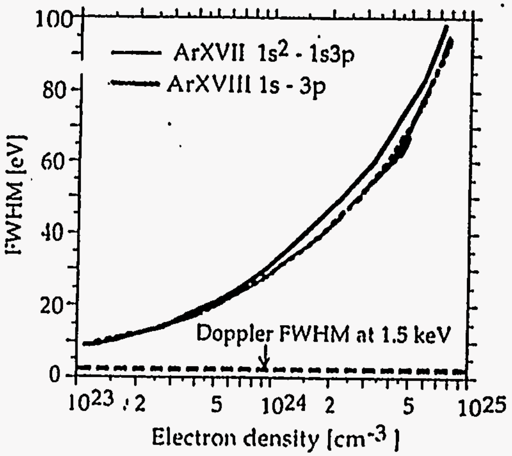

- Widths extracted from FLY
- Robust diagnostic since $N_e \propto FWHM^{2/3}$ (relatively independent of T_e)

Ion Dynamics Effects

Details of the shape of the ArXVII 1 - 3 transition provide insight into the nature of the line formation

- The central part of the line could be affected by various effects
  - Density gradient in the implosion core
  - Optical depth effects
  - Au emission
  - Ion dynamics
  - Satellite line transitions
- To find the intrinsic line profile, test the effect o low verses high Z ion perturbers

The ion dynamics can be investigated with different fill gases

- Investigate ion dynamics on the ArXVII $1s^2$ - $1s3p$ ^1P lineshape by varying the fill gas in the microsphere
- Keep N_e constant and try to ensure the hydrodynamics of the implosion is similar
- Fill gases:

D_2	-	50 atmospheres
CD_4	-	10 atmospheres
N_2	-	7 atmospheres
Ne	-	10 atmospheres

- Argon is introduced in trace amounts to ensure ArXVII 1-3 line remains optically thin and the argon does not effect the implosion
- Ion motion is greater for lighter ions
  - ion dynamics is most prominent for D_2

The electric field autocorrelation function is the key to ion dynamics

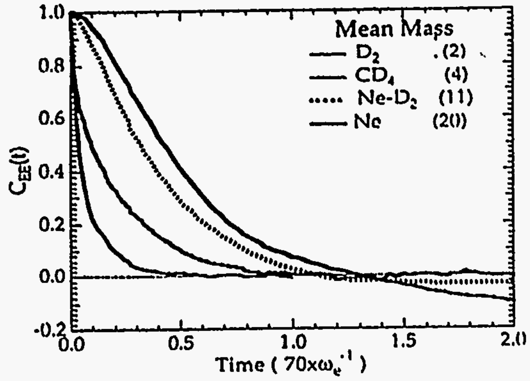

- $C_{EE}(t)$ for 4 gas fills at $N_e = 1.2\times10^{24}$ cm^{-3} and $T_e = 1.55$ keV
- By the fluctuation-dissipation theorem we can find, from the decay of $C_{EE}(t)$ ion microfield fluctuation rate υ

Ion dynamics alters the central part of the Ar XVII $1s^2$ - $1s3p^1P$ lineshape -- but not FWHM!

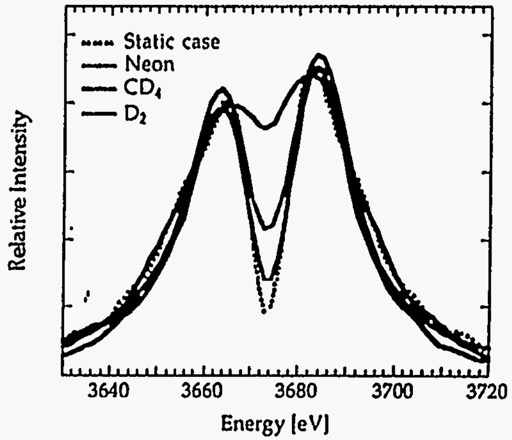

- Central dip in the lineshape is significantly altered through ion dynamics. Different fill gases may enable the effect of ion motion to be deter ed

Dielectronic Satellites

Li-like satellites to the He-like resonance transitions effect the width of the resonance at low T_e

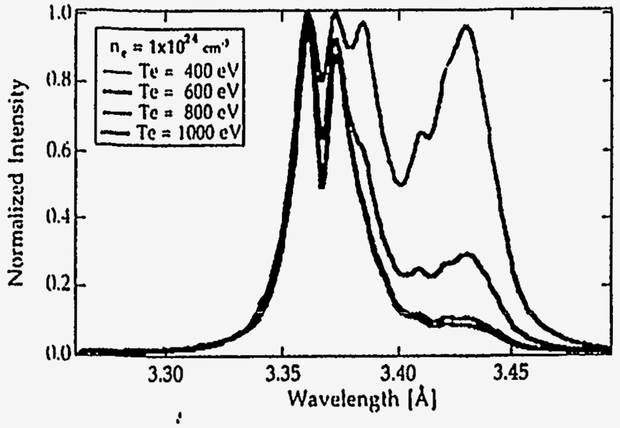

- Spectrum synthesis requires compatible kinetics and line shape calculations; atomic model contains all the 2l3l', 3l3l' and 3l4l' states
- At high T_e (< 1000 eV) satellites do not fill in the dip
- Shape and intensity of the Li-like Ar satellites to the He like Ar 1-3 line provides a T_e diagnostic

ICF implosions provide extreme conditions. Illustrates diagnostics, ion dynamics, and large-scale calculations for line shapes

- Experiments are performed at Nova using laser produced x-rays to implode a plastic capsule filled with a test gas.
  - Capsules are ~ 270 µm radius, with 50 atm of D_2 and 0.1 atm of Ar
  - Optical depth and emissivity of ArXVIII 1 to 3 lines controlled
  - Implosion compresses core plasma to high N_e & T_e, ≥ 10^{24} cm^{-3} & 1 keV
  - Time resolved imaging measures implosion core
  - Spectroscopy performed with x-ray crystal coupled streak camera

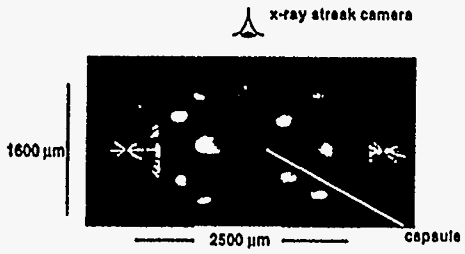

Argon emission spectrum from an imploding CD_4 filled capsule driven at 17 kJ

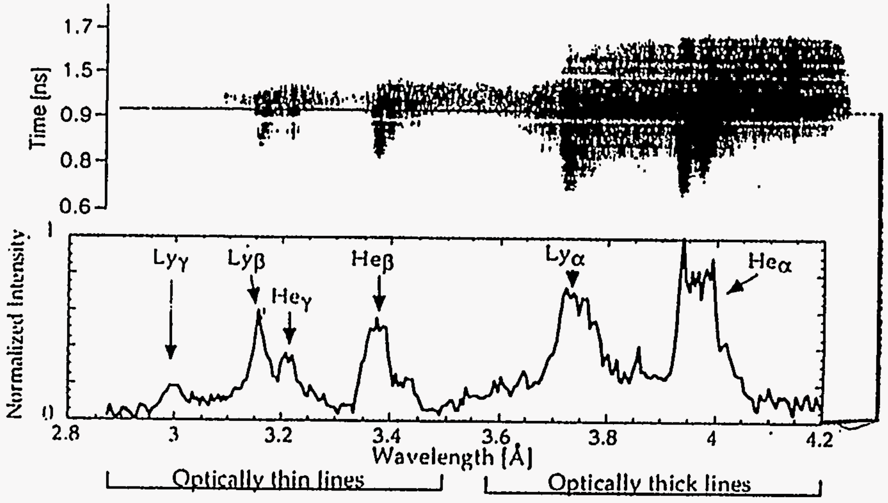

ote. dip in ArXVII 1-3 is not observed

ILE

Argon emission spectrum from an imploding D_2 filled capsule driven at 17 kJ

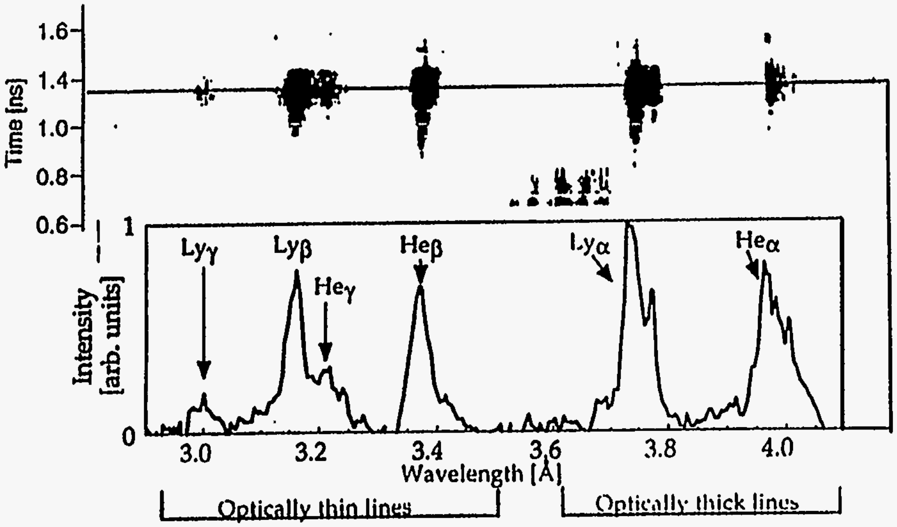

Ne(t) determined using the ArXVII $1s^2$-1s3p emission from an imploding D_2 microsphere

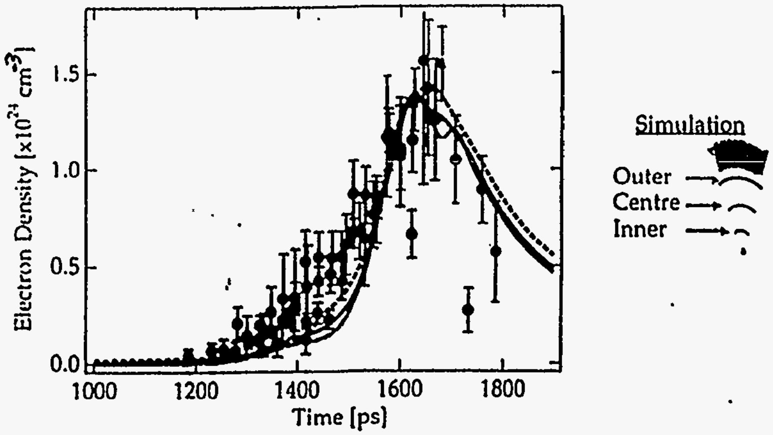

- 4 shots at ~19 kJ are represented
  HYADES simulation using a 16 kJ Planckian drive

Radiation-hydrodynamic simulations are used to understand the details of these implosions

- HYADES 1-D radiation hydrodynamics code
- SESAME EOS of state library
- Average atom atomic physics
- Multigroup radiation transport

- The radiation drive we used in the simulations is a Planckian source measured from a 2500 µm x 1600 µm diameter hohlraum irradiated with 16 kJ in a 1 ns temporally square laser pulse

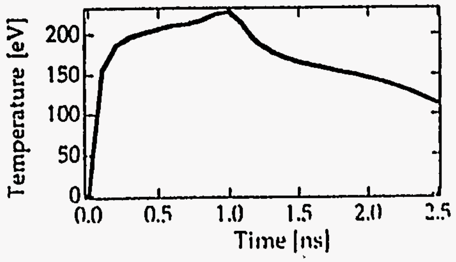

Interactive database / analysis software aids ArXVII n_e and T_e modelling

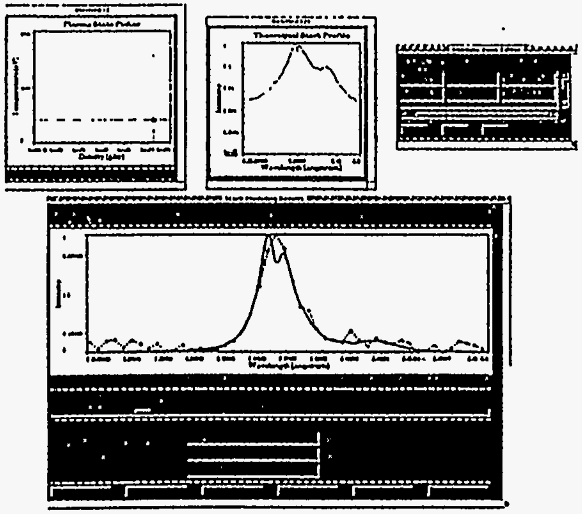

- Modelling software written by J. K. Nash
- Data base generated using TOTAL by J. C. Moreno

An interactive, database - driven application simplifies data analysis for Ar XII ne / Te diagnostics

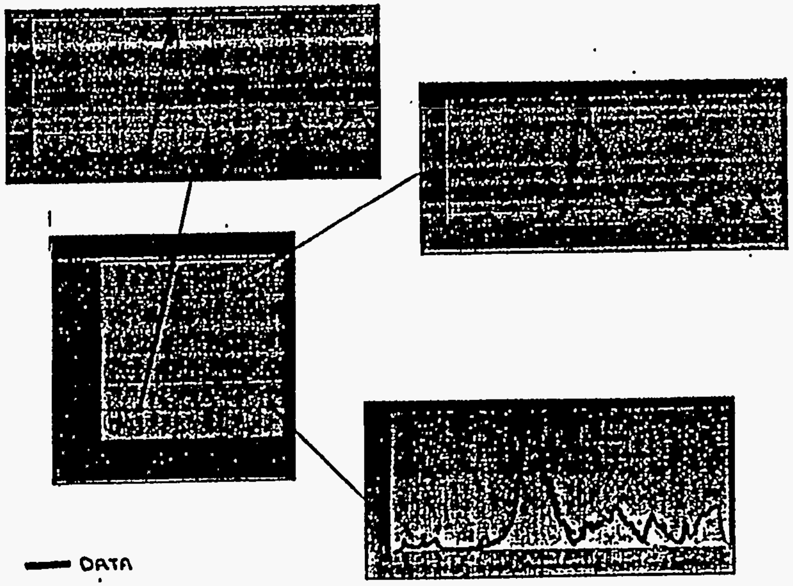

Summary: Density Diagnostics

- ArXVII $1s^2$-$1s3p^1P$ is a T_e, N_e diagnostic for hot d[illegible] systems
- Implosion cores provide a testbed for hydrodynamic simulations
- Implosion cores provide a testbed for theoretical lineshapes
- Implosion cores provide an excellent test of complex kinetics

Summary: Experiments

- Spectroscopic measurements have been made of indirectly driven implosions
- Dip in the ArXVII 1 - 3 with D_2, CD_4, and N_2 fills not observed
- The absence of the dip may be due to N_e T_e gradients in core.
    - This is supported by hydro-simulations
- Argon emission spectra not observed with neon filled targets
    - Predicted due to mismatch of T_e and N_e peaks
- $N_e(t)$ a test of hydrodynamics is determined from line widths
- Time histories are reproducible

Simulations of an imploding D_2 microsphere

Time history of the outer core radius cell and central core T_e and N_e

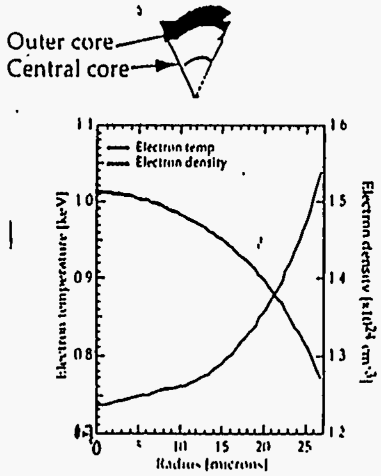

Spatial density and temperature profiles at peak density

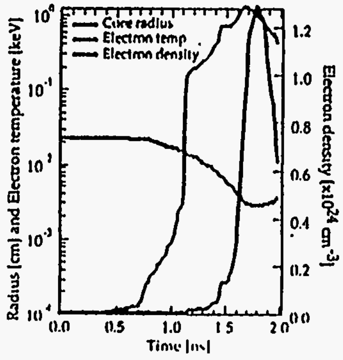

Ultra-Short Pulse Laser for High Energy-Density Science

Richard More
Lawrence Livermore National Laboratory

Ultra-Short Pulse Laser
for
High Energy-Density Science

Experiment:	Theory:
R. Stewart	R. More
D. Gold	E. Alley
G. Guethlein	M. Foord
D. Price	A. Osterheld
R. Shepherd	R. Walling
B. Young	(Z. Zinamon)

From the beginning, the LLNL USP Laser *was aimed at High Energy-Density Science*

- Chirped-pulse amplification, recompression, harmonic conversion produce

  0.3 Joules of 400 nm light in 100 fsec
  Prepulse intensity kept below 10^{-8}

- Diagnostics from LLNL test program
  - Reflected, scattered and transmitted light
  - Hydro expansion at small distance
  - Hydro expansion at large distance
  - Time-resolved x-ray emission
  - X-ray absorption
- Close contact with theory

Absorption is a first question— we measure it carefully

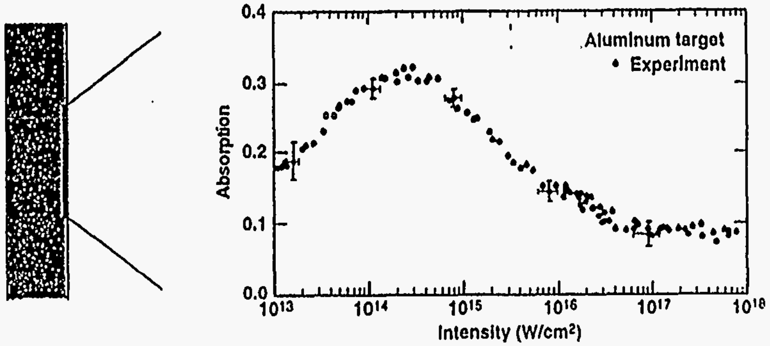

- Low prepulse
- Always irradiate fresh target material
- Measure pulse autocorrelation and spatial profile
- Measure incident, reflected and scattered energies

We understand the absorption

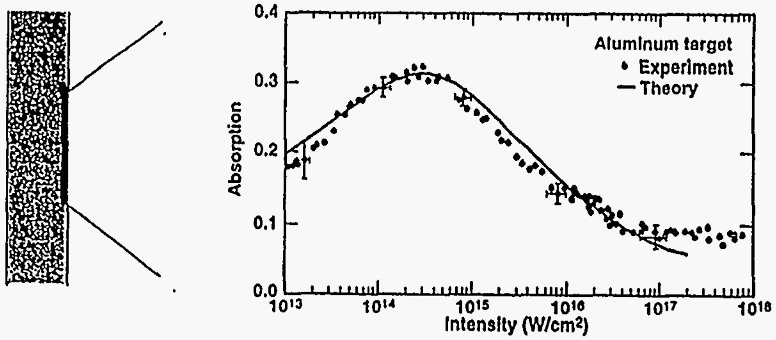

LASNEX MODEL

- Gaussian beam profile
- Realistic time–history
- Maxwell equations with correct AC conductivity
- 2T EOS and conductivity
- Hydrodynamic expansion
- Nominal heat flow

This excellent agreement is obtained for aluminum targets

Absorption depends on the target material

At high intensity, observe *Universal Plasma Mirror* reflection

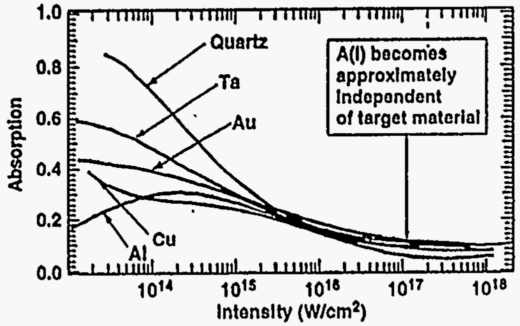

Low intensities:

- Conduction electron inverse bremsstrahlung
- Intra-atomic line absorption (interband transitions)

High intensities:

- Free electron/ion inverse bremsstrahlung
- Novel mechanisms above about 10^{18} Watts/cm²

We can test our understanding of absorption by future experiments on thin targets

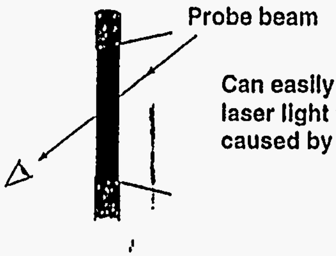

Can easily distinguish transmitted laser light from thermal emission caused by heat conduction

Electromagnetic skin depth $\delta = c/\sqrt{4\pi Z^* n_i e^2/m}$

Penetration is proportional to exp(-x/δ)

Transmission measurements will give us a direct measure of the ionization state Z*(T)

EOS is the linkage of thermodynamic variables specific to a given material

Thermodynamic variables: ρ, T, p, E, S

Thermodynamic functions which define en EOS: F(ρ,T), E(ρ,S), G(p,T), H(p,S)

- must know these in a 2-D region to form the derivatives...e.g., $p = \rho^2 \frac{\partial F}{\partial \rho}$ $S = \frac{\partial F}{\partial T}$

Incomplete or partial EOS:
p(ρ,T)
E(ρ,T)
p(ρ,T)

An Important Goal: to measure EOS using the USP Laser

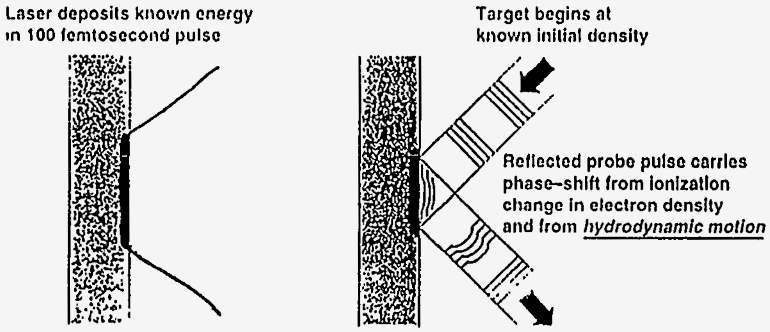

Analysis of spectoscopic interferometry:

- Measure phase shifts at various delays
- Separate ionization effect from hydrodynamic effect
- Determine expansion velocity vs time delay
- Extrapolate to early times

Variation of the phase with time in Aluminium

Gauthier et.al.,
Ecole Polytechnique

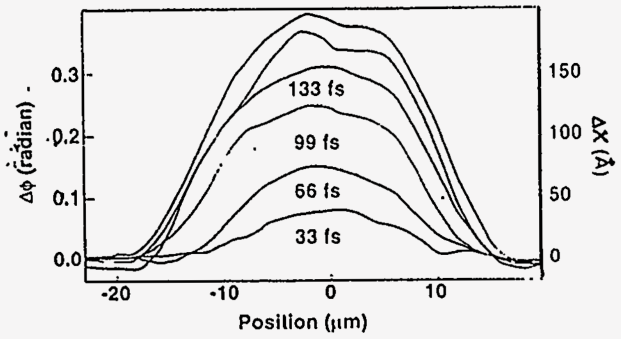

Frequency-Domain Interferometry

Accurate measurement of short pulse plasma expansion with femtosecond time resolution has been demonstrated.

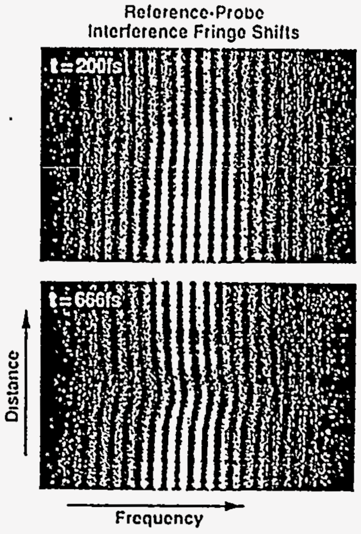
Reference-Probe Interference Fringe Shifts

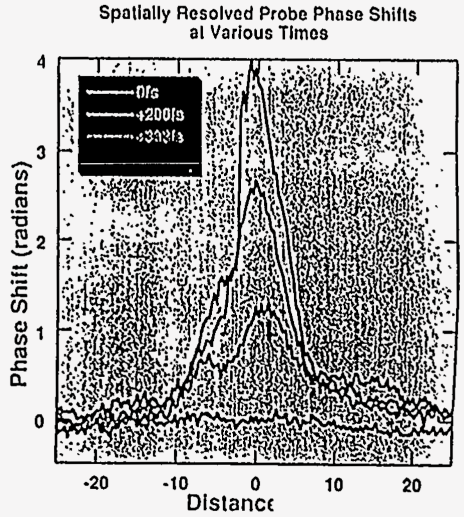
Spatially Resolved Probe Phase Shifts at Various Times

Ideal gas release velocity is 3 times the sound speed

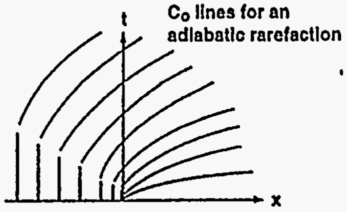

γ-law gas has $p \propto \rho^{\gamma}$ and $V(\infty) = \frac{2c}{\gamma-1}$

In fact, $v(x,t) + \frac{2c(x,t)}{\gamma-1} = \text{constant}$

Can these equations be generalized to an arbitrary equation of state?

Expansion velocity is related to dp/dρ for arbitrary EOS

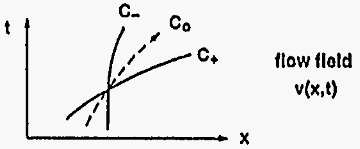

C_0 = particle track $\frac{dx}{dt} = v(x,t)$

$C_\pm$ = sound wave path $\frac{dx}{dt} = v(x,t) \pm c(x,t)$

Theorem (Bernhard Riemann):

$J_\pm(x,t) = v(x,t) \pm \int \frac{1}{c}\frac{dp}{\rho}$

is constant along $C_\pm$ path

$c^2 = \frac{dp}{d\rho}$

Application:

- Know initial value of $J_\pm(x, 0)$
- Measure v(x,t) from phase-shift data
- Then determine EOS integral by subtraction.

The EOS information is very much like that given by shock-wave experiments

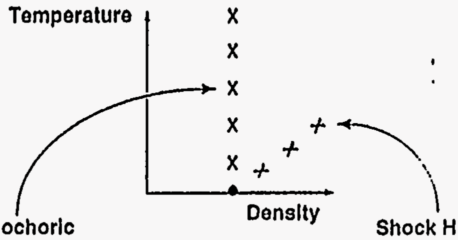

USP isochoric heating measures

$\boxed{\frac{\partial p}{\partial \rho}, \rho, E}$

- New technique
- Higher temperature
- Dominated by electron excitation

Shock Hugoniot experiment gives

$\boxed{p, \rho, E}$

- Higher precision
- Compression
- Dominated by bulk modulus

- Neither technique gives a complete equation of state, but the measured numbers serve to test theoretical EOS models

---

USP experiments can test EOS where it is most uncertain

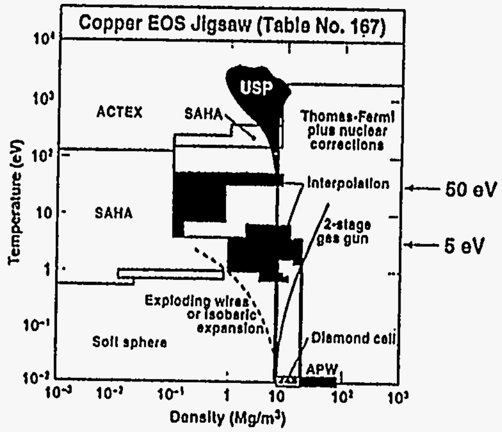

- No complete or conclusive theory (quantum + many–atom + disorder)
- No quantitative experiments (especially not above 10 eV temperature)
- Previous "high–quality" data–bases handled this region by interpolation

---

Do USP targets reach LTE in 100 fsec?

For this question we use codes and analytic formulas

- We expect to find

$$\boxed{T_{rad} << T_{ion} << T_e}$$

- Radiation is only a small part of the energy at conditions of our EOS experiments.
- Ion EOS can be 10% of the total, but only 1/2 of that is due to interactions and only about 1/4 (i.e., 2%) is uncertain
- However when $T_{ion} << T_e$, the ion contribution is much less

$$p = \underbrace{\frac{Z^*kTe}{V}}_{\text{electrons } 90\%} + \underbrace{\frac{kTi}{V}}_{\text{ion ideal } 5\%} + \underbrace{\text{Ion Grünelsen part}}_{\text{Ion Interactions } 5\%}$$

Are USP targets close enough to LTE to provide meaningful equation of state data? Evidently so, in the range where the EOS is most uncertain

- Electron-electron collision times are short enough that free electrons have an equilibrium (Maxwellian or Fermi-Dirac) distribution.

  (Typically τ_{ee} is 1 fsec)

- Impact ionization rates are large enough to ionize all but inner shell electrons in 10-20 fsec at 100 eV temperatures.
  Stepwise ionization leads to a steady-state.
  At solid density, impact ionization and three-body recombination are more rapid than radiative processes,
  producing approximately LTE populations.

- Numerical calculations agree.
  New X-ray spectra look like LTE emission.

How can we determine the temperature?

- X-ray emission spectrum
- Absorption of optical probe (Ng et al., UBC)
- Optical emission for known emissivity
- Ion velocities in TOF spectrum (Guethlein and Foord, LLNL)
- Emitted electron spectrum (Downer, U. Texas, Austin)
- Thin target calorimetry with known absorption

Near-term USP experiments test key physics of high enegy-density

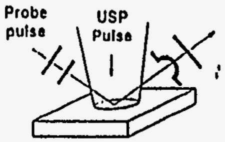

Surface release experiment
- Measure expansion velocity for known energy-deposition
- Tests EOS model under precisely-defined conditions

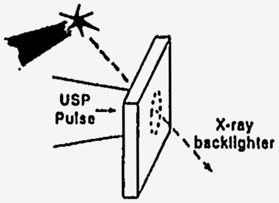

X-ray absorption experiment
- Measure high-density edge-shift and continuum lowering
- Tests opacity theory under precisely-defined conditions

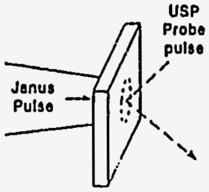

Shock-release experiment
- Chirped probe pulse gives unprecedented (sub-picosecond) time-resolution of surface release.

Femtosecond-Laser Driven Heat Waves in Solid

Andrew Ng
University of British Columbia

FEMTOSECOND-LASER DRIVEN HEAT WAVES IN SOLID

Andrew Ng, Andrew Forsman
University of British Columbia, Canada

Peter Celliers
Lawrence Livermore National Laboratory, U.S.A.

Femtosecond laser-driven heat waves in solid

- Inspired by the experiment of Vu *et al.*, Phys. Rev. Lett..(1994)

- 1-D hydrodynamic simulation
  - Examine roles of laser deposition, thermal conduction and hydrodynamics

---

PROBING THERMAL CONDUCTIVITY OF DENSE PLASMAS

- Propagation of heat front governed by thermal conductivity

- Experiment of Vu, Szoke and Landen [PRL 72, 3823 (1994)]
  - Glass target with top layer of 300 Å carbon irradiated with 100 fs, 616 nm pulse at 5×10^{14} W/cm^2
  - Laser deposition in carbon leads to heating of carbon-glass interface
  - Thermal conduction drives an ionization front into the glass

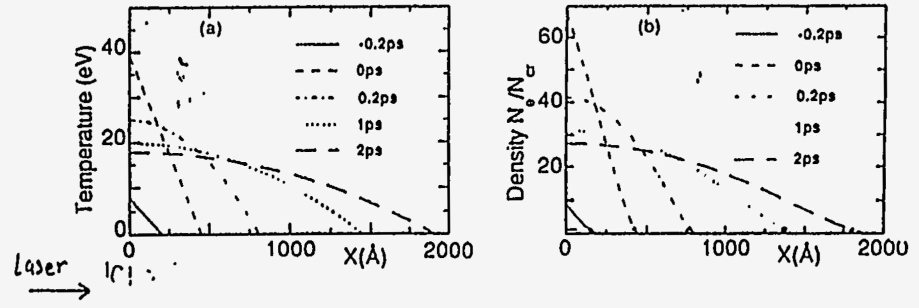

EXPERIMENT OF VU et al.

UBC

- Ionization front probed by 100 fs pulse at different time delays through target rear side
- Doppler shift in reflected probe pulse yields velocity of heat front
- Results in agreeement with diffusion calculations using Spitzer conductivity

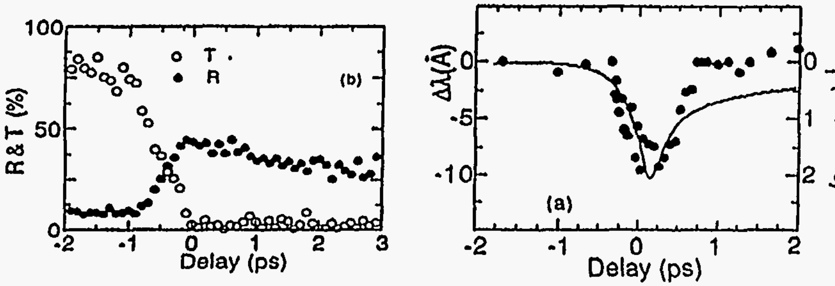

Difficulties with the study

UBC

- Experimental issues
  - Initial transmission of pump laser into glass due to finite opacity of 300 Å carbon
  - Plasma formation at extremely early times (-1 ps) of pump pulse at $\approx 10^9$ W/cm^2 might cause decoupling of laser from carbon-glass interface
  - Laser deposition at interface leads to laser heating of glass
- Modelling issues
  - Ionization in glass given by Saha equilibrium did not account for interband transitions
  - Laser deposition in carbon or glass, and plasma hydrodynamics not treated in thermal diffusion model
  - Use of Spitzer-type thermal conductivity might not be valid for dense plasmas

MODELLING OF LASER-DRIVEN HEAT FRONT

UBC

- Attempt to understand the phenomenon in a simple metal
- 1-dimensional hydrodynamic code
  - Laser-matter interactions treated with an EM wave solver (Helmholtz equations and dielectric function description).
  - Normal incidence for probing high densities
  - Examine effects of plasma conductivities on heat front propagation
  - Radiation transport, non-equilibrium effects of temperature and ionization not treated
- Aluminum irradiated with laser radiation of 400 nm, 100 - 500 fs (FWHM) at 10^{13} -10^{15} W/cm^2 show similar features
  - EOS and conductivity data availal r aluminum
  - Present 500 fs case for plausible time-resolved measurements

SNAP-SHOTS OF HEAT FRONTS AT EARLY TIMES

UBC

- Aluminum irradiated with 400 nm, 500 fs laser at 10^{15} W/cm^2
  QEOS; Lee & More conductivities; screened hydrogenic model
- Laser peak at $t = 0$; initial target front surface at $x = 0$

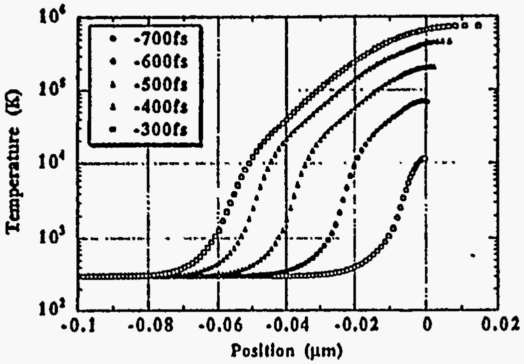

← Laser

Dominated by laser penetration process

Temperature and laser absorption profiles

UBC

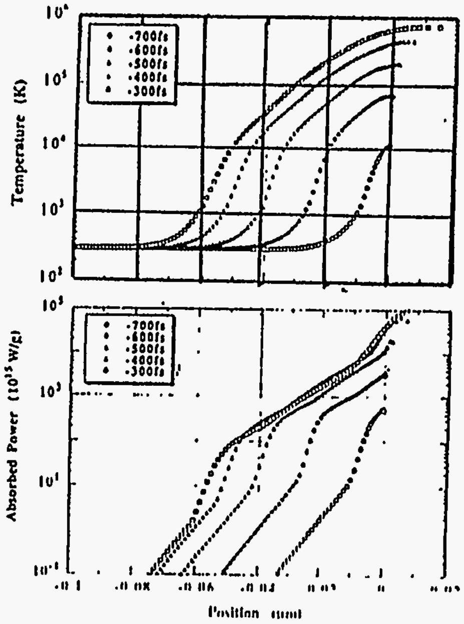

- At very early times, the heat front appears to move at similar speed as deposition front

SNAP-SHOTS OF HEAT FRONTS NEAR PEAK INTENSITY

- Aluminum irradiated with 400 nm, 500 fs laser at 10^{15} W/cm^2 QEOS; Lee & More conductivities; screened hydrogenic model
- Laser peak at t = 0 ; initial target front surface at x = 0

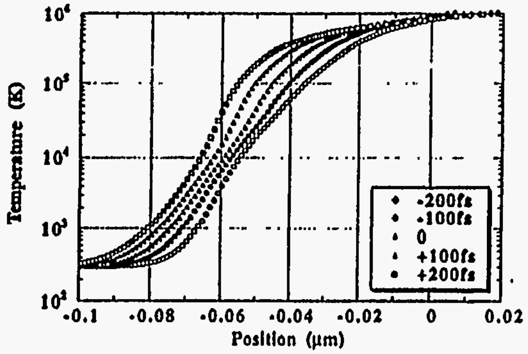

Laser

Steepening of temperature profile by nonlinear heat flow

Decoupling of laser deposition from heat front

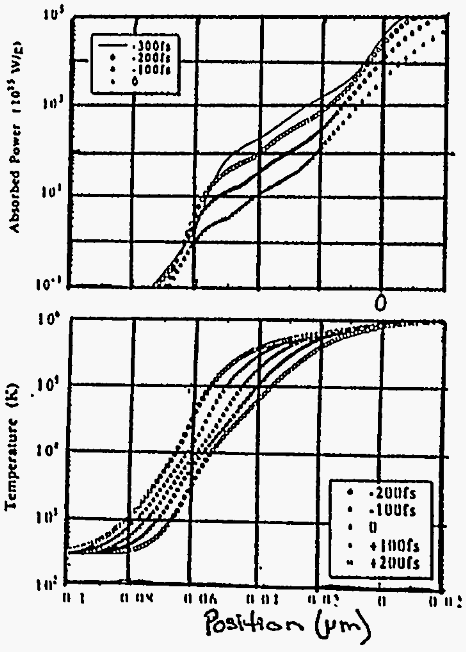

- As an expanding plasma forms, laser deposition begins to decouple from heat front
- As temperature rises, non-linear thermal conduction leads to steepening of heat front

SNAP-SHOTS OF HEAT FRONTS AT LATE TIMES

UBC

- Aluminum irradiated with 400 nm, 500 fs laser at 10^{15} W/cm^2
  QEOS; Lee & More conductivities; screened hydrogenic model
- Laser peak at $t = 0$; initial target front surface at $x = 0$

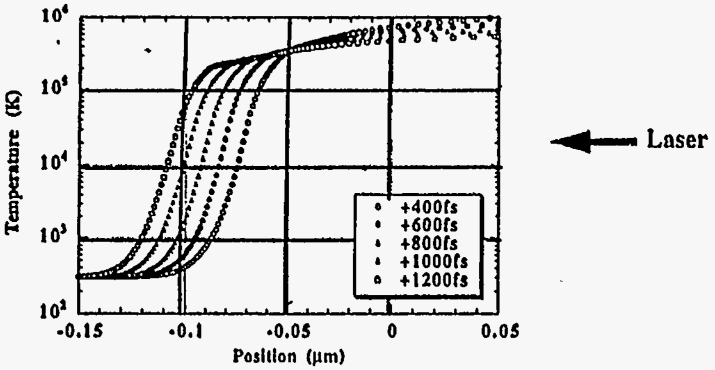

Plasma hydrodynamics producing shock waves

DEVELOPMENT OF SHOCK WAVES

UBC

- Significant compression occurs only after end of laser pulse

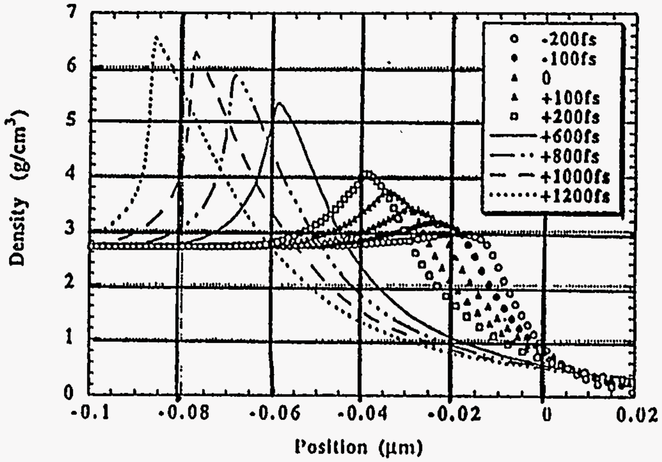

VELOCITY OF HEAT FRONT

UBC

- Consider the 10^4 K (sufficient to produce critical electron density in a solid) point on heat front for different conductivity models
  - At early times, velocity spike exceeding 10^7 cm/s
  - Before peak intensity, increase in velocity after minimum
  - At late times, steady but lower velocities

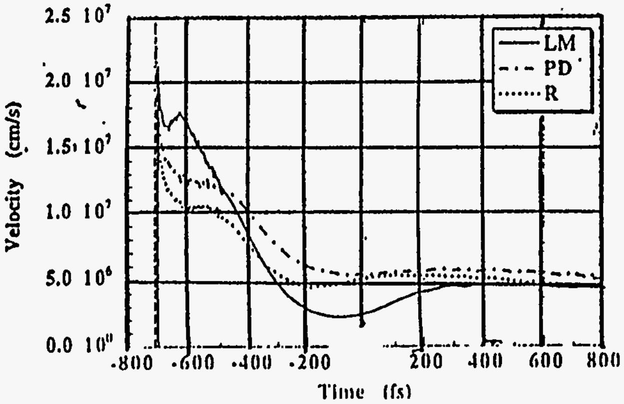

LM - Lee & More
PD - Perrot & Dharma-wardana
R - Rinker (Sesame)

10^4 K heat front speed and electrical conductivity

UBC.

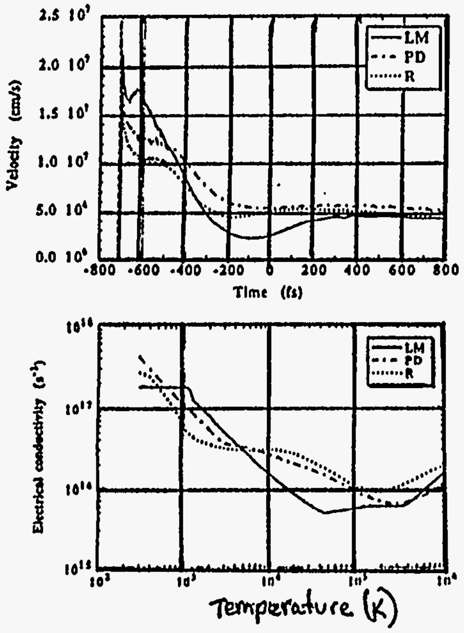

- At very early times, models with lower electrical conductivity allow deeper penetation of laser as an evanescent wave, leading to higher heat front speeds

10^4 K heat front speed and thermal conductivity

UBC

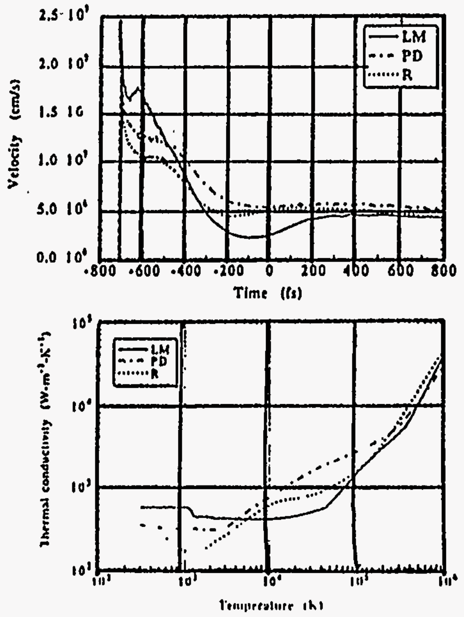

- When thermal conduction dominates, models with lower thermal conductivity yield slower heat front speeds

Conclusions on fs-laser driven heat waves

UBC

- Heat fronts produced in fs-laser heated solids characterized by three phases
  - Skin-depth deposition
  - Thermal conduction
  - Shock compression
- The high velocity (>10^7 cm/s) observed by Vu et al. might be due to laser penetration and not a measure of thermal conduction
  - Caveat : glass might behave very differently from aluminum
- Accurate measurements of heat front velocity may allow a complete test of models in electrical and thermal conductivities
  - New diagnostics required to provide sufficient sensitivity, accuracy and temporal resolution
- Details described in Phys. Rev. E 51, R5208 (1995)

Asteroseismology of White Dwarf Stars

Paul Bradley
Los Alamos National Laboratory

ASTEROSEISMOLOGY OF WHITE DWARF STARS

by

Paul Bradley
Los Alamos National Laboratory

Presented at
"Laboratory Astrophysics Experiments
With Large Lasers"
Workshop held at Lawrence Livermore National Laboratory
Feb. 26-27, 1996

1. Physics Regimes
2. Introduction and Motivation
3. Seismological Results
4. Astrophysical Implications
5. Comparison to Laser Plasmas

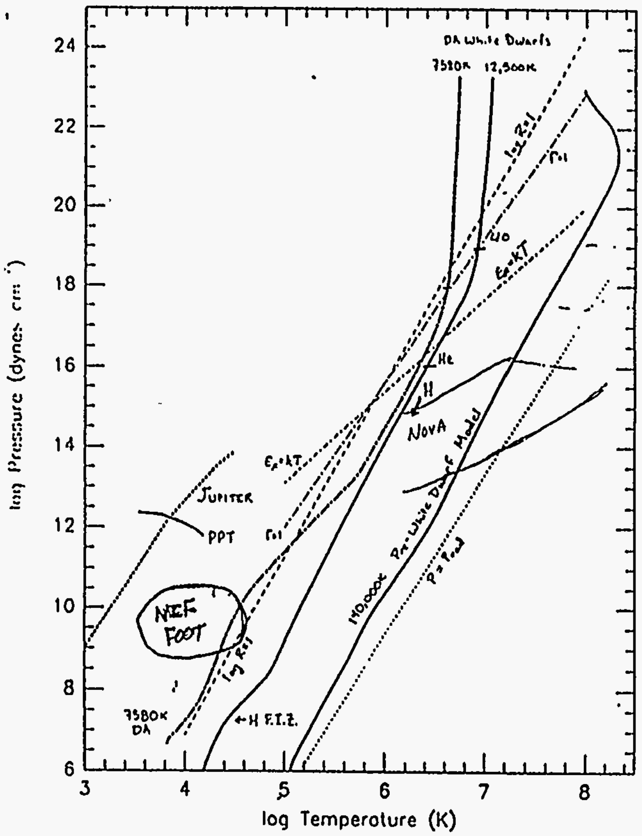

What Are White Dwarfs?

- General Properties

1. White dwarfs are the end result of stellar evolution for most stars. ($M_* \sim 1M_\odot$ to $5 - 8M_\odot$)
2. The average mass for planetary nebulae, PG1159 stars, and white dwarfs is $0.5 - 0.6M_\odot$ (Weidemann 1990; Bergeron, Saffer, & Liebert 1992; Werner 1992 Bergeron et al. 1995).
3. We believe the internal structure consists of a C/O core overlain by a thin surface layer. The composition of the surface layer and effective temperature determines what we call it.

   PG1159 stars are pre-white dwarfs. We see helium, carbon, and oxygen in their spectra and occasionally nitrogen is also present (see Dreizler et al. 1995). The surface temperatures ($\gtrsim 100,000$K) are too hot for hydrogen lines to appear in their spectra.

   DB white dwarfs have a modest helium layer at the surface and we only see lines of helium in their spectra.

   DA white dwarfs have only hydrogen lines in their spectra as a result of the thin hydrogen layer at the surface. The helium layer lies underneath due to gravitational settling because $\log g \sim 8$.

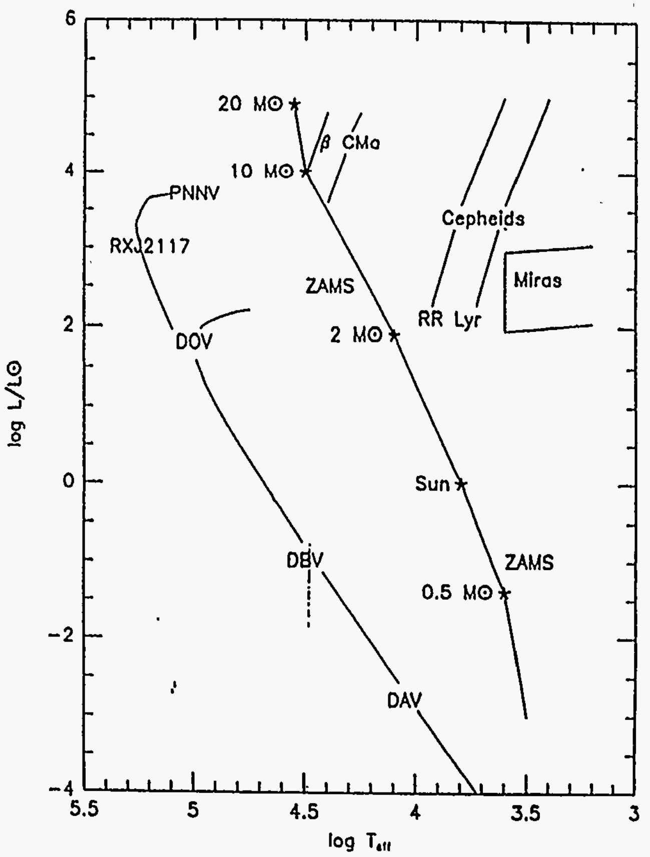

- **Pulsators**

  1. All 3 white dwarf classes mentioned above have a fraction of their members pulsating in nonradial *g*-modes They are called DOV stars in the PG1159 domain, DBV stars in the DB region, and DAV stars in the DA region.
  2. Pulsation driving comes from the κ,γ mechanism (heavily modified by convection/pulsation interactions) operating in the partial ionization zone (Winget 1981: Winget et al. 1982; Starrfield et al. 1983, 1984; Bradley & Dziembowski 1996). The different ionization potentials of the dominant element are responsible for the location of the instability strips.
  3. The observed light variations are due to changes in the surface temperature distribution (Robinson, Kepler, & Nather 1982).
  4. Various studies suggest the pulsators are otherwise normal white dwarfs that happen to be passing through an instability strip (Fontaine et al. 1985; Bergeron et al. 1995). What we learn about the pulsators should apply to white dwarfs in general.
  5. To resolve their complicated light curves into individual pulsation modes, we use multi-site observing campaigns with the Whole Earth Telescope.
  6. The multi-site nature of the Whole Earth Telescope allows us to minimize confusion in our data analysis due to daily gaps in the data one gets from sunrises at a single site.

Why Mess With White Dwarf Stars?

- The strong gravity of white dwarfs gives them a relatively simple "onion" structure.
- We do not have complicating effects like nuclear burning, heavy element (metal) enhancements, rapid rotation, or strong magnetic fields in most white dwarfs.
- The work of Bradley & Winget (1994) for GD 358 and Kawaler & Bradley (1994) for PG 1159-035 show that detailed seismology of white dwarfs is possible.

White dwarf seismology can help us with the following:

1. We can determine the total stellar mass, surface layer mass, depth and steepness of the chemical composition gradients, along with rotation rates and/or magnetic field strengths.
2. We can learn more about the properties of matter under extremes of density and temperature. This will help us with problems in the Equation-of-State (EOS), conductive+radiative opacities, viscosities, neutrino emission, and convection.
3. We can constrain the previous phases of stellar evolution in terms of what kind of progenitor gives rise to a particular class of white dwarf.
4. We can probe the previous history of star formation in the Galactic Disk and—eventually—the Halo.

Evolutionary Models

1. I use the White Dwarf Evolution Code (Lamb 1974; Lamb & Van Horn 1975; Wood 1990) to construct models of cooling white dwarfs
2. I do not include nuclear burning, but do include neutrino emission by dense matter (Itoh et al. 1996).
3. In my older models, I use the H, He, C, and O EOS for dense plasmas computed by Fontaine, Graboske, & Van Horn (1977) along with the Lamb (1974) C and O EOS for the strongly coupled plasma in the core.
4. I recently incorporated the OPAL opacities into WDEC, and use the conductive opacities of Itoh et al. (1983, 1984).
5. I also incorporated the new H and He EOS of Saumon, Charbrier, & Van Horn (1995). For now, I recast them onto a ρ,T grid for computational convenience.

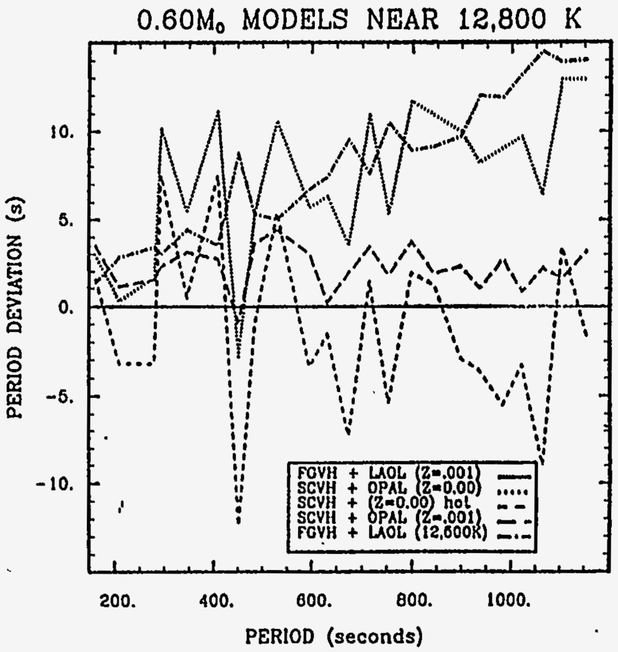

Comparison of Seismology Results to Other Results

1. Stellar Masses

- PG 1159-035 and PG 2131+066 has masses of 0 59M and $0.61M_{\odot}$.
- These masses are consistent with the mean mass ~ $0.6M_{\odot}$ for PNN (Weidemann 1990). It is larger than the masses (~ $0.5M_{\odot}$) suggested for extended horizontal branch objects (Heber 1992).
- GD 358 has a mass of $0.58M_{\odot}$, while PG 1115+158 is ~ $0.62M_{\odot}$, consistent with the mean mass of other DBs and the PG 1159 stars. (Oke, Weidemann, & Koester 1984).
- Our masses for the *DAV* stars are similar to the spectroscopically determined masses of Bergeron et al. (1995).

2. Surface Layer Mass

DOV stars:
- The surface layer mass of PG1159-035 is $4 \times 10^{-3}M_*$, thinner then the maximum allowed layer of $10^{-2}M_*$ (see Iben 1984 for example).
- PG 2131+066 has a similar surface layer mass of $6 \times 10^{-3}M_*$.
- However, it is similar to D'Antona & Mazzitelli's (1991) minimum surface layer mass of $2 \times 10^{-3}M_*$.
- Stellar evolution models are not yet able to duplicate the observed abundance patterns of the PG1159 type stars.

DBV stars:
- The helium layer masses of GD 358 is $2 \times 10^{-6}M_*$ and our limit for PG 1115+158 is $M_{He} \lesssim 10^{-4}M_*$.
- These are thinner than expected from stellar evolution theory ($M_{He} \lesssim 10^{-2}M_*$).
- However, Dehner & Kawaler (1995) show that if one allows diffusion to modify the composition profile of PG 1159-035, the main He/C composition transition occurs at ~ $2 \times 10^{-6}M_*$, consistent with what we see for GD 358.
- The total amount of helium in Dehner & Kawaler's models is about $6 \times 10^{-4}M_*$, consistent with what Pelletier et al. require to duplicate the carbon abundance trends in the DQ stars.

DAV stars:
- The hotter DAV stars have common trends in their periods that are consistent with their having a small range of hydrogen layer masses.
- These common pulsation spectra are consistent with their having hydrogen layer masses near $10^{-4}M_*$ to $10^{-5}M_*$.
- This is reasonably close to what stellar evolution theory predicts (Iben & MacDonald (1985, 1986).

Conclusions

- We are now able to perform seismology on white dwarfs, and have results for several DOV, DBV, and DAV white dwarfs.
- Seismology suggests that the DA and DB white dwarfs arise from different progenitors.
- We have suggestive evidence that DBs descend from He-rich PNN via the PG 1159 phase
- Most DA white dwarfs are descendants of H-rich PNN.
- White Dwarf models with the new OPAL opacities and new SCVH equation of state are not very different from previous models with older opacities and EOS.
- The previous two points say that previous seismological results are sound, and that we expect at most slight changes to earlier seismologically determined structural parameters.
- The biggest difference comes from using (more realistic) $Z = 0.0$ opacities, which were not available before.
- The Z=0.0 DA and DB models give the similar periods as before, but at about 500 K hotter temperatures.

Interaction Processes Between Exploding Plasmas and Media in Space

Anatolle Orishich
Novosibisirk State University

Anatoly Orishich

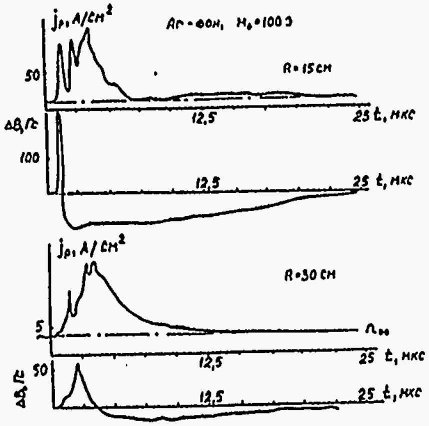

Oscillograms of electric j_p and magnetic ΔB probes at the cloud expantion in Ar-background at B_0=100 G.

$R_H^i < R^*, \quad R_H^* \gg R^*, \quad R_H R_H^* \gg R^*$

$\underline{M_A \simeq 25}$

The first Investigation problem

Collisionless deceleration of explouding plasmas in the conditions:

- Alfven-Mach number M_A>>1;
- λ>>R*, where λ - scale of collisional free-path of explouding plasmas ions, R*-gas dinamic scale, $R^* = (\frac{3M_A}{4\pi\rho^*})^{1/3}$, where ρ^* - background plasma density;
- magnetic Reynolds number Re_m>>1;
- $\beta = {}^{8\pi nT}/_{B_0^2} \ll 1$ - cold plasma.

Processes of Interaction:

- For a cold background plasma and M_A>5 the interaction between interpenetrating plasma flows due to charge-induced electric fields, both laminar and turbulent, is unlikely take place.
- The influence of the magnetic pressure upon to the deceleration of the cloud may be negligible, as it is M_A^2-times less then the dynamic pressure of the ambient plasma.
- Magnetic Laminar Mechanism (MLM) of interaction may be strong enough at M_A >>1. It is based on the action of a curl electric field $\vec{E}_\varphi$. An expanding diamagnetic cavity created by spherical cloud should effectively generate this field though $rot\vec{E}_\varphi = -{}^1/_c \frac{d\vec{B}}{dt}$. The necessary condition of this MLM interaction is the strong enough magnetization of ions. Larmour radius R_H and R_H* for cloud and background plasmas (calculation for cloud velosity) should be less than R^* ($R_H R_H^* < R^{*2}$).

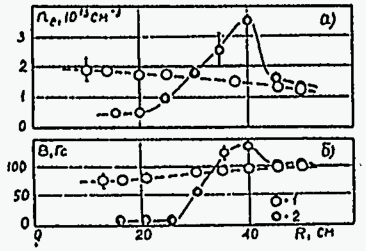

The structure of plasma (a) amd magnetic (b) cavities with the moving layer of compressed n_e and B_0 in the front, formed at the interaction of the cloud with H^+-background at $M_A \approx 5$ and $R_H R_H^* < R^{*2}$.
Dotted lines - initial distributions of n_e and B_0.

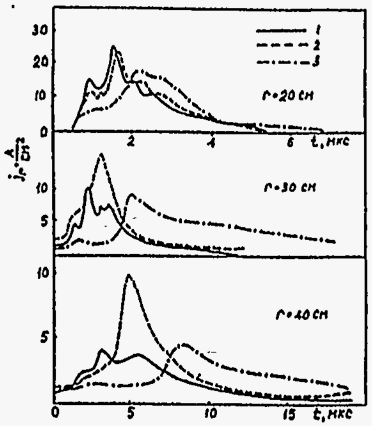

The influence of magnetic field $B_0 = 100$ G on the dynamics of radial flow of cloud ions in H^+-background at $R_H R_H^* < R^{*1}$:

1 - $n_1 = 2x10^{13} cm^{-3}$, $B_0 = 0$;

2 - $n_1 = 2x10^{13} cm^{-3}$, $B_0 = 75$ G, $M_A \approx 6$;

3 - $n_1 = 4x10^{13} cm^{-3}$, $B_0 = 65$ G, $M_A \approx 8$.

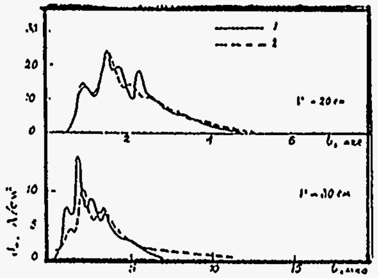

Dynamics of the radial flow of the ion cloud without magnetic field. (B = 0);
1 - n_1 = 0; 2 - n_1 = 210^{13}cm^{-3}. H^+- ions

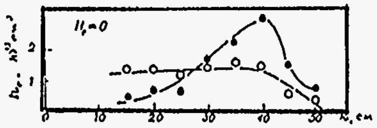

Plasma density distribution after the expansion of the cloud at B = 0. Light points - initial distribution .

Maoh nùmber $M_s = V_0/C_s \geq 3$
C_s - sound speed

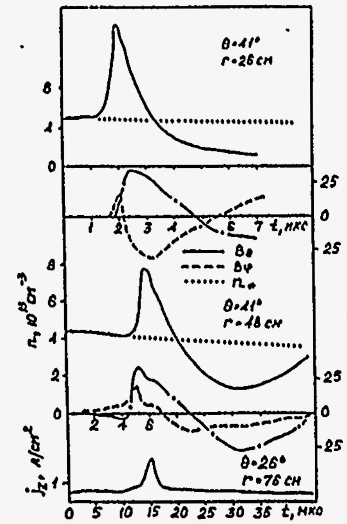

The structure of cloud-generated diturbances of H^+-background on the stage of their forming (R = 26 cm) and propagation (R = 48 and 76 cm) at various angles $\theta < 90°$ at $M_A > 3$ and $R_B R_B^* < R^{*3}$.

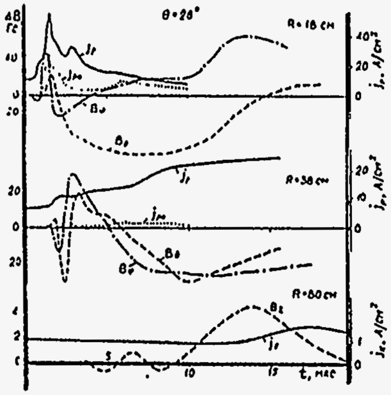

Dynamics of "quasi-parallel" disturbances of plasma and field at $M_A = 2$ ($R^* = 40$ cm).
j_{rr}, j_r - currents of the double probe at $n_1 = 0$, and $n_1 = 4 \times 10^{12} cm^{-3}$,
j_z - current of the collector.

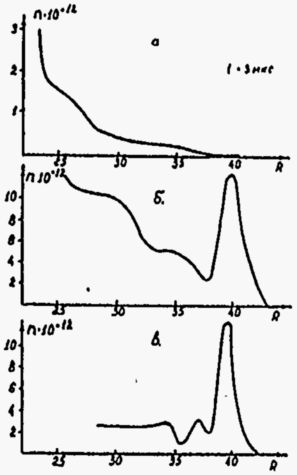

Typical radius distribution of concentration in laser plasma cloud.

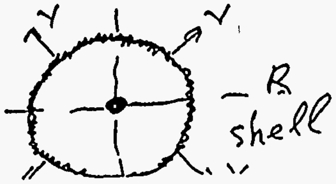

The second investigation problem:

The plasma cloud interaction with the vacuum magnetic field in the conditions:
- Alfven-Mach number $M_A << 1$;
- magnetic Reynolds $Re_m >> 1$, accoding to Coulomb collisions.

Processes of Interaction:

- Deceleration scale must be $R_s = (^{3E_0}/_{B_0})^{1/3}$, and its criteria must be $^{R_\pi}/_{R_s}$.
- Diffusion processes of $\vec{B}$ into the cloud may be turbulent.

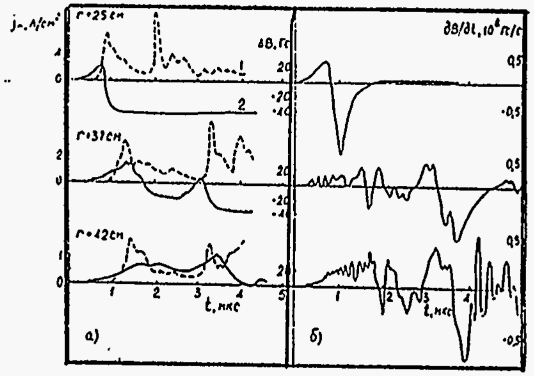

Dynamics of interaction of laser plasma cloud with the magnetic field B = 40 G in vacuum at $^{R_\pi}/_{R_s} > 1$ - the case of strong turbulent diffusion connected with the development of instability on lower hybrid frequency;
1 - j_1 at $B_0 = 40$ G;
2 - change of the perturbation of magnetic field ΔB.

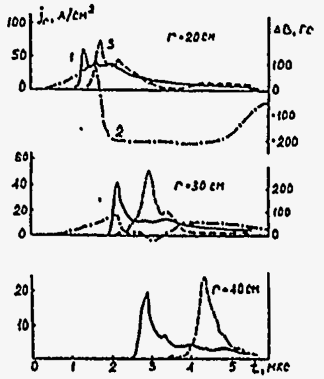

Dynamics of deceleration and following departure to R > R_s of the cloud with $R_н/R_s$ <1 at its interaction with magnetic field in vacuum:
1 - j_R at B_0 = 0; 2 - ΔB ; 3 - j_R at B = 260 G.

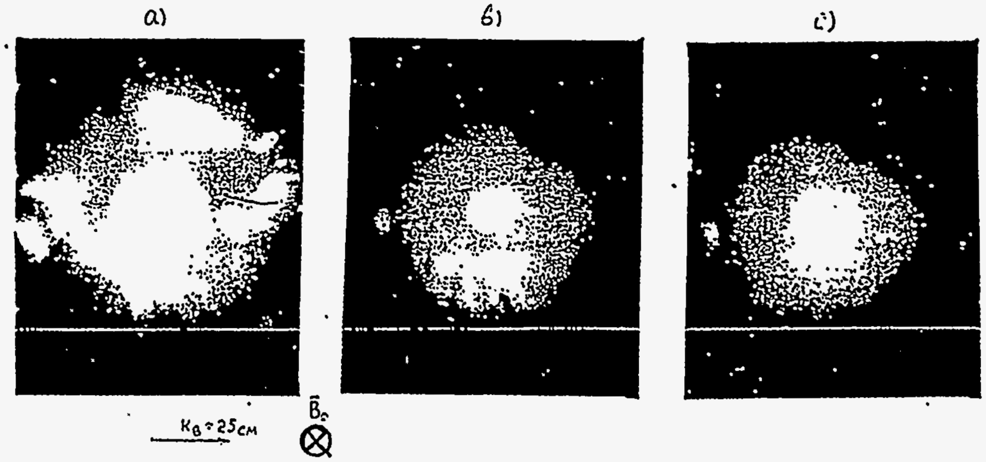

Fig.3 The control frame photo data (τ_{exp} ~100 ns), which demonstrate the effect of the [illegible]'s growth depression by a uniform H⁺-background with the density: [illegible] n_*=5·10^{11}cm^{-3} ; [illegible] 10^{12}cm^{-3} [illegible]

Summary and Conclusion:

1. The first confirmation of real efficiency of the Magnetic Laminar Methanism of the interaction between interpenetrating plasma flows at M_A > 5 and magnetization of ions was obtained. There are deceleration of the super-Alfvenic plasma flow and generation of the waves, travelling in the background at various angles with respect to $\vec{B}_0$.
2. At the plasma cloud interaction with B_0 (M_A < 1) there takes place microturbulent diffusion of magnetic field into the cloud (diamagnetic cavity), If the ions cloud magnetization is the strong enough ($R_н/R_s$ < 1), the cloud decelerates on the scale R_s, where plasma and field pressures becomes equal, and then continues to propogate with low velosity in perpendicular to $\vec{B}_0$ direction in the form of seperate flutes.
3. Obtained date may be used for analysis of natural explosive-type phenomena in space plasma like Supernova bursts, Barium releases of Ampte type or very greater plasma releases of "Starfish" type.

Laser plasma cloud simulation for investigation of a collisionless interaction processes between explouding plasmas and media in space.

V.M. Antonov, Yu.P. Zakharov, A.M. Orishich, A.G.Ponomarenko, V.G.Posukh, and V.N.Snytnikov.

Institute of Laser Physics, Siberian Branch of Russia Academy of Sience,
Novosibirsk State University

THE PROGRAM OF THE FACILITY KI-1 WORK.

MODELLED PHENOMENA.

1. Deceleration of Nova's and Supernova's shells in interstellar space.
2. Movement of plasmoids and artificial clouds in magnetosphere of the Earth.
3. Generation of interplanetary shock waves by solar flashes.
4. Evolution of planetary nebulae in galaxy field.

PROCESSES UNDER INVESTIGATION.

1. Collisionless interacton of superAlfvenic plasma flows.
2. Transformation of flows energy into collisionless disturbances of background.
3. Interaction of plasma flows with magnetic field, role of turbulence.
4. Plasma dynamics at non-stationary energy isolation, generation of compact plasma shells.
5. Ionization waves.

Principal scheme of the facility KI-1.

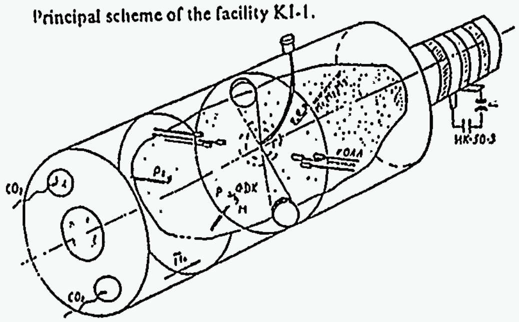

1. A large-scale (5 m long and 1.2 m in diameter) high-vacuum (10^{-3}torr) interactive chamber;
2. A system of CO_2 -laser and CO_2 -amplifier with output energy ~ 1 kJ.
3. A quasi-stationary source of a background plasma to fill the volume ~1 m^3 of the vacuum chamber by a highly-ionized density up to $n \sim 10^{13} cm^{-3}$. $T_e \approx 5 \div 10$ eV (H^+,Ar^+).
4. One or several carbon-hydrogen targets (Nylon) . Plasma clouds of an axially-symmetrical or near spherical form with energy E_0 up to 500 J and total mass M_0 up to 100μg has been obtained by two-sided irradiation of cylindrical and spherical targets.
5. Magnetic field $B_0 = 0 \div 1$ kG.
6. Diagnostic of the plasma density n_e, the ions flow j_{R*}, the perturbation of magnetic field ΔB, the electron temperature T_e.

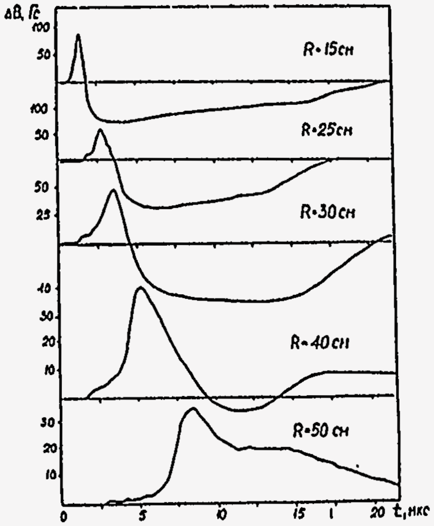

Dynamics of the magnetic field at the interaction of laser plasma cloud with H⁺ - background at $R_H R_H^* \le R^{*3}$, $M_A \ge 6$ ($n_i = 2x10^{11} cm^{-3}$, B_0=100 G).

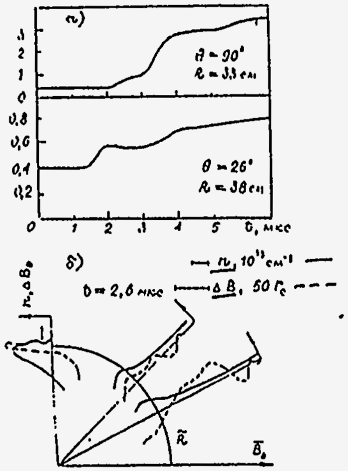

a) Disturbance of plasma concentration at various angles.
h) Regenerated space ditribution of n_r and B_0 in the experiment M_A= 1.5 and R^*= 40 cm.

Author Index

Participants

Alcock, Charles
LLNL L-413
(510) 423-0666
(510) 423-0238 FAX
alcock@igpp.llnl.gov
TOPICS OF INTEREST:
Low Mass Stars

Amendt, Peter
LLNL L-477
(510) 423-2162
amendt1@llnl.gov

Arnett, Dave
Steward Observatory
University of Arizona
Tucson, AZ 85721
(520) 621-9587
(520) 621-1532 FAX
dave@bohr.physics.arizona.edu

Azechi, Hiroshi
Institute of Laser Engineering
Osaka University
Osaka, Japan
azechi@ile.osaka.u.ac.jp

Back, Tina
LLNL L-473
(510) 422-6322
(510) 422-8395 FAX
tinaback@llnl.gov
TOPICS OF INTEREST:
Colliding Plasmas
Photo Pumping

Becker, Steven
Los Alamos National Laboratory
MS B-220
Los Alamos, NM 87545
(505) 667-8964
(505) 665-2227 FAX
sab@lanl.gov

Bernat, Tom
LLNL L-481
(510) 422-5915
bernat2@llnl.gov

Berning, Markus
LLNL L-399
(510) 424-4649
berning1@llnl.gov
UNIVERSITAT DUSSELDORF

Blain, Marc Antoine
DLPP/EPL
Centre de Limeil-Valenton
94195 Villeneuve-St-George
LLNL L-447

Blondin, John
North Carolina State Univ.
Dept. of Physics
P.O. Box 8202
Raleigh, NC 27695
(919) 515-7096
john_blondin@ncsu.edu
TOPICS OF INTEREST:
Modeling of Shock Instabilities
Supernova and Supernova Remnants

Blottiau, Patrick
CEA/DAM
Centre d'Etudes de Limeil-Valenton
94195- Villeneuve St Georges Cedex
France
33-(1) 45 95 60 63
33-(1) 43 86 74 20 FAX
TOPICS OF INTEREST:
Astrophysics
blottiau@limeil.cea.Fr

Bradley, Paul
XTA MS B-220
Los Alamos National Laboratory
Los Alamos, NM 87545
(505) 667-8999
(505) 665-2227 FAX
pbradley@lanl.gov
TOPICS OF INTEREST:
White dwarf astrophysics
Inertial Confinement Fusion (NIF)

Budil, Kim
LLNL L-018
(510) 423-8098
(510) 423-5112 FAX
budil1@llnl.gov
TOPICS OF INTEREST:
Laser experiments of
Hydrodynamics and transport

Campbell, E. Michael
LLNL L-466
(510) 422-5391
campbell5@llnl.gov

Castor, John
LLNL L-015
(510) 422-4664
(510) 422-5102 FAX
castor1@llnl.gov
TOPICS OF INTEREST:
Theory, modeling of laser experiments

Chevalier, Roger
Univ. of Virginia
Dept. of Astronomy
P.O. Box 3818
Charlottesville, VA 22903
(804) 929-4889
(804) 929-3109 FAX
rac5x@vifginia.edu
TOPICS OF INTEREST:
Supernovae/SN remnants

Colgate, Stirling —BANQUET SPEAKER
Los Alamos National Laboratory
Theoretical Div., T-6
MS 275B
Los Alamos, NM 87545
colgate@eagle.lanl.gov
TOPICS OF INTEREST:
All aspects of Supernova

Colvin, Jeff
LLNL L-473
(510) 422-3273
(510) 422-8395 FAX
colvin5@llnl.gov
TOPICS OF INTEREST:
Modeling of laser experiments

Cox, Arthur
Los Alamos National Laboratory
MS B288
P.O. Box 1663
Los Alamos, NM 87545
(505) 667-7648
anc@lanl.gov

Dearborn, Dave
LLNL L-022
(510) 422-7219
ddearborn@llnl.gov

Diamond, Patrick
Dept. of Phys. B019
University of CA.-- San Diego
La Jolla, CA 92093
(619) 534-4025
TOPICS OF INTEREST:
Hydrodynamic Instabilities
Shocks

Dimonte, Guy
LLNL L-043
(510) 423-0596
dimonte1@llnl.gov
TOPICS OF INTEREST:
Nonlinear hydrodynamics experiments

Drake, Paul
LLNL L-418, and
University of Michigan
Ann Arbor, MI
(510) 422-6706
(510) 422-2956 FAX
drake1@llnl.gov
TOPICS OF INTEREST:
Design of Nova Experiments
to Simulate the Circumstellar
Interactions Near SN 1987A

Dunn, Jim
LLNL L-251
(510) 423-1557
dunn6@llnl.gov

Estabrook, Kent
LLNL L-472
(510) 422-5441
estabrook2@llnl.gov
TOPICS OF INTEREST:
Modeling of laser experiments

Feldman, Uri
Naval Research Lab Code 7608
Space Science Division
4555 Overlook Ave. SW
Washington, DC 20375
(202) 767-5398

Fryxell, Bruce
NASA Goddard Space Flight Center
MS 934
Greenbelt, MD 20771
(301) 286-8567
(301) 286-1634 FAX
fryxell@neutrino.gsfc.nasa.gov
TOPICS OF INTEREST:
Supernova
Rayleigh-Taylor Instabilities
Computational Fluid Dynamics

Glendinning, S. Gail
LLNL L-473
(510) 423-3065
(510) 422-8395 FAX
glendinning1@llnl.gov
TOPIC OF INTEREST:
Laser experiments of
supernova hydrodynamics

Goldstein, William
LLNL L-047
(510) 422-2515
goldstein3@llnl.gov
TOPIC OF INTEREST:
Theory, modeling of
laser experiments

Grandy, Jeffrey M.
LLNL L-419
(510) 424-5626
(510) 422-8920 FAX
grandy1@llnl.gov
TOPICS OF INTEREST:
Large scale computing,
Fluid dynamics

Graziani, Frank
LLNL L-170
(510) 422-4803

Grun, Jacob
Code 6795
Naval Research Lab
Plasma Physics Division
4555 Overlook Ave. SW
Washington, DC 20375
(202) 767-9117
grun@NRLFS1.NRL.NAVY.MIL
TOPIC OF INTEREST:
Hydrodynamics laser experiments

Hatchett II, Steve
LLNL L-477
(510) 422-5916
(510) 423-9208 FAX
shatchett@llnl.gov

Iglesias, Carlos
LLNL L-041
(510) 422-7252
(510) 423-7228 FAX
IGLESIAS1@LLNL.GOV
TOPIC OF INTEREST:
Opacity

Iwamoto, Kohichi
Department of Astronomy, School of Science,
University of Tokyo
Bunkyo-ku, Tokyo 113
81-3-3813-9439 FAX
iwamoto@astron.s.u-tokyo.ac.jp
TOPICS OF INTEREST:
Linear stability of nuclear flames
2-D simulations of the Rayleigh-Taylor
instability in core collapse
Supernovae

Kallman, Tim
NASA/Goddard Space Flight Center
Code 665
Greenbelt, MD 20771
(301) 286-3680
TOPICS OF INTEREST:
Spectral modeling of x-ray
photoionized nebulae

Kane, Jave
LLNL L-413
University of Arizona/LLNL
TOPICS OF INTEREST:
Supernova modeling
Laser experiments

Kauffman, Bob
LLNL L-482
(510) 422-0419
(510) 422-4982 FAX
kauffman2@llnl.gov

Keane, Chris
LLNL L-477
(510) 423-4225
keane1@llnl.gov

Keedy, John
Los Alamos National Laboratory
Los Alamos, NM 87545

Khokhlov, Alexei
University of Texas/Austin
Astronomy Dept.
Austin, TX 78712
(512) 471-3397
(512) 471-6016 FAX
ajk@alla.as.utexas.edu
TOPICS OF INTEREST:
Instabilities in Thermonuclear Supernovae
Hydrodynamics of Interstellar Gas Interaction

Kilkenny, Joseph D.
LLNL L-488
(510) 423-4213
(510) 423 6212 FAX
kilkenny1@llnl.gov

Klein, Richard
LLNL L-023
(510) 422-3548
klein@mdhydro.berkeley.edu
TOPIC OF INTEREST:
Hydrodynamic Interaction of
Shock Waves with Interstellar Clouds

Kosaka, Keiji
Okayama University
Japan

Kruer, Bill
LLNL L-472
Livermore, CA 94550
(510)422-5437
(510)423-9969 Fax

Larsen, Jon
Cascade Applied Sciences, Inc.
6325 Trevarton Ln.
Longmont, CO 80503
larsen@casinc.com
TOPICS OF INTEREST:
Modeling of laser experiments

Levedahl, Kirk
DOE
Washington, DC
kirkl@icf.llnl.gov

Liang, Edison
Rice University
Dept. of Space Phys. & Astronomy
P.O. Box 1892
Houston, TX 77251
(713) 527-8101
TOPICS OF INTEREST:
Supernova ejecta-ring nebula collision

Liedahl, Duane
LLNL L-041
(510) 423-9647
liedahl1@llnl.gov
TOPIC OF INTEREST:
Spectroscopy of x-ray photoionized
nebulae and proposed laboratory expts.

Lindl, John
LLNL L-488
(510) 422-5430
lindl1@llnl.gov

Logory, Larry
LLNL L-419
(510) 423-6578
logory1@llnl.gov

London, Rich
LLNL L-477
(510) 423-2021
(510) 423-9208 FAX
rlondon@llnl.gov
TOPICS OF INTEREST:
All

Louis-Jacquet, Michel
CEA/DAM
Centre d'Etudes de Bruyeres le Chatel
BP 12
91680-Bruyeres le Chatel
France
33-(1) 69 26 77 53
Fax 33-(1) 69 26 70 15
TOPICS OF INTEREST:
Laser plasma physics

MacFadyen, Andrew
U.C. Santa Cruz
Dept. of Astronomy & Astrophysics
Santa Cruz, CA 95064
(408) 459-2774
andrew@ucolick.org
TOPICS OF INTEREST:
Supernovae
Hydrodynamic Instabilities

Max, Claire
LLNL L-413
(510) 422-5442
(510) 423-0238 FAX
max@llnl.gov
TOPICS OF INTEREST:
All

McCray, Richard
JILA, University of Colorado
Boulder, CO 80309-0440
(303) 492-7835
DICK@JILA.COLORADO.EDU
TOPIC OF INTEREST:
The impact of SN1987A with its
Circumstellar Ring
SuperNova ejecta-ring nebulae collision

Mihalas, Dimitri
University of Illinois
Astronomy Dept.
1002 W. Green St.
Urbana, IL 61821
(217) 333-5529
(217) 244-7638 FAX
dmihalas@altair.astro.uiuc.edu
TOPIC OF INTEREST:
Radiation Hydrodynamics

Mikaelian, Karnig
LLNL L-022
(510) 422-5449
TOPIC OF INTEREST:
Hydrodynamics
Modeling of laser experiments

Miller, Paul M.
LLNL L-022
(510) 423-6455
(510) 423 0925 FAX
pmiller@llnl.gov
TOPICS OF INTEREST:
Experiments on Richtmyer-
Meshkov mixing, jets

More, Richard M.
LLNL L-041
(510) 422-7208
more2@llnl.gov
TOPICS OF INTEREST:
Theory, modeling of
laser experiments

Murray, Stephen
LLNL L-023
(510) 423-9382
murray8@llnl.gov

Ng, Andrew
The University of British Columbia
Physics Department
6224 Agricultural Road
Vancouver, B.C.
V6T 1Z1, Canada
(604) 822-3191
nga@physics.ubc.ca
TOPICS OF INTEREST:
Detailed Opacities relevant to Stellar Interiors
Radiation and Thermal Transport
Dense Plasma Atomic Physics and EOS
X-ray Photoionized Plasmas

Orishich, Anatolle
Physics Department
Novosibisirk State University
Novosibisirk, Russia
011-738-32-3552 FAX

Pinto, Phil
University of Arizona
Steward Observatory
Tucson, AZ 85721
(602) 621-8678
ppinto@as.arizona.edu

Remington, Bruce
LLNL L-473
(510) 423-1699
(510) 422-8395 FAX
remington2@llnl.gov
TOPICS OF INTEREST:
Laser experiments

Rogers, Forrest
LLNL L-041
(510) 422-7351
rogers4@llnl.gov
TOPICS OF INTEREST:
Theory, modeling of
EOS, opacities

Rose, Steven
Bldg. R2, Rutherford-Appleton Lab
Chilton, Didcot
Oxon OX11 OQX, UK
8-011-44-1235-446344
8-011-44-1235-445888 FAX
s.j.rose@rutherford.ac.uk
TOPICS OF INTEREST:
Opacity and Radiative
Transfer experiments

Rosen, Mordy
LLNL L-472
(510) 422-5427
(510) 423-9969 FAX
rosen2@llnl.gov

Rubenchik, Alexander M. 'Sasha'
LLNL L-399
(510) 422-0976
rubenchik@llnl.gov
TOPICS OF INTEREST:
Theory
Modeling of Laser Experiments

Sangster, Craig
LLNL L-481
(510) 422-8176
sangster1@llnl.gov

Savin, Daniel
Dept. of Physics
University of California
Berkeley, CA 94720-7300
(510) 643-6863
savin@physics.berkeley.edu

Schappert, Gottfried
Los Alamos National Laboratory
Los Alamos, NM 87545
(505) 667-1294
(505) 665-4409 FAX
gts@lanl.gov

Shepherd, Ronnie
LLNL L-043
(510) 423-7456
shepherd1@llnl.gov

Shvarts, Dov
Physics Department
Nuclear Research Center Negev
P.O. Box 9001
Beer-Sheva, Israel
972-57-568736
972-57-567880 FAX
schwartz@bgumail.bgu.ac.il

Simmons, Kim
Los Alamos National Laboratory
Los Alamos, NM 87545

Springer, Paul
LLNL L-043
(510) 423-9221
(510) 423-5498 FAX
Springer6@llnl.gov
TOPICS OF INTEREST:
Experiments on Opacity
Stellar Evolution

Stone, James M.
Department of Astronomy
University of Maryland
College Park, MD 20742-2421
(301) 405-2103
(301) 314-9067 FAX
jstone@astro.umd.edu
TOPICS OF INTEREST:
shock-cloud interaction
radiation transport
radiation hydrodynamics

Strauss, Moshe
LLNL L-399
(510) 424-3101
strauss1@llnl.gov
UC Davis

Suzuki, Tomoharu
Department of Astronomy
School of Science
University of Tokyo
Bunkyo-ku, Tokyo 113
81-3-3813-9439 FAX
suzuki@astron.s.u-tokyo.ac.jp
TOPICS OF INTEREST:
3D simulations of the collision between Supernova
ejecta with Circumstellar material

Swenson, Fritz
Los Alamos National Laboratory
MS B220
P.O. Box 1663
Los Alamos, New Mexico 87545
(505) 667-4467
(505) 665-2227 FAX
fswenson@xdiv.lanl.gov

Townes, Charles
Dept. of Physics
Univ. of Calif., Berkeley
(510) 642-1128
(510) 643-8497 FAX
cht@sunspot.ssl.berkeley.edu
TOPICS OF INTEREST:
all

Wallace, Russ
LLNL L-482
(510) 423-7864
(510) 422-4982 FAX
wallace11@llnl.gov

Weaver, Robert
Los Alamos National Laboratory
X2 MS B220
P.O. Box 1663
Los Alamos, New Mexico 87545
(505) 667-4756
rpw@lanl.gov

Wilson Douglas
Los Alamos National Laboratory
XTA, MS B220
P.O. Box 1663
(505) 667-6154
(505) 665-2227 FAX
dcw@lanl.gov

Woolsey, Nigel
LLNL L-399
(510) 424-2175
(510) 423-6172 FAX
woolsey1@llnl.gov
AND
University of California at Berkeley
Berkeley, CA
(510) 643-1831
TOPICS OF INTEREST:
Laser Spectroscopy Experiments

Yoneda, Hitoshi
Institute of Laser Science
University of Electro Communications
Tokyo, Japan
81-424-83-2161
81-424-85-8960 FAX
yoneda@ils.uec.ac.jp

Unable to attend:

Aufderheide, Maurice
LLNL L-170
(510) 423-6174
aufderhe@viper.llnl.gov

Baldis, Hector
Laboratatoire LULI
Ecole Polytechnique
91128 Palaiseau Cedex
FRANCE
8-011-33-1-69-33-3713
8-011-33-1-69-33-3009 FAX
baldis@greco2.polytechnique.fr

Bell, Tony
Plasma Physics Group
Imperial College
London SW7 2BZ
0171-594-7638
0171-594-7658 FAX
t.bell@ic.ac.uk

Bildsten, Lars
Physics and Astronomy
UC Berkeley
Berkeley, CA 94720
bildsten@fire.berkeley.edu

Burrows, Adam
Univ. of Arizona
Steward Obs & Physics Dept.
Tucson, AZ 85721

Crandall, David
Director, Office of National Ignition Facility
Department of Energy
Defense Programs
DP16 FOR
Washington, DC 20585

Holm, Daryl
Los Alamos National Laboratory
MS
Los Alamos, NM 87545
(505) 667-6398

Laval, Guy
Centre de Physique Theorique
Ecole Polytechnique
91128 PALAISEAU Cedex
France

Livne, Eli
Recah Inst. of Physics
Hebrew University
Jerusalem, Israel

Mathews, Grant James
Department of Physics
University of Notre Dame
340B Nieuwland Science
Notre Dame, IN 46556
(219) 631-6919
(219) 631-5952 FAX
gmathews@bootes.phys.nd.edu
TOPICS OF INTEREST:
Stars
Stellar Interiors
White Dwarf Cooling, EOS

Nomoto, Kenichi
Univ. of Tokyo, School of Science
Dept. of Astronomy
Bunkyo-ku
113 Tokyo, Japan
011-3-3369-5079
nomoto@astron.s.u-tokyo.ac.jp

Takabe, Hideaki
Institute of Laser Eng.
Osaka University
Yamada-Oka 2-6
Suita, Osaka 565, JAPAN
8-011-81-06-879-8731
8-011-81-06-877-4799 FAX
takabe@ile.osaka-u.ac.jp

Vishniac, Ethan
University of Texas at Austin
College of Natural Sciences
Dept. of Astronomy
RLM 15-308
Austin, TX 78712
(512) 471-1429
ethan@astro.as.utexas.edu

Walling, Rosemary
(510) 422-4104
(510) 423-7228 FAX
rwalling@llnl.gov

Weaver, Tom
LLNL L-045
(510) 423-1850
(510) 422-1370 FAX
weaver-tom@llnl.gov

Wilson, Jim
LLNL L-161
(510) 422-4857
wjfrank@llnl.gov

Woosley, Stan
UC Santa Cruz
Board Study Astron./Astrophysics
Santa Cruz, CA 95064
408-459-2976